Dynamic Mathematical Modelling of Polymerization of Olefins Using Heterogeneous and Homogeneous Ziegler-Natta Catalysts

By

João B. P. Soares, M. Sc.

A Thesis

Submitted to the School of Graduate Studies

in Partial Fulfillment of the Requirements

for the Degree

Doctor of Philosophy

McMaster University

Hamilton, Ontario, Canada

Dynamic Mathematical Modelling of Polymerization of Olefins Using Heterogeneous and Homogeneous Ziegler-Natta Catalysts

To the *strong ones*:

my wife Fátima,

and my daughters Carolina, and Gabriela.

DOCTOR OF PHILOSOPHY (1994) **McMASTER UNIVERSITY**

(Chemical Engineering) Hamilton, Ontario

TITLE : Dynamic Mathematical Modelling of Polymerization of Olefins Using Heterogeneous and Homogeneous Ziegler-Natta Catalysts

AUTHOR : João B. P. Soares B. Chem. Eng. (Federal University of Bahia, Brazil)

M. Sc. (State University of Campinas, Brazil)

SUPERVISOR : Professor Archie E. Hamielec

NUMBER OF PAGES : xxix, 310

ABSTRACT

An integrated methodology based on Stockmayer's bivariate distribution for the dynamic mathematical modelling of the kinetics of olefin polymerization using heterogeneous and homogeneous Ziegler-Natta catalysts has been developed. This methodology uses polymer characterization via size exclusion chromatography (SEC), temperature rising elution fractionation (TREF), and carbon-13 nuclear magnetic resonance (^{13}C NMR) to estimate polymerization kinetics parameters and provide information about the types of active sites of the catalyst.

A novel and versatile mathematical model for the dynamic simulation of binary copolymerization of olefins using Ziegler-Natta catalysts has been proposed. This model calculates the complete distributions of chemical composition and molecular weight of polyolefins made with catalysts containing multiple active site types and subject to intraparticle mass and heat transfer resistances. This model has a very attractive mathematical formulation that permits easy adaptation to situations in which intraparticle mass and heat transfer resistances are negligible and can also be conveniently combined with mathematical models for the dynamic macroscopic simulation of polymerization reactors for process simulation, optimization and control studies.

The homopolymerization of propylene and ethylene using a titanium-based heterogeneous catalyst was investigated. The presence of hydrogen during the polymerization of propylene was found to increase the rate of propylene polymerization by creating new active site types. This was clearly shown using SEC and TREF analyses of the polypropylenes.

A systematic methodology for the deconvolution of the molecular weight distribution (MWD) of linear polyolefins made with multiple site type catalysts has been developed. The MWD of polyolefins measured by SEC is deconvoluted into individual most probable chain length distributions using a mathematical method that takes advantage of the conditional linearity of the optimization problem.

A mathematical model for simulation of TREF fractionation of binary copolymers made with multiple site type catalysts using Stockmayer's bivariate distribution has been developed. This is the first time a mathematical model is proposed to describe the MWD of TREF fractions using a phenomenological approach considering the influence of the bivariate distribution of molecular weights and copolymer composition in the fractionation. The modelling of TREF with this model provides an ideal limiting case for the fractionation of binary linear copolymers with broad molecular weight and composition distributions and is useful in interpreting TREF fractionation results.

ACKNOWLEDGMENTS

I wish to express my gratitude to several people that helped me during the course of my Ph.D. programme at McMaster University.

First, I am particularly indebted to my thesis supervisor, Professor Archie E. Hamielec, for his guidance and encouragement throughout this work. Working with Professor Hamielec for the past four years was certainly a privilege and an extremely enriching experience.

I owe special thanks to Dr. Jesus M. Vela-Estrada for his help with my experimental work and for our lively technical (or non-technical!) discussions during the two first years of my stay at McMaster University.

I would also like to express my gratitude to some of the present and former staff members of the McMaster Institute for Polymer Production Technology for their kind help during the past four years: Mr. Doug Keller, Mrs. Stienna Thomas, Ms. Lisa Morine, and Mr. Kris Kostanski.

I would like to show my appreciation to POLIBRASIL for sponsoring my Ph.D. programme, especially to Mr. Francisco Rocha and Mr. Alberto D'Almeida.

I would like to express my appreciation to two of my former professors in Brazil that had a decisive influence on my career and on my graduate studies: Professor Milton Mori of State University of Campinas, my former M.Sc. thesis supervisor, for his constant encouragement and friendship during and after my M.Sc. thesis work, and Professor Antonio C. T. Franco of Federal University of Bahia, for his friendship over the past ten years and guidance during the first years of my industrial career.

Several friends outside McMaster University contributed indirectly to this thesis by reminding me that even Ph.D. candidates must have a social life. I would like to extend my thanks to these special friends: Regina and Wilson Pascheto, Joaquín and Lourdes Mingorance, and André and Valéria de Almeida.

I am very grateful to my parents, for all their patience, encouragement and support, not only during this Ph.D. programme, but also during all my life. Above all, I wish to thank them for being the best role models one could wish to have. This work could not have been accomplished without their lifelong guidance.

I also wish to thank my brother for his support and friendship, and for showing me that, no matter how unrealistic it might seem, one is able to make one's dream come true.

Finally, and most important, I wish to thank my wife, Fátima, and my daughters, Carolina and Gabriela for being the best wife and daughters that one can possibly have. Their constant support, patience and love were certainly the most important encouragement I could have had during my Ph.D. programme.

TABLE OF CONTENTS

	Page
ABSTRACT	iii
ACKNOWLEDGMENTS	v
LIST OF FIGURES	xi
LIST OF TABLES	xxi
NOMENCLATURE	xxiv
CHAPTER 1 - INTRODUCTION	1
CHAPTER 2 - LITERATURE REVIEW	9
Heterogeneous Catalysts	9
Soluble Conventional Ziegler-Natta and Metallocene Catalysts	18
Cationic Metallocenes	44
Supported Metallocenes	45
Polymerization Mechanism and Kinetics	55
Polymer Characterization	63
Size Exclusion Chromatography (SEC)	63
Temperature Rising Elution Fractionation (TREF)	66
Nuclear Magnetic Resonance (NMR)	78
Mathematical Modelling	80
CHAPTER 3 - MATHEMATICAL MODELLING OF MASS AND HEAT TRANSFER RESISTANCES IN THE POLYMER PARTICLE	88
Model Development	88
Kinetics	90
Monomer Profile	92
Temperature Profile	93
Population Balances	94
Copolymer Composition	98
Stockmayer Bivariate Distribution	100
Particle Growth - Grid Updating	104

Table of Contents (continued) Page

Numerical Solution 105
Results and Discussion 108
Conclusion 133

CHAPTER 4 - MATHEMATICAL MODELLING OF POLYMERIZATION IN A SERIES OF CONTINUOUS STIRRED TANK REACTORS USING ZIEGLER-NATTA CATALYSTS IN A SLURRY PROCESS 135
Model Development 135
Kinetics 137
Monomer and Temperature Radial Profiles in the Polymer-Catalyst Particle 137
Population Balances 138
Chain Length Averages and Copolymer Composition 138
Macroscopic Balance Around the Polymerization Reactor 138
Energy Balance 143
Process Control Equations 144
Numerical Solution 145
Results and Discussion 146

CHAPTER 5 - POLYMERIZATION EXPERIMENTS 163
Introduction 163
Catalyst and Cocatalyst Sampling 164
Diluent Purification 166
Polymerization Reactor System 168
Polymerization Procedure 170
Estimate of Propylene and Ethylene Concentration in Diluent 171
Propylene Polymerization 174
Ethylene Polymerization 180
Discussion 188

Table of Contents (continued) Page

CHAPTER 6 - POLYMER CHARACTERIZATION 192
Introduction 192
Determination of Molecular Weight Distributions of Ethylene and Propylene Homopolymers with High Temperature SEC 192
Experimental Details 192
Evaluation of SEC - Sample Degradation, Reproducibility, and Peak Broadening 195
Experimental SEC Results for Polypropylene and Polyethylene 199
Determination of Stereoregularity and Chemical Composition Distributions Using TREF and ^{13}C NMR 203
Experimental Details 204
Experimental Results for TREF Fractionation 207
Ethylene-1-Octene Copolymer (LLDPE) 207
Propylene-Ethylene Impact Copolymer 208
Polypropylene Made by Heterogeneous Ziegler-Natta Catalyst 219
Polypropylene Made by a Metallocene Catalyst 223

CHAPTER 7 - MATHEMATICAL MODELLING OF SEC AND TREF 228
Introduction 228
Deconvolution of SEC Chromatograms 228
Representation of WCLD as a Weighted Sum of Most Probable WCLDs 229
Numerical Solution 231
Obtaining First Estimates and Increasing the Number of Site Types 232
Simulation Results 234
Mathematical Modelling of TREF Using Stockmayer's Bivariate Distribution 248
Equations for Each Site Type 249
Equations for the Total Polymer Produced on All of the Active Site Types, Instantaneously 251

Table of Contents (continued) Page

Equations for TREF Fractions 252
Simulation Results and Discussion 254
Conclusion 268

SIGNIFICANT RESEARCH CONTRIBUTIONS TO POLYMER SCIENCE AND ENGINEERING 271

APPENDIX A: Alternative Numerical Method for Solving the Gas-Liquid Equilibrium Equations of the Macroscopic Model 274

APPENDIX B: Particle Size Distribution in a Series of Continuous Stirred Tank Reactors Using Heterogeneous Ziegler-Natta Catalysis in a Slurry Polymerization Process 277
Equations for particle growth when there is no catalyst deactivation 277
Equations for particle growth when there is catalyst deactivation 281
Algorithm for solving the equations 282
Simulation Results 284

APPENDIX C: ^{13}C NMR - Experimental Conditions 289

REFERENCES 290

LIST OF FIGURES

CHAPTER 1		Page
Figure 1	Instantaneous molecular weight distribution (MWD) of a polyolefin made with a multiple site type catalyst as a superposition of four individual Flory's most probable MWDs.	6
Figure 2	Instantaneous chemical composition distribution (CCD) of a binary olefin copolymer made with a multiple site type catalyst as a superposition of five individual Stockmayer's CCDs considering all chain lengths.	6
CHAPTER 2		
Figure 1	Chain structures of polyethylene.	10
Figure 2	Fragmentation of heterogeneous Ziegler-Natta catalyst (secondary) particles during polymerization.	15
Figure 3	Generic structure of a metallocene catalyst.	20
Figure 4	Polymerization catalyzed by homogeneous metallocene/aluminoxane and Ziegler-Natta systems.	21
Figure 5	Structure of bis(cyclopentadienyl) zirconium dichloride (Cp_2ZrCl_2).	25
Figure 6	Types of polypropylene chains produced with metallocene/aluminoxane catalysts.	30
Figure 7	Polymerization of propylene with meso and racemic forms on indenyl derivative catalysts.	31
Figure 8	Active site and chain end stereochemical control mechanisms for syndiotactic polymerization of propylene.	35
Figure 9	Types of polymerization kinetics curves of Ziegler-Natta catalyst.	58
Figure 10	Chain structure and crystallinity: Effect of short chain branching and stereoregularity.	67
Figure 11	Precipitation and elution stages of TREF fractionation.	68
Figure 12	Generic TREF profiles of some commercial polyolefins.	71

Figure 13 Levels of mathematical modelling. 80
Figure 14 Some important physical models for heterogeneous Ziegler-Natta polymerization. 83

CHAPTER 3

Figure 1 Schematic representation of the polymeric multilayer model. 90
Figure 2 Effect of monomer diffusivity for low activity catalyst. 110
Figure 3 Effect of monomer diffusivity for medium activity catalyst. 111
Figure 4 Effect of monomer diffusivity for high activity catalyst. 111
Figure 5 Effect of monomer diffusivity for high activity catalyst. 112
Figure 6 Effect of monomer diffusivity for high activity catalyst. 112
Figure 7 Chain length distribution for high activity catalyst. 114
Figure 8 Effect of monomer diffusivity for high activity catalyst. 114
Figure 9 Effect of varying the propagation constant of a catalyst particle with large initial radius. 115
Figure 10 Radial profile of number average chain length for propylene polymerization under severe mass transfer limitations. 115
Figure 11 Radial profile of number average chain length for propylene polymerization under severe mass transfer limitations. 116
Figure 12 Time variation of polydispersity index for propylene polymerization under severe mass transfer limitations. 116
Figure 13 Chain length distribution for propylene polymerization under significant mass transfer limitations. 117
Figure 14 Effect of initial concentration of active sites. 118
Figure 15 Effect of initial concentration of active sites. 118
Figure 16 Effect of monomer diffusivity for a low activity catalyst during copolymerization. 120
Figure 17 Effect of monomer diffusivity for a low activity catalyst during copolymerization. 120

List of Figures (continued) Page

Figure 18	Effect of monomer diffusivity for a low activity catalyst during copolymerization.F1 - mol fraction of propylene in copolymer.	121
Figure 19	Effect of monomer diffusivity for a low activity catalyst during copolymerization.	121
Figure 20	Effect of monomer diffusivity for a high activity catalyst during copolymerization.	122
Figure 21	Effect of monomer diffusivity for a high activity catalyst during copolymerization.	123
Figure 22	Effect of monomer diffusivity for a high activity catalyst during copolymerization.	123
Figure 23	CCD of different polymer layers for propylene-ethylene copolymerization.	125
Figure 24	Average CCD for propylene-ethylene copolymerization.	125
Figure 25	Copolymerization over a 3 site type catalyst.	127
Figure 26	Copolymerization over a 3 site type catalyst.	128
Figure 27	Copolymerization over a 3 site type catalyst.	129
Figure 28	CCD's for each site type over all layers for propylene-ethylene copolymerization.	130
Figure 29	CCD's considering all site types in different polymer layers for propylene-ethylene copolymerization.	131
Figure 30	Chain length distribution for each site type over all layers for propylene-ethylene copolymerization.	132

CHAPTER 4

Figure 1	Series of two CSTRs for the polymerization of olefins using Ziegler-Natta catalysts.	136
Figure 2	Number average molecular weight profiles of a binary copolymerization of olefins with a two site type Ziegler-Natta catalyst in four CSTRs in series.	151

List of Figures (continued) Page

Figure 3	Polydispersity index profiles of a binary copolymerization of olefins with a two site type Ziegler-Natta catalyst in four CSTRs in series.	152
Figure 4	Copolymer composition profiles of a binary copolymerization of olefins with a two site type Ziegler-Natta catalyst in four CSTRs in series.	153
Figure 5	Reactor pressure profiles of a binary copolymerization of olefins with a two site type Ziegler-Natta catalyst in four CSTRs in series.	153
Figure 6	Polymer yield profiles of a binary copolymerization of olefins with a two site type Ziegler-Natta catalyst in four CSTRs in series.	154
Figure 7	Concentration profiles of monomer 1 in gas phase of a binary copolymerization of olefins with a two site type Ziegler-Natta catalyst in four CSTRs in series.	155
Figure 8	Concentration profiles of hydrogen in gas phase of a binary copolymerization of olefins with a two site type Ziegler-Natta catalyst in four CSTRs in series.	156
Figure 9	Concentration profiles of monomer 1 in liquid phase of a binary copolymerization of olefins with a two site type Ziegler-Natta catalyst in four CSTRs in series.	156
Figure 10	Dimensionless concentration profiles of monomer 1, monomer 2, and hydrogen in gas phase of a binary copolymerization of olefins with a two site type Ziegler-Natta catalyst in four CSTRs in series.	157
Figure 11	Concentration profiles of poison in gas phase of a binary copolymerization of olefins with a two site type Ziegler-Natta catalyst in four CSTRs in series.	158
Figure 12	Number average molecular weight profiles of a binary copolymerization of olefins with a two site type Ziegler-Natta catalyst in four CSTRs in series.	158

Figure 13 Polydispersity index profiles of a binary copolymerization of olefins with a two site type Ziegler-Natta catalyst in four CSTRs in series. 159
Figure 14 Polymer production profiles of a binary copolymerization of olefins with a two site type Ziegler-Natta catalyst in four CSTRs in series. 159
Figure 15 Decrease of the global heat transfer coefficient in the second reactor due to fouling by copolymer. 160
Figure 16 Temperature profiles of polymerization reactor and cooling water during a binary copolymerization of olefins with a two site type Ziegler-Natta catalyst in two CSTRs in series. 161
Figure 17 Number average molecular weight profiles during a binary copolymerization of olefins with a two site type Ziegler-Natta catalyst in two CSTRs in series. 162
Figure 18 Polydispersity index profiles during a binary copolymerization of olefins with a two site type Ziegler-Natta catalyst in two CSTRs in series. 162

CHAPTER 5

Figure 1 Schlenk type catalyst slurry bottle. 165
Figure 2 Sampling procedure for catalyst slurry and cocatalyst solution. 166
Figure 3 Solvent storage and purification bottle. 167
Figure 4 Polymerization reactor. 168
Figure 5 Polymerization reactor system. 169
Figure 6 Concentration of propylene in isoparaffin 2025 as a function of propylene pressure at different temperatures. 173
Figure 7 Concentration of propylene in isoparaffin 2025 as a function of temperature at different partial pressures of propylene. 173
Figure 8 Concentration of ethylene in isoparaffin 2025 as a function of temperature (partial pressure of ethylene = 70 psi). 174

Figure 9	Effect of hydrogen pressure on polymerization rate of propylene at 70 °C.	177
Figure 10	Effect of hydrogen pressure on polymerization rate of propylene at 60 °C.	177
Figure 11	Effect of hydrogen pressure on polymerization rate of propylene at 50 °C.	178
Figure 12	Reversibility of hydrogen effect on polymerization rate of propylene at 70 °C.	179
Figure 13	Arrhenius law plot for polymerization of propylene in presence of hydrogen.	181
Figure 14	Arrhenius law plot for polymerization of propylene in absence of hydrogen.	181
Figure 15	Effect of catalyst prepolymerization with propylene on the polymerization rate of ethylene at 60° C.	184
Figure 16	Effect of hydrogen pressure on polymerization rate of ethylene at 60 °C with prepolymerized catalyst.	187
Figure 17	Effect of hydrogen pressure on polymerization rate of ethylene at 60 °C with regular catalyst.	187
Figure 18	Arrhenius law plot for polymerization of ethylene with catalyst prepolymerized with propylene, considering runs with and without hydrogen.	188

CHAPTER 6

Figure 1	Universal calibration curve for SEC using narrow MWD polystyrene standards.	195
Figure 2	Degradation of polypropylene as a function of dissolution time at 145 ^{0}C.	196
Figure 3	SEC curve of a high molecular weight polypropylene sample made with LYNX 900 ($T = 60$ °C, $P_{H_2} = 0$).	201
Figure 4	Cooling Section of TREF.	204
Figure 5	Heating Section of TREF.	205

List of Figures (continued) Page

Figure 6	Preparative TREF profile for an ethylene-1-octene copolymer (LLDPE) made with a heterogeneous Ziegler-Natta catalyst.	207
Figure 7	Relation between short chain branching and TREF fraction average elution temperature for an ethylene-1-octene copolymer (LLDPE) made with a heterogeneous Ziegler-Natta catalyst.	208
Figure 8	Preparative TREF profile of propylene-ethylene impact copolymer made with LYNX 900.	209
Figure 9	Preparative TREF fractionation of propylene-ethylene impact copolymer made with LYNX 900 below 90 °C.	210
Figure 10	DSC curves of TREF fractions of propylene-ethylene impact copolymer made with LYNX 900.	211
Figure 11	FTIR spectra of TREF fractions of propylene-ethylene impact copolymer made with LYNX 900.	214
Figure 12	^{13}C NMR peak assignments of the TREF fraction of propylene-ethylene impact copolymer made with LYNX 900 collected between 60 - 90 °C.	215
Figure 13	^{13}C NMR of TREF fractions of propylene-ethylene impact copolymer made with LYNX 900.	218
Figure 14	Preparative TREF profile of polypropylene made with LYNX 900 at 70 °C and hydrogen partial pressure of 5 psi.	220
Figure 15	^{13}C NMR of TREF fractions of polypropylene with LYNX 900.	221
Figure 16	Preparative TREF profile of polypropylene made with LYNX 900 at 70 °C in absence of hydrogen.	222
Figure 17	Preparative TREF profile of propylene made with $Et(Ind)_2ZrCl_2$/MAO.	224
Figure 18	^{13}C NMR of TREF of polypropylene made with $Et(Ind)_2ZrCl_2$/MAO.	226
Figure 19	^{13}C NMR of TREF of polypropylene made with $Et(Ind)_2ZrCl_2$/MAO.	227

CHAPTER 7

Figure 1	Model chain length distribution generated for a six site type catalyst.	235
Figure 2	Deconvolution of a model chain length distribution generated for a six site type catalyst into two and three most probable chain length distributions.	236
Figure 3	Deconvolution of a model chain length distribution generated for a six site type catalyst into four most probable chain length distributions and residuals of the predicted four site type chain length distribution and the model six site type chain length distribution.	237
Figure 4	Deconvolution of a model chain length distribution generated for a six site type catalyst into five most probable chain length distributions and residuals of the predicted five site type chain length distribution and the model six site type chain length distribution.	238
Figure 5	Deconvolution of a model chain length distribution generated for a six site type catalyst into six most probable chain length distributions and residuals of the predicted six site type chain length distribution and the model six site type chain length distribution.	239
Figure 6	Experimental polypropylene chain length distribution.	242
Figure 7	Deconvolution of an experimental polypropylene chain length distribution into four most probable chain length distributions and residuals of the predicted four site type chain length distribution and the experimental polypropylene chain length distribution.	243
Figure 8	Deconvolution of an experimental polypropylene chain length distribution into five most probable chain length	244

distributions and residuals of the predicted five site type chain length distribution and the experimental polypropylene chain length distribution.

Figure 9 Deconvolution of an experimental polypropylene chain length distribution into six most probable chain length distributions and residuals of the predicted six site type chain length distribution and the experimental polypropylene chain length distribution. 245

Figure 10 TREF curve of whole polymer and of active site types. 257

Figure 11 Chain length distribution of whole polymer and of active site types. 258

Figure 12 Composition of TREF fractions. 260

Figure 13 Chain length distribution of TREF fractions 1 to 7. 261

Figure 14 Absolute percentage deviations (wt%) between corrected and uncorrected composition distributions for differing monomer molecular weights. 262

Figure 15 Theoretical TREF curve of a LLDPE made with a five site type catalyst. 264

Figure 16 Theoretical TREF curve of isotactic polypropylene made with a five site type catalyst. 267

APPENDIX B

Figure B.1 Algorithm for solving the equations. 283

Figure B.2 Particle size distribution of catalyst before polymerization. 284

Figure B.3 Comparison of particle size distribution of polymer made in five CSTRs of volume V in series and that obtained when only one CSTR with volume equal to $5V$ is used. 285

Figure B.4 Particle size distribution of polymer-catalyst particles after and before polymerization. 285

Figure B.5 Non-ideal residence time distribution (RTD) obtained as a linear combination of two ideal RTDs. 287

Figure B.6	Effect of nonideal residence time distribution on the particle size distribution.	287
Figure B.7	Deactivation profile of a model catalyst composed of stable (C^*_{ss}) and unstable (C^*_{uns}) active sites.	288
Figure B.8	Effect of catalyst deactivation on particle size distribution.	288

LIST OF TABLES

		Page
CHAPTER 1		
Table 1	Industrial processes for the production of polyethylene and polypropylene using Ziegler-Natta catalysts.	2
CHAPTER 2		
Table 1	Development of Ziegler-Natta catalysts for propylene polymerization.	13
Table 2	Comparison between analytical and preparative TREF.	70
CHAPTER 3		
Table 1	Range of studied parameters.	109
CHAPTER 4		
Table 1	Reactor operation conditions at beginning of simulation.	147
Table 2	Physical properties of reagents.	148
Table 3	Polymerization kinetics parameters.	149
Table 4	Operation condition changes of impact copolymer manufacture in CSTR in series (figures 2 to 10).	150
CHAPTER 5		
Table 1	Experimental design of propylene polymerization runs.	175
Table 2	Experimental conditions and yield of propylene polymerization runs.	176
Table 3	Effect of hydrogen on catalyst activity of propylene polymerization.	178
Table 4	Experimental design of ethylene polymerization runs.	182
Table 5	Experimental conditions and yield of ethylene polymerization runs.	183
Table 6	Effect of prepolymerization with propylene in catalyst activity of ethylene polymerization.	184

Table 7	Statistical significance of the influence of hydrogen on the polymerization rate of ethylene.	185
Table 8	Effect of hydrogen on catalyst activity of ethylene polymerization.	186

CHAPTER 6

Table 1	Polystyrene standards of narrow MWD used for SEC calibration.	194
Table 2	Mark-Houwink constants for universal calibration curve of SEC.	194
Table 3	Reproducibility of SEC using polypropylene.	197
Table 4	Evaluation of symmetrical and skewing peak broadening in SEC with polystyrene standards.	199
Table 5	Molecular weight averages and polydispersities of polypropylene made with LYNX 900.	200
Table 6	Molecular weight averages and polydispersities of polyethylene made with LYNX 900 (measured by high temperature SEC).	203
Table 7	Characteristics and operational conditions of TREF apparatus.	206
Table 8	TREF fractionation results for ethylene-propylene impact copolymer made with LYNX 900.	209
Table 9	Differential scanning calorimetry measurements of melting point temperature (maximum peak temperature, T_m) and heats of fusion, ΔH_f, of TREF fractions of ethylene-propylene impact copolymer made with LYNX 900.	211
Table 10	TREF fractionation results for polypropylene made with LYNX 900 at 70 °C and partial pressure of hydrogen of 5 psi.	219
Table 11	TREF fractionation results for polypropylene made with LYNX 900 at 70 °C in absence of hydrogen.	223

Table 12 TREF fractionation results for polypropylene made with $Et(Ind)_2ZrCl_2$/MAO. 225

CHAPTER 7

Table 1 Model chain length distribution parameters. 235
Table 2 Sum of the squares of residuals as a function of number of site types for prediction of the model chain length distribution. 240
Table 3 Computational times and number of iterations required for convergence as a function of number of site types for the model chain length distribution. 241
Table 4 Sum of the squares of residuals as a function of number of site types for prediction of the GPC chain length distribution of polypropylene. 246
Table 5 Converged parameters of the five and six site types model for the GPC chain length distribution of polypropylene. 247
Table 6 Computational times and number of iterations required for convergence as a function of number of site types for the GPC chain length distribution of polypropylene. 247
Table 7 Simulation parameters. 255
Table 8 Averages per site type and whole polymer. 255
Table 9 TREF fraction averages. 259
Table 10 Deviation between chain length averages of TREF fractions calculated by uncorrected and corrected Stockmayer's distributions. 263
Table 11 Simulation parameters (LLDPE). 265
Table 12 Averages per site type and whole polymer (LLDPE). 265
Table 13 TREF fraction averages (LLDPE). 265
Table 14 Simulation parameters (isotactic polypropylene). 266
Table 15 Averages per site type and whole polymer (isotactic polypropylene). 266

NOMENCLATURE

A	cocatalyst, total heat transfer area
A_j, B_j, C_j	radial discretization weights
$B_i(j)$	moles of monomer type i bound to polymer at site type j
$c(t)$	analog controller action
$[C^*]$	average concentration of active sites in reactor
C_n	digital controller action at time n
C_p	heat capacity
D_{M_i}	effective diffusion coefficient of monomer type i in the polymeric particle
D_p	diameter of polymer-catalyst particle exiting the reactor
D_p^0	initial diameter of catalyst particle
$e(t)$	deviation from set point
E	average activation energy of polymerization
f_i	fraction of monomer i in liquid phase
$F_i(j)$	copolymer composition of site type j
H_2	hydrogen
ΔH_r	heat of polymerization
IM	impurity
$k_a(j)$	impurity desorption rate constant for site type j
$k_{dIM}(j)$	deactivation by impurities rate constant for site type j
$k_{d_s}(j)$	spontaneous deactivation rate constant for site type j
K_c	controller proportional gain
k_e	thermal conductivity of polymeric particle
k_i	Henry's law constant, i = monomer type, H_2, N_2, D, A, imp
$k_f(j)$	formation rate constant
k_p	average propagation constant
k_{p0}	propagation rate constant pre-exponential factor (Arrhenius law)
$k_{tA_i}(j)$	transfer to cocatalyst rate constant for a site of type j with terminal monomer of type i
$k_{tH_i}(j)$	transfer to hydrogen rate constant for a site of type j with terminal monomer of type i

Nomenclature (continued)

$k_{tm_{ij}}(j)$	rate constant of transfer to monomer of type j for a site of type j with terminal monomer of type i
$k_{ts_i}(j)$	spontaneous transfer rate constant for a site of type j with terminal monomer of type i
$k_{H_A}(j)$	initiation by cocatalyst rate constant for site type j
$k_{H_i}(j)$	rate constant of initiation by monomer of type i for site type j
$k_{i_i}(j)$	initiation by monomer rate constant for site type j with monomer of type i
$k_{p_{ij}}(j)$	rate constant of propagation of monomer type j for site type j with terminal monomer of type i
k_p	average (over all site types) propagation constant
$l_j(r)$	lagrangian interpolating polynomial
m	number of monomers
$\dot{m}$	mass flow rate of monomer to reactor, g/min
$m(j)$	weight or mass fraction of polymer made by site type j
m_k	mass of polymer in layer k
$[M]$	monomer concentration in diluent
M_i	monomer of type i
M_g	mass of monomer in the headspace of the reactor, g
M_l	mass of monomer dissolved in diluent, g
M_n	number average molecular weight
M_t	total mass of monomer in the reactor, g
mw	molecular weight
$\overline{mw}$	average molecular weight of comonomers
M_w	mass average molecular weight
MW_1, MW_2	molecular weights of monomer type 1 and type 2
$\overline{MW}$	average molecular weight of the monomers
n	number of site types
$\dot{n}_{in}$	mol flow rate of a given chemical component to the reactor
N	number of radial grid points
N_i	moles of a given chemical component i in the reactor, i = monomer type, H_2, N_2, D, A, imp

Nomenclature (continued)

$N^*(j)$	potential sites of type j
$N(0,j)$	initiation sites of type j
$N_d(j)$	deactivated sites of type j
$N_{dIM}(0,j)$	deactivated by impurity sites of type j
$N_{dIM_H}(0,j)$	deactivated by impurity sites of type j
$N_i(r,j)$	growing polymer of chain length r in site type j with terminal monomer of type i
$N_H(0,j)$	sites of type j terminated by hydrogen
$\overline{N_N}(j)$	cumulative number average chain length
$N_T(r,j)$	total growing polymer of chain length r at sites of type j
$\overline{N_W}(j)$	cumulative weight average chain length
P	reactor pressure, atm
P^{sat}	saturated vapour pressure of diluent
$\overline{PDI}$	average cumulative polydispersity
$Q(r,j)$	dead polymer of chain length r formed at sites of type j
Q_p	total heat of polymerization
r	polymer chain length or radial position in the growing polymeric particle
r_i	reaction ratio of a given chemical component, i = monomer type, H_2, N_2, D, A, imp
$r_1(j), r_2(j)$	reactivity ratios
R	universal gas constant
R_{p_i}	polymerization rate of monomer type i
t	time
Δt	acquisition time interval
T	temperature
U	global heat transfer coefficient
V_j^i	volume of layer j at time i
V_t	volume of diluent in the reactor
V_p	volume of polymer-catalyst particle exiting the reactor
V_p^0	initial volume of catalyst particle

Nomenclature (continued)

ΔV_p	volume increase of polymer-catalyst particle due to polymerization
V_r	reactor volume
V_t	total volume of reactor
$w(r,y,j)$	instantaneous chain length and composition distribution of site type j
$w(r,j)$	instantaneous chain length distribution of site type j
$w(y,j)$	instantaneous composition distribution of site type j
$W(r)$	cumulative chain length distribution of the whole polymer (all site types)
$\hat{W}(r)$	estimated instantaneous weight chain length distribution of the whole polymer produced by n site types
$W(y)$	cumulative composition distribution of the whole polymer (all site types)
x_i	mol fraction of a given chemical species dissolved in the diluent, i = monomer type, H_2, N_2, D, A, imp
$X_i(j)$	i^{th} moment of dead polymer produced by site type j
y	deviation from mean copolymer composition
y_i	mol fraction of a given chemical species in gas phase, i = monomer type, H_2, N_2, D, A, imp
Y	polymer yield
$Y_i(j)$	i^{th} moment of living polymer at site type j

Greek Letters

α_T	effective thermal diffusivity of the polymeric particle
ε_n	deviation from set point at acquisition time n
$\dot{v}_{out}$	volumetric flow rate from reactor
$\phi_i(j)$	fraction of sites of type j with terminal monomer of type i
ρ_p, ρ_{pol}	polymer density
$\tau(j)$	ratio of rate of production of dead polymer chain to rate of propagation
τ_I	controller integral time constant

Nomenclature (continued)

τ_D	controller derivative time constant

Subscripts

0	initial conditions in the reactor
1,2,....n	monomer type, unless stated otherwise
A	cocatalyst
cw	cooling water
D	diluent
H_2	hydrogen
imp	impurities or catalyst poisons
N_2	nitrogen or any inert gas

Superscripts

T	liquid and gas phases
g	gas phase
l	liquid phase
min	minimum value of a certain control variable
max	maximum value of a certain control variable

Abbreviations

CCD	Chemical composition distribution
CLD	Chain length distribution
CSTR	Continuous stirred tank reactor
DSC	Differential scanning calorimetry
DEAC	Diethylaluminum chloride
EPDM	Ethylene-propylene-diene
FTIR	Fourier transform infrared
HDPE	High density polyethylene
HP-LDPE	High pressure low density polyethylene
IBAO	Isobutylaluminoxane
LCB	Long chain branching
LDPE	Low density polyethylene

Nomenclature (continued)

LLDPE	Linear low density polyethylene
LYNX 900	Titanium-based, heterogeneous Ziegler-Natta catalyst
MAO	Methylaluminoxane
MDPE	Medium density polyethylene
MW	Molecular weight
MWD	Molecular weight distribution
^{13}C NMR	Carbon-13 nuclear magnetic resonance
PDI	Polydispersity index
PE	Polyethylene
PID	Proportional-integral-derivative
PP	Polypropylene
SCB	Short chain branching
SEC	Size exclusion chromatography
TCB	trichlorobenzene
TEA	triethylaluminum
TIBA	triisobutylaluminum
TMA	trimethylaluminum
TREF	Temperature rising elution fractionation
WCLD	Weight chain length distribution
ZN	Ziegler-Natta

CHAPTER 1 - INTRODUCTION

Polyolefins are among the most important modern commodity polymers. Polyethylene and polypropylene are today the major tonnage plastic materials worldwide, accounting for 44% of all U.S. plastic sales in 1988 and reaching a capacity of about 45 million tons in 1990 (Elias, 1992; Whiteley et al., 1992).

Polyolefins are commercially produced using free-radical initiators, Phillips type catalysts, and Ziegler-Natta catalysts. Of those processes, the ones based on Ziegler-Natta catalysts are the most important because of their very broad range of applications.

Ziegler-Natta catalysts have evolved considerably since their discovery by Ziegler and Natta in the early 50s until today, with the development of new catalyst generations and industrial processes. This class of catalysts has been used in homogeneous, heterogeneous and colloidal forms to synthesize high-density polyethylene, isotactic polypropylene, ethylene-propylene copolymers, cis-1,4-polybutadiene, and cis-1-4-polyisoprene among other products. Recently, the discovery of a new class of soluble Ziegler-Natta catalyst, the metallocene/aluminoxane catalysts, seems to have opened the doors to a new revolution in the production of polyolefins. Metallocene/aluminoxane catalysts are able to produce polyolefins at a very high productivity with a degree of microstructural control not possible to achieve using conventional Ziegler-Natta catalysts.

The industrial importance of Ziegler-Natta catalysts is truly remarkable. Several industrial processes using a variety of reactor types exist today for the production of polyolefins using these catalysts (table 1).

Before the discovery of Ziegler-Natta catalysts, polyethylene was produced commercially only with free-radical initiators at high polymerization temperatures and pressures. As a consequence of the mechanism of polymerization, the polymer chains obtained with free-radical processes contain both short and long chain

Industrial Process	Polyethylene		Polypropylene	
	Reactor type	Licensor	Reactor type	Licensor
Gas-phase	fluidized bed	Union Carbide	fluidized bed	Union Carbide/Shell
			vertical stirred bed	BASF
			horizontal stirred bed	Amoco
Slurry (diluent suspension)	autoclave	Hoescht	autoclave	Mitsubishi
	autoclave	Mitsubishi	autoclave	Montedison
Liquid Monomer			loop reactor	Himont
			autoclave	Amoco
			autoclave	Mitsui
Solution	autoclave	Du Pont	autoclave	Eastman-Kodak
	autoclave	Dow Chemical		
	autoclave	Mitsui		

Table 1 - Industrial processes for the production of polyethylene and polypropylene using Ziegler-Natta catalysts.

branches. The short chain branches because of their abundance significantly decrease the density of the polymer (low density polyethylene - LDPE) and affect several other rheological and mechanical properties. LDPE is used predominantly for making films because of its limp feel, transparency and toughness. The high level of long chain branching gives excellent processability and high melt tension.

Probably the most important innovation introduced in the manufacture of polyethylene by Ziegler-Natta catalysts was the synthesis of linear high-density polyethylene (HDPE) and copolymers of ethylene and α-olefins. HDPE has few or no short chain branches and no long chain branches. HDPE is used in structural applications because of its greater rigidity. Copolymerization of ethylene with α-olefins disrupts the order of the linear polyethylene chain by introducing short chain branches. As a consequence, the density, crystallinity, and rigidity of the polymer is decreased (Linear low density polyethylene - LLDPE). By varying the amount and type of α-olefin, the type of catalyst, and the polymerization conditions, one can produce several grades of copolymers to meet specific market demands. LLDPE shares the market with LDPE made by free-radical processes. Those polymers are used predominantly for films.

Perhaps an even more important innovation in the field of polyolefins manufacture introduced with Ziegler-Natta catalysts was the production of highly isotactic and syndiotactic polypropylene. Several types of Ziegler-Natta catalysts are stereospecific, i.e. the insertion of asymmetric monomers into the growing chain in a given orientation is favoured over all other possible orientations. Only atactic polypropylene is obtained in free-radical polymerization. Isotactic polypropylene is used in several injection molding and extrusion processes due to its excellent rigidity, toughness and temperature resistance. Atactic polypropylene has little commercial value.

Most industrial processes today utilize heterogeneous Ziegler-Natta catalysts. Conventional soluble Ziegler-Natta catalysts have not found widespread industrial applications, mainly because of insufficient catalytic stability and stereochemical control. This picture, however, will probably change in the future with the advent of metallocene/aluminoxane catalysts.

Although there are many different types of heterogeneous Ziegler-Natta catalysts, most of them have a common intriguing characteristic: they yield polymer with broad molecular weight distribution (MWD) and, in the case of copolymerization, broad chemical composition distribution (CCD). There is now a general agreement that heterogeneous Ziegler-Natta catalysts possess more than one type of active site, each one with distinct ratios of chain transfer to propagation rates, comonomer reactivity ratios and stereoselectivities. Since polymer chains made by each site type have different average chain lengths, comonomer compositions, comonomer sequence lengths and, in the case of asymmetric monomers, different degrees of stereoregularity, the bulk polymer made by heterogeneous ZN catalysts is in reality a mixture, at the molecular level, of polymer chains having dissimilar average properties. These dissimilar average properties are reflected in the broad MWDs and CCDs that are frequently observed in polymers made with heterogeneous Ziegler-Natta catalysts. Additionally, intraparticle heat and mass transfer resistances during the polymerization may broaden even further these distributions.

On the other hand, polyolefins made with most soluble Ziegler-Natta catalysts have narrow MWD, and copolymers also have narrow CCD. This behaviour supports the multiple-site type hypothesis for heterogeneous catalysts. Soluble Ziegler-Natta catalysts consist of reasonably well defined, single catalytic species, probably not subject to heat and mass transfer resistances during polymerization.

The complexity of MWDs and CCDs of polyolefins made with Ziegler-Natta catalysts constitutes a challenging problem for polymer quality control. Most properties of polyolefins are routinely measured only as average values. Measurements of melt flow index (as an estimator for molecular weight averages), melt flow index ratio (as an estimator of polydispersity) and bulk density (as an estimator of copolymer composition or degree of chain branching) are common practice in industry. However, it is important to recall that the macroscopic properties of polymers in general, and polyolefins in particular, can not be uniquely determined by average values, since polymers that have some average properties in common can possess other properties that differ markedly. Even a knowledge of the full molecular weight distribution for polypropylene may not be sufficient for many practical applications, due to stereoirregularities. In the same way, determining

average compositions of copolymers or average degrees of branching will not entirely define the polymer in question. The whole distribution of composition in addition to chain length is necessary to accomplish this task. This issue becomes even more complex with polyolefins made with Ziegler-Natta catalysts because polymers with broad and sometimes multimodal MWDs and CCDs are often produced.

The concern about the breadth of MWD and CCD of polyolefins is far from academic. Those distributions affect the final mechanical and rheological properties of polyolefins and ultimately determine their applications. Polyethylenes with broad MWD are easier to process because of greater flowability in the molten state at high shear rate, while polyethylenes with narrow MWD have greater dimensional stability, higher impact resistance, greater toughness at low temperatures, and higher resistance to environmental stress cracking. For polypropylene, narrow MWD is required for rapid molding of products with good mechanical properties.

It is useful to interpret the broad MWD and CCD of polymers obtained with Ziegler-Natta catalysts as resulting from the superposition of individual MWDs and CCDs of polymer chains produced on each type of active site.

It is generally accepted that, under most polymerization conditions, the effect of multiple site types is far more important than mass and heat transfer resistances. Under these conditions, each site type instantaneously produces polymer that has Flory's most probable MWD. Therefore, the instantaneous MWD of accumulated polymer made with heterogeneous Ziegler-Natta catalysts can be considered an average of that produced by the individual site types, weighted by the weight fraction of polymer produced by each site type (figure 1).

The same treatment can be extended to copolymers by using Stockmayer's bivariate distribution to describe the instantaneous bivariate distribution of chain length and composition. Therefore, if one assumes that each site type produces copolymer that obeys distinct bivariate distributions of chain length and composition, the bivariate distribution of the accumulated copolymer can be considered an average

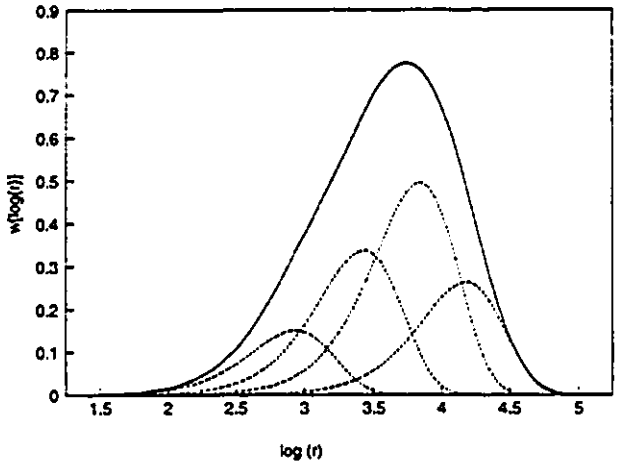

Figure 1 - Instantaneous molecular weight distribution (MWD) of a polyolefin made with a multiple site type catalyst as a superposition of four individual Flory's most probable MWDs (Solid line indicates MWD of accumulated polymer and dotted lines represent MWDs of polymer made on distinct active sites).

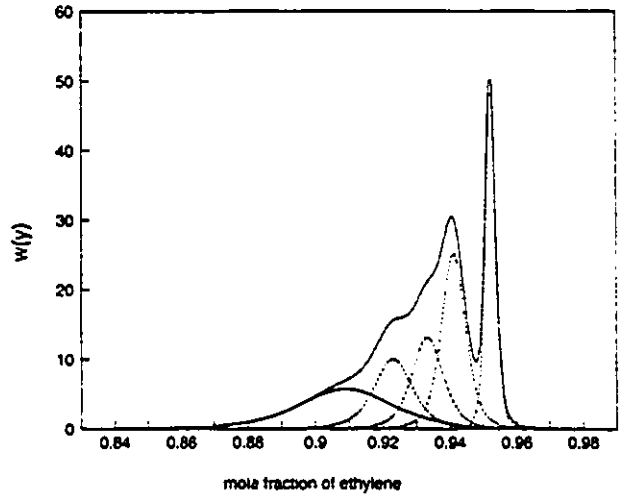

Figure 2 - Instantaneous chemical composition distribution (CCD) of a binary olefin copolymer made with a multiple site type catalyst as a superposition of five individual Stockmayer's CCDs considering all chain lengths (Solid line indicates CCD of accumulated polymer and dotted lines represent CCDs of polymer made on distinct active sites).

of that produced by the individual site types. Figure 2 shows the average and individual CCDs of a binary olefin copolymer obtained by integrating Stockmayer's bivariate distribution over all chain lengths.

The objective of this research is to study the factors that affect the microstructure of polyethylene and polypropylene produced with Ziegler-Natta catalysts, through an integrated methodology of mathematical modelling, polymerization kinetics determination, and polymer characterization using high temperature size exclusion chromatography (SEC), temperature rising elution fractionation (TREF), and carbon-13 nuclear magnetic resonance spectroscopy (^{13}C NMR).

The effect of the presence of multiple site types and heat and mass transfer resistances on MWD and CCD of polyolefins is analyzed using a novel dynamic mathematical model for copolymerization of linear olefins with heterogeneous and soluble Ziegler-Natta catalysts.

This mathematical model is also applied to simulate the copolymerization of olefins in a series of slurry continuous stirred tank reactors (CSTR) to study how operation conditions affect polymer quality and transitions between different polymer grades. Series of CSTRs are commonly used in the polyolefin industry to produce homopolymers, random copolymers and impact copolymers.

A semi-batch slurry reactor is used to study the kinetics of ethylene and propylene homopolymerization with a titanium trichloride heterogeneous Ziegler-Natta catalyst (LYNX-900). The microstructure of polymer produced during this stage is further analyzed with SEC, ^{13}C NMR, and TREF.

The MWDs of polyethylene and polypropylene produced with LYNX-900 are experimentally determined using SEC. Information about the nature of the active sites present in the catalyst is obtained by the deconvolution of the MWD of the accumulated polymer into individual, most probable MWDs using two mathematical optimization methods.

The stereoregularity distribution of polypropylene produced with LYNX-900 is analyzed by TREF and ^{13}C NMR. A mechanistic model based on Stockmayer's bivariate distribution is used to interpret TREF results and make semi-quantitative predictions about MWDs of TREF fractions.

MWD and stereoregularity distribution of polypropylene made with LYNX-900 is also compared to the ones experimentally measured for a polypropylene produced with bis(indenyl) zirconium dichloride/methylaluminoxane, a soluble metallocene/aluminoxane catalyst.

Finally, the CCD of impact copolymers of ethylene and propylene produced with a heterogeneous, titanium-based Ziegler-Natta catalyst in an industrial process containing five CSTRs in series will be thoroughly analyzed using TREF and ^{13}C NMR.

The importance of having a detailed understanding of the polymerization phenomena in Ziegler-Natta catalysis can not be overstated. Product quality has been a growing concern in almost all industrial sectors and the polymer industry is not an exception. Polymers are heterogeneous materials and product quality is directly related to polymer microstructure. A mathematical model that can predict polymer microstructure as well as reactor macroscopic behavior from process conditions is a convenient way to summarize this knowledge and can be a valuable tool for process and quality control.

CHAPTER 2 - LITERATURE REVIEW

Heterogeneous Catalysts

The discovery of Ziegler-Natta catalysts started a new era in polyolefins research and production. Those catalysts were first used by Ziegler in 1953 to polymerize ethylene at low pressure and further developed by Natta in 1954 to produce isotactic polypropylene. Since then this field has grown incessantly with the development of improved catalysts and new industrial processes. This class of catalysts has been used in homogeneous, heterogeneous and colloidal forms to synthesize high density polyethylene, linear low density polyethylene, isotactic polypropylene, ethylene-propylene copolymers, cis-1,4-polybutadiene, and cis-1,4-polyisoprene among other products (Boor, 1979). Commercial reactors also assume various configurations and involve diverse processes: solution, slurry, gas-phase and bulk-liquid (Whiteley et al., 1992). The discovery of Ziegler and Natta had such an impact on polymer manufacture and research that they were awarded the 1963 Nobel prize in chemistry.

Before the discovery of Ziegler-Natta catalysts, polyethylene was produced commercially with free-radical initiators under severe polymerization conditions in autoclave (150-200 MPa, 180-290 °C) or tubular reactors (200-350 MPa, 140-180 °C). Polyethylene chains manufactured under these conditions contain both long and short chain branches (LCB and SCB) as a consequence of the polymerization mechanism with free-radical initiators (Hamielec et al., 1987). Since LCB and SCB decrease the density of polyethylene as compared to a linear chain, polyethylene made by these free-radical processes is known as low density polyethylene (LDPE).

In contrast to free-radical synthesis, ethylene polymerized with Ziegler-Natta catalysts produces unbranched, linear, high density polyethylene (HDPE) at moderate polymerization pressure and temperature. The copolymerization of ethylene and α-olefins with those catalysts produces copolymer with various levels of comonomer units or SCB, for applications where lower densities are required. The structures of LDPE, LLDPE, and HDPE are illustrated in figure 1.

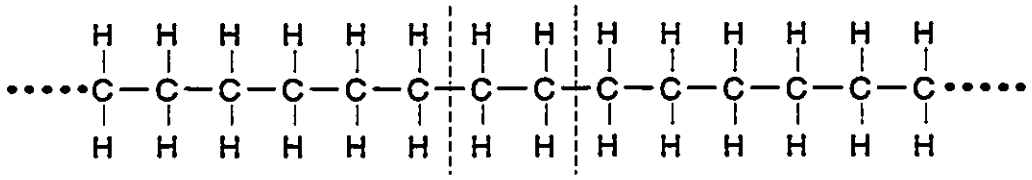

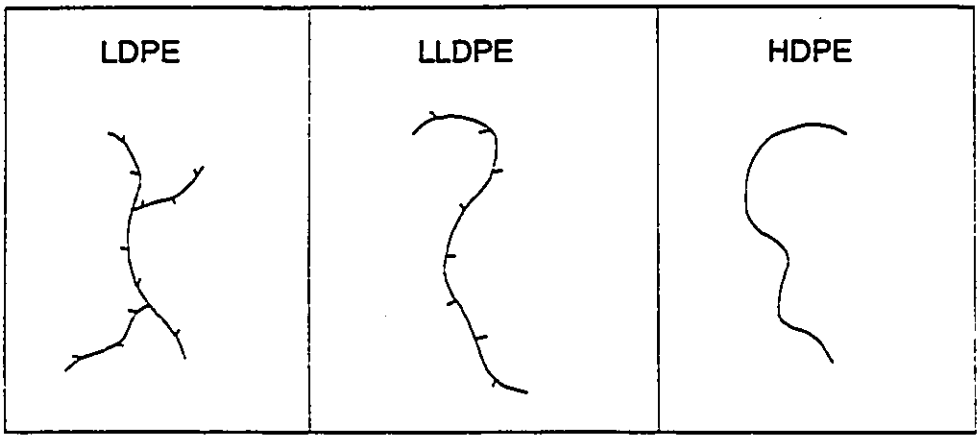

Figure 1 - Chain structures of polyethylene (LDPE - low density polyethylene; LLDPE - linear low density polyethylene; HDPE - high density polyethylene).

Although propylene can be polymerized with free-radical initiators, only low molecular weight, atactic polypropylene is formed due to lack of stereochemical control in free-radical polymerization. Atactic polypropylene has little commercial value (Whiteley et al., 1992). On the other hand, polypropylene made with stereospecific Ziegler-Natta catalysts contains mainly isotactic chains (90-98 wt%). At present, isotactic polypropylene is one of the most important commercial thermoplastics (Lieberman and Barbe, 1986).

In its broadest definition, Ziegler-Natta catalysts are composed of a transition metal salt of metals of groups IV to VIII (known as the *catalyst*) and a metal alkyl of a base metal of groups I to III (known as the *cocatalyst* or *activator*). However not all combinations are equally efficient and can be used for all monomers. For industrial use, most Ziegler-Natta catalysts are based on titanium salts and aluminium alkyls (Boor, 1979).

Ziegler-Natta catalysts can be either soluble or insoluble in the reaction medium. Conventional soluble Ziegler-Natta catalysts have not found widespread industrial applications. However, a new type of soluble Ziegler-Natta system, metallocene/aluminoxane catalysts, is becoming increasingly important from the industrial point of view (Soares and Hamielec, 1994e). These catalyst systems will be reviewed in the next section.

Four main steps can be recognized in the development of Ziegler-Natta catalysts: 1) In 1953 Ziegler's original catalyst was produced *in situ* as a precipitate by the reaction of a soluble transition metal halide with a soluble metal alkyl. This catalyst had high activity for ethylene polymerization at moderate pressure and temperature but produced mainly atactic, low molecular weight poplypropylene; 2) Natta discovered in 1954 that preformed solid transition metal halides in lower valence states produced more isotactic polypropylene than Ziegler's formulation; 3) It was later discovered that the addition of certain Lewis bases could increase the stereospecificity of propylene polymerization and alter the polymerization rate(2^{nd} generation catalysts); 4) It was also found that the activity of titanium compounds could be dramatically increased by supporting them onto several inorganic carriers or supports, especially $MgCl_2$ (3^{rd} generation catalysts). Some further improvements of some supported catalysts led to the 4^{th} generation, super high active catalysts (Simonazzi et al., 1991).

Some of those stages in the evolution of Ziegler-Natta catalysts are illustrated in table 1 for polypropylene. Catalyst generations are differentiated by a considerable increase in catalyst productivity and stereochemical control.

Those steps in catalyst evolution reflect what can be considered the catalyst targets for polyolefin production (Tait, 1989; Simonazzi et al., 1991):

1) Elimination of catalyst deactivation and removal procedures. High level catalyst residues in the polymer may cause polymer degradation during storage and processing or contamination of substances in contact with the polymer. Industrial processes that use 1^{st} and 2^{nd} generation catalysts usually include an expensive stage of catalyst deactivation and removal (deashing) and a treatment station for the aqueous waste generated in this

process. However, the productivity of 3rd generation catalysts is so high that it is generally not necessary to remove catalyst residues (Galli and Haylock, 1991; Brockmeier, 1983).

2) Stereoregularity control. Atactic polymer production is undesirable because of the low price for atactic polymer and for the need to separate the atactic and isotactic fractions, thus increasing production costs. The production of atactic polymer with 3rd generation catalysts is so low that the atactic fraction can remain incorporated into the isotactic matrix without negative consequences (Simonazzi et al., 1991; Galli and Haylock, 1991).
3) High productivities.
4) Good control of molecular weight distribution (MWD) and chemical composition distribution (CCD). Both MWD and CCD have a marked effect on the mechanical and rheological properties of the polymer. The control of MWD and CCD of polymers obtained with heterogeneous Ziegler-Natta catalysts is complicated, if not impossible, because of catalyst surface irregularities and the presence of multiple active site types (Tait and Berry, 1989).
5) Production of polymer with controlled particle size distribution, morphology and density. Those properties will affect polymer processability (Galli et al., 1981).

Several factors influence the performance of Ziegler-Natta catalysts: 1) metal alkyl structure - choice of metal and nature of ligands; 2) transition metal structure - choice of metal, nature of ligands, crystal structure, and valence; 3) polymerization conditions - absolute and relative concentrations of catalyst and cocatalyst, catalyst aging, polymerization temperature, and polymerization time (Boor, 1979; Caunt, 1977).

The precise role of the alkyl aluminium or cocatalyst is still subject to speculation. One of the main roles of the cocatalyst is certainly the reduction and alkylation of the transition metal (Dusseault and Hsu, 1993):

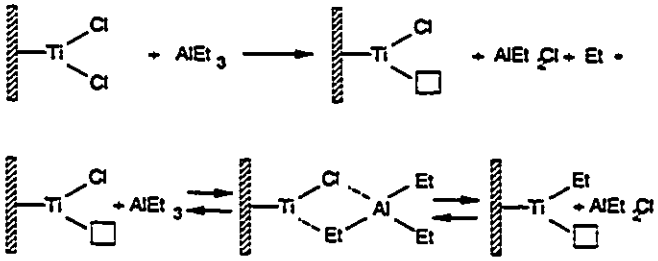

Catalyst system	Activity (kg PP/g cat)	wt% insoluble in boiling heptane*	Plant process
1st generation 1957 - 1970 $TiCl_3 \cdot AlEt_2Cl$	0.8 - 1.2	88 - 93	deash atactic removal
2nd generation 1970 - 1980 $TiCl_3 \cdot AlEt_2Cl$ + Lewis base	3.0 - 5.0	92 - 97	deash atactic removal (optionally)
3rd generation 1980-1994 $MgCl_2/TiCl_4 \cdot AlEt_3$	5.0 - 20	> 98	no deash no atactic removal

Table 1 - Development of Ziegler-Natta catalysts for propylene polymerization (Source: Whiteley et al., 1992).
* The degree of stereoregularity of polypropylene is generally correlated to the fraction of polymer insoluble in boiling heptane (isotactic index). Highly isotactic polypropylene is mainly insoluble in boiling heptane.

However, since it is necessary to have a ratio of aluminum/transition metal higher than stoichiometic (generally 5 to 50) and given that the type and excess of cocatalyst also influence stereochemical control, molecular weight distribution and catalyst productivity, other roles such as scavenger and complexation with monomer have also been proposed for the cocatalyst (Dusseault and Hsu, 1993). Some

researchers proposed that the active site for polymerization is actually a bimetallic center, formed by the combination of catalyst and cocatalyst. This hypothesis has today few supporters (Tait and Watkins, 1989).

One of the most common 1st and 2nd generation commercial heterogeneous Ziegler-Natta catalysts is $TiCl_3$ and its derivatives. $TiCl_3$ can occur in different crystalline forms: α-$TiCl_3$ is obtained from the reduction of $TiCl_4$ with hydrogen above 400 °C; α-$TiCl_3$•0.33$AlCl_3$ by the reduction of $TiCl_4$ with metallic aluminium or aluminium alkyls in hydrocarbon medium at 250 °C; β-$TiCl_3$ by the reduction of $TiCl_4$ with metallic aluminium or aluminium alkyls at low temperature; γ-$TiCl_3$ by heating β-$TiCl_3$ above 150 °C; and δ-$TiCl_3$ by prolonged grinding of α- or γ-$TiCl_3$. The α and γ-forms have lower activity than the δ-form, while the β-form produces polymer that is essentially amorphous (Tait, 1989).

Those crystalline forms have the following modes of packing: α-$TiCl_3$, close hexagonal; γ-$TiCl_3$, close cubic; δ-$TiCl_3$, random alternation of α and γ packing. The β-form shows a fiber-shaped structure (Boor, 1979).

δ-$TiCl_3$ is obtained as porous, secondary particles of 20-40 μm diameter formed by loosely aggregated primary particles of 0.03-0.04 μm diameter (Tait, 1989). During polymerization, these secondary particles are fragmented by the growing polymer, forming an expanding particle containing primary particles and living and dead polymer chains (figure 2). This catalyst fragmentation mechanism has been documented for most types of heterogeneous Ziegler-Natta catalysts (Buls and Higgins, 1970; Kakugo et al., 1989; Galli and Haylock, 1991; Simonazzi et al., 1991). One of its consequences is the well known *replication phenomenon*: the particle size distribution of the polymer particles at the end of batch or semi-batch polymerization closely approximates the particle size distribution of the catalyst at the beginning of polymerization (Simonazzi et al., 1991). Good replication is supposed to occur when there is an adequate balance between the mechanical strength of the particle and catalyst activity. If the reactivity is too high and the particle very weak, the fast growing polymer can explode the catalyst particle forming undesirable fine polymer powder. On the other hand, if the particle is too strong, there will be little or no fragmentation and the pores will be blocked by polymer chains, making the internal

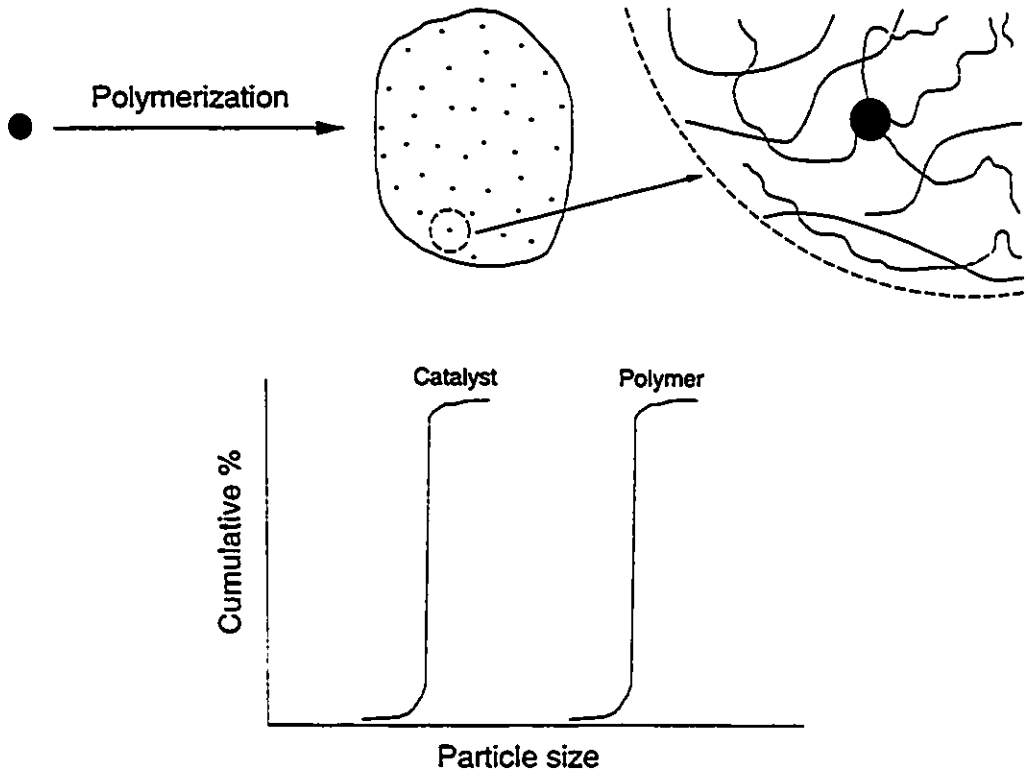

Figure 2 - Fragmentation of heterogeneous Ziegler-Natta catalyst (secondary) particles during polymerization. The growing polymer chains break the secondary catalyst particles into primary particles, forming an expanding particle made of catalyst fragments surrounded by dead and living polymer chains. This phenomenon is responsible for the replication phenomenon observed in heterogeneous Ziegler-Natta catalysis.

active sites inaccessible to monomer. Replication factors of 40-50 (ratio of average polymer particle diameter to average catalyst particle diameter) can be obtained with 3rd generation catalysts (Galli and Haylock, 1992).

The realization that electron donors such as Lewis bases could increase the stereochemical control and alter the productivity (increase or decrease) of heterogeneous Ziegler-Natta catalysts led to the development of 2nd generation catalysts. Although the function of an electron donor is not completely understood, some of its possible roles are: 1) Complex formation with active center. This may lead to deactivation of atactic producing centers (*achiral centers*), formation of centers of increased stability and/or improved stereoregularity (*chiral centers*), and

blocking of active centers; 2) Complexation with aluminium alkyls with consequent decrease in their reducing power. There is some evidence that Ti^{III} sites are active for polyethylene and isotactic polypropylene production while Ti^{II} sites are active only for polyethylene and atactic polypropylene production; 3) Complexation with aluminium dialkyl dihalides, produced during catalyst formation or surface alkylation reactions. Those substances might act as catalyst poisons; 4) Catalyst modification reactions, such as removal of $AlCl_3$ from δ-$TiCl_3$•0.33$AlCl_3$, increasing the porosity of the catalyst particle. A reasonably weak structure is important during catalyst break-up to ensure good powder morphology of the final polymer (Tait, 1989; Tait and Watkins, 1989).

It was soon realized that most transition metal atoms of 1st and 2nd generation catalysts are inaccessible to monomer. Most of these atoms are located inside the crystalline lattice and only atoms located on the lateral faces and edges and crystal defects act as active sites for polymerization (Galli and Haylock, 1992). It is estimated that for 2nd generation catalysts, less than 1% of the total transition metal atoms are available for polymerization (Galli and Haylock, 1991). As mentioned earlier, the presence of catalyst residues in the final product is highly undesirable. Supporting the catalyst on porous carriers makes more of the transition metal atoms accessible for monomer polymerization and eliminates the need of catalyst removal from the polymer. Supported catalysts are generally classified as 3rd generation catalysts.

Several inorganic carriers can be used to support Ziegler-Natta catalysts. $TiCl_4$ can be attached to the surface of supports containing hydroxyl groups, such as SiO_2 and Al_2O_3, by a substitution reaction:

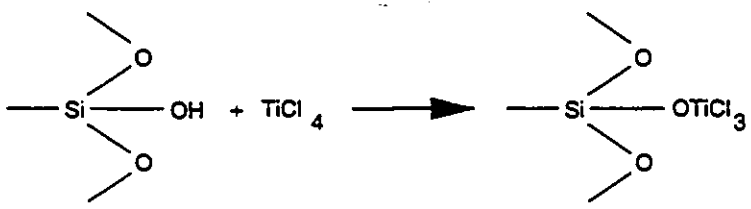

Magnesium alkoxides and magnesium alkyls have also been used as carriers. The process of supporting the catalyst is similar to the one used for hydroxyl group containing supports (Tait, 1989).

Those catalysts show high activity for the polymerization of ethylene but have poor stereochemical control. Apparently the stereochemical control of the catalyst is lost during the supporting process due to the change in the structural order of $TiCl_4$ crystallites.

However, if $MgCl_2$ is used as the support for $TiCl_4$, not only high activities but also increased stereochemical control can be obtained (using Lewis bases) when compared with 1st and 2nd generation catalysts. $MgCl_2$ acts as an effective dispersant of the active titanium and, because of its ability to mimic $TiCl_3$, it is able to maintain the structure responsible for stereochemical control (Ti^{3+} and Mg^{2+} have similar ionic radii and δ-$MgCl_2$ resembles δ-$TiCl_3$). $TiCl_4$ is not fixed to the surface by a substitution reaction. Instead, a surface mixed crystal is attributed to the system (Dusseault and Hsu, 1993).

$MgCl_2$/$TiCl_4$ alone have poor stereochemical control. Stereospecificity requires the presence of a Lewis base during catalyst preparation (*internal donor*) by: 1) mechanical treatment of $MgCl_2$/internal base/$TiCl_4$ mixture, or 2) mechanical treatment of $MgCl_2$/internal base mixture and subsequent contact with $TiCl_4$ above 80°C, or 3) treatment of active $MgCl_2$ with both internal base and $TiCl_4$ above 80 °C. Additionally, those catalysts require the presence of a second Lewis base (*external donor*) and cocatalyst during polymerization (Barbe et al., 1987; Galli and Haylock, 1992).

One of the functions of the internal donor is to selectively poison the sites responsible for producing stereoirregular polymer; if in excess, the internal donor will poison stereospecific sites as well (Dusseault and Hsu, 1993).

Ethyl benzoate is commonly used as both internal and external base. Apparently comilling $MgCl_2$ with ethyl benzoate reduces its size since ethyl benzoate is able to stabilize $MgCl_2$ crystallites by coordination, inhibiting their reaggregation. This mechanical treatment exposes more sites for fixation of $TiCl_4$ (Dusseault and Hsu, 1993):

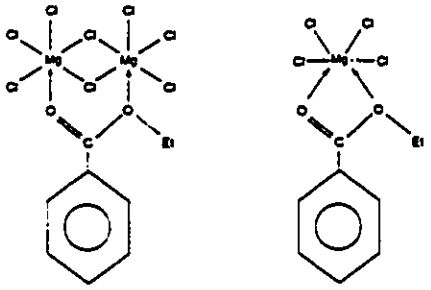

$TiCl_4$ diplaces part of ethyl benzoate from unsaturated portions of $MgCl_2$ crystallite to form the active sites (Tait and Watkins, 1989; Dusseault and Hsu, 1993):

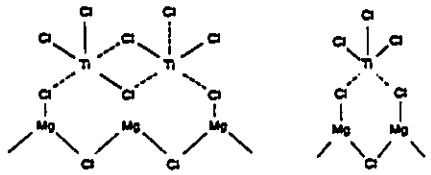

Those catalysts are very complex systems. It is proposed that the internal base, $TiCl_4$ and $MgCl_2$ either form a complex that is the active center, or that the internal base only stabilizes the $MgCl_2/TiCl_4$ active center, or even that both processes occur, leading to more then one type of active site. Cocatalyst and external base can also interact, producing new components that might also interact with the catalysts leading to the formation of more types of active sites (Barbe et al., 1987; Simonazzi et al., 1991; Dusseault and Hsu, 1993). The presence of multiple active site types has been considered the main cause of the characteristic broad molecular weight and chemical composition distributions of polymers and copolymers made by heterogeneous Ziegler-Natta catalysts (Soares and Hamielec, 1994a-c).

Soluble Conventional Ziegler-Natta and Metallocene Catalysts

Homogeneous Ziegler-Natta catalysts are soluble in the reaction medium. However, the polymer generally precipitates as it is formed (if the reaction temperature and pressure are not sufficiently high).

Conventional soluble Ziegler-Natta catalysts have little industrial interest because they usually have low activity and produce polymer with commercially unacceptable powder morphology and no, or low, stereoregularity in the case of isotactic polypropylene production (Corradini et al., 1989).

Important exceptions are some vanadium-based systems such as VCl_4-$AlEt_3$ and VCl_4-$AlEt_2Cl$, for the production of ethylene-propylene copolymers, ethylene-propylene-diene terpolymers (Cooper, 1976; Tait, 1989) and syndiotactic polypropylene (Corradini et al., 1989). Copolymers made with soluble Ziegler-Natta catalysts generally have narrow molecular weight and chemical composition distribution (Cozewith and VerStrate, 1971; Tait and Berry, 1989).

Those catalysts have been studied mainly for academic purposes. Since they are not subject to surface heterogeneity nor to mass and heat transfer limitations present in heterogeneous Ziegler-Natta catalysts, they are more suitable for investigating the elementary steps of polymerization (Sinn and Kaminsky, 1980; Tait and Watkins, 1989). However, their behaviour is complicated by deactivation processes and formation of colloids or precipitation from solution during polymerization (Tait, 1989).

The activity of bis(cyclopentadienyl) and tri(cyclopentadienyl) zirconium derivatives, both low-activity, soluble catalysts for the polymerization of ethylene when used with organoaluminum cocatalysts (Andressen, 1976), was found to be greatly enhanced by addition of traces of water (Sinn, 1980; Kaminsky, 1986a). This increased activity was related to the formation of aluminoxanes. This discovery led to the development of an entirely new class of soluble Ziegler-Natta catalytic systems: the metallocene/aluminoxane catalysts. Metallocene/aluminoxane catalysts have found widespread academic and industrial interest, and today are the most promising branch of Ziegler-Natta catalysis.

Metallocenes are organometallic coordination compounds in which two cyclopentadienyl or substituted cyclopentadienyl rings are bonded to a central transition metal atom (figure 3). By varying the nature and number of the rings and substituents (S), the type of transition metal (M) and its substituents (R), and by changing the type and length of the bridge (B) between the rings (or completely removing it), it has been possible to synthesize a whole range of active centre types suitable for the polymerization of linear and cyclic olefins and diolefins, producing polymers with entirely novel properties.

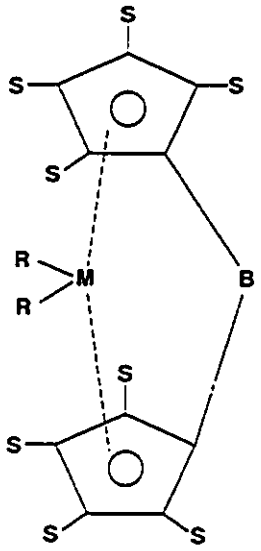

M : transition metal of groups 4b, 5b or 6b
R : hydrocarbyl, alkylidene, halogen radicals
S: hydrogen, hydrocarbyl radicals
B: alkylene, alkyl radicals, heteroatom groups

Figure 3 - Generic structure of a metallocene catalyst.

Metallocene/aluminoxane catalysts, being homogeneous systems, behave very differently compared with heterogeneous Ziegler-Natta catalysts. There is much experimental evidence indicating that several metallocene/aluminoxane catalysts have only one active site type (Kaminsky, 1986b, 1991b). In this case, the polymerization catalyzed by metallocenes may proceed in the way exemplified in figure 4. In this scenario, the active sites are dissolved in a proper solvent. The monomer molecules are inserted in the metal-carbon bond at the active site to form a generally insoluble polymer chain that separates from the catalytic site by β-hydride elimination or by transfer to a small molecule, leaving the catalytic species in solution and free to propagate another chain. It is not certain how accurate this picture is, but it is a useful idealization to understand the behaviour of metallocenes and other soluble Ziegler-Natta catalysts.

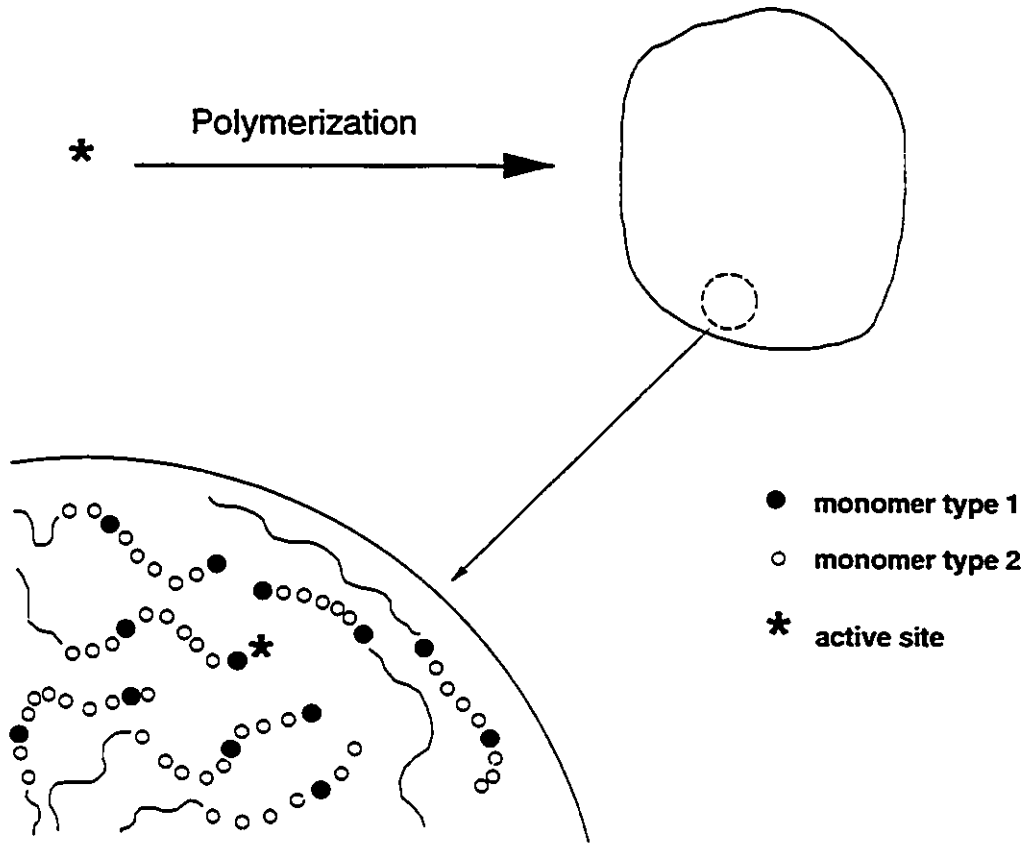

Figure 4 - Polymerization catalyzed by homogeneous metallocene/aluminoxane and Ziegler-Natta systems.

If the assumption that there is only one active species type is correct, then the CLD and CCD would be adequately described by Stockmayer's distribution and the polymer would have a PDI equal to 2 and a very narrow CCD for the long polymer chains. This indeed seems to be true for several metallocene/aluminoxane systems studied and reported in the literature (Soares and Hamielec, 1994e). Some other systems, however, produce polymer with broad CLD and CCD, and this has been attributed, analogously to conventional heterogeneous ZN catalysts, to the presence of more than one active species type or to the transformation of the active species in time from one type to another.

Although polymers made by metallocene/aluminoxane catalysts, due to their narrow CLD, are adequate for applications such as injection molding and precision injection, several other commercial uses (extrusion molding, thermoforming, rotational molding, plate casting and production of films) require exactly the opposite, i.e., a broad CLD (or a narrow MWD with sufficient long chain branching). By the appropriate combination of different metallocenes it is possible to design a multi-site type catalyst to make polymer with tailor-made properties. In this way, CLD and CCD can not only be broadened but can also be designed to be uni, bi. tri or multimodal as the need for the appropriate blend of polymer properties demands.

One or more types of metallocenes can also be supported on inorganic and organic carriers to form a uni to multi-site type heterogeneous catalyst. The advantage of these systems over the conventional heterogeneous ZN catalysts is the better control over the number and type of active species present on the support, at the same time benefiting from the use of heterogeneous catalysts in processes such as gas-phase polymerization and the ability to make polymer with controlled particle properties.

The greatest drawback associated with metallocene/aluminoxane catalysts is likely the high aluminoxane/metallocene ratio required in most systems to obtain adequate activity levels and stereochemical control. Aluminum/transition metal ratios varying from 1.000 to 50.000 are commonly reported in the literature. Aluminoxanes are difficult to synthesize and hence are expensive, and since they are required in great amounts it is necessary to remove the residues from the polymer, increasing production costs. Much research has been devoted to the problem of minimizing the level of aluminoxane required (for instance by supporting the catalysts) or by completely eliminating its use as with the cationic metallocene catalyst systems.

Aluminoxanes are obtained by the reaction of an alkylaluminum with water. Water should be present in dilute or less accessible form such as in wet solvents or hydrated salts since the reaction between water and alkylaluminuns is extremely rapid and highly exothermic. Several methods for synthesizing aluminoxanes have been published in the literature (Wild et al., 1982; Kaminsky et al., 1983b,1985c; Giannetti et al., 1985).

Even though the exact structure of aluminoxanes is still a matter of controversy, they supposedly exist as a mixture of different cyclic or linear oligomers with degree of oligomerization commonly varying from 6 to 20. Methylaluminoxane (MAO), the most commonly used aluminoxane, might have the following structures:

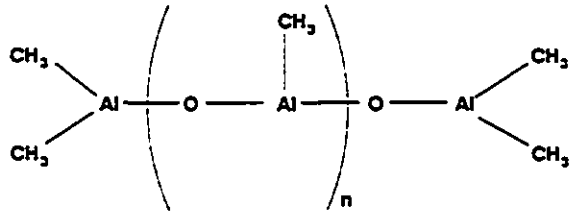

Linear

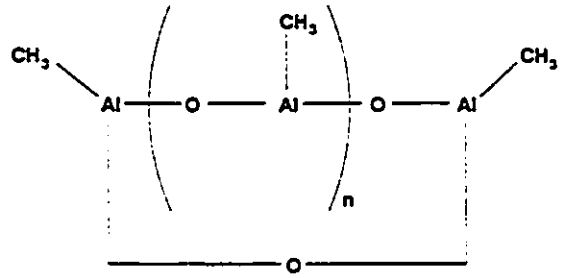

Cyclic

The synthesis of aluminoxanes by the above mentioned routes is associated with several serious limitations such as long reaction times, low yields, potential of explosion and formation of solid by-products.

Recently some alternate methods have been proposed to produce aluminoxanes: 1) *in situ* production of aluminoxane by feeding wet monomer to a solution of metallocene and alkylaluminum in the polymerization reactor (Chang, 1989b; Luker, 1991); 2) bubbling wet nitrogen to a solution of alkylaluminum (Stricklen, 1991); 3) reaction of alkylaluminum and hydrocarbylboroxine (Welborn, 1991b); 4) reaction of alkylaluminum and water vapour at low temperature, 0 °C (Resconi et al., 1992); 5) reaction of trimethylaluminum (TMA), a polyalkyldialuminoxane containing alkyl groups (ethyl or higher), and optionally water (Crapo and Malpass, 1992).

The type of aluminoxane has a marked influence on the efficiency of a metallocene/aluminoxane catalytic system. MAO seems to be more effective as a cocatalyst then other aluminoxanes such as ethylaluminoxane (EAO) and

isobutylaluminoxane (IBAO) (Kaminsky and Steiger, 1988b). More remarkably, the catalytic activity of the metallocene complex is directly proportional to the degree of oligomerization of the aluminoxane (Sinn et al., 1980).

Despite its marked influence on catalytic performance, the exact role of the aluminoxane component is not known precisely. Experimental evidence seems to indicate that besides acting as an alkylation agent it is involved in the formation of active sites and preventing their deactivation by bimolecular processes by stabilization of the active species and scavenging of impurities.

Chien and Wang (1988b) unequivocally demonstrated that the functions of the aluminoxane component go beyond alkylation of the metallocene. When 99% of MAO is substituted by trimethylaluminum (TMA), which also acts as an effective alkylation agent, polymerization rates are reduced by one third to one fourth of the value obtained when pure MAO is used. MW is also lowered by 40% when TMA/MAO = 10 but remains unaffected when TMA/MAO < 2.

Ethylene was the first olefin to be polymerized using metallocene/aluminoxane catalysts. The high reactivity of ethylene and absence of stereochemical isomerism in polyethylene chains make ethylene an ideal monomer for testing new non-stereoselective catalytic systems for synthesis of polyolefins.

The most commonly used catalysts for polyethylene (PE) production are achiral cyclopentadienyl derivatives of Zr, Ti and Hf (figure 5). Ti and Hf catalysts show a smaller activity and are less stable at temperatures above 50 °C than zirconocenes (Kaminsky, 1986b; Kaminsky and Steiger, 1988b).

One of the most striking features of these catalysts is their elevated polymerization rates. Kaminsky (1991b) reports activities as high as 40,000 kg PE $(g\ Zr.h)^{-1}$ for bis(cyclopentadienyl) zirconium dichloride (Cp_2ZrCl_2) and MAO at a polymerization temperature of 95 °C and ethylene pressure of 8 bars. Considering that all Zr atoms form active catalytic sites (Tait et al., 1988), the interval between two monomer insertion steps was estimated to be smaller then 0.1 ms.

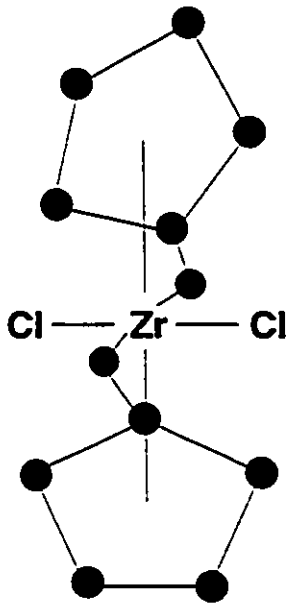

Figure 5 - Structure of ethylenebis(cyclopentadienyl) zirconium dichloride (Cp_2ZrCl_2).

Catalytic activity is a strong function of Al/metal ratio (Chien and Razzavi, 1988a). The catalytic activity of Cp_2ZrCl_2/MAO for ethylene polymerization increases steadily from 25.000 kg PE (g Zr.h.atm)$^{-1}$ to 480,000 kg PE (g Zr.h.atm)$^{-1}$ by varying Al/Zr ratio from 1,070 to 46,000 (Chien and Wang, 1988b).

The activity of Cp_2ZrCl_2/MAO can last for days (Kaminsky, 1986a). This behaviour has been incorrectly called "living polymerization" because the polymerization could be restarted after withdrawal of monomer for a determined period of time and then supplying the reactor with fresh monomer (Sinn et al., 1980). The same is observed for bis(neomenthylcyclopentadienyl) zirconium dichloride ($(NMCp)_2ZrCl_2$) and MAO: the polymerization of ethylene interrupted for 0.5, 1 and 12 hours can be restarted with only minimal decrease in catalytic activity (Chien and Razavi, 1988a). This catalyst site stability should permit one to produce polymer blends mixed on a molecular level as is done in the manufacture of high impact polypropylene by varying reactor operation conditions in time or by using a series of reactors at different operation conditions.

The number average molecular weight (M_n) of polymer made by Cp_2ZrCl_2/MAO is very sensitive to temperature, ranging from 1,000,000 at 0 °C to 1,000 at 100 °C (Sinn et al., 1980). Most homogeneous metallocene catalysts show the same relation between M_n and temperature, presumably due to an intensification of β-hydride elimination with increasing temperature. At temperatures below -20 °C transfer reactions are so reduced that the molecular weight becomes only a function of time, thus behaving as in a real living polymerization system (Kaminsky, 1986b). β-hydride elimination and transfer to monomer both produce dead polymer chains with terminal vinyl unsaturation. These chain ends can add to active metal centres to produce trifunctional long chain branches. With α-olefins vinylidene end groups can also be produced but these terminal C=C bonds are far less reactive than vinyl end groups.

Hydrogen is an efficient chain transfer agent when used with metallocenes. However, contrary to what is observed with conventional Ziegler-Natta catalysts, only traces of hydrogen are necessary to achieve MW control. The presence of hydrogen also lowers the activity of Cp_2ZrCl_2/MAO (Kaminsky and Luker, 1984) but the effect is reversible; removal of hydrogen increases the polymerization rate. For ethylene polymerization with Cp_2ZrCl_2/MAO, MW is a linear function of hydrogen pressure (Kaminsky and Luker, 1984).

The decrease of average molecular weight of PE with increasing metallocene concentration has been attributed to bimetallic interruption processes or to transfer reactions (Kaminsky et al., 1986e; Chien and Razavi, 1988a).

When metallocene/aluminoxane catalysts are supported on inorganic supports the rate of β-hydride elimination is reduced and hydrogen must be used to obtain desirable molecular weights.

More remarkably, the polydispersity index (PDI) of PE produced by these metallocenes under most experimental conditions approaches 2 (Kaminsky, 1986b, 1991b), which strongly supports the hypothesis that only one type of catalytic site is involved in the polymerization.

By altering the chemical environment around the central transition metal atom it is possible to considerably change the nature of the active centre and the catalytic behaviour of the metallocene. Kaminsky et al. (1986e) used bis(pentamethyl cyclopentadienyl) zirconium dichloride ($(CpMe_5)_2ZrCl_2$) and MAO

to catalyze ethylene polymerization. The catalyst is 5 to 10 times less active than Cp_2ZrCl_2/MAO but it produces polymer with twice the MW and a much broader molecular weight distribution (MWD) under the same polymerization conditions. PDI varied from 6 to 15. This behaviour is attributed to the presence of two catalytic site types formed sequentially during the contact of metallocene and aluminoxane. An initial fast step produces active sites that are less reactive and make PE with lower molecular weight. If left to age without contact with ethylene, some of those sites can be transformed to a more reactive site type that makes PE with higher molecular weights.

$(NMCp)_2ZrCl_2$/MAO can also be used to catalyze the homopolymerization of ethylene (Chien and Razavi, 1988a). The catalytic activity is not as high as for Cp_2ZrCl_2/MAO and the melting point of the produced PE is low (113.5 - 132.9 °C), indicating structural defects or low molecular weights.

As mentioned before, non-chiral cyclopentadienyl derivatives produce PE at high productivities and narrow MWD and CCD. Different types of metallocenes can be combined to obtain PE with broad MWD and CCD (Ewen, 1990b,1990c; Stricklen, 1991). Those polymers are generally easier to process because they have a faster throughput rate with lower energy requirements and show reduced melt flow perturbations. According to Stricklen, MWD can be controlled not only by the relative amounts of the metallocene types but also by the concentration of hydrogen when one of the metallocenes is more sensitive to the chain transfer agent than the other. Improved processability can also be obtained by varying the degree of long chain branching in copolymers of ethylene and α-olefins using a monocyclopentadienyl metallocene catalyst (Lai et al., 1993).

It is possible to synthesize polyolefins with long and short chain branches and totally novel properties by the copolymerization of ethylene and α-olefins under controlled conditions using monocyclopentadienyl derivatives of transition metals (Lai et al., 1993). Polyolefins with long chain branches can not be obtained with conventional Ziegler-Natta catalysts because β-hydride elimination with the required formation of terminal vinyl unsaturations does not occur at sufficiently high rates. Those polyolefins have been called "substantially linear" to indicate that they might possess up to 3 long chain branches per 1000 carbon atoms. Polyolefins synthesized using this process can possess narrow molecular weight distribution (PDI = 2.5)

showing excellent mechanical properties but still have good processability. As a rule, polymers with narrow molecular weight distribution are difficult to process because of low shear sensitivity, low melt elasticity and melt fracturing. However, it is claimed that "substantially linear" polyolefins combine the processability of HP-LDPE with strength and other physical properties of LLDPE.

Contrarily to polyolefins made with heterogeneous Ziegler-Natta catalysts, the melt flow index ratio of these resins is practically independent of polydispersity. This result is probably achieved by varying the concentration of long and short chain branches in the polymer chain while keeping the same narrow molecular weight distribution. The formation of long chain branches is probably a consequence of the open structure of the monocyclopentadienyl catalyst as well as the availability of terminal vinyl unsaturations. This facilitates the addition of dead polymer chains containing active terminal double bonds to the active sites. Dead polymer chains containing active terminal double bonds (usually vinyl double bonds) are formed by β-hydride elimination reactions at higher temperature.

Although slurry, liquid and gas phase processes are also claimed in this patent, these polyolefins are preferentially produced by solution processes. It is likely that the enhanced mobility of the polymer chains in solution plays a decisive role in controlling the average number of long chain branches of the final polymer.

PE and ethylene-α-olefin waxes can be obtained using catalysts with substituted and unsubstituted cyclopentadienyl derivatives of Zr, Hf and Ti using H_2 as the chain transfer agent (Luker, 1991). Due to the high sensitivity of these catalysts to H_2, only minor amounts of H_2 are required to considerably lower MW, which makes the process attractive from the industrial point of view.

Substitution of one cyclopentadienyl ligand with a heteroatom ligand such as dimethylsilyltetramethyl produces a metallocene which can polymerize ethylene to high MW PE and LLDPE (Canich, 1991). Also, the use of a third organoaluminum component, such as dialkylaluminum alkoxides, leads to catalysts that make PE with narrow MWD and CCD, high polymerization activity and bulk density and excellent powder properties (Kioka et al., 1993). The use of a third component was also proposed by Fujita (1990), in this case a silicon compound having a Si-O-C bond, such as tetraethyl silicate. The silicon compound together with the metallocene and

aluminoxane are contacted inside the reactor before polymerization. It is claimed that this catalyst makes polymer with higher MW than when the silicon compound is not present. Unfortunately no explanation was provided to account for the increase in MW. Tentatively we may assume that the third component acts like a support for the active species, decreasing chain transfer by β-hydride elimination.

MW of polyolefins made by metallocene/aluminoxane catalysts shows a strong inverse relation to the polymerization temperature. A process for obtaining high MW, narrow MWD PE at high temperature and high monomer pressure (T_p > 120 °C, P > 500 bars) was invented by Welborn and Speed (1992b). As usual, combination of different metallocenes can be used to broaden MWD while keeping a high MW average.

The use of metallocene/aluminoxane catalysts for polymerization of propylene is complicated because of stereoisomerism of the polypropylene chains. By the appropriate selection of metallocene catalysts it is possible to produce polypropylene (PP) with atactic, isotactic, syndiotactic, isotactic-stereoblock, atactic-steroblock and hemiisotactic configurations (figure 6). More remarkably, it is also possible to synthesize PP chains that have optical activity.

The metallocenes commonly used for ethylene polymerization, such as achiral cyclopentadienyl derivatives, are also able to polymerize propylene with productivities of 550 kg PP $(g\ Zr)^{-1}$, but only atactic chains are produced.

Ewen (1984) was the first to report the synthesis of isotactic PP by using bis(cyclopentadienyl) titanium diphenyl (Cp_2TiPh_2) and ethylenebis(indenyl) titanium dichloride ($Et(Ind)_2TiCl_2$) and MAO. The first catalyst produces isotactic PP with helix inversions at low temperatures, according to a chain end control mechanism (Ewen, 1984; Grassi et al., 1988; Zambelli and Ammendola, 1988). $Et(Ind)_2TiCl_2$ is produced as a mixture of 56% racemic and 44% meso forms. Of the total PP produced, 63% is isotactic, and the mechanism of monomer insertion is site controlled. The meso form of the catalyst is supposed to produce the 37% atactic fraction.

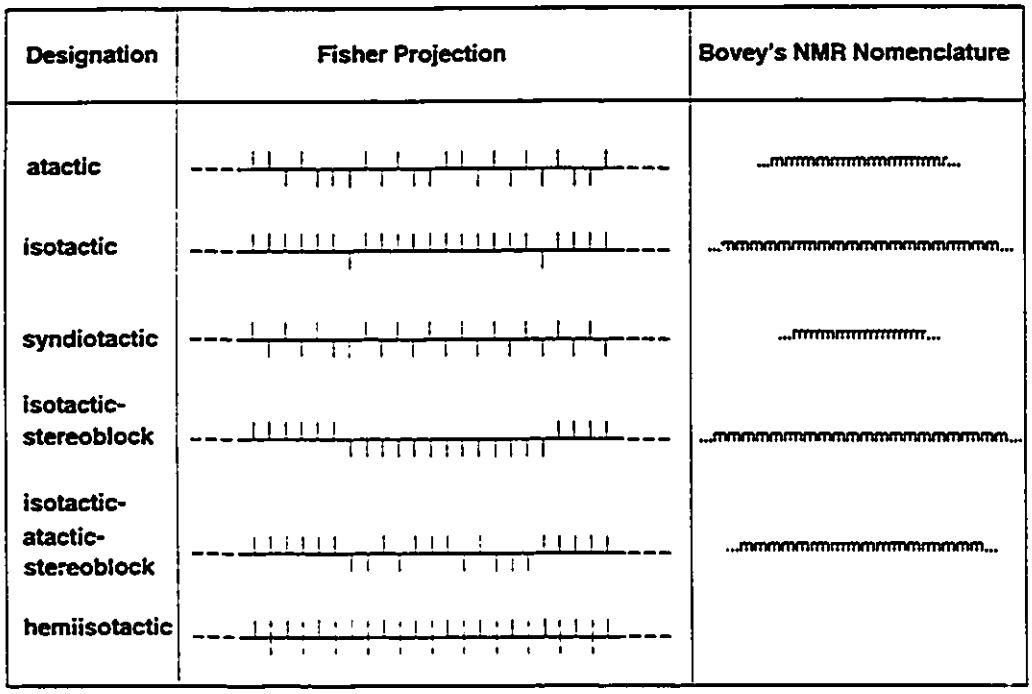

Figure 6 - Types of polypropylene chains produced with metallocene/aluminoxane catalysts.

The bridge extending between the two indenyl rings imparts stereorigidity to the metallocene complex, preventing the rotation of the rings about their coordination axes. In the case of the chiral racemic isomeric forms, their spatial arrangement favours the coordination of propylene molecules in such a way as to produce mainly isotactic chains. For the meso form, both monomer orientations are equally favoured and therefore only atactic chains are formed (figure 7).

However, chiral metallocenes such as ethylenebis(tetrahydro indenyl) zirconium dichloride ($Et(H_4Ind)_2ZrCl_2$) can make PP with high degree of stereoregularity. These zirconocenes are generally obtained as a racemic mixture of the d and l forms. The concentration of the meso form is very low (Wild et al., 1985).

Highly isotactic PP was first produced by Kaminsky et al. (1985a,1986d) using $Et(H_4Ind)_2ZrCl_2$/MAO. The reported solubility of PP in toluene is only 0.2% and the triad distribution measured by ^{13}C NMR is mm = 95%, mr = 3.2%, rr = 0.9%. Besides, the catalyst is more active for propylene than the non-chiral biscyclopentadienyl derivatives, reaching activities of 7,700 kg PP (mol Zr.h)$^{-1}$ at

60 °C. At conventional polymerization temperatures the number average molecular weight (M_n) is low (12,000 at 60 °C) but increases with decreasing polymerization temperature (300,000 at -20 °C). MWD is narrow with PDI = 1.9 to 2.6.

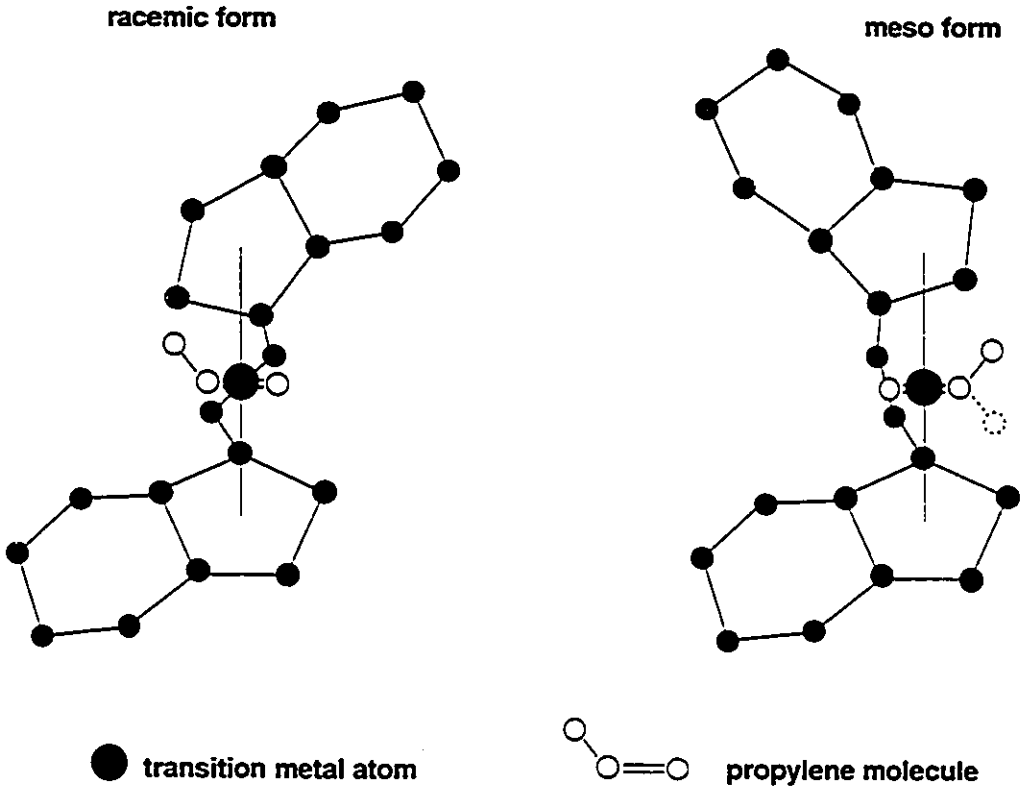

Figure 7 - Polymerization of propylene with meso and racemic forms on indenyl derivative catalysts.

The performance of $Et(H_4Ind)_2ZrCl_2$ and its non-hydrogenated equivalent $Et(Ind)_2ZrCl_2$ were compared by Kaminsky et al. (1986b,1986e,1987). $Et(Ind)_2ZrCl_2$ is more active then $Et(H_4Ind)_2ZrCl_2$. The rate of polymerization of both catalysts depends linearly on monomer and catalyst concentration. MW and stereoregularity are very sensitive to temperature because of the flexibility of the ligands; more atactic polymer is formed and β-hydride elimination is more frequent at higher temperatures. The catalysts are also regioselective, since no significant amount of 2,1-insertions is observed in the ^{13}C NMR spectra of the polymer. The Ti equivalent catalyst is less active by a factor of 100 than the zirconocene and makes more atactic PP.

Optically active PP can be produced by fractionating the racemic mixture of $Et(H_4Ind)_2ZrCl_2$ or $Et(Ind)_2ZrCl_2$ into pure enantiomeric forms (Kaminsky et al., 1986b,1986e,1987). The polymer made by the S-enantiomer has higher isotacticity than the one made by the racemic mixture but its catalytic activity is lower. The so formed polymer chains remain stable and show optical activity unless treated at high temperatures or being completely dissolved.

Soga et al. (1987) fractionated PP made by the S-enantiomer of $Et(H_4Ind)_2ZrCl_2$ into boiling heptane soluble (C_7-sol) and insoluble (C_7-ins) fractions. The polymer was produced at -10 °C in toluene solution. In contradiction with previous reported results (Kaminsky et al., 1985a,1986d) the MWD of the whole polymer is broad and bimodal, with PDI equal to 5.8. The MWDs of the two fractions are much narrower, with PDI of 2.8 and 2.6 for the C_7-ins and C_7-sol fractions respectively. The MW of the C_7-sol fraction is considerably smaller than that of the C_7-ins fraction. The melting point of the C_7-ins fraction is 160 °C while that of the C_7-sol fraction is considerably lower (149 °C). The C_7-ins fraction ^{13}C NMR spectrum is that of a conventional isotactic PP, while the one of the C_7-sol fraction shows a series of secondary peaks related to 1,3-insertions of the propylene units or less probably to contamination by ethylene. The mm triad content of whole polymer, C_7-ins and C_7-sol fractions are 98.15%, 98.57% and 96.14% respectively. Unfortunately, the amount of each fraction was not reported. Estimating from the mm content of the whole polymer and fractions, one obtains 83% for the C_7-ins and 17% for the C_7-sol fractions. Considering that the polymerization temperature is very low and that the S-enantiomer catalyst produces polypropylene of higher isotacticity than the racemic mixture, the C_7-sol fraction is considerably large. The broad MWD and presence of fractions of different microstructures are attributed to the existence of two types of active sites, one of which may undergo hydrogen-transfer polymerization (1,3-insertion).

The effect of operational conditions on the polymerization of propylene by $Et(Ind)_2ZrCl_2$/MAO was extensively studied by Rieger et al. (1990). The polymerization rate increases with temperature from -55 to 80 °C. The Arrhenius plot is linear over this range of polymerization temperatures and the estimated values for the activation energy of propagation and chain transfer are 10 kcal/mol and 15 kcal/mol, respectively. Increasing the polymerization temperature broadens the

melting temperature curve (as measured by DSC) and decreases the melting point temperature of the polymer (T_m). Decreasing the polymerization temperature increases MW and narrows MWD: PDI is equal to 2.69 at 80 °C, 1.3 at 0 °C, and 1.52 at -20 °C. Activity and MW increase with increasing Al/Zr ratio but PDI decreases. The polymer was fractionated by successive extraction in acetone, ether, pentane, hexane, and heptane. Even when the polymerization temperature is as low as - 55 °C, only 86.2% of the produced PP is insoluble in refluxing heptane. As expected, ^{13}C NMR of the fractions showed increasing mmmm and mmmr pentad contents from acetone to heptane soluble fractions. The PP chains show a preference for crystallizing in the γ-form, which is unstable for high MW isotactic PP. This anomalous behaviour was attributed to the inversion of the helix configuration of the chain.

Chien and Sugimoto (1991b) and Chien (1992) compared propylene polymerizations catalyzed by $Et(H_4Ind)_2ZrCl_2$/MAO and $Et(Ind)_2ZrCl_2$/MAO. The activity of $Et(H_4Ind)_2ZrCl_2$ is smaller than that of $Et(Ind)_2ZrCl_2$ but the activation energies of propagation of both catalysts are around 10 kcal/mol. The activity of both catalysts is strongly dependent on Al/Zr ratio but showed distinct behaviour. While the activity versus Al/Zr ratio curve for $Et(H_4Ind)_2ZrCl_2$ is S-shaped, the one for $Et(Ind)_2ZrCl_2$ is bell-shaped. The authors proposed that MAO could coordinate in a weaker way with $Et(H_4Ind)_2ZrCl_2$ than with $Et(Ind)_2ZrCl_2$; an excess of MAO in the latter case could cause partial or total blocking of the active sites. More than one active site type is supposed to be present since the polymer could be fractionated by extraction with different solvents. Metallocene complexes with different coordination states with MAO are assumed to be responsible for the formation of different types of catalytic sites. The authors argued that the depression in T_m caused by decreasing Al/Zr ratio or by increasing the polymerization temperature could not be explained by the small amount of 1,3-insertions observed by ^{13}C NMR analysis. They believe that inversion of the helix configuration is a more reasonable explanation.

Tsutsui et al. (1989a,1989b) compared PP made by $Et(Ind)_2ZrCl_2$/MAO and the heterogeneous system $MgCl_2/TiCl_4$/triethylaluminum. The polymer was fractionated by successive extractions with boiling pentane (C_5), hexane (C_6), heptane (C_7), and trichloroethylene (T) and the fractions were analyzed by ^{13}C NMR,

GPC and DSC. Most of the PP made by the soluble zirconocene catalyst is C_6-ins/C_7-sol or C_7-ins/T-sol; small amounts are C_5-sol and no T-ins polymer is formed. This indicates good homogeneity of the polymer samples in terms of stereoregularity as well as molecular weight. The PDI of the samples varies between 1.77 to 2.9 and the maximum number average molecular weight (M_n) obtained is low (40,000 to 50,000) even at low polymerization temperatures (-20 to -30 °C). The characteristics of PP made by the heterogeneous system are markedly different: polymer fractions range from C_5-sol to T-ins and PDI is 5.53. The ^{13}C NMR data are particularly elucidative. For the polymer made by the Zr catalyst the mmmm pentad ranges from 94.6 to 95.4 for the C_7-ins/T-sol fraction and from 86.3 to 88.6 for the C_5-ins/C_6-sol fraction. On the other hand, for the polymer produced by the heterogeneous catalyst, the mmmm pentad is 23.4 for the C_5-sol fraction and 93.5 for the T-ins fraction. The higher solubility of PP made by the metallocene catalyst (no T-ins fractions were obtained) was attributed to 2,1- and 1,3-insertion defects as verified by ^{13}C NMR analysis. Those defects are absent in the polymer made by the heterogeneous catalyst and they were considered to account for the different properties of PP made by the metallocene catalyst, rather than due simply to a lower degree of stereoregularity.

Isotactic PP can also be produced by dimethylsilylenbis(substituted - cyclopentadienyl)metal dichloride compounds (Mise et al., 1989). Under some polymerization conditions PP with higher MW and stereoregularity than that made by indenyl derivative catalysts can be obtained. MWD is also narrow, with PDI close to 2. The catalytic activity, however, is significantly lower than that for $Et(Ind)_2ZrCl_2$/MAO.

Ewen et al. (1988b) reported the production of syndiotactic PP using isopropyl(cyclopentadienyl-1-fluorenyl) hafnium dichloride ($iPr(Flu)(Cp)HfCl_2$) and MAO and the equivalent Zr catalyst. High MW (52,000 - 777,000) and narrow MWD (PDI = 1.8 - 2.6) are obtained at conventional polymerization temperatures (25 - 70 °C). ^{13}C NMR determined rrrr pentads are between 0.74 and 0.86. The main chain defects are mm triads, which is consistent with a site stereochemical control mechanism (figure 8). From the results reported, MW of polymer made by the Hf catalyst is significantly higher (8 to 11 times) than the one made by the Zr catalyst.

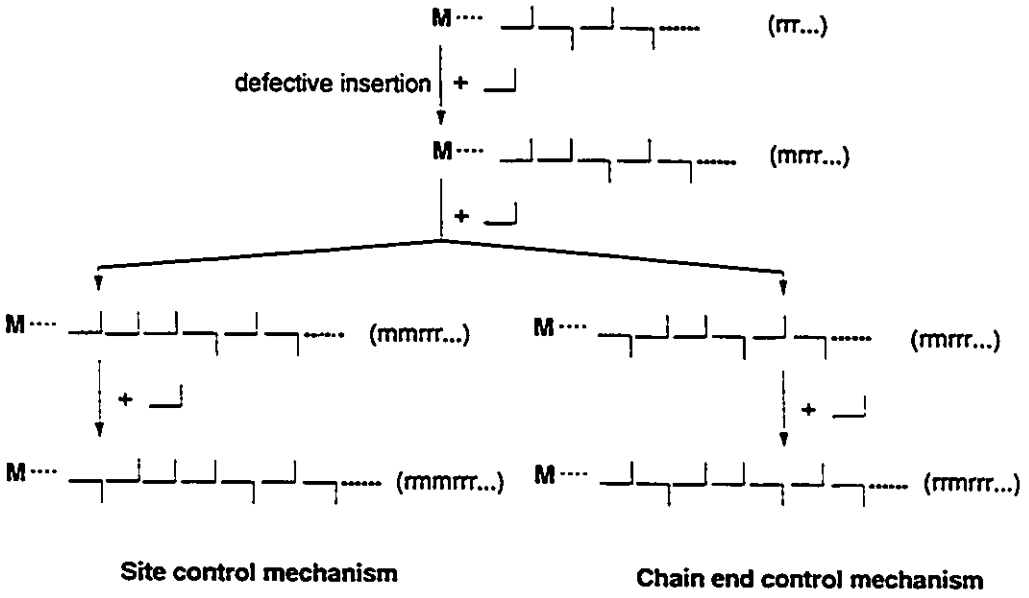

Figure 8 - Active site and chain end stereochemical control mechanisms for syndiotactic polymerization of propylene.

By varying the ligands around the central transition metal atom, PP with novel chain structures can be obtained. $(NMCp)_2ZrCl_2$/MAO produces stereoblock PP (Kaminsky and Bushermohle, 1987; Kaminsky and Steiger, 1988b) with sequence lengths between 2 and 7 and narrow MWD. Sequence lengths are inversely proportional to polymerization temperature.

Mallin et al. (1990) and Chien et al. (1991c) used ethylidene (1-tetramethylcyclopentadienyl)(1-indenyl) titanium dichloride ($Et(Me_4Cp)(Ind)TiCl_2$) and MAO and $Et(Me_4Cp)(Ind)TiEt_2$/MAO to produce PP having the attributes of a thermoplastic elastomer (TPE). According to the authors, that is the first example of a TPE comprising a single monomer. The activity of the catalyst is 250 kg PP (mol Ti.h.atm)$^{-1}$ at 50 °C. The polymer is mainly soluble in ethyl ether and has narrow MWD with PDI = 1.7 to 1.9. To account for the properties of the new PP, the authors suppose that the active sites can exist in two different states, one stereospecific and the other non-stereospecific. Since they can change states during the lifetime of a polymer molecule, the chain has alternating blocks of atactic and isotactic PP. The isotactic domains act as physical cross-links and give the polymer its elastomeric properties.

An extensive ^{13}C NMR peak assignment for PP made by $Et(Ind)_2ZrCl_2$/MAO, $Et(IndH_4)_2ZrCl_2$/MAO and $Me_2Si(Ind)_2ZrCl_2$/MAO was done by Cheng and Ewen (1989). The dominating propagation mechanism of those catalysts is 1,2-insertion, with a much lower amount of 2,1- and 1,3-insertions. For the isotactic fraction, when a 2,1-insertion occurs it does not propagate, which is consistent with a site controlled propagation mechanism. For the atactic fraction all tactic sequences are identified, indicating random statistics in stereoselectivity. However, even in the atactic fraction, 1,2-insertions appear to be predominant, suggesting that the regiochemistry of propagation is still site controlled.

Taking as model catalysts $Et(H_4Ind)ZrCl_2$ (isotactic PP) and $iPr(Flu)(Cp)HfCl_2$ (syndiotactic PP), Spaleck et al. (1990) synthesized several metallocene catalysts by varying the ligand type, the bridge between ligands, and the substituents on the bridge and on the ligands. All 14 modifications proposed have smaller catalytic activity and produce polymer with decreased steroregularity and MW. This behaviour was attributed to a decrease in the difference of the energy levels of the two possible modes of insertion of the monomer in the new catalysts.

Several patents deal with the isospecific homo and copolymerization of propylene. Isotactic-stereoblock PP can be obtained at temperatures lower then 0 °C by employing Cp_2TiPh_2 (Ewen, 1985). By elevating the polymerization temperature the isotactic block lengths decrease and the polymer changes from an insoluble, crystalline product to an elastomer and finally to a sticky, amorphous material. PP with high degree of isotacticity can be obtained by the bridged racemic Cp derivatives at ambient and higher temperatures. Ewen (1988c) claims that hafnocenes of that type produce isotactic PP with higher MW than the equivalent Ti and Zr systems. The addition of TMA to this system causes a transformation over time, with decrease of MW and change of the unimodal, narrow MWD to a broader, bimodal MWD, probably caused by the formation of a new catalytic species.

Attempts to make stereoregularity less dependent on polymerization temperature have resulted in some new patents. Metallocenes for the isospecific polymerization of propylene and higher α-olefins with improved thermal stability were invented by Kaminsky and Buschermohle (1989a). The metallocene contains at least one Cp ring substituted by chiral groups, such as $(NMCp)_2ZrCl_2$. It is claimed that such complexes are stable in dilute solution at temperatures of 80 °C and make

polymer with high isotacticity. Improved isotacticity at conventional polymerization temperatures can also be obtained by silicon bridged chiral metallocene catalysts (Welborn, 1991c,1992c). In a similar way, it is claimed that metallocenes containing Cp ligands bridged by a Si or Ge compound, in which the Cp rings contain one branched C_4 to C_{10} alkyl radicals possess improved stereochemical control (Rieger et al., 1992).

A synthesis route for the production of racemic silyl bridged metallocenes essentially free from meso forms was invented by Rohrmann and Herrmann (1992). The racemate is obtained by the reaction of an alkali metal salt of a silylindenyl compound with a Ti, Zr or Hf halide at low temperature. Unfortunately, no polymerization results of catalysts produced in this way were shown in the patent. Razavi (1992) also proposed a new method for preparation of a great variety of metallocenes that dispenses with purification steps. Slaugh and Schoenthal (1987) invented a method for stabilizing metallocene/aluminoxane catalysts against aging during storage periods prior to use by maintaining them in an organic solvent containing at least 1 mole of 3,3,3-trialkyl-1-propene per mole of metallocene.

Broad MWD and/or CCD PP and copolymers can be obtained either by combining different types of metallocenes (Ewen, 1990d) or by the use of systems that can alone produce them (Kaminsky and Buschermohle, 1989b; Antberg and Bohm, 1993).

Accordingly to Ewen and Razavi (1990a), syndiotactic poly-α-olefins can be produced by bridged metallocenes in which one of the Cp rings is substituted in a different manner from the other ring, such as iPr(CpFlu)$HfCl_2$. It was found that the use of metallocenes with sterically different Cp rings produces predominantly syndiotactic chains. Contrary to vanadium based homogeneous ZN catalysts, the mechanism of monomer insertion seems to be controlled by the active site instead of the chain end, as inferred from ^{13}C NMR analysis. When only one type of catalyst is used, PDI is close to 2. As usual, mixtures of different types of metallocenes can be employed to broaden MWD.

Very high indices of syndiotacticity (up to 90%) have been claimed for catalysts such as diphenylmethylene (FluCp)$HfCl_2$ and methylphenyl-methylene (FluCp)$HfCl_2$ (Winter et al., 1992b). More remarkably, those systems show a direct

relation between polymerization temperature and MW: At low temperatures, low MW and narrow MWD are obtained, changing to high MW and broad MWD as the polymerization temperature is increased.

Hemiisotactic PP can be produced by bridged metallocenes having dissimilar Cp groups and no bilateral symmetry such as iPr(3-MeCp-1-Flu)$ZrCl_2$ (Ewen, 1991). The polymer made by this complex has an isotactic structure affecting only every other asymmetric carbon atom. The remaining methyls on asymmetric carbon atoms can be either on the same side or on the opposite side of the polymer chain. Reactor blends of hemiisotactic PP and syndiotactic PP or isotactic PP can be made by combining the above catalyst with iPr(CpFlu)$ZrCl_2$ or Et(H_4Ind)$_2ZrCl_2$, respectively. Hemiisotactic PP is noncrystalline and would act in these blends as a plasticizer.

Waxes of PP or propylene-ethylene or higher α-olefin copolymers with narrow MWD can be obtained by using catalysts such as $(NMCp)_2ZrCl_2$ and comparatively small amounts of H_2 as chain transfer agent (Winter et al., 1990a). By including at least one heteroatom in the bridge between the Cp rings, compact, spherical particles having narrow grain size distribution and high bulk density can be prepared (Winter et al., 1990b). Comonomers are incorporated predominantly as isolated units in the polymer chains, which results in an optimal reduction of crystallinity and hardness (Winter et al., 1992a).

Few applications of metallocene/MAO systems for linear olefins other then ethylene and propylene have been reported in any detail in the literature. Kaminsky et al. (1985a,1986b,1987) studied butene-1 and hexene-1 homopolymerizations with metallocene catalysts but presented very few experimental results.

One remarkable feature of some chiral metallocene catalysts is that they can polymerize cycloalkenes to isotactic polycycloalkenes without ring opening. Although some conventional Ziegler-Natta catalysts are also able to polymerize cycloalkenes, 20 to 30% of the rings are opened during the polymerization, providing the polymer with elastomeric properties (Kaminsky et al., 1988a) in contrast to highly crystalline polycycloalkanes made by chiral metallocene catalysts. If some of the rings open during polymerization the polymer obtained contains double bonds which can lead to chain crosslinking, considerably restricting the processability of the material by extrusion and injection molding.

Kaminsky et al. (1988a,1988b) used $Et(Ind)_2ZrCl_2$/MAO to polymerize cyclopentene. The catalyst activity at 30 °C is 2.2 kg polycyclopentene (g Zr.h)$^{-1}$. The polymer is highly crystalline and is insoluble in aromatic or aliphatic hydrocarbons. The melting point of this polymer is 395 °C. Cylopentene can also be polymerized by $Me_2Si(Ind)_2ZrCl_2$/MAO (Kaminsky 1991a) at a catalyst activity higher then that of $Et(H_4Ind)_2ZrCl_2$/MAO.

Cyclobutene and norbornene are also polymerized by $Et(Ind)_2ZrCl_2$/MAO to crystalline, high melting point polycycloalkenes (Kaminsky et al., 1991a,1991b). At the same conditions, the activity of cyclobutene is 5 times higher then that of cyclopentene. The polymerization rate of norbornene is significantly lower. The melting point of polycyclobutene is 485 °C and of polynorbornene is over 600 °C.

Polycycloolefins and copolymers of cycloolefins, linear olefins and dienes can be obtained by using chiral metallocenes such as $Et(Ind)_2ZrCl_2$ (Kaminsky and Spiehl, 1993b). The preferred cycloolefin is cyclopentene; linear olefins are ethylene and propylene; and the diene is butadiene. The rate of incorporation of the cycloolefin increases with decreasing temperature. No significant ring opening takes place and the polymer is isotactic with melting point above 250 °C. MWD is broader (PDI from 3 to 6) than when propylene is polymerized by the same system (PDI around 2), indicating that the type of monomer is an important factor in the catalytic behaviour. Brekner et al. (1992) noticed the same MWD broadening by polymerizing polycyclic, monocyclic and acyclic olefins to obtain polymers with glass transition temperature above 100 °C.

A process for cyclopolymerization of non-conjugated diolefins, particularly 1,5-hexadiene to form polycyclopentene was invented by Waymouth (1993). Two catalytic systems are used: achiral metallocenes such as Cp_2ZrCl_2 or chiral metallocenes such as $Et(Ind)_2ZrCl_2$. When produced in a bulk monomer reactor, the polymer is poorly soluble in chlorinated organic solvents, probably indicating crosslinking, but when polymerized in toluene solution by slowly adding the monomer the polymer can be fractionated by conventional boiling solvent extraction techniques. Achiral metallocenes show trans selectivity: 80% of the monomer units show trans configuration when the polymer is obtained at 25 °C, but the polymer is atactic. With chiral catalysts the polymer is isotactic but the trans selectivity decreases to only 60%.

Several types of copolymers can be successfully produced by metallocene catalysts. The most remarkable property of these catalysts, besides high productivities, is the potential to make copolymer with much narrower CCD than the ones produced by heterogeneous Ziegler-Natta catalysts, opening the possibility for a much tighter control of copolymer composition.

Cp_2TiMe_2/MAO was used by Kaminsky (1986a) to copolymerize ethylene and propylene. Copolymers with 10 to 90% of propylene can be synthesized by this catalyst. The highest catalyst productivity reported is 137 kg copolymer $(g\ Ti)^{-1}$ at 20 °C at MAO/Ti ratio of 143. The propylene units were reported to be distributed at random in the copolymer but no data were shown to support this claim.

Propylene and ethylene can also be copolymerized by $Et(Ind)_2ZrCl_2$/MAO (Drogemuller et al., 1988). In comparison with Cp_2TiMe_2/MAO and Cp_2ZrMe_2/MAO the reactivity ratio of ethylene is lower and that of propylene is higher than unity, permitting a greater incorporation of propylene in the copolymer under the same polymerization conditions. MW and polymerization rate are proportional to ethylene concentration in the reactor and PDI = 2.5 to 4.5.

Tsutsui et al. (1989a) employed $Et(Ind)_2ZrCl_2$/MAO to copolymerize ethylene and propylene. The activity is enhanced to a maximum of eight times by incorporating 22% ethylene units in the copolymer. From ^{13}C NMR analysis, it seems that the presence of ethylene facilitates 2,1-insertions of propylene units in the copolymer: 2,1-insertions increase from 0.58% in absence of ethylene to 0.88% when the ethylene content is 22%.

Linear low density polyethylene (LLDPE) can be produced by copolymerizing butene-1 or hexene-1 and ethylene using cyclopentadienyl-metallocene catalysts. Although almost no detail about the polymerization conditions is given, a linear relationship between PE density and hexene incorporation is presented by Kaminsky (1986a).

Kaminsky and Schlobohm (1986c) copolymerized ethylene and butene-1 using Cp_2ZrCl_2/MAO. For the same degree of butene-1 incorporation, the melting point of the copolymer made by the zirconocene catalyst is lower than for a copolymer made by the heterogeneous catalyst $TiCl_3$/TEA. This indicates that the

comonomer is more regularly distributed in the copolymer chain when the zirconocene catalyst is used. Further evidence of copolymer regularity comes from the small values of PDI observed (2 to 3).

Cp_2ZrMe_2/MAO can be used to produce LLDPE by copolymerizing hexene-1 and ethylene (Kaminsky, 1986b). The hexene fraction during polymerization has a peculiar influence on polymerization rate: If the amount of hexene is lower than that of ethylene, the polymerization rate is the same order as that for homopolymerization of ethylene. However, upon increasing the amount of hexene above that of ethylene, a period of increase in the polymerization rate is followed by a final decrease. This behaviour occurs at different Zr concentrations and temperatures. The reactivity ratios were estimated to be 55 for ethylene and 0.005 for hexene. The content of hexene diads, as measured by ^{13}C NMR, is relatively low. Hexene seems to favour transfer to monomer reactions since it decreases MW compared to that of the PE made at the same conditions and increases the number of vinylidene groups in the copolymer. PDI is close to 2. EPDM can also be produced by this catalyst but it may take 10 hours until the system reaches its maximum polymerization rate. This rate is stable for several days and typical activities lie between 10 to 100 kg polymer (g Zr.h)$^{-1}$.

Acceleration rate effects were observed for the copolymerization of ethylene and hexene-1 by iPr(FluCp)$ZrCl_2$/MAO and $Me_2Si(Ind)_2ZrCl_2$/MAO and were related to the increase in the number of active sites or of the propagation rate constant (Herfert et al. 1993). Sequence length distributions were explained in terms of a two-site type terminal model or a one-site type penultimate model. Ethylene and 1,3-butadiene can also be copolymerized by Cp_2ZrMe_2/MAO (Kaminsky and Schlobohm, 1986c).

Copolymerization of ethylene and 4-methyl-1-pentene can be achieved using $Et(Ind)_2ZrCl_2$/MAO (Kaminsky et al., 1988a). Catalytic activity is in the range of 3 kg (mol Zr.h)$^{-1}$. The rate of copolymerization of ethylene is about 3 times higher then the rate of homopolymerization using $Et(Ind)_2ZrCl_2$/MAO.

Cross-linkable polymers can be made by the copolymerization of ethylene and small amounts of $\alpha-\omega$–diolefins. Although not showing detailed experimental

results, Kaminsky (1986a) claims that a PE with 2% of $\alpha-\omega$–octadiene has no defined melting point but shows rubber elasticity, being insoluble in organic solvents but swelling more than five times its original volume.

Propene was copolymerized with cyclopentene using $Et(Ind)_2ZrCl_2$/MAO (Kaminsky et al., 1991a). The catalyst activity is between that of the homopolymerization of both comonomers by the same catalyst. MWs are low (35,000 at 0 °C and 17,000 at 30 °C) and the maximum reported content of cyclopentene is 5%.

Ethylene and norbornene can be copolymerized by $Et(Ind)_2ZrCl_2$/MAO and $Et(H_4Ind)_2ZrCl_2$/MAO with an activity 100 times higher then that of Cp_2ZrCl_2/MAO (Kaminsky et al., 1991a). Remarkably, the reactivity ratio for ethylene is only 1.5 to 3.2 for $Et(H_4Ind)_2ZrCl_2$/MAO, which means that copolymers containing more than 50% of norbornene can be synthesized. These copolymers have narrow MWD, with PDI values around 2.

Kaminsky and Bark (1992a) used $Et(H_4Ind)_2ZrCl_2$/MAO and $Et(Ind)_2ZrCl_2$/MAO to catalyze the copolymerization of ethylene and dimethanooctahydronaphthalene (DMON). $Et(H_4Ind)_2ZrCl_2$ is the most active catalyst and MW is inversely proportional to DMON concentration.

Terpolymerization of ethylene-propylene-ethylidene norbornene can be catalyzed by $(C_2H_5)_2ZrMe_2$/MAO (Kaminsky and Miri, 1985b). The catalytic activity (100 - 1000 kg (mol Zr.h.bar)$^{-1}$)is higher then that of vanadium catalysts at the same polymerization conditions, but MW is lower (40,000 to 160,000). Average PDI = 1.7. The presence of the diene lowers the catalyst activity, especially at low ethylene/propylene ratios. By using a cationic metallocene catalyst, Chien and Xu (1993) reported ideal copolymerization (fraction incorporated in the copolymer equals fraction in reactor bulk phase) of ethylidene norbornene without reduction of polymerization rate.

Narrow MWD and CCD ethylene-propylene elastomers can be produced by Cp derivatives, principally zirconocenes containing tetrahydroindenyl ligands (Hoel, 1989a). Reactor fouling can be minimized by supporting and prepolymerizing the catalyst. Predominantly crystalline ethylene-propylene copolymers with less then 15% propylene incorporation are made by catalysts such as $Pr(1\text{-}(3\text{-}Me_3\text{-}Si\text{-}Ind))_2ZrCl_2$, $Pr(Ind)_2ZrCl_2$ and $(Me_5Cp)_2ZrCl_2$ (Antberg, 1992).

Those catalysts have particularly high selectivity towards the small ethylene molecule which leads to high ethylene incorporation even when the polymerization is carried out in liquid propylene. By selection of appropriate polymerization conditions, HDPE, MDPE and LLDPE can also be produced. PDIs are very high, varying from 6.5 to 35.8 in the presented examples. In some cases multimodal melting curves are observed.

A process for production of EPDM copolymers was invented by Floyd and Hoel (1993). Among the desirable properties of an elastomer are a relatively high diene content to permit a fast cure rate, a low degree of crystallinity, weight average MW of at least 110,000 and narrow MWD. Those conditions are met by using alkylene or silanylene or mixed alkylene-silanylene bridged bis(substituted Cp) derivatives of group 4b transition metals. The catalyst is preferably supported and the reaction takes place in liquid α-olefin.

A completely novel use of metallocene catalysts was invented by Malanga and Newmann (1990) for the syndiotactic polymerization of vinyl aromatic monomers, especially styrene. The suspending agent must evidently be a non solvent and not react with the metallocene: fluorinated aliphatic compounds, such as perfluoromethylcyclohexane, are the most adequate. The most preferred metallocenes are monocyclopentadienyl titanium trialkoxides. Because the suspending agent is a nonsolvent for the catalyst or monomer or polymer, very little reactor fouling occurs and the polymer is recovered as beads with diameters varying from 100 μ to 1.0 cm.

Graft polymerization with biomass is possible with substances containing free hydroxyl groups, such as cellulose, starch and lignin (Kaminsky, 1986a,1986b). Those hydroxyl surface groups can be used to hydrolyze alkylaluminums and make aluminoxane analogous structures. The metallocene is then added to the alkylaluminum treated surface. By varying the polymerization time it is possible to regulate the polymer/support ratio. Kaminsky claims that the polymerization can take place on the catalyst coated surface and that the polymer is adsorbed after chain termination. Unfortunately, few experimental results were disclosed.

Cationic Metallocenes

Cationic metallocenes are catalysts in which the transition metal atom is positively charged. The metallocene complex is therefore a cation associated with a stable anion. It may be that, with further study, it will be shown that all active center types operative with metallocenes are cationic.

They are generally prepared by combining at least two components. The first is a metallocene and the second is an ion exchange compound comprising a cation and a non-coordinating anion. The cation reacts irreversibly with at least one of the first component's ligands. The anion must be capable of stabilizing the transition metal cation complex and must be labile enough to be displaced by the polymerizing monomer. The relationship of the counterion to the bridged structure controls monomer insertion and isomerization (Elder et al., 1992).

Jordan et al. (1986,1988) used a cationic metallocene catalyst, $Cp_2Zr(CH_3)(THF)^+$, to produce PE in the absence of an aluminum cocatalyst. Even though the polymerization rate is low, the activity of this catalyst supports the hypothesis that a cationic complex is the active species in metallocene catalysis and that the aluminum cocatalyst acts mainly as an alkylation agent and activator. This idea has been further supported by noticing that copolymers of ethylene/propylene and ethylene/propylene/ethylidene norbornene made in presence of $Et(Ind)_2ZrCl_2$/MAO or $[Et(Ind)_2ZrEt]^+[B(C_6F_5)_4]^-$ have similar microstructures (Chien, 1993). The same catalyst can be used to produce highly isotactic PP at a temperature of -55 °C (Chien et al., 1991d).

The hypothesis that the catalytic center is polar or ionic is further supported by the eletronic effects observed in some metallocenes of the type $(X_2C_9H_5)_2ZrCl_2$/MAO where X can be a Cl, H or F atom or a CH_3 or OCH_3 group (Piccolrovazzi et al., 1990; Lee et al., 1992). It was observed that for ethylene polymerization, electron withdrawing groups such as F significantly lower the catalytic activity and MW while electron donors such as CH_3 have little influence over the polymerization. For the case of polypropylene synthesis, electron withdrawing groups reduce considerably the stereochemical control of the catalyst.

This has been related to changes in the degree of association of the metallocene and the MAO counterion or to increase in the strength of the metal-carbon bond between metallocene and ligands.

Zambelli et al. (1989) prepared a MAO free isotactic specific homogeneous catalyst based on group 4 metallocenes and a mixture of TMA-DMF (DMF = $AlMe_2F$). Polymers made in the presence of one particular group 4 metallocene and either MAO or TMA-DMF have similar stereochemical structure. The ability of MAO to activate group 4 metallocenes towards propylene polymerization has been tentatively attributed to the formation, in presence of MAO, of cationic complexes such as $[M(IV)L_2R]^+$, where M is a group 4 metallocene, L is a ligand and R is an alkyl ligand (CH_3 or growing polymer chain) which would be the actual active species:

$$L_2MX_2 + AlMe_3 + AlMe_2F \rightarrow L_2MMeF + 2\ AlMe_2X$$

$$L_2MMeF + AlMe_3 \rightarrow L_2MMe_2 + AlMe_2F$$

$$L_2MF + 2\ AlMe_3 \rightarrow [L_2MMe]^+ + [Al_2Me_6F]^-$$

It is speculated that the use of TMA-DMF leads to the same cationic active species obtained when MAO is used as cocatalyst.

High MW, narrow MWD and CCD (Hlatky and Turner, 1992; Turner et al., 1993) as well as syndiotactic selectivity (Elder et al., 1992) have been claimed for those systems.

A neutral, aluminoxane free metallocene catalyst was invented by Jordan and Crowther (1993) to produce low MW PE and PP oligomers. The uninegative Cp ligand of cationic metallocenes is substituted by a dinegative dicarbollide ligand and a neutral complex is produced that does not require a cocatalyst to generate a counterion. However, alkylaluminums do improve the performance of these catalysts and the inventors recognize that beside acting as a scavenger it might also function as a cocatalyst.

Supported Metallocenes

Since most of the conventional polyolefins industrial plants were designed to use heterogeneous Ziegler-Natta or Phillips catalysts, the commercial application

of homogeneous metallocenes involves not only the synthesis of a catalyst that makes polymer with convenient final properties but also the design of an entirely new plant or the expensive adaptation of existing ones to operate with a soluble catalyst. One way of overcoming this problem is by supporting the metallocene catalyst on an "inert" inorganic support hopefully without significantly losing its activity, stereochemical control and ability to make polymer with narrow MWD and CCD.

Another incentive for supporting metallocenes is the enhancement of stereochemical and regiochemical control of those catalysts to make PP with properties closer to those obtained with the use of conventional Ziegler-Natta catalysts. PP made by homogeneous catalysts generally has a higher number of chain defects such as 2,1- and 1,3-insertions which cause a decrease in its T_m. Also, these polymers also possess low MW, apparently due mainly to significant β-hydride elimination. Supporting the catalyst may lead to more rigid catalytic structures that produce polymer with improved regio and stereoregularity and higher MW.

Metallocenes can be effectively supported on several inorganic oxides. The type of the support as well as the technique used for supporting the metallocene and/or MAO have a crucial influence on catalytic behaviour. By the appropriate choice of conditions, stereo and regioselectivity can be improved and transfer reactions can be minimized with consequent production of polymers with higher MW. Those changes have been attributed to a more rigid catalytic structure that results from the interaction between metallocene and the surface of the support. Unfortunatelly, particularly with $MgCl_2$-supported catalyts, those interactions may lead to the formation of additional site types leading to broadening of MWD.

Additionally, supported catalysts usually require smaller Al/metal ratios than the soluble systems and some can be activated in the absence of MAO by commom alkylaluminums such as trimethylaluminum (TMA), triethylaluminum (TEA) and triisobutylaluminum (TIBA). This reduced dependence on MAO with lower Al/metal ratios has been related to reduction in catalyst deactivation by bimolecular processes due to the immobility of the active sites on the surface of the support. However, usually the catalytic activity is inferior to that observed for soluble systems, probably due to deactivation or inefficient production of active sites during the supporting process.

Chien and He (1991a) reported four methods of supporting $Et(Ind)_2ZrCl_2$ on SiO_2. The only successful approach consisted in contacting MAO with dried SiO_2 in a first step, followed by addition of the metallocene in a later stage. The Zr content of the catalyst was 0.62 wt% at an Al/Zr ratio of 50. Contacting $Et(Ind)_2ZrCl_2$ or $Et(Ind)_2ZrMe_2$ with SiO_2 prior to MAO leads to no or very low amounts of supported Zr. Contacting $Et(Ind)_2ZrCl_2$ with TMA treated SiO_2 and then MAO produced a catalyst of very low activity (20 kg PP (mol Zr.h.bar)$^{-1}$). When compared to the unsupported catalyst, the catalyst made by the first method makes ethylene-propylene copolymer with about the same composition and density. More remarkably, it remains active at lower Al/Zr ratios which supports the hypothesis that immobilization of the metallocene in the support prevents deactivation of active sites by bimolecular processes. No evidence of significant extraction of the metallocene from the surface during polymerization was found by the authors.

Chien and He (1991a) also studied the partial substitution of MAO by IBAO, TIBA and TMA. Increasing the amount of any alkylaluminum diminished the polymerization rate and increased the amount of ethylene incorporated in the copolymer, that is, reduced the reactivity ratio for the α-olefin.

Kaminaka and Soga (1991) polymerized propylene using Al_2O_3, $MgCl_2$ and SiO_2 supported $Et(IndH_4)_2ZrCl_2$. TEA or TMA were used in place of MAO. The SiO_2 supported catalyst is inactive and so is the homogeneous catalyst if TEA or TMA are used in place of MAO. $MgCl_2$ and Al_2O_3 supported catalysts, on the other hand, polymerize propylene with good activity in absence of MAO. When compared to PP made by the homogeneous system, the one made by the supported catalyst shows higher isotacticity (as measured by ^{13}C NMR) and higher melting point. $Et(Ind)_2ZrCl_2/Al_2O_3$ produces polymer with PDI around 2 in the same fashion as the homogeneous catalyst. However, the MWD of PP made by $Et(Ind)_2ZrCl_2/MgCl_2$ is much broader, with PDI varying from 4 to 5. In this case, some interaction between support and metallocene seems to have created different types of active sites.

Kaminaka and Soga (1992) also polymerized propylene by supporting $iPr(Flu)(Cp)ZrCl_2$ and Cp_2ZrCl_2 over Al_2O_3, $MgCl_2$ and SiO_2 with TEA in place of MAO. Once again, the SiO_2 catalysts were unable to produce PP while

iPr(Flu)(Cp)$ZrCl_2$ and Cp_2ZrCl_2 supported over Al_2O_3 or $MgCl_2$ made syndiotactic PP and atactic PP, respectively. The syndiotactic PP made by the supported catalyst has higher melting point then the one produced by the homogeneous system.

Soga and Kaminaka (1992) were able to polymerize propylene using SiO_2 supported $Et(IndH_4)_2ZrCl_2$ without adding additional MAO to the polymerization reactor. The support was treated with MAO before the addition of the metallocene. The supported catalyst alone shows almost no activity but when combined with TMA, TEA or TIBA becomes active. It is assumed that the metallocene combines with the MAO fixed on the SiO_2 surface forming an inactive complex. This complex is activated by the addition of alkylaluminum. The catalyst activity is dependent on the following cocatalyst type in order of decreasing activity: TIBA > TEA > TMA. TIBA also makes polymer with higher MW. The melting point and mmmm pentads of PP made by this catalyst are higher then the ones made by the equivalent homogeneous catalysts.

Collins et al. (1992) used fully hydroxylated, partially dehydroxylated and dehydroxylated Al_2O_3 and SiO_2 to support $Et(Ind)_2ZrCl_2$ and $Et(IndH_4)_2ZrCl_2$ for the polymerization of propylene. The metallocenes were adsorbed directly onto the oxide surface. In all cases, the amount of adsorbed metal is less than that predicted by monolayer coverage of the surface, indicating that the metallocenes are adsorbed on specific sites. The highest activities attained are those of partially dehydroxylated Al_2O_3 and SiO_2 when both are pre-treated with TMA. In any case, however, catalytic activities are lower than that of the homogeneous systems. Polymer properties such as stereoregularity, MWD and degree of crystallinity are not much affected. Although an excess of MAO has to be present for the catalysts to be active, the Al/Zr ratio applied (8.5) is significantly lower than that required for homogeneous catalysts. Apparently metallocenes react with surface hydroxyl groups to form inactive species, as attested by the higher activities of TMA-treated supported catalysts and by the increasing activity of SiO_2 supported catalyst as the surface is dehydroxylated.

Kaminsky (1993a) suggested three possible ways of supporting a metallocene: (1) adsorption of MAO onto the support followed by addition of the metallocene; (2) immobilization of the metallocene on the support followed by contact with MAO in the polymerization reactor; (3) immobilization of the metallocene on the support followed by treatment with MAO, producing a catalyst

that does not require additional MAO during polymerization. Method (1) excludes direct interaction of support and metallocene and therefore performs similarly to a homogeneous catalyst. $Et(Ind)_2ZrCl_2$ was supported on SiO_2 using methods (2) and (3). Catalysts (2) and (3) behave similarly, but (3) requires a lower Al/Zr ratio and is more convenient to use since no additional MAO is required during the polymerization. When compared with PP made by the homogeneous catalyst at the same reaction conditions the supported catalyst shows lower activity (10 kg PP (mol Zr.h)$^{-1}$) but a significantly smaller Al/Zr ratio was required (100 to 200). The PP made by the supported catalyst, however, possesses properties closer to that made by conventional heterogeneous Ziegler-Natta systems. Compared to PP made by the homogeneous catalysts, the one made by the supported catalysts possesses higher T_m (136-160 °C), about 30 times higher MW, and mm triads 9% higher. Results for ethylene polymerization follow the same trends. This may be explained by the more stable structure resulting from the direct contact of the metallocene and the surface of the support.

Soga and Kaminaka (1993) supported $Et(IndH_4)_2ZrCl_2$, $iPr(Flu)(Cp)ZrCl_2$, and Cp_2ZrCl_2 on Al_2O_3, $MgCl_2$, MgF_2, CaF_2 and SiO_2. All resulting catalysts are activated by using ordinary alkylaluminums in absence of MAO, except for SiO_2 that has to be treated with MAO before supporting the metallocene. PDI is close to 2 for all supported catalysts, except for $MgCl_2$-supported catalysts that make polymer with broader MWD. PP made with the supported $Et(Ind)_2ZrCl_2$ has fewer chain defects, as measured by ^{13}C NMR, than that made with the homogeneous catalyst.

In a recent article, Janiak et al. (1993) suggest the use of "polymeric MAO" as support for metallocene catalysts. "Polymeric MAO" is produced as a three dimensional lattice in the reaction between MAO and 1,10-dodecanediol or 1,6-dodecanediol. The authors affirm that preliminary results show that zirconocene dichlorides have higher activity when supported on "polymeric MAO" than on SiO_2.

Several patents have been issued regarding supporting technology for metallocene catalysts. They can be conveniently classified according to the way the aluminoxane catalyst is synthesized. Aluminoxanes can be either synthesized by the techniques mentioned above and be contacted with an adequately dried support in a later step or they can be produced *in situ* by reacting an alkylaluminum directly with the water adsorbed on a support such as silica gel.

Chang (1989a-b, 1990a-f, 1991a, 1991b, 1992a, 1992b) obtained several patents applying the direct synthesis of aluminoxanes for homopolymerization and copolymerization of 1-olefins in slurry and gas phase reactors, especially for the production of HDPE and LLDPE.

The support most commonly used is silica gel containing naturally occurring adsorbed water from 5 to 20 % by weight (*undehydrated* silica gel). In some patents this amount can be increased up to 50 % by adding water to commercially available silica gel (*water impregnated* silica gel).

A single type, preferably TMA, or a mixture of trialkylaluminums is added to the moist support. The reaction between the adsorbed water and the trialkylaluminum produces the equivalent aluminoxane *in situ*. The aluminoxane coated support is then contacted with a metallocene solution to form the final catalyst. This solid catalyst can be dried for subsequent use or immediately used for polymerization. Following the same procedure, Chang (1991d) also proposed a catalyst for producing broad molecular weight distribution HDPE and LLDPE by substituting the metallocene with a vanadium compound such as vanadium trichloride.

The metallocenes employed are cyclopentadienyl derivatives of transition metals. Bis(substituted cyclopentadienyl) zirconium compounds show higher activities.

The order of addition of silica gel and trialkylaluminum is important. It is known that the activity of the metallocene-aluminoxane catalyst is proportional to the degree of oligomerization of the aluminoxane. Therefore the slow addition of silica gel to a solution of trialkylaluminum forces the reaction to proceed under water deficient conditions and produce an aluminoxane with degree of oligomerization between 6 and 25. If the reverse order of addition is chosen the final catalyst has low activity.

When used alone for producing the aluminoxane, TMA generates a catalyst with the highest activity. However its cost is higher than that of other alkylaluminums such as TEA or TIBA. Chang proposed two ways of partially replacing TMA by a cheaper alkylaluminum without significantly decreasing the final activity of the catalyst. In the first (1990b.1990c.1990d) the aluminoxane coated silica is prepared by reacting the wet silica gel with TEA and then contacting it with a TMA treated

metallocene solution. Alternatively (1991a) the aluminoxane can be produced by reacting the wet silica gel with a mixture of TMA and TIBA and then contacting the aluminoxane coated silica with a metallocene solution. Chang claims that both modifications produce catalysts that have a level of activity comparable to the one obtained by using TMA alone.

The molecular weight of the polymer can be controlled in several ways. In terms of catalyst design, it is influenced by the ratio of aluminoxane to metallocene in the catalyst, by the type of substituents in the cyclopentadienyl ring and by the use of ligands in the metallocene. In terms of reactor operation, increases in hydrogen concentration and temperature decrease the average molecular weight of the polymer.

The comonomer content can also be controlled by the selection of the metallocene used in the catalyst synthesis or by changing the comonomer ratio in the reactor.

Many applications of polyolefins require that the polymer possess broad molecular weight distribution. In the case of copolymers, broad chemical composition distribution may also be desirable for some applications. Conventional heterogeneous Ziegler-Natta catalysts generally possess more then one type of active site and therefore produce polymer that fit these requirements. On the other hand, at least from the theoretical point of view, metallocene/aluminoxane catalysts have only one site type and therefore will produce polymer with narrow MWD and CCD.

One way of using metallocene/aluminoxane catalysts to produce polymer with broad MWD and CCD is by combining different metallocene compounds on the same support, therefore engineering a multisite type catalyst. If each metallocene type has distinct ratios of chain transfer to propagation rates as well as different reactivity ratios, copolymers of tailored MWD and CCD can be synthesized by the planned selection of metallocene types and their relative proportions.

With this line of thought Welborn (1987,1991,1992,1993) invented a supported catalyst comprised of at least one metallocene, at least one non-metallocene transition metal compound, an aluminoxane and an organometallic compound. By carefully selecting the proportion of the components, Welborn claims that it is possible to produce LLDPE and HDPE with polydispersities between 2.5 and 100 and average molecular weights from 500 to 2,000,000. The disadvantage

of high polydispersities is the lower mechanical properties. This can be overcome by using a narrow MWD with appropriate levels of long chain branching (Lai et al., 1993).

The support can be any inorganic oxide or even a finely divided polyolefin. It has to be dried by thermal or chemical means prior to contact with the other catalyst components. Surface modification of the support may be employed by reacting with an organometallic compound having hydrolytic character, such as magnesium and aluminum alkyls.

The metallocene is a cyclopentadienyl derivative of a transition metal, and the other transition metal compound is any conventional Ziegler-Natta catalyst, such as $TiCl_4$.

Preferably the dry support is contacted firstly with the metallocene/non-metallocene compound and then with the aluminoxane/organometallic compound. The product of this reaction is then dried and can be used to catalyze 1-olefin polymerizations in gas or slurry processes.

In a similar way, Welborn (1989,1990) developed a supported catalyst system comprised of at least one metallocene and an aluminoxane. By using more than one type of metallocene it is possible again to modify the MWD and CCD of HDPE and LLDPE. The catalyst can be used in both gas and slurry processes.

When polyolefins are to be used as elastomers, narrow MWD and especially narrow CCD are required. If the polymer has broad CCD some chains might possess long sequences of one monomer type, which increases the crystallinity of the polymer. This is undesirable in elastomers.

With this line of thought, Hoel (1989,1991) developed a metallocene/aluminoxane supported catalyst for producing ethylene-1-olefin elastomers with narrow MWD and CCD in a slurry process. The support is again any finely divided inorganic porous material treated to remove adsorbed water. The aluminoxane is preferably added to the support firstly, followed by the metallocene. Prepolymerization with ethylene or ethylene and 1-olefins is used to obtain good powder properties and to keep small particles from sticking to the reactor walls. The polydispersities of the quoted examples are between 2.2 and 4.0.

Chang (1991) developed a metallocene/aluminoxane supported catalyst for polymerizing ethylene and 1,4-hexadiene. The product of this reaction is polymer of narrow MWD and CCD containing pendant double bonds for posterior crosslinking or functionalization. The process for supporting the catalyst is similar to the one used by Hoel (1989).

Tsutsui et al. (1992) developed a catalyst made of an organometallic compound, an aluminoxane, a fine particle carrier, a metallocene of group IVB transition metal and an olefin product obtained during the prepolymerization of the catalyst. Electron donors may also be used if required.

The support can be any finely divided inorganic porous material or a polyolefin. Preferred organometallic compounds are trialkylaluminums having branched alkyl radicals. Metallocenes are cyclopentadienyl and indenyl derivatives of transition metals.

The process for supporting the catalyst is somewhat more elaborate then the ones presented before. Firstly the organometallic compound and the aluminoxane are contacted with the dry support, preferably in that order. The aluminoxane is then precipitated from solution by, for instance, adding a bad solvent. The organometallic compound/aluminoxane coated support is then contacted with the metallocene, followed by prepolymerization (with ethylene or ethylene-1-olefin) in an inert hydrocarbon medium. When the prepolymerization is finished, the soluble fraction is separated from the insoluble one which is then dried and used as the final catalyst.

Narrow MWD polymer can be produced by $MgCl_2$-supported metallocenes by the process invented by Bailly et al. (1992). $MgCl_2$ is prepared by precipitation in the presence of an electron donor free from labile hydrogen to ensure its homogeneous distribution over the support. The catalyst resulting from supporting zirconocenes produces PE with PDI varying from 2 to 5.

The polymerizations can be carried out both in slurry or gas phase reactors for producing HDPE and LLDPE. Additional aluminoxane and/or organometallic compound may be used for enhancing the activity of the catalyst. The inventor claims that the polymer produced possesses narrow CCD and MWD. In the examples shown, HDPE is obtained with polydispersity always less than 3.

Antberg et al. (1993) use a siloxane-substituted metallocene to improve the attachment of the metallocene to the surface of the support. They state that when a metallocene and an aluminoxane are applied together from solution onto a silicate support the bonds between support and the components of the catalyst are not permanent and they can be extracted from the surface during the polymerization.

Supports can be inorganic oxides having hydroxyl groups at the surface. The transition metal compound is strongly bonded to the surface by the presumed following reaction:

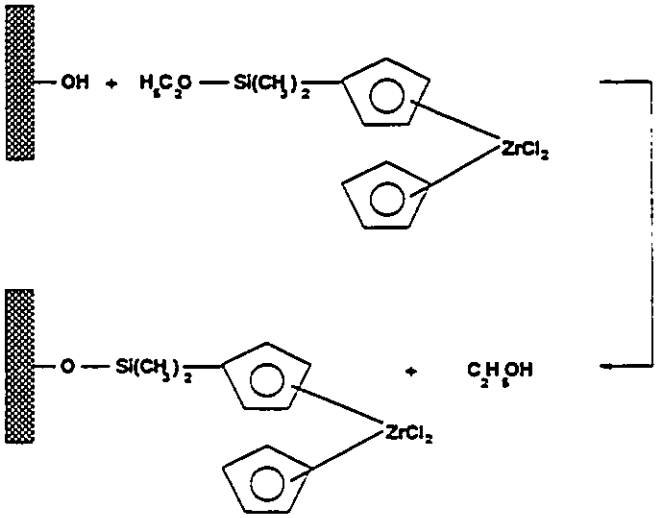

The resulting catalyst is used together with an aluminoxane in gas or slurry phase reactors for polymerizing 1-olefins.

Some patents propose a totally different method of obtaining a heterogeneous metallocene catalyst than the ones reviewed above. Instead of depositing the metallocene/aluminoxane over a support, they propose routes to heterogenize these components.

Antberg et al. (1991) developed a process for the preparation of a heterogeneous metallocene catalyst by reacting a substituted metallocene with a poly(methylhydrogensiloxane) over a hydrosilation catalyst as follows:

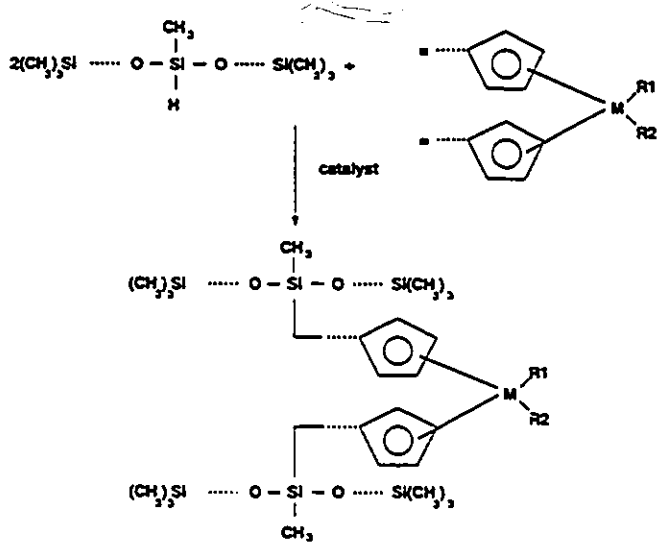

The so obtained catalyst can be used with MAO for the polymerization of 1-olefins, cyclic olefins, diolefins and cyclic diolefins. In the examples presented for ethylene, the polydispersity was always less than 4.

Antberg et al. (1992b) synthesized a heterogeneous metallocene catalyst for the polymerization of linear or cyclic olefins by polymerizing substituted metallocenes containing a vinyl group, such as Cp(Cp-vinyl)$ZrCl_2$, or by copolymerizing them with vinyl and divinyl aromatic compounds, such as divinylbenzene. The polymerization is initiated by heat or free radicals. Aluminoxanes are not essential, but should be used for polymerization of cycloolefins.

By reacting a metallocene and an aluminoxane and recovering the solid product, Turner (1988a-b) claims to obtain a heterogeneous catalyst that has good activity at significantly lower Al/metal ratios (12 to 100) than most conventional metallocene catalysts. It is not clear, however, if the catalyst does not dissolve again during the polymerization, thus behaving as a homogeneous catalyst.

Polymerization Mechanism and Kinetics

Despite the intense research activity, no definite, unequivocal polymerization mechanism has yet been defined to describe the behavior of Ziegler-Natta catalysts. This is hardly surprising, given the complex nature of the catalytic systems studied:

the catalyst may be soluble or insoluble in the reaction medium, a cocatalyst is generally required but some catalysts are able to polymerize olefins alone, the monomers may be liquid or gaseous, electron donors may be present or not, and the polymerization can be in gas phase, liquid monomer or slurry with various residence time distributions.

However, in an effort to unify the knowledge in this field, several attempts have been made to propose a mechanism that could be applied to all Ziegler-Natta catalyzed polymerizations. Recent reviews of polymerization mechanisms were published by Zakharov et al. (1983); Tait and Watkins (1989), and Corradini et al. (1989).

Mechanisms for Ziegler-Natta polymerization can be divided into two main categories: *Bimetallic* mechanisms assume that propagation occurs at the aluminum-carbon bond, while *monometallic* mechanisms assume that propagation takes place in the transition metal-carbon bond (Boor, 1979).

With bimetallic mechanisms, polymer growth occurs *via* insertion of monomer into the aluminum-carbon bond and the role of the catalyst surface is to complex with the monomer and, by polarization, promote insertion into the cocatalyst-alkyl bond. Natta and Mazzanti (1960) were among the first to suggest a bimetallic mechanism for Ziegler-Natta polymerization:

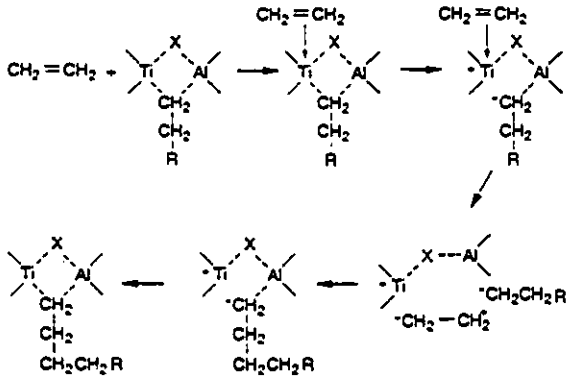

In this schematic, X is a halogen ligand, and R is a growing polymer chain or alkyl group.

Some experimental evidence apparently supports bimetallic mechanisms. For instance, catalytic activity and stereoregularity may depend on size, ionic nature,

and complexing ability of the metal alkyl. However, differences in the ability to alkylate or reduce the transition metal can also explain the influence of the cocatalyst on catalytic activity and stereochemical control (Tait and Watkins, 1989).

It is well established now that the two key steps in polymerization are the complexation between the monomer and the active centre followed by insertion into the growing polymer chain (Zakharov et al., 1983; Tait and Watkins, 1989; Corradini et al., 1989). In those monometallic mechanisms the cocatalyst acts as an alkylating and reducing agent and polymer growth takes place *via* insertion of monomer into the transition metal-carbon bond.

One of the models with greatest impact on the further development of monometallic polymerization mechanisms was proposed by Cossee (1960, 1964):

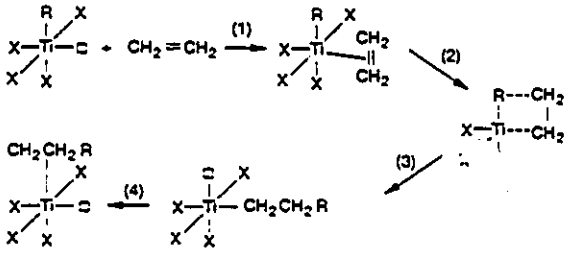

In this schematic, X is a halogen ligand, R is a growing polymer chain or alkyl group, and the open square indicates a ligand vacancy.

In Cossee's model, the active site is composed of a titanium atom having an octahedral configuration, with four chlorine ligands from the crystal lattice, an alkyl group introduced by the cocatalyst, and a coordination vacancy. According to Arlman (1964), coordination vacancies are required to ensure the electroneutrality of the crystal.

Step 4 is probably the weakest assumption of Cossee's model. In order to explain isotacticity, the polymer chain has to flip back to the position occupied before the monomer insertion step. Besides, several important phenomena such as monomer reaction orders higher then 1 and copolymerization rates higher then homopolymerization rates of both comonomers can not be explained by Cossee's model (Ystenes, 1991).

Several alternative monometallic models have been proposed based on Cossee's model (Zakharov et al., 1983; Tait and Watkins, 1989, Corradini et al., 1989; Ystenes, 1991). There is no agreement about the general validity of these models, but it is generally accepted that Cossee's model provides the best representation to date of the leading mechanisms governing polymerization by Ziegler-Natta catalysts (Dusseault and Hsu, 1993).

The polymerization rate curves for Ziegler-Natta polymerizations are generally classified as the two types illustrated in figure 9 (Keii, 1972). The *decay type curve* shows three distinct regimes. At the *build-up or acceleration period* (I), the polymerization rate increases until it reaches a maximum value that is followed by the *decay period* (II) where the polymerization rate decreases until it approaches the *constant rate period* (III) after which decay is negligible. In the *acceleration or build-up type curve* the decay period is absent; the build-up period is immediately followed by the constant rate period.

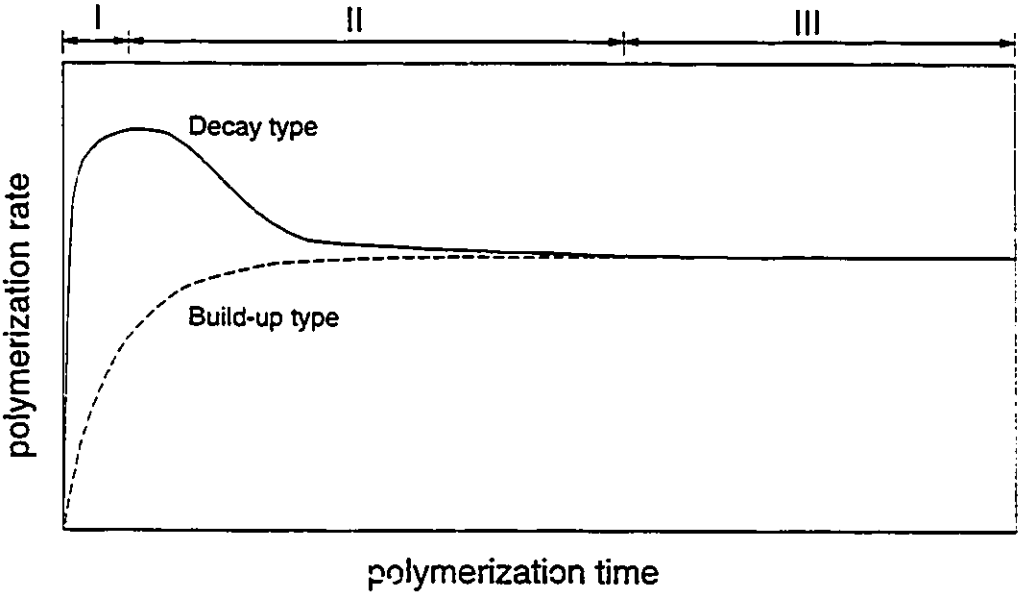

Figure 9 - Types of polymerization kinetics curves of Ziegler-Natta catalyst (I - acceleration or build-up period, II - decay period; III - constant rate period).

Several 1st generation catalysts when used with dialkylhalides have a build-up type curve, with a relatively long acceleration period (20-60 min) followed by a steady-state period (Natta, 1959b; Burfield et al., 1972; Chumaevskii et al., 1976;

Burfield et al., 1976; Doi et al., 1980). The acceleration period has been related to the break-up of the catalyst particles, exposing more active sites for polymerization. This assumption is supported by the significant reduction of the acceleration period observed when the catalyst particles are submitted to mechanical grinding before polymerization (Natta, 1959b; Wilchinsky, 1973).

2nd generation catalysts, such as Solvay ether-treated type, have a weaker porous structure and are therefore easily fragmented during the first seconds of polymerization. As a consequence, there is little or no acceleration period. A slow decay period, if present, is generally followed by a steady-state polymerization rate (Yoon and Ray, 1987; Tait and Watkins, 1989; Jejelowo et al., 1991).

Generally, 3rd generation, supported catalysts have a decay type polymerization curve. The acceleration period is generally short and can be completely absent for some polymerizations (Munoz-Escalona and Villalba, 1977; Keii, 1982; Chien et al., 1985; Tait and Wang, 1988; Marques et al., 1993).

The acceleration period is said to occur because of the formation of the active sites and in heterogeneous catalysts is additionally related to the break-up of the catalytic particles exposing new sites for polymerization (Natta, 1959a). This stage can take from minutes to hours, depending on the catalyst type and polymerization conditions.

The decay period is generally related to a decrease in the number of or to a reduction in the activity of the catalytic sites (Boor, 1979). The encapsulation of the catalyst particle with polymer and the consequent increase in mass transfer resistance has also been related to decay in catalyst activity but has encountered few supporters (Yoon and Ray, 1987; Soares and Hamielec, 1994b).

Besides catalyst type, several other variables can affect the Ziegler-Natta polymerization kinetics: cocatalyst type, monomer pressure, temperature, monomer type, and diluent type (Boor, 1979; Tait and Watkins, 1989).

Metallocene/aluminoxane catalyzed polymerizations also conform well to this classification. Of the few polymerization kinetic curves that have been reported in the literature, most of them can be classified as decay type (Chien et al., 1988a,1988b,1989,1990,1991b,1992; Huang and Rempel, 1992; Vela-Estrada and Hamielec, 1994) but some copolymerizations catalyzed by $Cp_2Zr(CH_3)_2$ show a characteristic build-up type curve (Kaminsky and Miri, 1985b; Kaminsky, 1986b).

The effect of TMA/MAO ratio on the kinetics of ethylene polymerization by Cp_2ZrCl_2/MAO was studied by Chien and Wang (1988b). The polymerization curve at low TMA/MAO ratios (less than 10) is a decay type, with stationary rates of about half of the maximum polymerization rate. However, at higher TMA/MAO ratios it changes to a build-up type regimen with an induction time of approximately 10 minutes. Aging the catalyst for 5 minutes decreases its activity to about one-half the original value. Surprisingly, longer aging times do not alter the induction time but increase the activity. A catalyst aged for one hour has about the same activity as the unaged catalyst. The induction period observed at high TMA/MAO ratio was tentatively explained by Chien in terms of a complexation of TMA with MAO which could retard the alkylation of Cp_2ZrCl_2.

Vela-Estrada and Hamielec (1994) studied the same system using a two level factorial design for temperature, MAO and Zr concentration. Two different types of kinetic behaviour were identified at the two studied temperatures. Polymerization rate and MWD results could be well represented by a two site type model. This was the first study to use GPC to establish the number of active site types quantitatively. In fact, a bimodal distribution gave PDI of 2 for each mode.

The polymerization kinetic curve of ethylene by $(NMCp)_2ZrCl_2$/MAO is also of decay type (Chien and Razavi, 1988a). Interruption of the polymerization by several hours does not significantly alter the polymerization kinetics.

The type of the propylene polymerization kinetics curve catalyzed by $Et(IndH_4)_2ZrCl_2$/MAO can be altered by varying the Al/Zr ratio (Chien and Sugimoto, 1991b). At high Al/Zr ratios commonly used in metallocene catalyzed polymerizations, the polymerization curve is of the conventional decay type. At low Al/Zr ratios, however, two build-up stages are present which may be attributed to the formation of active sites of distinct types at different rates.

Huang and Rempel (1992) found that $Et(Ind)_2ZrCl_2$/MAO catalyzed propylene polymerization can present two different types of polymerization kinetics curves. Although all rate curves obtained at 70 °C are of the decay type, some polymerizations at 50 °C show a build-up type curve with constant rates that are 1/4 to 1/3 of that obtained with the decay type curve. The authors assume that two active site types are present during the polymerization. Site type I is unstable and very active and can be converted into site type II. Site type II is stable but only mildly

active. Recent molecular weight measurements have, however, shown polydispersities very close to 2 suggesting that one active site type is operative, even though the rate versus time curves are complex.

The copolymerization kinetics of ethylene-hexene, propylene-ethylene and propylene-ethylene-diene by Cp_2ZrCl_2/MAO have a build-up type rate curve (Kaminsky and Miri, 1985b; Kaminsky, 1986b).

Supporting $Et(Ind)_2ZrCl_2$/MAO on SiO_2 does not alter the type of polymerization rate curve (Chien and He, 1991a). Even though the duration of the acceleration, decay and stationary periods vary between supported and soluble systems, both show a decay type curve.

Several elementary polymerization steps have been recognized in polymerizations catalyzed with Ziegler-Natta catalysts: 1) chain initiation - insertion of first monomer molecule into the transition metal-alkyl group bond, 2) chain propagation - insertion of a monomer molecule into the transition metal - polymer bond, 3) chain transfer to small molecule - a small molecule (monomer, cocatalyst, or transfer agents such as hydrogen) attaches to the active center forming a dead polymer chain, 4) spontaneous chain transfer (β-hydride elimination) - transfer of a hydrogen of the β-carbon to the active center, forming a dead polymer chain containing a terminal double bond (Boor, 1979; Kissin, 1985; Tait and Watkins, 1989).

Several chain transfer mechanisms occur simultaneously in polymerizations with Ziegler-Natta catalysts. These mechanisms of chain transfer were proposed in the early sixties by Natta and co-workers and further verified by other researchers (Boor, 1979; Kissin, 1985).

Hydrogen is commonly used as a chain transfer agent to control the molecular weight of polymers manufactured with heterogeneous Ziegler-Natta catalysts. The transfer reaction to hydrogen during propylene polymerization can be described by the chemical equation:

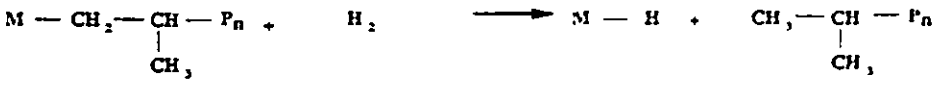

where P_n and M indicate growing polymer chains and catalytic active sites, respectively. Although illustrated for propylene polymerization, this and the next transfer reactions can occur during the polymerization of any linear olefin.

Another efficient chain transfer agent for these catalytic systems is $ZnEt_2$ but hydrogen is generally preferred since it is cheaper and leaves no residues in the polymer. The mechanism of chain transfer to $ZnEt_2$ is equivalent to the one with aluminum alkyls:

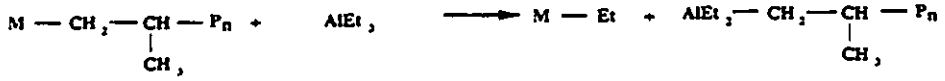

$ZnEt_2$ is a more efficient chain transfer agent than aluminum alkyls. This has been attributed to the fact that $ZnEt_2$ exists alone in solution while aluminum alkyls are generally present as dimers.

Monomer can also act as a chain transfer agent. This is even more significant for the copolymerization of ethylene and α-olefins, especially α-olefins higher then propylene. Chain transfer to monomer follows the chemical equation:

and results in terminal vinylidene unsaturation.

Chain termination by thermal degradation is generally of little importance for the polymerization of ethylene and propylene using heterogeneous catalysts. However, for the case of homogeneous metallocene catalysts, this transfer mechanism can be the most significant one in the absence of hydrogen. This mechanism involves the abstraction of a β-hydrogen atom and is therefore known as β-hydride elimination:

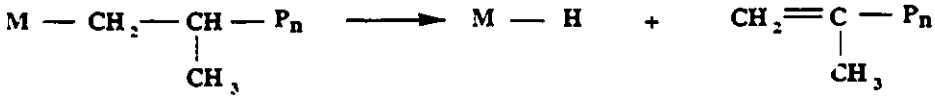

Termination by β-hydride elimination and transfer to monomer produce polymer with vinylidene end groups and terminal unsaturation; with ethylene, terminal vinyl unsaturation occurs. These chain transfer mechanisms are essential

to produce polymer with long chain branches. The terminal double bond, particularly with vinyl unsaturation, can add to the active centre to generate a trifunctional long branch.

Another mechanism of thermal degradation has also been reported for high polymerization temperatures, forming polymer chains with vinyl end groups:

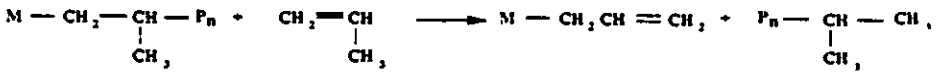

Some kinetic models use the above polymerization steps together with Rideal or Langmuir-Hinshelwood rate laws to describe polymerization catalyzed with Ziegler-Natta systems (Burfield et al., 1972; Bohm, 1978; Tait and Wang, 1988; Marques et al., 1993)

Polymer Characterization

Three techniques for polymer characterization are reviewed in this section. Size Exclusion Chromatography is a liquid chromatography technique for the determination of the molecular weight distribution of polymers. Temperature Rising Elution Fractionation is an analytical and preparative method for the fractionation of semi-crystalline polymer chains according to their crystallinity. Carbon-13 Nuclear Magnetic Resonance spectroscopy can be used to provide very detailed structural information about polymer chains, particularly after TREF fractionation.

Size Exclusion Chromatography (SEC)

Polymers differ from most small molecules in the sense that they can not be unequivocally described using average properties. While it is possible to characterize a small molecule by its molecular weight, such an average value for polymers must be used with caution since these complex materials almost always (the only exception being monodisperse polymers in which all chains possess the same length) present a distribution of chain lengths and, consequently, of molecular weights that in some cases can be very complex and broad (Billingham, 1989).

In general, the molecular weight distribution (MWD) of polyolefins synthesized with heterogeneous Ziegler-Natta catalysts is very broad, with polydispersity indices varying from 5 to 20. This is due principally to the polymerization mechanism and multiple site types for catalysts used in the polymerization (Zucchini and Cecchin, 1983). With the newer metallocene/aluminoxane catalysts, it is becoming possible to tailor the MWD of polyolefins from narrow, unimodal distributions to broad, multimodal distributions (Soares and Hamielec, 1994e).

The detailed knowledge of the molecular weight distribution of those polymers is of paramount importance to understand the catalytic processes taking place during polymerization (Soares and Hamielec, 1994c; Vickroy et al., 1993) and to determine their final rheological and mechanical properties. The shape of the MWD of a polyolefin has a significant influence on its application: Polymers with narrow MWD are adequate for injection molding and precision molding, but a broad MWD for linear chains is required for extrusion molding, thermoforming, rotational molding, plate casting and production of films (Ewen and Welborn, 1990b).

Size Exclusion Chromatography (SEC) is the most effective analytical technique for determining the molecular weight distribution of polymers. This technique is based on the fractionation of polymer chains according to their size in solution in a series of columns filled with packing of different pore sizes (Styring and Hamielec, 1989). Smaller chains penetrate into more pores then larger chains and therefore take a longer time to elute from the column. A detector (generally a differential refractometer) at the end of the last column monitors the polymer concentration in solution as a function of elution time.

If the hydrodynamic volume of the polymer is only a function of chain length, solvent type and temperature, then it is relatively easy to obtain a calibration curve relating retention time and molecular weight, provided there are available standards for calibration.

Calibration standards must possess a very narrow distribution of molecular weights (ideally unimodal) and be of the same type as the polymer being analyzed. Unfortunately, as a consequence of the mechanism of polymerization of olefins,

polyolefins have broad MWD. Calibration with broad MWD standards is also possible (Balke et al., 1969) but instrumental peak broadening may have to be taken into account (Styring and Hamielec, 1989).

A more attractive calibration technique for polyolefin analysis is the use of the universal calibration curve. Since SEC fractionation is governed by the hydrodynamic volume of the polymer chains in solution, the product of the molecular weight and intrinsic viscosity can be used as a universal parameter for SEC calibration, regardless of the chemical nature of the polymer being analyzed (Hamielec, 1989). In this way it is possible to establish a universal relation between elution time and molecular weight using readily available polystyrene narrow MWD standards. It is important to notice that this relation is not valid for complex polymer mixtures in which the hydrodynamic volume in the detector cell is the same, however compositions, stereoregularity, branching structure, and molecular weight might differ (Hamielec, 1982; Garcia-Rubio et al., 1983; Lew et al., 1993).

The universal calibration curve is commonly used for SEC analysis of polyolefins (Kok and Omens, 1982; Scholte et al.; 1984; Grinshpun et al., 1984; Grinshpun and Rudin, 1985; Lew et al., 1988a-b; Lew et al., 1993).

For the determination of MWD of polyolefins, it is necessary to use high temperature SEC, since most polyolefins are only soluble at high temperatures. High temperature SEC is essentially the same as SEC and has become the standard method for the determination of MWD of polyolefins (Haddam and Hay, 1988).

The analysis of polyethylenes and polypropylenes by SEC can be complicated by incomplete dissolution of the polymers. If dissolution times are not adequate, stable, multimolecular aggregates can be present in trichlorobenzene solutions of polyethylene and polypropylene at 145 °C (Grinshpun et al., 1984; Grinshpun and Rudin, 1985). Polyethylene aggregates can be eliminated by heat treatment at 160 °C for 1 hour (Grinshpun et al., 1984). Grinshpun and Rudin (1985) observed degradation of polypropylene under the same heat treatment but Ekmanis and Skinner (1991) did not report similar problems. Some researchers recommend longer dissolution times (30 - 50 hours) at 145°C for polypropylene (Grinshpun and Rudin, 1985; Lew et al., 1988a).

Temperature Rising Elution Fractionation (TREF)

TREF can be concisely defined as a technique to fractionate semicrystalline polymers according to their solubility-temperature relationship and thus to their composition and molecular structure. Two important parts of this definition must be stressed. First, TREF fractionates semicrystalline polymers. It is not applicable for amorphous polymers because TREF is mainly sensitive to differences in polymer crystallinity/solubility. Second, TREF fractionates polymer chains according to molecular structure that affects crystallinity/solubility. Distinct molecular structures of semicrystalline polymers are reflected in different crystallinity/solubility. TREF is sensitive to these differences.

A complementary definition is: TREF is sensitive to and fractionates according to the relation between molecular structure, chain crystallinity and dissolution temperature. Therefore, different molecular structures will be reflected in distinct crystallinities that will have dissimilar dissolution temperatures. TREF operates in the reverse order: by making use of the differences in dissolution temperature that arise due to the dissimilar crystallinities of polymer chains one can infer their molecular structure.

Figure 10 illustrates these ideas. The upper chain is the homopolymer, high density polyethylene (HDPE). It has very high structural order and it crystallizes in the form of a hard and brittle polymer. However, if one of the hydrogens attached to the backbone is substituted by another chemical group (R), the structural order of the original chain is disrupted. Now this unit may not crystallize with the other regular chains, and therefore the crystallinity of the polymer will be lower than that of the original fully regular one (Whiteley et al., 1992). This is done commercially with polyethylenes in order to alter the macroscopic properties of the polymer, and the products are known as linear low density polyethylene (LLDPE). The extraneous monomer unit or comonomer can be, for instance, 1-butene, 1-hexene or 1-octene.

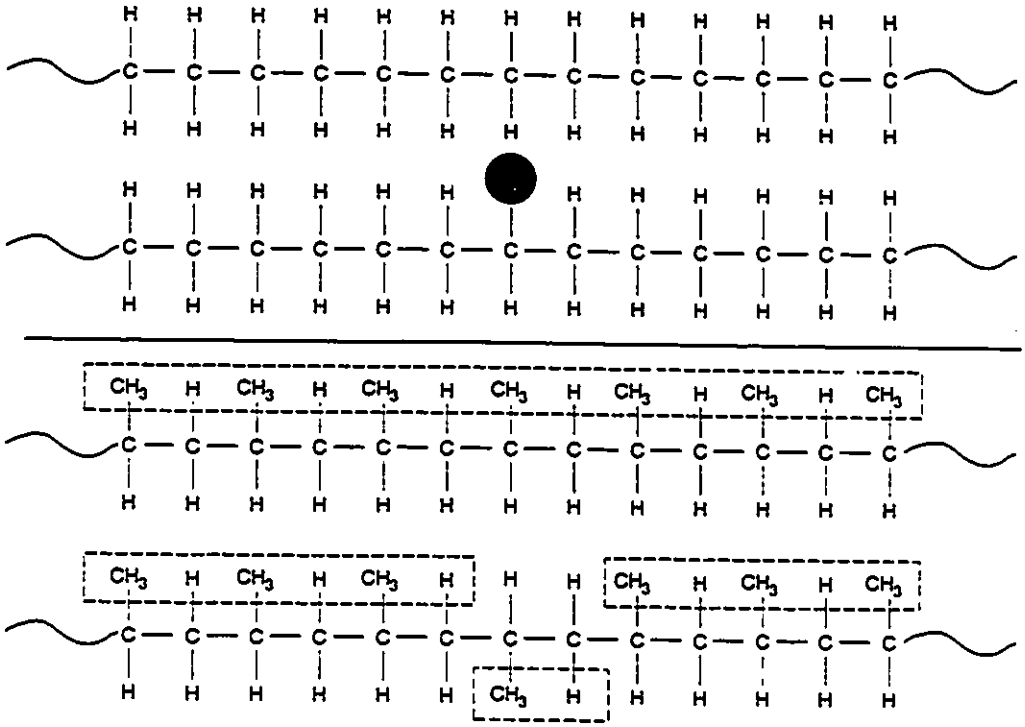

Figure 10 - Chain structure and crystallinity: Effect of short chain branching and stereoregularity.

In a similar manner, when considering a homopolymer that can experience stereoisomerism such as polypropylene, the crystallinity of the original chain can be altered by the introduction of the same monomer but in the inverse position, known as an atactic placement (lower chain in the figure). This polymer will be less crystalline than the one where all methyl groups are on the same side of the chain.

TREF makes use of the effect of these differences in molecular structure or solubility to fractionate the polymer chains.

TREF can be divided into two sequential stages, as illustrated in figure 11: Precipitation and Elution. In the precipitation step, the polymer is dissolved in a good solvent and put in contact with an inert support. Solvents commonly used are trichlorobenzene (TCB), o-dichlorobenzene (ODCB), xylene or α-chloronaphthalene. Usual supports are: Chromosorb P, glass beads, silica gel or stainless steel shots. The precipitation or crystallization is done under a well controlled, slowly decreasing temperature. Polymer fractions that remain in solution

are removed as the first TREF fraction. Mirabella (1987) proposed that the polymer coats the support in layers of different crystallinity as seen in greatly exaggerated dimension in the detail of this figure. The layers that are closer to the surface of the support were precipitated at higher temperatures and therefore are more crystalline than the external ones. This step can be performed in a stirred vessel or directly in the TREF column.

In the second step the polymer layers are eluted from the support in the reverse order they were precipitated. Solvent flows through a column packed with the polymer coated support while the temperature is slowly increased. If the column is connected to a mass concentration detector an elution curve is obtained on-line: less crystalline fractions elute first at lower temperatures while the most crystalline fractions are only eluted at higher temperatures at the end of the fractionation.

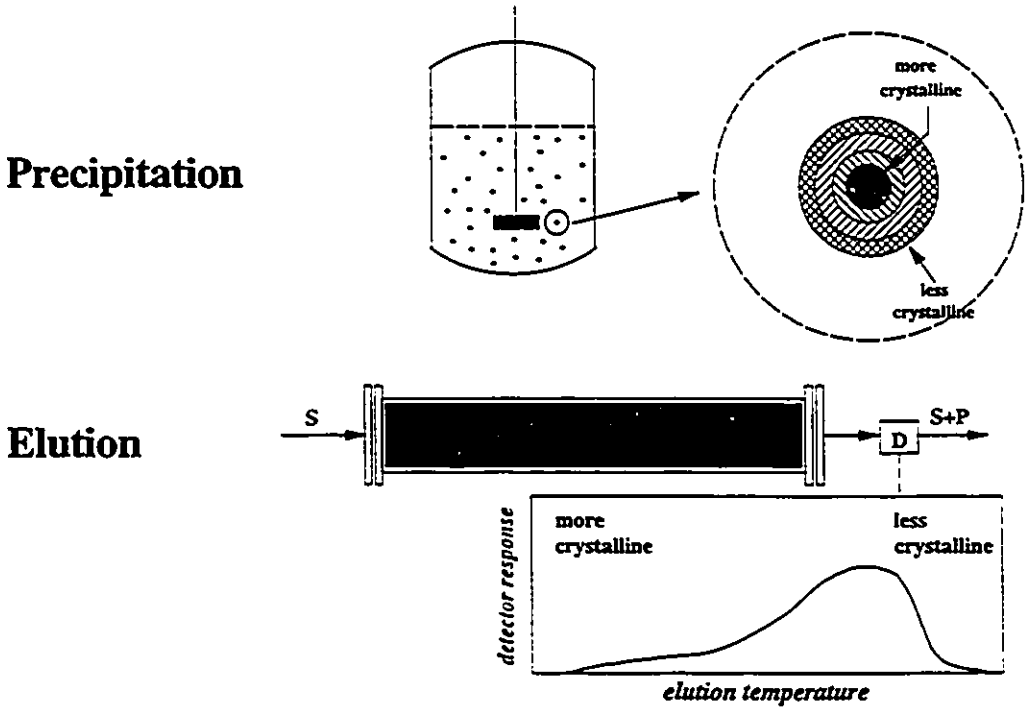

Figure 11 - Precipitation and elution stages of TREF fractionation.

TREF can be operated in two ways, in preparative or analytical mode. Preparative TREF is a separation technique in which polymer fractions are collected at predetermined temperature intervals. Those fractions are then analyzed offline to

determine their microstructures. Analytical TREF is an analytical technique in which the mass concentration of the eluted polymer is continuously monitored with an on-line detector. In this case no further analysis of the fractions is normally done if a calibration curve that relates elution temperature to the investigated property, for instance degree of short chain branching in LLDPE, was previously determined. Since standards of narrow composition distribution for TREF calibration are not easy to obtain, generally they have to be previously obtained by Preparative TREF.

The basic features of preparative and analytical TREF are shown in table 2. Preparative TREF requires larger columns to hold larger samples so that the fractions are big enough to be analyzed offline. Analytical techniques such as ^{13}C NMR, FTIR, DSC and GPC are commonly used on the fractions and give a wealth of information about the molecular structure of the polymer. Clearly, more information about the samples can be obtained by using preparative TREF than analytical TREF. Preparative TREF is, however, more time consuming than analytical TREF, not only in operation but also in the time required for filtering, drying and analyzing the fractions.

Generic TREF profiles of some common polyolefins are presented in figure 12. Atactic polypropylene has a disorganized molecular structure and therefore does not crystallize. It elutes as the first TREF fraction since it is soluble even at room temperature in the solvents commonly used. The crystallinity of LLDPE is decreased by the presence of short chain branches, causing it to elute at lower temperatures. Since there will be a distribution of branching, the TREF profile is broad and generally multimodal. The high temperature peak is generally attributed to HDPE, formed simultaneously with LLDPE in the reactor. Finally, highly isotactic polypropylene is also highly crystalline and since it is generally less soluble it elutes at temperatures even higher than polyethylene. Stereoregularity defects and monomer inversions can broaden the TREF profile as shown in the TREF response in figure 12.

Preparative TREF	Analytical TREF
Fractions are collected at predetermined temperature intervals	Continuous operation
Information about molecular structure is obtained offline by additional analytical techniques	Information about molecular structure is obtained online by means of a calibration curve
Requires larger columns and larger sample sizes	Requires smaller columns and smaller samples sizes
Time consuming but can generate detailed information about polymer microstructure	Faster than preparative TREF but generates less information about polymer microstructure

Table 2 - Comparison between analytical and preparative TREF.

The most important step in TREF fractionation is the sample crystallization. As mentioned before, during the crystallization step polymer chains of different crystallinity are separated. The elution step is simply the careful recovery of the already fractionated polymer. Therefore, one has to be very careful in order to avoid secondary effects such as cocrystallization and molecular weight influences during the precipitation step. This is accomplished by a slow cocling rate. Wild et al. (1982) suggested an upper limit of 2 °C/h for a variety of polyethylene types. This is evidently the limiting slow step of the technique. In the case of copolymers of polypropylene, for example, where it might be necessary to cool the polymer solution from 140 °C to room temperature, it takes about 2 1/2 days to complete the precipitation step.

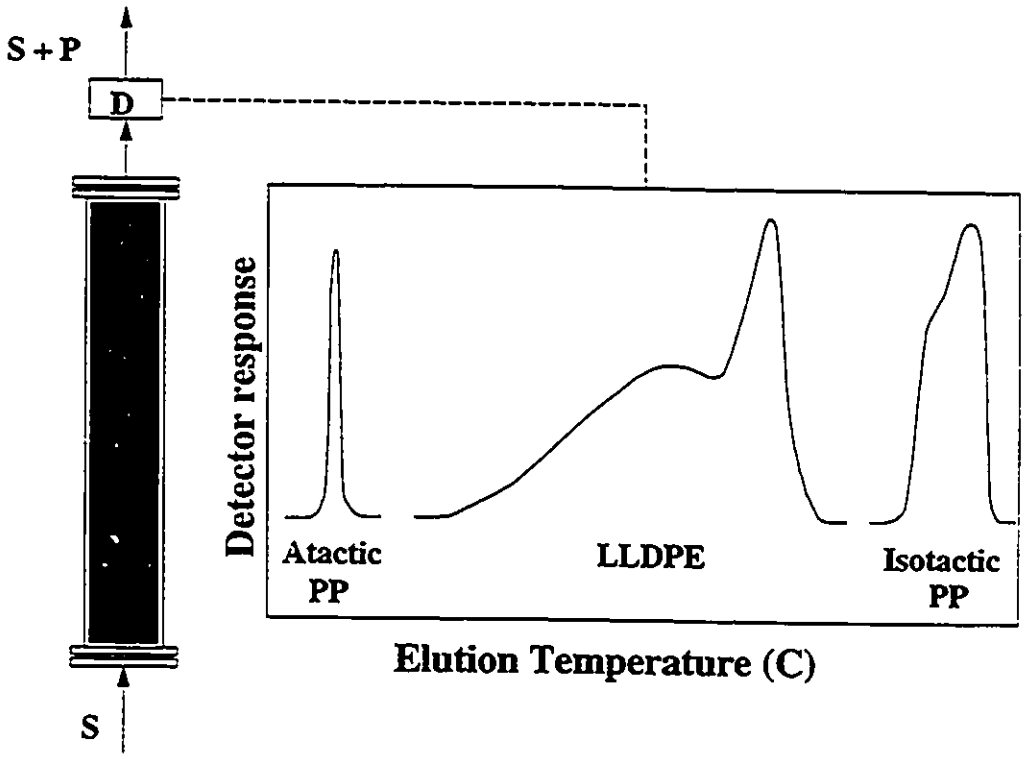

Figure 12 - Generic TREF profiles of some commercial polyolefins.

The effect of molecular weight on the fractionation of linear polyethylene of narrow molecular weight distribution was studied by Wild et al. (1982). The elution temperature is virtually molecular weight independent for values larger than 10,000. For shorter chains, the effect of the noncrystallizable chain ends (Flory, 1953) becomes more pronounced and the elution temperature decreases. It seems, therefore, that for common commercial copolymers of high molecular weight, the influence of molecular weight on TREF fractionation is negligible.

Cocrystallization is another concern when one deals with TREF. If chains of different structure crystallize at the same time, then TREF usefulness as a separation technique is severely reduced. However, if the precipitation step is done carefully, this does not seem to be the case. Wild (1982) compared the analytical TREF profile of a mixture of equal parts of 3 fractions of polyethylene obtained by preparative TREF with the analytical TREF profiles of the same fractions obtained individually. He found that there was very good agreement between the two curves and at least

for that case cocrystallization effects did not seem to be important. Similar results were reported for blends of HP-LDPE/LLDPE and EVA/LLDPE (Kelusky et al., 1987).

Solvent type does not seem to play a significant role in TREF as far as fractionation resolution is concerned. Glockner (1990) compared calibration curves for polyethylene using four different solvents (xylene, o-dichlorobenzene, trichlorobenzene, α-chloronaphthalene). The calibration curves were almost parallel. In general, the better the solvent, the lower the elution temperature for a polymer of a given molecular structure. Notice that this is also in excellent agreement with Flory's theory of melt point depression by solvents (Flory, 1953).

TREF has been mainly applied for characterizing polyolefins, especially polyethylenes, polypropylenes and their copolymers. Some applications have also been reported for polymer blends which are specially interesting for the evaluation of cocrystallization in TREF fractionation. Some extensive reviews of TREF applications have been published recently (Wild, 1990; Soares and Hamielec, 1994d).

High pressure low density polyethylene (HP-LDPE) was the first polyolefin to be studied by a TREF related technique. One of the earliest attempts to fractionate HP-LDPE according to degree of short chain branching in an apparatus based on increasing temperature fractionation was performed by Desreux and Spiegels (1950). Hawkins and Smith (1958) applied Desreux's technique to the, by that time, new HDPE produced by heterogeneous Ziegler-Natta catalysts. A linear relation between short-chain branching SCB and elution temperature was obtained for four types of HDPE and one type of HP-LDPE.

With a somewhat different approach, Shirayama et al. (1965) fractionated HP-LDPE according to molecular weight by the solvent gradient method. The fractions obtained were further fractionated according to SCB by a temperature elution method. It was found that SCB distribution was broader when the average molecular weight of the fractions was lower. Notice that this result is in good agreement with the Stockmayer bivariate distribution in which a broader composition distribution (or SCB distribution) is expected for chains with lower average molecular weights.

The acronym TREF was first proposed by Wild and Ryle (1977). The authors showed how the principles of increasing temperature fractionation could be adapted to an analytical technique to determine SCB of LLDPE. The suggested approach was to obtain fractions of narrow SCB distribution having different SCB averages using increasing temperature fractionation techniques (later called preparative TREF) and use them to determine a calibration curve of SCB as a function of elution temperature for the analytical TREF. A linear relation between SCB and elution temperature was obtained.

TREF also proved to be useful in fractionating "composite" HP-LDPE molecules synthesized by varying the operation conditions of different regions of an autoclave reactor (Bergstrom and Avela, 1979). A linear relation between methyl group concentration and elution temperature was only observed for a sample of LLDPE (ethylene-1-butene copolymer).

Nakano and Goto (1981) proposed a combination of analytical TREF and GPC in an automated composition fractionation-molecular weight distribution measurement mode. The TREF fractions were collected in a stepwise mode and directly injected in the GPC. Four low density polyethylenes (0.921-0.924) and one HDPE (0.978) and their mixture were analyzed to assess the usefulness of the system. The fractionation of one sample took about 10 h to complete. This analytical system is very attractive because it permits the determination of the complete bivariate distribution online. Care should be exercised, however, in the interpretation of the GPC results, since this technique is sensitive to the radius of gyration of a polymer in solution which depends both on molecular weight and chemical composition of the polymer (Hamielec, 1982).

Probably the most substantial work to date defining the applicability and limitations of analytical TREF was published by Wild et al. (1982) and has already been discussed in detail above. Optimal operation conditions, influence of molecular weight, determination of a calibration curve from fractions obtained using preparative TREF, and cocrystallization effects were covered in this paper.

TREF has also often been used to study the nature of polymerization catalysts. In a very interesting paper, Usami et al. (1986) compared four LLDPE samples made by different processes with one HP-LDPE sample. While the HP-LDPE sample presents a relatively narrow, low elution temperature range, all four LLDPE samples

show considerably broader and bimodal TREF profiles. All LLDPE samples were produced by different processes; therefore this behaviour could not be linked to reactor operation conditions. Since LLDPE was produced by catalytic processes, it was proposed that there were at least two different types of active sites on the catalyst, one producing almost exclusively linear homopolymer polyethylene and the other LLDPE of broad composition distribution.

Bimodal, broad TREF curves for LLDPE and narrower, unimodal curves for HP-LDPE were also observed by Wild et al. (1986) comparing three different LLDPE samples and one HP-LDPE sample using both analytical and preparative TREF. By cross-fractionation with SEC the authors concluded that the lower molecular weight species tended to be more branched, this dependence being more important for HP-LDPE than for LLDPE.

Hazlit and Moldovan (1989) and Hazlit (1990) proposed an automated analytical TREF apparatus in order to speed the fractionation using a modified process control GC analyzer. It is claimed that the system can fractionate eight samples of LLDPE in 24 hours. Four independent TREF columns are operated in parallel and data acquisition is done by a microprocessor. To achieve faster analysis rates the reported cooling and heating rates are much higher than those usually considered adequate to avoid molecular weight effects during the precipitation/fractionation.

Mirabella (1987a, 1987b) used analytical TREF to compare HDPE, HP-LDPE and LLDPE. TREF profiles of HDPE were unimodal and sharp, of HP-LDPE were unimodal and broad and of LLDPE were trimodal. DSC of TREF fractions showed that the melting point and heat of fusion increased with elution temperature, i.e., with decreasing amount of SCB.

Schouterdan et al. (1987) fractionated LLDPE by successive solution fractionation (molecular weight controlled) followed by analytical TREF. TREF curves of all molecular weight fractions were bimodal, except for the first one. DSC curves of the molecular weight fractions were also complex and multimodal. The authors concluded that the SCB is broader for the lower molecular weight fractions. Notice that this is again in agreement with Stockmayer's bivariate distribution in which the lower molecular weight species show broader composition distribution than the higher molecular weight ones.

Kulin et al. (1988) compared TREF with a liquid-liquid phase separation technique for the fractionation of HP-LDPE. The fractions were characterized by SEC, light-scattering, viscosity, IR, DSC and ^{13}C NMR. It was concluded that the fractionation mechanism of the liquid-liquid method was regulated by molecular weight while TREF was regulated by SCB. However, TREF did not seem to fractionate well according to long chain branching, supposedly because the levels of long chain branches are much smaller than that for short chain branches (< 3/1000 C atoms) and behave essentially as main chains and therefore have little effect on chain crystallinity.

Vela-Estrada and Hamielec (1993) reviewed some techniques to determine the bivariate distribution of semicrystalline and amorphous copolymers. For crystalline copolymers the combination of TREF and GPC is suggested as the most efficient method. For amorphous copolymers GPC and adsorption HPLC has been successfully employed in some cases. Some results of their preparative TREF fractionation of ethylene/octene-1 copolymers were also shown.

Wilfong (1990) used analytical TREF to study the crystallization behaviour of ethylene/octene-1 copolymers. Small Angle Light Scattering was used to determine spherulite size, and it was found that it decreased with increasing degree of short chain branching.

Kakugo (1991) analyzed ethylene-1-hexene copolymers using TREF and determined a trimodal composition distribution. This was attributed to the presence of three types of catalyst sites: the most common producing 1-hexene rich random copolymer, the intermediate, ethylene rich random copolymer, and the least numerous a copolymer containing long sequences of ethylene.

The influence of sequence length distribution on TREF fractionation was studied by Karbashewsky et al. (1993). From the comparison of four LLDPE samples with different degrees of comonomer "blockiness", it was concluded that a universal calibration curve relating elution temperature to degree of SCB can not be obtained since TREF is influenced by the comonomer sequence length distribution of the copolymer.

Few works have been published about TREF fractionation of polypropylene. While the TREF fractionation of LLDPE is regulated by SCB, the fractionation of polypropylene is determined mainly by the stereoregularity of the polymer chains.

One of the first attempts to fractionate isotactic polypropylene by an increasing temperature fractionation technique was reported by Wijga et al. (1960) and compared to the fractionation of polypropylene by the elution gradient method (in which the fractionation is done by increasing the fraction of solvent in a solvent/non-solvent mixture at constant temperature). The first method was concluded to be regulated mainly by molecular weight while the second by both molecular weight and stereoregularity of the polypropylene molecules.

Probably the first insight on the leading mechanism regulating the efficiency of TREF fractionation was reported by Kamatah and Wild (1966). The fractional crystallization of polypropylene from dilute solution was found to be mostly dependent on stereoregularity and almost independent of molecular weight. The precipitations were done in a flask at constant temperature under conditions such as "*the molecules should certainly be able to precipitate out of solution according to their crystallizability under tantamount equilibrium conditions and without experiencing any physical hindrance from neighbouring molecules.*" The refining of those ideas would lead to the development of TREF in its modern form.

Mainly isotactic polypropylene made by a $TiCl_4/MgCl_2$ catalyst with and without electron donors was fractionated by Kioka et al. (1994) over a wide temperature range (-65°C to 140°C). The samples made without electron donor showed much broader distributions of molecular weight and isotacticity. The average molecular weight of the fractions increased with elution temperature, but not enough to suggest that the fractionation was influenced by molecular weight effects. Melting point and isotacticity indexes also increase with elution temperature indicating that the fractionation mechanism is controlled by stereoregularity.

TREF curves of polypropylene synthesized using a titanium-based heterogeneous Ziegler-Natta catalyst and using a chiral metallocene/aluminoxane catalyst were compared by Soares and Hamielec (1994d). The TREF profile of polypropylene made with the heterogeneous catalyst is significantly broader than the TREF profile of the polypropylene made with the metallocene catalyst. This supports the hypothesis of the presence of multiple-site types in heterogeneous Ziegler-Natta catalysts as opposed to one or few site types for metallocene catalysts.

Other copolymers besides LLDPE have also been investigated by TREF, mainly propylene/ethylene or propylene/higher α-olefin elastomers and impact copolymers.

Kakugo et al. (1988) used preparative TREF to investigate the active catalytic sites during the formation of ethylene-propylene and propylene-1-butene copolymers. The fractions were analyzed by ^{13}C NMR and the authors concluded that the lower isospecific catalytic centers were more active toward ethylene but that its activity did not change as much for 1-butene.

Kakugo et al. (1989) also fractionated random ethylene-propylene copolymers made by three different catalytic systems by preparative TREF and solvent extraction. Using ^{13}C NMR they found that their samples were a mixture of polyethylene, random copolymer and copolymer containing long sequences of ethylene.

Cheng and Kakugo (1991) combined preparative TREF with ^{13}C NMR to characterize compositional heterogeneity in ethylene-propylene copolymers produced by a Ti based heterogeneous Ziegler-Natta catalyst. The triad sequences of each fraction were determined by ^{13}C NMR. Using these measurements, reaction probabilities and relative weight fractions were estimated for different multiple-site statistical models. A Bernoullian model containing 3 to 4 active site types gave the best data representation.

Another copolymer of great commercial importance studied by TREF is the high impact copolymers of propylene and ethylene. This copolymer is produced in at least two reactors in series. Only propylene is fed to the first reactor, and it makes isotactic polypropylene. The effluent of the first reactor is fed to the second reactor as well as a mixture of propylene and ethylene. In this way, the effluent of the second reactor contains a mixture, at a molecular level, of polypropylene and propylene-ethylene copolymer. The copolymer portion is rubbery and helps to dissipate stress, making the brittle polypropylene more resistant to impact. A lot of speculation about the nature of this copolymer can be found in the literature and the use of TREF is probably the most efficient way to solve this puzzle.

Mirabella (1992, 1993) was the first to fractionate this polymer by analytical TREF, identifying three different copolymer zones. The rubbery propylene-ethylene copolymer fractions are soluble at room temperature (zone 1). At somewhat higher temperatures, fractions of crystallizable ethylene-propylene copolymer are present (zone 2). Unexpectedly, at even higher temperatures, a fraction of ethylene rich copolymer can be recovered (zone 3). Finally, isotactic polypropylene formed in the first reactor is recovered in the end of the fractionation. Similar results were also reported by Usami et al. (1993) and Soares and Hamielec (1994d).

In a recent paper, Mirabella (1994) proposed a method to determine the ethylene concentration distribution in random copolymers of ethylene and propylene with fractions of ethylene varying from 1 to 5 weight percent. A calibration curve for analytical TREF was obtained from analytical TREF analysis of preparative TREF fractions. It was found that the content of ethylene in the copolymer correlated adequately with the weight-average elution temperature of the analytical TREF chromatograms of the preparative TREF fractions. TREF curves of several commercial ethylene-propylene random copolymers were shown to be broad and significantly different in shape. Unfortunately no information about catalyst type and reactor operation conditions for production of the copolymer samples analyzed by TREF was presented.

Nuclear Magnetic Resonance (NMR)

Nuclear magnetic resonance (NMR) spectroscopy, especially ^{13}C NMR, is now a well established analytical technique for the investigation of the microstructure of polymer chains.

^{13}C nuclei act as magnets and can interact with an externally applied magnetic field, assuming one of two possible orientations or states (parallel or antiparallel to the magnetic field) that have different energies. If radio waves of proper frequency irradiate the nuclei, the ones at the lower energy state change to the higher energy state (resonance). The electron clouds surrounding the nuclei also act as magnets under an externally applied magnetic field. These local fields act in opposition to the applied field so that every non-equivalent nucleus in a molecule feels a slightly

different magnetic field. Because of this phenomenon, it is possible to observe sharp resonance lines for each non-equivalent kind of carbon atom in the molecule with ^{13}C NMR (McMurry, 1984).

The use of ^{13}C NMR has several advantages over other techniques for studying polymer microstructure, such as Fast Fourier Transform Infra-Red spectroscopy (FT-IR). Firstly, ^{13}C NMR is a quantitative technique, i.e., each resonance area is proportional to the number of contributing species (Randall, 1977). FT-IR is also frequently used to determine the composition of ethylene-propylene copolymers but it requires a calibration curve to generate quantitative results. Besides, there is still some controversy about peak assignments (Corish, 1961; Smith et al., 1962; Drushel and Iddings, 1963; Corish and Tunnicliffe, 1964; Wei, 1969; Gardner et al., 1973). Secondly, ^{13}C NMR is more sensitive to subtle structural details than FT-IR. Chemical shift differences can be caused by rearrangement of repeat units, head-to-tail inversions, configuration sequences from two to seven units in length, and stereochemical configurations (Randall, 1977).

Chemical shifts for isotactic, syndiotactic and atactic polypropylene as well as for ethylene-α-olefin copolymers have been extensively reported in the literature. The classic reference for these polymers is certainly the book by Randall (1977) but several other complementary studies have been published (Carman and Wilkes, 1971; Carman et al., 1973; Ray et al., 1977; Randall, 1978a; Kakugo et al., 1982; Zhu et al., 1983; Kissin and Brandolini, 1991).

^{13}C NMR spectra have been used to calculate reactivity ratios, number average sequence lengths of comonomer blocks, tacticity, and copolymer average composition of polyolefins (Randall, 1978b; Cheng, 1984; Martuscelli et al., 1985; Abis et al., 1986; Locatelli et al., 1988).

Reaction probability models have also been extensively used in conjunction with ^{13}C NMR spectra to study kinetics and mechanism of polymerization by Ziegler-Natta catalysts (Carman et al., 1977; Cheng, 1982; Doi et al., 1983; Ionue et al., 1984; Hayashi et al., 1988; Cheng, 1988).

Mathematical Modelling

As suggested by Ray (1988), mathematical models for polymerization processes can be divided in three levels, microscale, mesoscale and macroscale. At the *microscale* level, chemical phenomena occur that are the main cause of the molecular weight and chemical compositional characteristics of the polymer. Interphase and intraphase phenomena take place at the *mesoscale* level, such as heat and mass transfer in the polymeric particle and its boundary layer. The macroscopic behaviour of the reactor, such as imperfect mixing, residence-time distribution, gas-liquid mass transfer and heat of reaction removal are described at the *macroscale* level. The final application of the model determines the degree of complexity required in each level. Figure 13 depicts schematically these three levels of mathematical modelling.

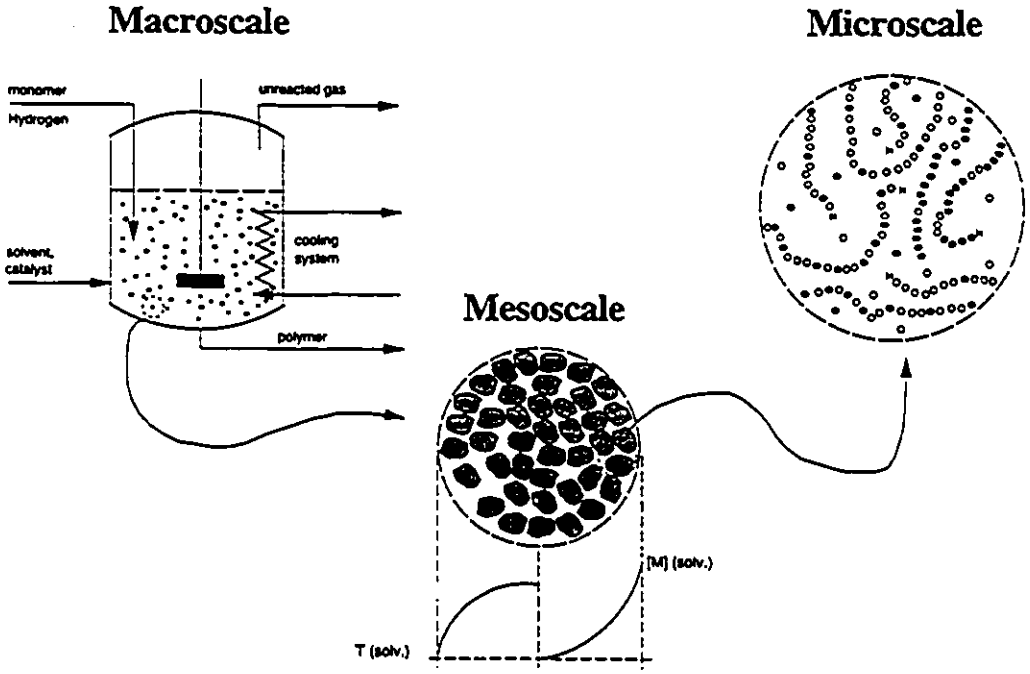

Figure 13 - Levels of mathematical modelling.

The very broad molecular weight distribution (MWD), broad composition chemical distribution (CCD), and reaction rate decay observed in heterogeneous and in some homogeneous Ziegler-Natta catalyzed polymerizations have been the

subject of considerable study. It is believed that physical and chemical phenomena at the microscale and mesoscale levels are mainly responsible for this characteristic behaviour of Ziegler-Natta catalysts.

Different explanations for this unusual phenomenon have been proposed, but most of them can be classified into two main categories. One proposes that mass and heat transfer resistances during polymerization are entirely responsible for the phenomena while the other neglects transfer effects and explains the same phenomena invoking the existence of multiple catalytic active site types.

Polymerization with heterogeneous Ziegler-Natta catalysts involves complicated phenomena. In the early stages of polymerization, the original catalyst, be it supported or not, is broken up by the nascent polymer and the catalyst fragments are dispersed in the growing polymer. As the polymerization proceeds, this *polymeric particle* grows due to monomer propagation reactions as new polymer molecules form. Based on this well known experimental evidence (Boor, 1979; Wilchinsky et al., 1973; Kakugo et al., 1989; Buls and Higgins, 1970; Hock, 1966) some researchers advocate that, due to diffusion resistances, catalyst fragments in different radial positions are exposed to different monomer and hydrogen concentrations (the main chain transfer agent) and consequently produce polymer with chain length averages which differ spatially. For copolymerization, different monomer transfer rates and reactivities may be responsible for spatial compositional heterogeneity in the polymeric particle. In addition, if there is appreciable heat transfer resistance, hot spots can occur inside the polymer particle altering reaction rates and increasing the polymer molecular weight and compositional heterogeneity, causing broad MWD and CCD.

Different mathematical models have been proposed based on this approach. Some are very simplified pictures of the polymerization process and are only useful as reference for comparison with more sophisticated models. Among those the most usual are the solid core model and the polymeric core model. With the first, the catalyst breakup is not modelled and the polymer is considered to grow around a solid catalyst core containing all active sites on its surface. This model using a single site catalyst type cannot predict broad MWD. With the second, polymer grows around a non-expanding polymeric core formed by polymer and catalyst particles. Although

this model is an improvement over the first one, it still is not able to explain the complex behaviour of heterogeneous Ziegler-Natta polymerization, the broad MWD and CCD.

The models that best represent the polymerization in this category of single site type transfer controlled models are the so-called *expansion models*. Two will be considered in detail below: the polymeric flow model and the multigrain model.

With the polymeric flow model, growing polymer and catalyst particles are considered to form a continuum. Diffusion of reagents as well as heat transfer occurs in this polymeric particle. If the reaction is diffusion controlled the monomer concentration profiles in the particle may cause MWD and CCD broadening. The effective mass and heat transfer parameters in the polymeric particle have to be estimated to use this model.

On the other hand, the multigrain model considers two levels of mass and heat transfer. The polymeric particle, called *macroparticle* in this model, is formed by an agglomerate of *microparticles*. Each microparticle consists of a solid catalyst particle, with all the active sites on its surface, surrounded by growing polymer. The number of microparticles and the transfer parameters in the microparticle and macroparticle have to be estimated in this model.

Figure 14 depicts the generic representation of those four models. In this figure, the black circles indicate catalyst cores containing catalyst sites on the surface, shadowed areas represent a mixture of catalyst fragments surrounded by growing and terminated polymer chains, and the white areas indicate growing and terminated polymer chains free of catalyst fragments. The relative dimensions are not in scale.

In the second category, heat and mass transfer resistances are neglected and a multiple number of active site types is proposed based also on vast experimental evidence (Boor, 1979; Zucchini and Cecchin, 1983; Usami et al., 1986; Cheng and Kakugo, 1991; Cozewith and VerStrate, 1971; Keii, 1982; Keii et al., 1984; Spitz, 1987; Chien et al., 1985). Each site has its own kinetic constants and produces polymer with often very different MWDs, CCDs, and stereoregularity.

Recently, due to the realization that both phenomena, multiple active site types and transfer resistances, may contribute simultaneously to the actual behaviour of heterogeneous Ziegler-Natta catalysis, models combining these two approaches

have been proposed. Both the polymeric flow model and the multigrain model were modified to include more than one active site type (Galvan and Tirrell, 1986b; Floyd et al., 1988).

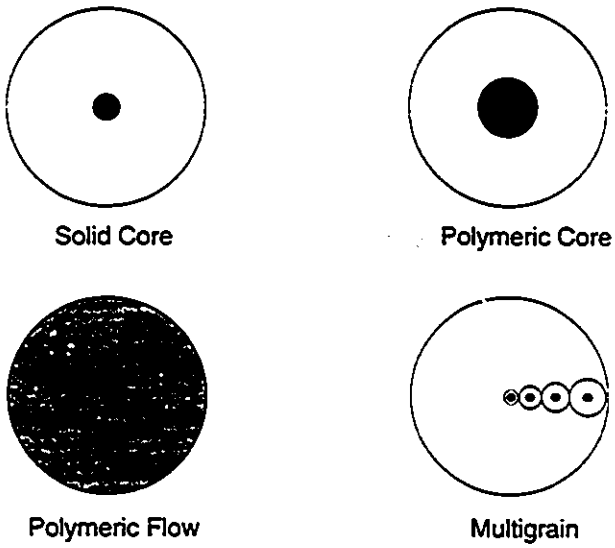

Figure 14 - Some important physical models for heterogeneous Ziegler-Natta polymerization.

Since there is no formal nomenclature regarding mathematical models for Ziegler-Natta polymerization it is important to define certain terms that will be used to describe these models in the following paragraphs. Models that consider only mass and heat transfer resistances will be called *physical models*. Models that disregard these effects and utilize more than one active catalytic site type will be called *chemical models*. Models that combine these two approaches will be called *hybrid models*.

Schmeal and Street (1971,1972) compared the ability of four different physical models to predict polymerization rate decay and MWD broadening, using very simple kinetics. The solid core model, polymeric core model, polymeric flow model and a non-expanding polymeric flow model, called by the authors base model, were compared. All four models were able to predict rate decay when the reaction was diffusion controlled. For this case, all but the solid core model could predict

broad MWD (large polydispersities). For the same conditions, the larger polydispersity was predicted by the polymeric flow model. When the reaction was not diffusion controlled, the predictions of the four models were practically the same.

Singh and Merrill (1971) compared three different physical models: the polymeric core model, the polymeric flow model and a variation of the polymeric flow model in which the active center concentration is considered uniform and constant, named uniform site conservation model by the authors (USC). All three models were able to anticipate MWD broadening for high values of the Thiele modulus. For the same conditions, the USC model predicted the highest polydispersity.

Brockmeier and Rogan (1976) adjusted the solid core model to data collected in a semi-batch reactor and used this model to predict the behaviour of a continuous reactor. The predictions were accurate for polymer yield. No molecular weight results were shown.

Chien (1979) proposed some criteria to evaluate the relative importance of diffusion resistance in Ziegler-Natta polymerization. Some of these criteria were based on experimental evidence while others were based on mathematical models. Applying his criteria to data from different sources, he found that for all cases studied, except for Phillips catalyst, diffusion resistances were negligible.

Nagel et al. (1980) compared the solid core model with the multigrain model for homopolymerization of ethylene or propylene. The solid core model could not predict MWD broadening even for extreme reaction conditions. On the other hand, the multigrain model could predict polydispersities up to 7 using reasonable physical parameters. The more sensitive parameters in the model were the effective diffusivity in the macroparticle and the number of microparticles in one macroparticle. Those parameters determine the monomer diffusion rate in the macroparticle. In other words, the penetration levels for monomer in different regions of the growing macroparticle are the main cause of broader MWD's or larger polydispersities.

Taylor et al. (1983) presented a comprehensive review of polymerization models for heterogeneous Ziegler-Natta catalysis, with focus on the physical models. The multigrain model was presented as the most detailed and likely most valid model to date, followed by the polymeric flow model.

Floyd et al. (1986a, 1986b, 1986c) applied the multigrain model in an extensive and detailed study of heat and mass transfer resistances for the homopolymerization of ethylene and propylene in slurry and gas-phase reactors. Intraparticle as well as interparticle resistances were analyzed. For the case of slurry reactors, gas-liquid mass transfer resistances were evaluated for sparged and unsparged reactors. They concluded that: (1) in most cases, intraparticle temperature gradients are negligible; (2) concentration gradients in the macroparticles are likely to be more important in slurry reactors while for gas-phase reactors these gradients may be significant in the microparticles; (3) interparticle effects are negligible except for high activity catalysts; (4) gas-liquid mass transfer effects are generally negligible for sparged reactors but can be important for unsparged reactors. A methodology was proposed to predict when this factor could be determinant.

Galvan and Tirrell (1986b) used a hybrid model to study MWD broadening in propylene polymerization. They modified the polymeric flow model by including active site types. Even when diffusion effects were not important, the model could predict broad MWD's, provided that the difference in reactivities at the two site types was large enough. The broadening of MWD was attributed to the presence of multiple site types and not to diffusion effects. The numerical method used, orthogonal collocation, was introduced in a previous paper (Galvan, 1986a) to solve the conventional polymeric flow model. However, his formulation was in error making the position of the collocation points time dependent.

Honig et al. (1987) modeled the polymerization rate and MWD for butadiene polymerization for a soluble Ziegler-Natta catalyst using a chemical model. Only one site was used. The model fit well monomer conversion and number average molecular weight but underpredicted mass average molecular weight.

Floyd et al. (1987) presented a comprehensive review of the applications of the multigrain model including an extension for multiple site types. Heat and mass transfer effects were analyzed. The authors recognized that intraparticle effects alone could not account for the broad MWD observed with heterogeneous Ziegler-Natta catalysts, although it could provide some broadening of the MWD. The main influence of intraparticle transfer effects was on the apparent polymerization rate. Intraparticle temperature effects were only important in gas phase reactions for highly active and large catalyst particles. Mass diffusion effects, however, could

play an important role even for low activity catalysts early in the polymerization. These conclusions were confirmed and extended in a subsequent paper (Floyd, 1988).

Hutchinson and Ray (1988) used the multigrain model to analyze the influence of monomer adsorption on the surface of the microparticle. In the multigrain model, before diffusing into the microparticle, the monomer has first to adsorb on the outer surface of the microparticle formed by the growing polymer. Rate enhancement in copolymerization and differences between slurry and vapor phase reaction were explained based on differences of solubilities in each case. The more crystalline the polymer layer, the lower are the solubility and effective diffusion coefficient of the monomer.

Ray (1988) presented a detailed review of the multigrain model. The main conclusion was that multiplicity of site types was the principal factor in explaining the typical behaviour of Ziegler-Natta catalysts (broad MWD and CCD) but heat and mass transfer effects could play an important role, especially for highly active and large size catalyst particles.

De Carvalho et al. (1989) proposed a multisite type model for olefin copolymerization with very detailed kinetics. The model was able to predict broad MWD's as well as broad CCD's. A methodology to estimate the model parameters using TREF, GPC and NMR was proposed.

Rincon-Rubio et al. (1990) applied a two-site model for the homopolymerization of propylene. Parameters were estimated from semi-batch experiments in a slurry reactor. Good results were obtained for polymerization rate, polymer yield and number average molecular weight but not for polydispersity.

McAuley et al. (1990) applied the model after de Carvalho et al. (1989) for two-site types to simulate the copolymerization of ethylene and α-olefins in a fluidized bed reactor. No diffusion effects were considered. The model could track industrial data for a UNIPOL reactor reasonably well.

Lorenzi et al. (1991) presented a multisite type model for high temperature, high pressure polymerization of ethylene and butene-1 (220 - 260 °C, 800 bar). No diffusional effects were considered. The experimental runs were done in a high-pressure continuous reactor and the polymer was analyzed by IR and GPC. The model was fit to the experimental data by minimizing one objective function

comprising differences in polymer production rate, number and weight average molecular weight, short chain-branching (or copolymer composition) and double bond index between experimental and calculated results. Three site types were necessary to fit the model to the experimental data.

Sarkar and Gupta (1991) proposed a new model called polymeric multigrain model that combines features of the multigrain model with some of the more simplified flow models. The authors found that their model could predict higher polydispersities than the multigrain model for single site, non-deactivating catalysts.

Hutchinson et al. (1992) further expanded the multigrain model to describe particle growth and morphology.

CHAPTER 3 - MATHEMATICAL MODELLING OF MASS AND HEAT TRANSFER RESISTANCES IN THE POLYMERIC PARTICLE

Model Development

This chapter defines the microscale and mesoscale mathematical models. These models describe the kinetics of polymerization, the presence and nature of active site types, mass and heat transfer resistances, and the growth of the polymer particle. Macroscale models for the simulation of CSTRs in series are covered in chapter 4.

Two models describe reasonably well the phenomena at the mesoscale level during a polymerization using a heterogeneous Ziegler-Natta catalyst: the polymeric flow model and the multigrain model.

Despite the more comprehensive description of the mesoscale phenomena achieved by the multigrain model, much of the results presented in the literature seem to justify the use of the simpler model, particularly in view of the much greater importance of multiple site types compared to transfer resistances for these polymerizations. Transfer resistances may in most cases be considered a second-order effect, with multiple site types, a first-order effect.

From the extensive works published in the literature using the multigrain model (Taylor et al., 1983; Nagel et al., 1980; Floyd et al., 1986a, 1986b, 1986c, 1987, 1988) , the most important mass and heat resistances for almost all of the cases studied were found to be at the macroparticle level. One possible exception happens during gas-phase polymerization using highly active catalysts, when mass transfer limitations in the microparticles may be significant. Besides, it is very difficult to precisely estimate the effective transfer parameters in both microparticle and macroparticle. Additionally, the number of microparticles in one macroparticle is an adjustable parameter that can only be estimated arbitrarily.

For the polymeric flow model it is necessary to estimate transfer parameters only for the whole polymeric particle. It also can predict reasonably high polydispersities, as shown by Schmeal and Street (1971, 1972), Singh and Merrill (1971) and Galvan and Tirrel (1986a, 1986b).

In the model developed herein (the polymeric multilayer model) the particle is divided into concentric spherical layers as in the multigrain model but microparticles are not considered. Initially all layers have the same concentration of active sites as the whole particle, i.e., there is no radial profile of active site concentration. Monomer concentration and temperature are calculated at the boundaries of each layer using a 3 point Lagrangian interpolation polynomial (Crank, 1990). Average concentrations of monomer in the layers are used to calculate the population balance equations of the layers in each time interval. The volume of each layer is updated according to the amount of polymer formed in that time interval. The monomer and temperature profiles are recalculated for the new boundary positions and the process is repeated for the next time interval. The species present in the layers are not allowed to cross its boundaries.

The convenience of this approach will be noticed in the following derivations. The population balances derived for each layer are the same as those for a model with no mass and heat transfer resistances. If these resistances are found to be of little importance the same equations can still be used with the bulk monomer concentrations.

Additionally, the multilayer model estimates the distributions of molecular weight and chemical composition for each site type, model layer, and whole polymer particle using a theoretically sound equation, Stockmayer's bivariate distribution. The former expansion models published in the literature could only estimate molecular weight and composition averages.

A schematic picture of the polymeric multilayer model is shown in figure 1.

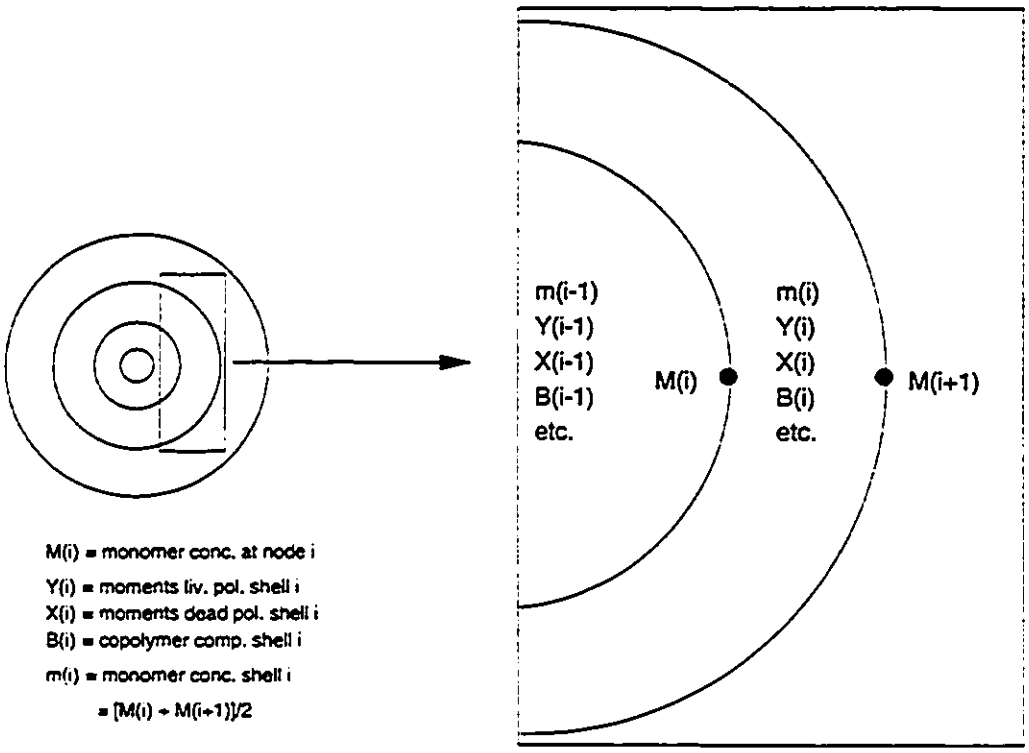

Figure 1 - Schematic representation of the polymeric multilayer model.

Kinetics

The reaction kinetics include steps of site formation, initiation, propagation, transfer to monomer, transfer to co-catalyst, transfer to hydrogen, spontaneous transfer (such as β-hydride elimination), deactivation and reaction with impurities.

In the kinetic equations below, N^* stands for a potential catalyst site, N represents a live polymer chain (a live polymer chain is chemically bonded to the active metal centre) and Q is a dead polymer chain. Monomer molecules are indicated by M, cocatalyst by A, hydrogen by H_2 and impurities by IM. The subscript j indicates active site type, i and k are monomer types either chemically bound to active centers or free in the reactor. Finally r,0 and l represent chain length of the polymer molecule.

Site Formation:	$N^*(j)+A \rightarrow N(0,j)$	$k_f(j)$
Initiation:	$N(0,j)+M_i \rightarrow N_i(1,j)$	$k_{i_i}(j)$
Propagation:	$N_i(r,j)+M_k \rightarrow N_k(r+1,j)$	$k_{p_{ik}}(j)$
Transfer to monomer:	$N_i(r,j)+M_k \rightarrow N_k(1,j)+Q(r,j)$	$k_{tm_{ik}}(j)$
Transfer to co-catalyst:	$N_i(r,j)+A \rightarrow N_2(1,j)+Q(r,j)$	$k_{tA_i}(j)$
Transfer to hydrogen:	$N_i(r,j)+H_2 \rightarrow N_H(0,j)+Q(r,j)$	$k_{tH_i}(j)$
	$N_H(0,j)+M_i \rightarrow N_i(1,j)$	$k_{H_i}(j)$
	$N_H(0,j)+A \rightarrow N_2(1,j)$	$k_{H_A}(j)$
Spontaneous transfer:	$N_i(r,j) \rightarrow N_H(0,j)+Q(r,j)$	$k_{ts_i}(j)$
Deactivation:	$N_i(r,j) \rightarrow N_d(j)+Q(r,j)$	$k_{d_i}(j)$
	$N_H(0,j) \rightarrow N_d(j)$	$k_{d_i}(j)$
	$N(0,j) \rightarrow N_d(j)$	$k_{d_s}(j)$

Reaction with impurities:

$$N_i(r,j)+IM \rightarrow N_{dIM_H}(0,j)+Q(r,j) \qquad k_{dIM}(j)$$

$$N_H(0,j)+IM \rightarrow N_{dIM_H}(0,j) \qquad k_{dIM}(j)$$

$$N(0,j)+IM \rightarrow N_{dIM}(0,j) \qquad k_{dIM}(j)$$

$$N_{dIM_H}(0,j) \rightarrow N_H(0,j)+IM \qquad k_a(j)$$

$$N_{dIM}(0,j) \rightarrow N(0,j)+IM \qquad k_a(j)$$

Implicit in the kinetic equations above is the concept of the terminal model for copolymerization, as described by Hamielec et al. (1983, 1987, 1989). In a few words, the terminal model assumes that the reactivity of the growing polymer molecules depends only on the monomer molecule chemically bonded to the chain at the active site.

Monomer Profile

The monomer radial profile in the polymeric particle can be described by the diffusion-reaction equation in spherical polar coordinates (Froment and Bischoff, 1979):

$$\frac{\partial M_i}{\partial t} = D_{M_i}\left(\frac{2}{r}\frac{\partial M_i}{\partial r}+\frac{\partial^2 M_i}{\partial r^2}\right)-R_{p_i} \tag{1}$$

where the total polymerization rate of monomer type i is expressed by:

$$R_{p_i} = M_i \sum_{j=1}^{n} k_{p_{Ti}}(j) Y_0(j) \tag{2}$$

$Y_0(j)$ is the total concentration of live chains on active sites of type j, defined by the equation:

$$Y_0(j) = \sum_{i=1}^{m}\sum_{r=1}^{\infty} N_i(r,j) \quad = \quad \sum_{r=1}^{\infty} N_T(r,j) \tag{3}$$

Only propagation reactions are considered when calculating the polymerization rate since the consumption of monomer by other reaction types is generally negligible. This hypothesis is valid for long chains and is known as *long chain approximation* (Biesenberg and Sebastian, 1983).

The following initial and boundary conditions apply:

$$M_i(r,0) = 0 \tag{4}$$

$$\frac{\partial M_i}{\partial r}(0,t) = 0 \tag{5}$$

$$M_i(R,t) = M_{i_0} \tag{6}$$

Temperature Profile

The temperature radial profile is expressed by the conduction heat transfer equation in spherical polar coordinates (Froment and Bischoff, 1979):

$$\frac{\partial T}{\partial t} = \frac{k_e}{\rho_p C_p}\left(\frac{2}{r}\frac{\partial T}{\partial r} + \frac{\partial^2 T}{\partial r^2}\right) - Q_p \tag{7}$$

where the total heat of polymerization is expressed as:

$$Q_p = \sum_{i=1}^{m}\left(-\Delta H_{p_i}\right) M_i \sum_{j=1}^{n} k_{p_{T_i}}(j) Y_0(j) \tag{8}$$

The following initial and boundary conditions apply:

$$T(r,0) = T_0 \tag{9}$$

$$\frac{\partial T}{\partial r}(0,t) = 0 \tag{10}$$

$$T(R,t) = T_0 \tag{11}$$

Population Balances

Population balances for the active species are defined for each concentric layer. We use pseudo-kinetic rate constants in these equations to simplify the mathematical treatment (Hamielec and McGregor, 1983). The pseudo-kinetic rate constants concept permits the description of copolymerization with the same expressions used for homopolymerization when appropriate pseudo-kinetic rate constants are defined.

The following pseudo-kinetic rate constants, which are consistent with the terminal model for copolymerization, are used in the model:

$$k_i(j) = \sum_{i=1}^{m} k_{i_i}(j) f_i \tag{12}$$

$$k_p(j) = \sum_{i=1}^{m} \sum_{k=1}^{m} k_{p_{ik}}(j) \phi_i(j) f_k \tag{13}$$

$$k_{p_k}(j) = \sum_{i=1}^{m} k_{p_{ik}}(j) \phi_i(j) \tag{14}$$

$$k_{tm}(j) = \sum_{i=1}^{m} \sum_{k=1}^{m} k_{tm_{ik}}(j) \phi_i(j) f_k \tag{15}$$

$$k_{tH}(j) = \sum_{i=1}^{m} k_{tH_i}(j) \phi_i(j) \tag{16}$$

$$k_H(j) = \sum_{i=1}^{m} k_{H_i}(j) f_i \tag{17}$$

$$k_{tA}(j) = \sum_{i=1}^{m} k_{tA_i}(j) \phi_i(j) \tag{18}$$

$$k_{ts}(j) = \sum_{i=1}^{m} k_{ts_i}(j) \phi_i(j) \tag{19}$$

The mole fraction of monomer i at the active center, f_i, and the fractions of growing chains on site type j terminating with monomer i, $\phi_i(j)$, are defined by the equations:

$$f_i = \frac{M_i}{\sum_{i=1}^{m} M_i} \tag{20}$$

$$\phi_i(j) = \frac{\sum_{r=1}^{\infty} N_i(r,j)}{\sum_{i=1}^{m} \sum_{r=1}^{\infty} N_i(r,j)} \tag{21}$$

We can calculate $\phi_i(j)$ by making the stationary state hypothesis (Hamielec and McGregor, 1983). For a multicomponent copolymerization with m different types of monomers we can define m-1 equations of the form:

$$\sum_{i=1,\neq k}^{m} k_{p_{ik}}(j)\phi_i(j)f_k - \sum_{i=1,\neq k}^{m} k_{p_{ki}}(j)\phi_k(j)f_i = 0 \quad k = 1, m-1 \tag{22}$$

Those m-1 equations can be solved together with,

$$\sum_{i=1}^{m} \phi_i - 1 = 0 \tag{23}$$

to obtain the fractions of growing chains on site type j terminating with each type of monomer that participates in the copolymerization.

For the case of a binary copolymerization, the expression above can be explicitly solved for ϕ_1:

$$\phi_1(j) = \frac{k_{p_{21}}(j)f_1}{k_{p_{12}}(j)f_2 + k_{p_{21}}(j)f_1} \quad ; \qquad \phi_2(j) = 1 - \phi_1(j) \tag{24}$$

Using the proposed kinetic model, the population balances for living polymer of chain length r are given by the expressions:

$$\frac{dN_T}{dt}(1,j) = k_i(j)N(0,j)\overline{M}_T + k_{fm}(j)\overline{M}_T\left\{\sum_{r=1}^{\infty} N_T(r,j) - N_T(1,j)\right\} \tag{25}$$

$$+ k_H(j)N_H(0,j)\overline{M}_T + k_{H_A}(j)N_H(0,j)A$$

$$+ k_{tA}(j)A\left\{\sum_{r=1}^{\infty} N_T(r,j) - N_T(1,j)\right\}$$

$$- N_T(1,j)\{k_p(j)\overline{M}_T + k_{tH}(j)H_2 + k_{ts}(j)$$

$$+ k_{ds}(j) + k_{dIM}(j)IM\}$$

$$\frac{dN_T}{dt}(r,j) = k_p(j)\overline{M}_T\{N_T(r-1,j) - N_T(r,j)\} \tag{26}$$

$$- N_T(r,j)\{k_{tm}(j)\overline{M}_T + k_{tH}(j)H_2$$

$$+ k_{tA}(j)A + k_{ts}(j) + k_{ds}(j) + k_{dIM}(j)IM\} \qquad r \geq 2$$

where,

$$\overline{M}_T = \sum_{i=1}^{m} \overline{M}_i \tag{27}$$

$$N_T(r,j) = \sum_{i=1}^{m} N_i(r,j) \tag{28}$$

and $\overline{M}_i$ is the average concentration of monomer type i in the layer.

The mole balance for all molecules of living polymer is thus obtained by summing the equation (26) from r equal to 2 to infinity plus equation (25).

$$\frac{dY_0}{dt}(j) = K_I(j) - \{K_T(j) + K_D(j)\}Y_0(j) \tag{29}$$

where,

$$Y_0(j) = \sum_{r=1}^{\infty} N_T(r,j) \tag{30}$$

$$K_I(j) = \overline{M}_T\{k_i(j)N(0,j) + k_H(j)N_H(0,j)\} + k_{H_A}(j)N_H(0,j)A \tag{31}$$

$$K_T(j) = k_{tH}(j)H_2 + k_{ts}(j) \tag{32}$$

$$K_D(j) = k_{ds}(j) + k_{dIM}(j)IM \tag{33}$$

To calculate the total number of moles of living polymer in the reactor using the above equation, it is necessary to know $N(0,j)$ and $N_H(0,j)$.Developing population balances for these species, the following expressions are derived:

$$\frac{dN}{dt}(0,j) = k_f(j)N^*(j)A + k_a(j)N_{dIM}(0,j) - N(0,j)\{k_i(j)\overline{M}_T + K_D(j)\} \tag{34}$$

$$\frac{dN^*}{dt}(j) = -k_f(j)N^*(j)A \tag{35}$$

$$\frac{dN_{dIM}}{dt}(0,j) = k_{dIM}(j)N(0,j)IM - k_a(j)N_{dIM}(0,j) \tag{36}$$

$$\frac{dN_H}{dt}(0,j) = Y_0(j)K_T(j) + k_a(j)N_{dIM_H}(0,j) - N_H(0,j)\{k_H(j)\overline{M}_T + k_{H_A}(j)A + K_D(j)\} \tag{37}$$

$$\frac{dN_{dIM_H}}{dt}(0,j) = k_{dIM}(j)IM\{Y_0(j) + N_H(0,j)\} - k_a(j)N_{dIM_H}(0,j) \tag{38}$$

In an analogous way, the population balance for dead polymer of chain length r is easily derived:

$$\frac{dQ}{dt}(r,j) = N_T(r,j)\{K_T(j) + K_D(j)\} \tag{39}$$

where,

$$K_T(j) = k_{tm}(j)\overline{M}_T + k_{tH}(j)H_2 + k_{tA}(j)A + k_{ts}(j) \tag{40}$$

The mol balance for dead polymer of *all* chain lengths is thus obtained by summing equation (39) from *r* equal to 2 to infinity:

$$\frac{dX_0}{dt}(j) = \{Y_0(j) - N_T(1,j)\}\{K_T(j) + K_D(j)\} \tag{41}$$

where,

$$X_0(j) = \sum_{r=2}^{\infty} Q(r,j) \tag{42}$$

Copolymer Composition

The calculation of copolymer composition is straightforward. Making the long chain approximation the mole balance for monomer bound in polymer is:

$$\frac{dR_{P_i}}{dt}(j) = k_{p_i}(j)Y_0(j)\overline{M}_i \tag{43}$$

Thus, the polymer composition on each site is given by the expression:

$$F_i(j) = \frac{R_{P_i}(j)}{\sum_{i=1}^{m} R_{P_i}(j)} \tag{44}$$

Chain Length Averages

Chain length averages are estimated using the method of moments. The number average chain length is expressed as the ratio of the first moment to the zeroth moment of the molecular weight distribution. In the same way, the mass

average chain length is expressed as the ratio of the second moment to the first moment. Thus, the number average, mass average chain lengths, and polydispersity are calculated accordingly to the expression:

$$\overline{N_N} = \frac{\sum_{j=1}^{n} \{X_1(j) + Y_1(j)\}}{\sum_{j=1}^{n} \{X_0(j) + Y_0(j)\}} \tag{45}$$

$$\overline{N_W} = \frac{\sum_{j=1}^{n} \{X_2(j) + Y_2(j)\}}{\sum_{j=1}^{n} \{X_1(j) + Y_1(j)\}} \tag{46}$$

$$\overline{PDI} = \frac{\overline{N_W}}{\overline{N_N}} \tag{47}$$

where,

Y_n = n^{th} moment of the living polymer.

X_n = n^{th} moment of the dead polymer.

The n^{th} leading moment of some generic distribution *f(r)* is defined by the equation:

$$\mu_n = \sum_{r=1}^{\infty} r^n f(r) \tag{48}$$

The zeroth moments of living and dead polymer have been already expressed in equations (29) and (41).

The first and second moments of the living polymer are obtained by multiplying equation (26) by r and r^2 respectively and summing from 2 to infinity plus equation (25):

$$\frac{dY_1}{dt}(j) = Y_0(j)\{k_p(j)\overline{M}_T + k_{tm}(j)\overline{M}_T + k_{tA}(j)A\} \tag{49}$$

$$-\{K_T(j) + K_D(j)\}Y_1(j) + K_f(j)$$

$$\frac{dY_2}{dt}(j) = Y_0(j)\{k_p(j)\overline{M}_T + k_{tm}(j)\overline{M}_T + k_{tA}(j)A\} \tag{50}$$

$$+2k_p(j)\overline{M}_T Y_1(j) - \{K_T(j) + K_D(j)\}Y_2(j) + K_f(j)$$

In an analogous way, expressions for the first and second moments of dead polymer are derived from equation (39):

$$\frac{dX_n}{dt}(j) = \{Y_n(j) - N_T(1,j)\}\{K_T(j) + K_D(j)\} \tag{51}$$

Stockmayer Bivariate Distribution

For the special case of a binary copolymerization, Stockmayer's bivariate distribution (Stockmayer, 1945) can be calculated in each layer and later summed over time and spatially in the particle to get the bivariate distribution for the accumulated polymer. It permits the calculation of the complete CCD's and MWD's instead of only average values. However, it has to be kept in mind that the steady state hypothesis applied to chains of all lengths made by Stockmayer may not be valid, especially during the initial moments of the polymerization. Nevertheless, this is a very powerful approach and should always be used when possible for modelling binary copolymerization. Unfortunately, a generally valid trivariate distribution has not been developed to date and for terpolymerization or higher one can calculate analytically the full molecular weight distribution; however, if the assumption that terpolymer chains produced "instantaneously" all have the same chemical composition is significantly in error, then the trivariate distribution of chain length and compositions of monomers 1 and 2 in the terpolymer chain cannot be calculated analytically.

The method of moments should only be used for linear chains when the full distribution of chain lengths is not required (e.g., in process control). For polymers with long chain branching, the method of moments is also a useful alternative method.

Stockmayer (1945) used the general copolymerization theory proposed by Simha (1944) to derive a simple expression for the bivariate distribution of chain length and composition valid for linear binary copolymers with long chains. Both monomers were assumed to have the same molecular weight. Tacx (1988) added a minor correction term to Stockmayer's distribution tc account for comonomers with distinct molecular weights. For the case of a multisite type catalyst copolymerizing ethylene and propylene, Tacx's correction is negligible for most of the copolymer chains (Soares and Hamielec, 1994a).

In our model, we assume that each catalytic site type instantaneously produces polymer that follows an individual Stockmayer bivariate distribution. For a given chain length the composition will be normally distributed around the mean value and the chain length distribution, considering all compositions, will be equal to the most probable weight chain length distribution.

Having determined the bivariate distribution of each site type it is possible to derive expressions for the different layers and the whole polymer.

The instantaneous chain length and composition mass distribution proposed by Stockmayer and corrected for different molecular weights is expressed by the equation:

$$w_k(r,y,j)dr\,dy = [1+y(j)\delta(j)]\tau_k^2(j)r\exp[-\tau_k(j)r]dr \qquad (52)$$

$$\frac{1}{\sqrt{2\pi\beta_k(j)/r}}\exp\left[-\frac{y^2(j)r}{2\beta_k(j)}\right]dy$$

where,

$$\beta_k(j) = \overline{F}_{1,k}(j)\,(1-\overline{F}_{1,k}(j))K_k \qquad (53)$$

$$K_k = \{1+4\overline{F}_{1,k}(j)\,(1-\overline{F}_{1,k}(j))\,(r_{1,k}(j)r_{2,k}(j)-1)\}^{0.5} \qquad (54)$$

$$\delta_k(j) = \frac{y_k(1 - MW_2/MW_1)}{MW_2/MW_1 + \overline{F}_{1,k}(j)(1 - MW_2/MW_1)} \tag{55}$$

and,

r	chain length.
y	deviation from average copolymer composition.
$\tau(j)$	transfer to propagation rate ratio.
$\overline{F}_1(j)$	average mole fraction of monomer type 1 in copolymer.
r_1, r_2	reactivity ratios.
j	active site type.
k	catalyst particle layer.
MW_1	molecular weight of monomer type 1.
MW_2	molecular weights of monomer type 2.

It is evident from the equation above that the correction term is more significant for copolymer chains with compositions that considerably deviate from the average composition.

To obtain the instantaneous chain length distribution, we integrate Stockmayer's distribution with respect to y, from $-\infty$ to ∞:

$$w_k(r,j) = \int_{-\infty}^{\infty} w_k(r,y,j)dy = \tau_k^2(j) r \exp[-\tau_k(j) r] \tag{56}$$

Analogously, for composition distribution over all chain lengths:

$$w_k(y,j) = \int_0^{\infty} w_k(r,y,j)dr = w'_k(y,j)\,[1+\delta_k(j)y_k] \tag{57}$$

where,

$$w'_k(y,j) = \frac{3}{4\sqrt{2\beta_k(j)\tau_k(j)}\,(1+y_k^2/2\beta_k(j)\tau_k(j))^{5/2}} \tag{58}$$

To obtain the equivalent cumulative distributions per layer for all types of active sites, we integrate equations (56) and (57) in time and sum over all site types:

$$W_k(r) = \frac{\sum_{j=1}^{n}\int_0^t R_{p.k}(j)w_k(r,j)dt}{\sum_{j=1}^{n}\int_o^t R_{p.k}(j)dt} \tag{59}$$

$$W_k(y) = \frac{\sum_{j=1}^{n}\int_0^t R_{p.k}(j)w_k(y,j)dt}{\sum_{j=1}^{n}\int_o^t R_{p.k}(j)dt} \tag{60}$$

Finally for the whole catalyst particle, we sum equations (59) and (60) over all l spherical layers.

$$W(r) = \frac{\sum_{k=1}^{l} m_k W_k(r)}{\sum_{k=1}^{l} m_k} \tag{61}$$

$$W(y) = \frac{\sum_{k=1}^{I} m_k W_k(y)}{\sum_{k=1}^{I} m_k} \tag{62}$$

where m_k is the mass of polymer in the spherical layer k.

Chain length averages are easily calculated from these distributions:

$$\overline{N_N} = \left\{ \int_0^{\infty} \frac{W(r)}{r} dr \right\}^{-1} \tag{63}$$

$$\overline{N_W} = \int_0^{\infty} r W(r) dr \tag{64}$$

Particle Growth - Grid Updating

Layer volumes and boundary positions are updated after a predetermined time interval. Monomer concentrations and the zeroth moment of living polymer in the previous time step are used in these computations.

In the equations below, superscripts indicate time and subscripts indicate radial position.

$$V_j^0 = \frac{4}{3}\pi\left((r_{j+1}^0)^3 - (r_j^0)^3 \right) \tag{65}$$

$$V_j^{i+1} = V_j^i \left[\frac{k_{p_{TT}} (\overline{M}_T)_j^i (Y_0)_j^i \overline{MW} \Delta t}{\rho_p} + 1 \right] \tag{66}$$

$$\overline{MW} = \frac{\sum_{i=1}^{m} B_i MW_i}{\sum_{i=1}^{m} B_i} \tag{67}$$

$$r_{j-1}^{i+1}=\left(\frac{3}{4\pi}V_j^{i+1}+r_j^{i+1}\right)^{1/3} \tag{68}$$

Numerical Solution

Monomer and temperature radial profiles are calculated using a 3 point Lagrangian interpolating polynomial as defined below:

$$M_i(r)=\sum_{j=1}^{3} l_j(r)M_i(r_j) \tag{69}$$

$$l_j(r)=\frac{p_3(r)}{(r-r_j)p_3'(r_j)} \tag{70}$$

$$p_3(r)=(r-r_{k-1})(r-r_k)(r-r_{k+1}) \tag{71}$$

where k stands for the radial position in the polymeric particle.

Therefore, the first and second derivatives of monomer concentration can be expressed as:

$$\frac{1}{2}\frac{d^2M_i}{dr^2}(r)=\frac{M_i(r_{k-1})}{(r_{k-1}-r_k)(r_{k-1}-r_{k+1})}+ \tag{72}$$

$$\frac{M_i(r_k)}{(r_k-r_{k-1})(r_k-r_{k+1})}+\frac{M_i(r_{k+1})}{(r_{k+1}-r_{k-1})(r_{k+1}-r_k)}$$

$$\frac{dM_i}{dr}(r)=\frac{(r-r_k)+(r-r_{k+1})}{(r_{k-1}-r_k)(r_{k-1}-r_{k+1})}M_i(r_{k-1})+ \tag{73}$$

$$\frac{(r-r_{k+1})+(r-r_{k-1})}{(r_k-r_{k-1})(r_k-r_{k+1})}M_i(r_k)+$$

$$\frac{(r-r_{k-1})+(r-r_k)}{(r_{k-1}-r_{k-1})(r_{k+1}-r_k)}M_i(r_{k+1})$$

Using equations (72) and (73) in equation (1) to express the first and second radial derivatives and after some algebraic manipulations we arrive at the following expression for monomer concentration profile at the interior points:

$$\frac{dM_i}{dt}(r_k) = 2D_{M_i}[A_k M_i(r_{k-1}) B_k M_i(r_k) + C_k M_i(r_{k+1})] \qquad (74)$$

$$-R_{p_i}(r_k) \qquad k = 2, N-2$$

where the discretization weights are expressed by:

$$A_j = \frac{2r_j + r_{j+1}}{r_j(r_{j-1} - r_j)(r_{j-1} - r_{j+1})} \qquad j = 2, N-2 \qquad (75)$$

$$B_j = \frac{3r_j - r_{j+1} - r_{j-1}}{r_j(r_j - r_{j-1})(r_j - r_{j+1})} \qquad j = 2, N-2 \qquad (76)$$

$$C_j = \frac{2r_j - r_{j-1}}{r_j(r_{j+1} - r_{j-1})(r_{j+1} - r_j)} \qquad j = 2, N-2 \qquad (77)$$

and N is the total number of grid points or the number of shells plus 1.

Equation (74) becomes indefinite when r=0. Applying L'Hospital rule to the derivative term of equation (1) we obtain:

$$\frac{\partial M_i}{\partial t} = 3D_{M_i}\frac{\partial^2 M_i}{\partial r^2} - R_{p_i} \qquad (78)$$

Expanding M_i in Taylor series around the origin and substituting the boundary condition we obtain an expression for the second derivative:

$$\frac{\partial^2 M_i}{\partial r^2}(r_0) = 2\frac{M_i(r_1) - M_i(r_0)}{(r_1 - r_0)^2} \qquad (79)$$

Using the expression above we obtain the discretized monomer profile at the center of the particle:

$$\frac{dM_i}{dt}(r_0) = D_{M_i}[B_0 M_i(r_0) + C_0 M_i(r_1)] - R_{p_i}(r_0) \qquad (80)$$

where,

$$B_0 = -\frac{6}{(r_1 - r_0)^2} \tag{81}$$

$$C_0 = -B_0 \tag{82}$$

We use the same approach for the temperature radial profile. The resulting equations are:

$$\frac{dT}{dt}(r_k) = 2\alpha_T[A_k T(r_{k-1}) B_k T(r_k) + C_k T(r_{k+1})] \tag{83}$$

$$-Q_p(r_k) \qquad k = 2, N-2$$

$$\frac{dT}{dt}(r_0) = \alpha_T[B_0 T(r_0) + C_0 T(r_1)] - Q_p(r_0) \tag{84}$$

where,

$$\alpha_T = \frac{k_e}{\rho_p C_p} \tag{85}$$

The resulting set of equations for monomer concentration, particle temperature, active species, copolymer composition and molecular weight averages can be solved by any commercial package for ordinary differential equations that can deal with stiff systems.

Although the model can be directly solved in the presented form, some simplifications are very useful to reduce the stiffness of the system but do not significantly reduce the accuracy of the simulation results.

For the present simulations, the following simplifications were made:

- Monomer and temperature profiles are considered stationary at each time step, i.e. *dMi/dt* and *dT/dt* = 0. Therefore both monomer and temperature profiles can be calculated by solving a system of algebraic equations. Note that the profiles are recalculated at each update of the layer volumes.

- The stationary-state hypothesis (SSH) was made for the short-lived species, $N(0,j)$, $N_H(0,j)$, $N_T(1,j)$, $N_{dlM}(0,j)$, $N_{dlMH}(0,j)$. In this way the resulting system of equations is not stiff and the numerical solution is much faster.

The basic steps for solving the model are:

1. Input data
2. Calculate initial layer sizes and boundary positions
3. Set initial conditions
    4. Calculate discretization weights for monomer profile
    5. Estimate monomer and temperature profiles
    6. Calculate average monomer concentrations in the shells
    7. Calculate pseudo-kinetic constants in each shell
    8. Calculate active species profiles from $t \rightarrow t + \Delta t$
    9. Increment time
    10. Update shell volume and boundary positions
    11. Save intermediate results
    12. If time less then end time return to step 4
13. End

Results and Discussion

We will first use our model to evaluate the importance of mass transfer resistance in homopolymerization for a non-deactivating, single-site type, heterogeneous catalyst. We will focus our attention on results for ethylene and propylene polymerization in a slurry reactor but the analysis that follows can be applied to any olefin polymerization.

The majority of experimental data and mathematical modelling results seems to indicate that Ziegler-Natta heterogeneous catalysts have more then one active site type. However, with the advent of supported metallocene catalysts technology (Soares and Hamielec, 1994b), such catalysts may be available commercially in the near future. Since those catalysts are generally highly active, mass and heat transfer resistances might have a significant influence on their performances.

To simplify the interpretation of the results we assumed that: (1) all initiation constants were equal to the equivalent propagation constants, (2) transfer to hydrogen is the only significant chain transfer reaction, (3) no deactivation reactions take place, (4) no impurities are present, (5) there is no significant radial gradient of hydrogen concentration, (6) there is no significant radial gradient of temperature.

The parameters used in the simulation are shown in table 1. These values are realistic estimations for heterogeneous Ziegler-Natta catalysts in slurry reactors (Floyd, 1986d). The broad range of propagation constants covers low activity, first generation catalysts to high activity, supported catalysts. Concentrations of monomers are those commonly encountered in slurry reactors. Diffusion coefficients for monomers are in the range of commonly reported values in the literature for slurry reactors. Catalyst radius and active site concentration are also in the range of values reported in the literature.

$k_{P_{propylene}}$	30 - 5,000	l/mol.s
$k_{P_{ethylene}}$	300 - 50,000	l/mol.s
[propylene]	2 - 4	mol/l
[ethylene]	0.5 - 1	mol/l
R_0	0.001 - 0.01	cm
$D_{propylene}$	10^{-6} - 10^{-5}	cm^2/s
$D_{ethylene}$	10^{-6} - 10^{-5}	cm^2/s
C^*	0.001 - 0.1	mol/l

Table 1: Range of studied parameters.

Figure 2 shows the effect of the diffusion coefficient on the number average chain length for a low activity catalyst. Even for the lower limit of diffusivity, mass transfer resistances do not significantly affect the number average chain. For a moderately active catalyst, as presented in figure 3, the effect of mass transfer resistance is more pronounced but still small. For a very highly active catalyst the influence of diffusion resistances is more important, as shown in figure 4. In this case, a clear decrease in the number average molecular weight with increasing mass transfer resistance is noticed. Polydispersity, however, is not appreciably influenced even for the very active catalysts under strong mass transfer limitations, as depicted in figure 5.

The radial profiles of monomer concentration are shown in figure 6 for the high activity catalyst. Radial positions 1 and 11 indicate the innermost layer and the polymer particle/diluent interface, respectively. When monomer diffusivity is high, the radial profile of monomer is flat and the average chain lengths are spatially uniform. However, for low monomer diffusivity there is a significant decrease in monomer concentration towards the center of the particle with consequent decrease in the average molecular weights of the polymer.

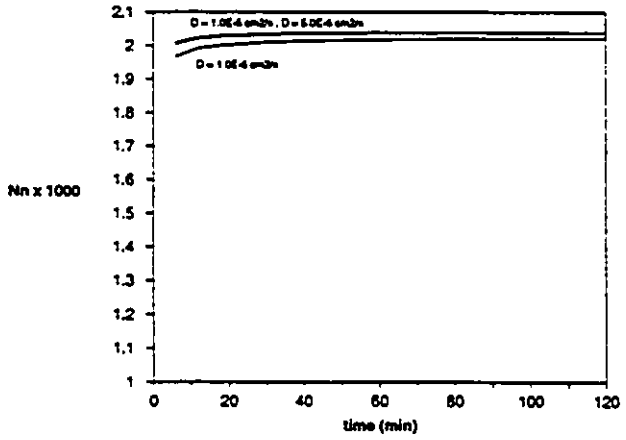

Figure 2 - Effect of monomer diffusivity for low activity catalyst.
$k_p = 95 l/mol.s$; $[M_0] = 4 mol/l$; $C^* = 0.01 mol/l$; $R_0 = 0.001 cm$

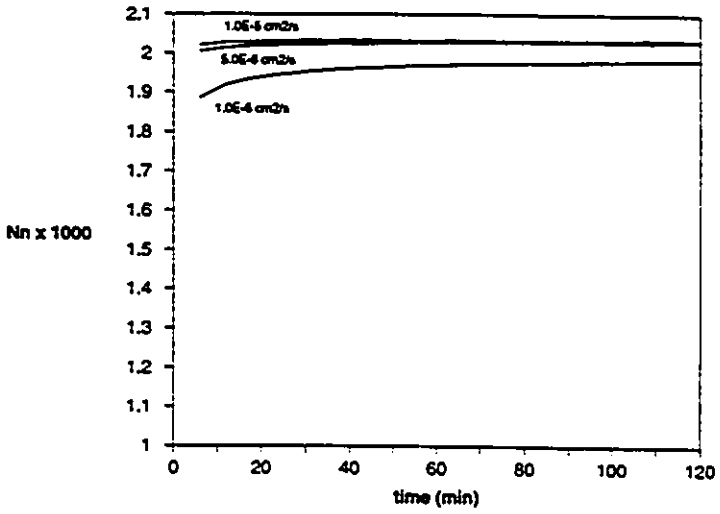

Figure 3 - Effect of monomer diffusivity for medium activity catalyst. $k_p = 500 l/mol.s$; $[M_0] = 4 mol/l$; $C^* = 0.01 mol/l$; $R_0 = 0.001 cm$

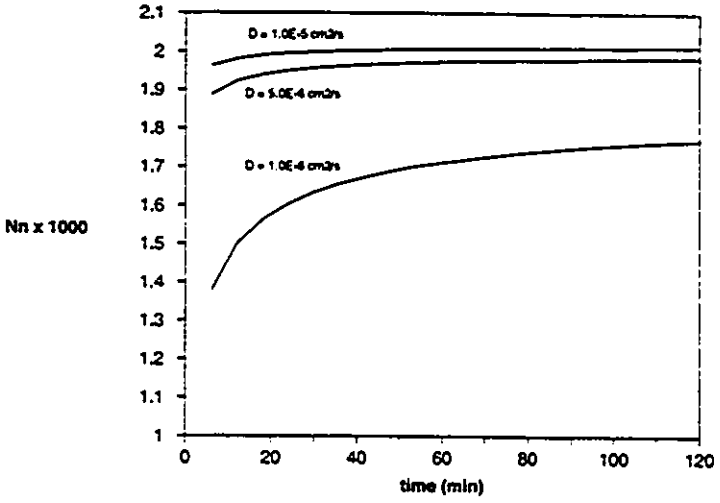

Figure 4 - Effect of monomer diffusivity for high activity catalyst. $k_p = 5000 l/mol.s$; $[M_0] = 4 mol/l$; $C^* = 0.01 mol/l$; $R_0 = 0.001 cm$

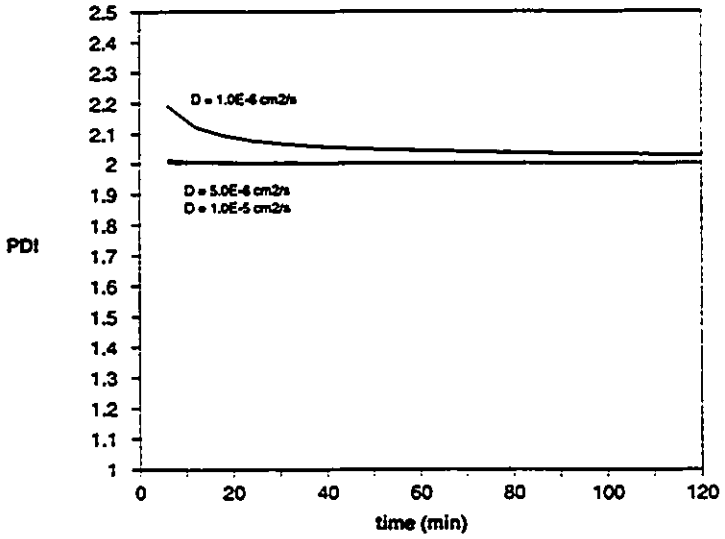

Figure 5 - Effect of monomer diffusivity for high activity catalyst.
$k_p = 5000 l/mol.s$; $[M_0] = 4 mol/l$; $C^* = 0.01 mol/l$; $R_0 = 0.001 cm$

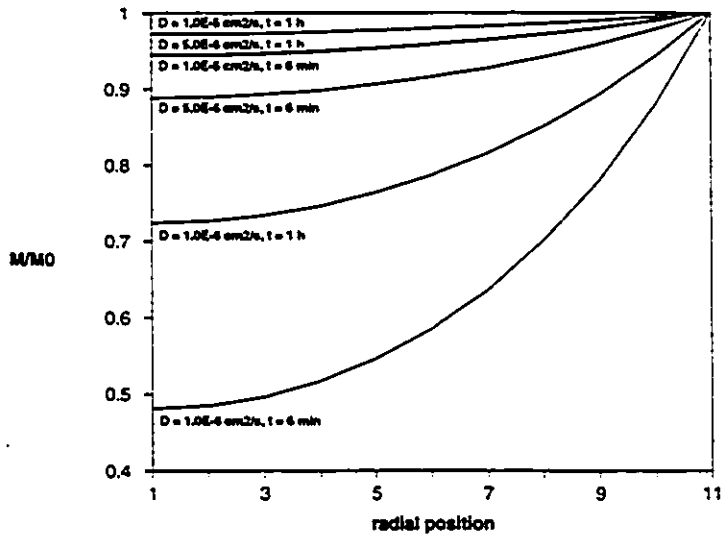

Figure 6 - Effect of monomer diffusivity for high activity catalyst.
$k_p = 5000 l/mol.s$; $[M_0] = 4 mol/l$; $C^* = 0.01 mol/l$; $R_0 = 0.001 cm$
Radial position: 1 = particle centre, 11 = particle/diluent interface
M/M0 - dimensionless monomer concentration, M0 - monomer concentration in diluent.

Figure 7 shows the chain length distributions of polymer made with the highly active catalyst after two hours of polymerization for two values of monomer diffusivity. The formation of smaller chains when monomer diffusivity is smaller shifts the distribution to the left without significantly broadening it.

Figure 8 presents the particle growth profile for the high activity catalyst for 3 different levels of mass transfer resistance. As can be seen, only for the lower limit of diffusivity is there a significant decrease in particle growth due to mass transfer resistances. It is likely that the residence-time distribution plays a much more important role in determining the polymer particle size distribution than mass transfer resistances within the particle.

The effect of varying the propagation rate constant for larger catalyst particles is illustrated in figure 9. Increasing the initial size of the catalyst decreases considerably the number average chain length of the polymer as compared with results shown in figures 2 and 3, where the initial radius of the catalyst is ten times smaller. The radial profile of the number average chain length for the more active catalyst is shown in figure 10. After 6 minutes of polymerization there is a steep radial profile of the number average chain length indicating that in the central regions of the particle, catalyst sites are monomer starved. This number average chain length profile is still significantly steep even after two hours of polymerization.

Figure 11 shows the monomer radial profile for the same conditions presented in figure 10. The points on the curves indicate the layer limits used for the simulation. The steep radial profile of the monomer causes the layers to expand at very different rates during the simulation. At time zero all layers have the same spacing. After 6 minutes of simulation, only the outer layers expand significantly, since monomer is not reaching the center of the particle. For longer times, however, the radial profile of the monomer flattens and the inner layers start to expand at a higher rate.

Higher polydispersities will also be achieved if we have highly active catalyst particles with large initial radii. Figure 12 shows that the polydispersity of a polymer made with a moderately active catalyst can be significantly greater than 2, especially during the initial stages of the polymerization. The polydispersity, however, moves toward 2 as the polymerization proceeds due to catalyst particle expansion.

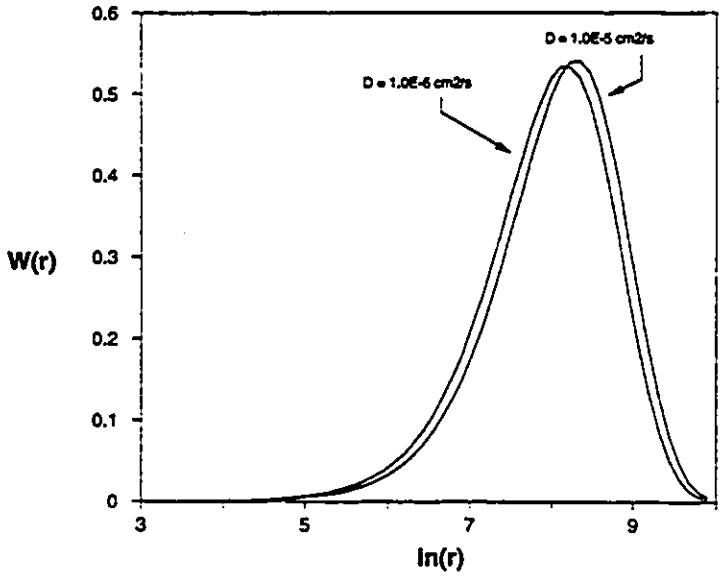

Figure 7 - Chain length distribution for high activity catalyst. $k_p = 5000 l/mol.s$; $[M_0] = 4 mol/l$; $C^* = 0.01 mol/l$; $R_0 = 0.001 cm$; $t = 120$ min

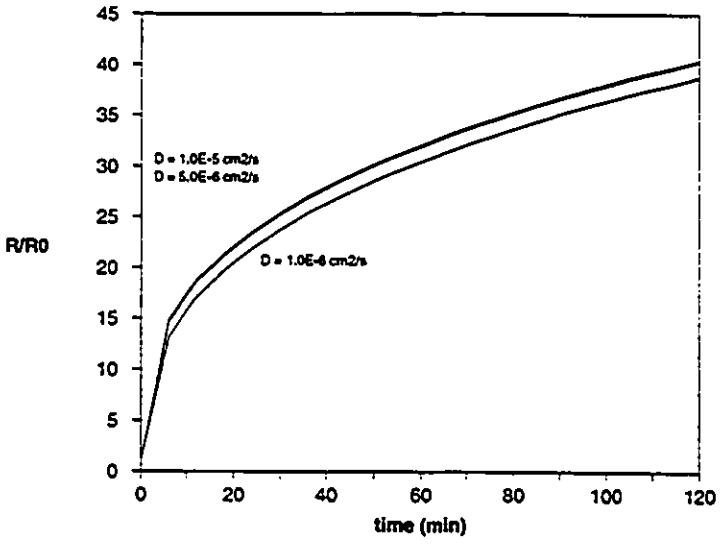

Figure 8 - Effect of monomer diffusivity for high activity catalyst.
$k_p = 5000 l/mol.s$; $[M_0] = 4 mol/l$; $C^* = 0.01 mol/l$; $R_0 = 0.001 cm$
R/R0 - dimensionless radial position, R0 - polymeric particle radius (time function).

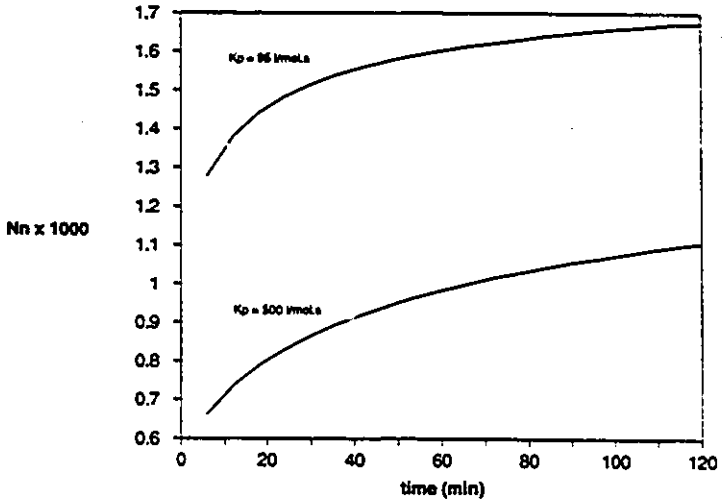

Figure 9 - Effect of varying the propagation constant of a catalyst particle with large initial radius.
$D = 5x10^{-6} cm^2/s$; $[M_0] = 4 mol/l$; $C^* = 0.01 mol/l$; $R_0 = 0.01 cm$

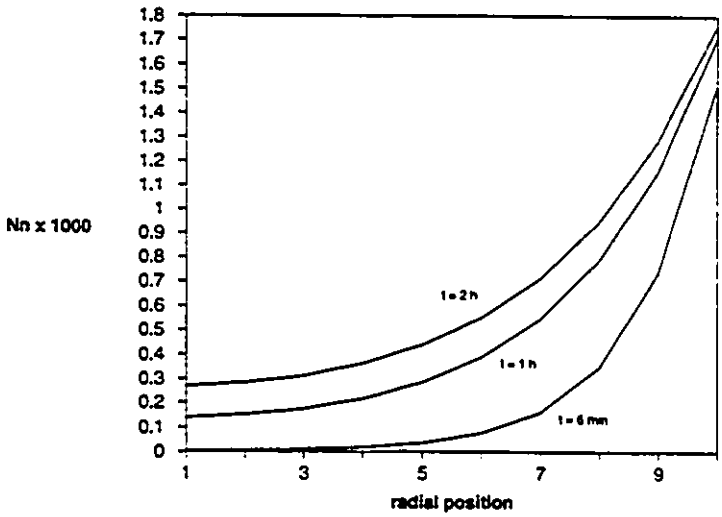

Figure 10 - Radial profile of number average chain length for propylene polymerization under severe mass transfer limitations.
$k_p = 500 l/mol.s$; $D = 5x10^{-6} cm^2/s$; $[M_0] = 4 mol/l$; $C^* = 0.01 mol/l$; $R_0 = 0.01 cm$
Radial position: 1 = particle centre, 11 = particle/diluent interface.

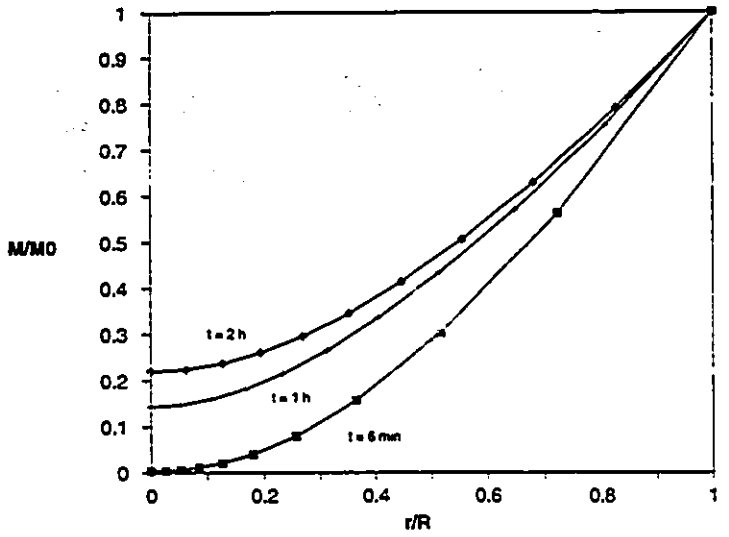

Figure 11 - Radial profile of number average chain length for propylene polymerization under severe mass transfer limitations.
$k_p = 500 l/mol.s$; $D = 5x10^{-6} cm^2/s$; $[M_0] = 4 mol/l$; $C^* = 0.01 mol/l$; $R_0 = 0.01 cm$
M/M0 - dimensionless monomer concentration, M0 - monomer concentration in diluent, r/R - dimensionless radial position, R - polymeric particle radius (time function).

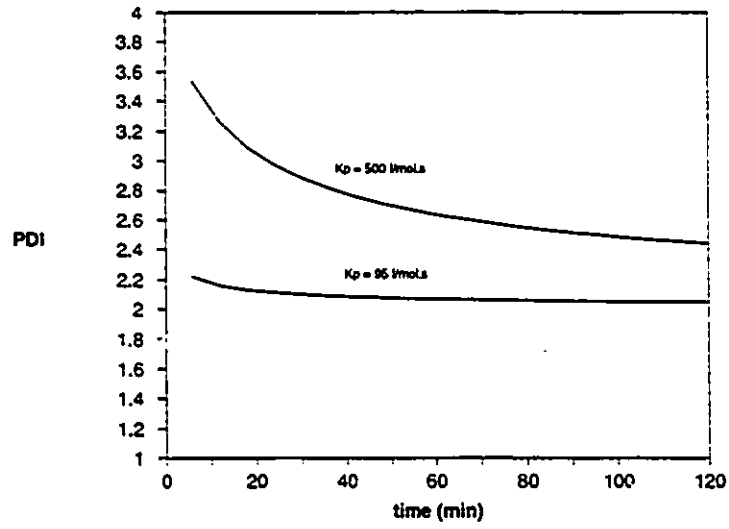

Figure 12 - Time variation of polydispersity index for propylene polymerization under severe mass transfer limitations.
$D = 5x10^{-6} cm^2/s$; $[M_0] = 4 mol/l$; $C^* = 0.01 mol/l$; $R_0 = 0.01 cm$

Figure 13 depicts how the chain length distributions vary in the different layers of the model when k_p = 500 l/mol.s. There is a significant shift of the distribution towards smaller chain lengths when one moves from the surface to the interior of the particle. In figure 13, layer 1 is in the central position and layer 10 is the most exterior position.

The effect of active site concentration is presented in figures 14 and 15 for the highly active catalyst. The higher the concentration of the active sites, the lower the number average chain length of the produced polymer. A high concentration of active sites causes a steep monomer radial profile which decreases the average sizes of the polymer chains. This is a very important conclusion for supported catalysts, since it dictates the limits of the number of active centers to be deposited on the catalyst support to avoid diffusion controlled polymerization. Figure 15 shows how the polydispersity varies with active site concentration. The effect on polydispersity is limited and tends to be less important as the polymerization proceeds.

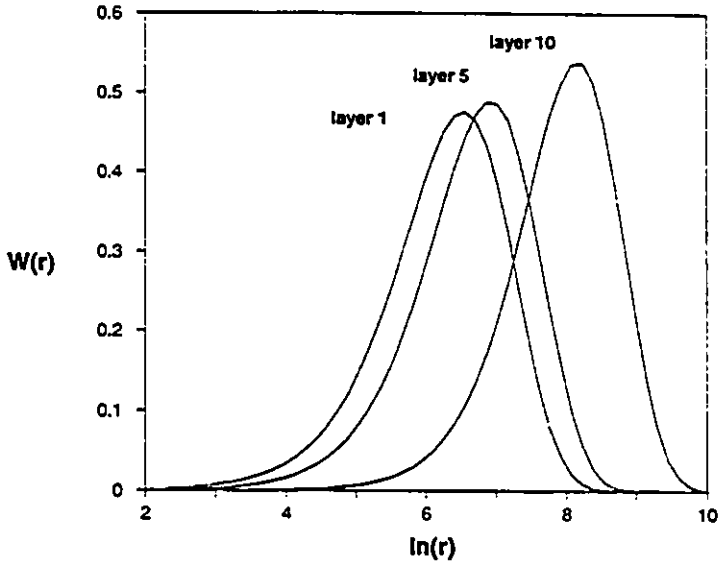

Figure 13 - Chain length distribution for propylene polymerization under significant mass transfer limitations.
$D = 5x10^{-6} cm^2/s$; $[M_0] = 4 mol/l$; $C^* = 0.01 mol/l$; $R_0 = 0.01 cm$ $k_p = 500 l/mol.s$; $: = 2h$
Layer 1 = innermost layer, layer 10 = external layer.

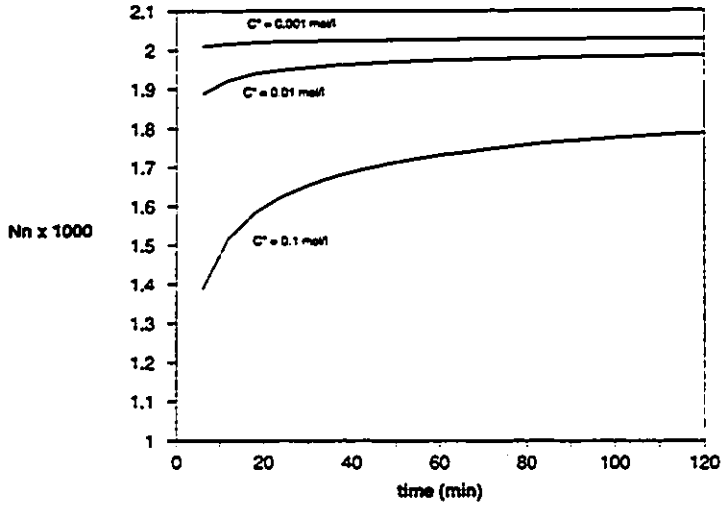

Figure 14 - Effect of initial concentration of active sites.
$k_p = 5000 l/mol.s$; $[M_0] = 4 mol/l$; $D = 5x10^{-6} cm^2/s$; $R_0 = 0.001 cm$

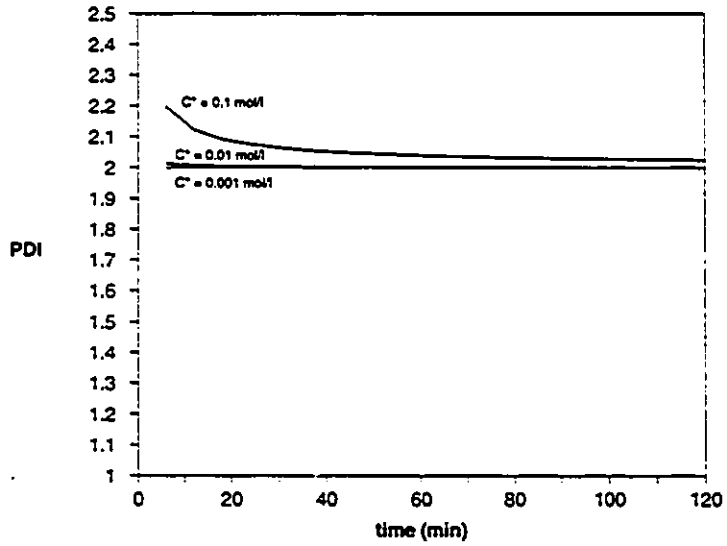

Figure 15 - Effect of initial concentration of active sites.
$k_p = 5000 l/mol.s$; $[M_0] = 4 mol/l$; $D = 5x10^{-6} cm^2/s$; $R_0 = 0.001 cm$

These simulation results confirm the predictions of both multigrain and polymeric flow models. It is clear that mass transfer resistances alone can not explain the large polydispersities observed with heterogeneous Ziegler-Natta catalysts. They may, however, especially for high activity catalysts with large particle size, significantly decrease the molecular weight averages of the final product. High active site concentration can also increase mass transfer resistance effects and should be carefully considered especially for the case of supported catalysts.

The results for copolymerization of ethylene-propylene over a low activity catalyst are shown in figures 16 to 19. Propylene is monomer 1. Number average molecular weight and polydispersity are not altered significantly for all the range of diffusivities used. The results for copolymer composition are more interesting. Figure 18 shows that for small monomer diffusivities the mol fraction of propylene in the copolymer increases. This behaviour can be attributed to the higher reactivity of ethylene. Since ethylene is more reactive then propylene it will experience higher mass transfer limitations and its concentration will drop faster as we move to the center of the growing particle. In this way, the inner layers will make polymer that is richer in propylene than ethylene. This can be seen in figure 19 for two values of diffusivity and three reaction times. For a large value of the diffusivity, the radial profile of composition is almost flat. However, for smaller diffusivities the composition radial profile becomes more prominent, especially for short reaction times. It is important to notice that this effect is less marked for longer reaction times due to particle expansion.

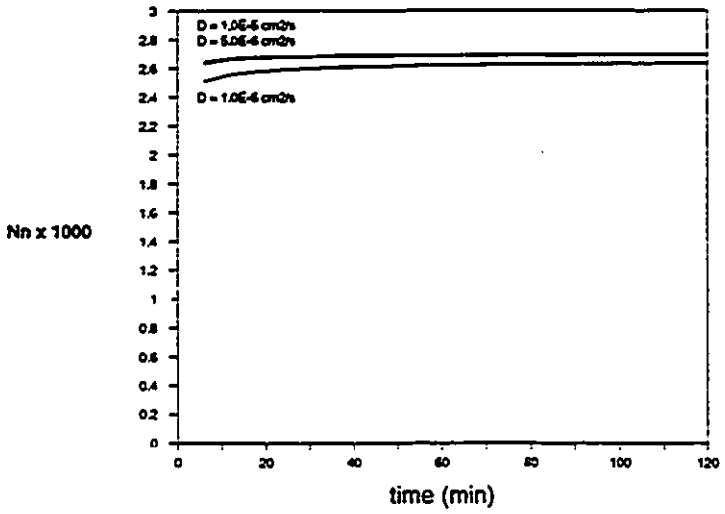

Figure 16 - Effect of monomer diffusivity for a low activity catalyst during copolymerization.
$k_{P_{1,1}} = k_{P_{2,1}} = 95 l/mol\,s$; $k_{P_{1,2}} = k_{P_{2,2}} = 950 l/mol\,s$; $[M_{0_1}] = 4 mol/l$; $[M_{0_2}] = 0.13 mol/l$; $C^* = 0.01 mol/l$; $R_0 = 0.001 cm$; $D_1 = D_2$

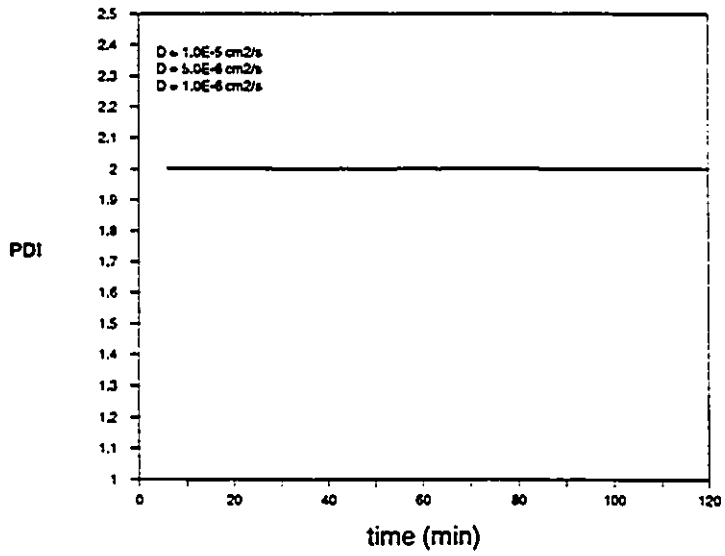

Figure 17 - Effect of monomer diffusivity for a low activity catalyst during copolymerization.
$k_{P_{1,1}} = k_{P_{2,1}} = 95 l/mol\,s$; $k_{P_{1,2}} = k_{P_{2,2}} = 950 l/mol\,s$; $[M_{0_1}] = 4 mol/l$; $[M_{0_2}] = 0.13 mol/l$; $C^* = 0.01 mol/l$; $R_0 = 0.001 cm$; $D_1 = D_2$

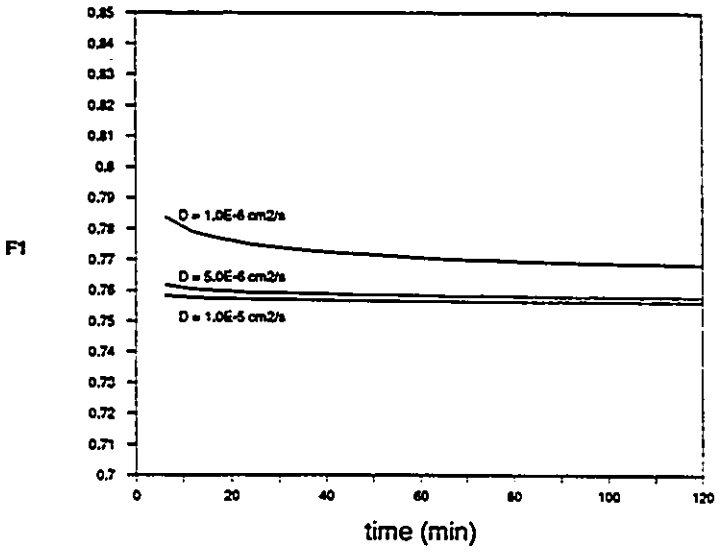

Figure 18 - Effect of monomer diffusivity for a low activity catalyst during copolymerization.
$k_{P_{1,1}} = k_{P_{2,1}} = 95 l/mol.s$; $k_{P_{2,2}} = k_{P_{1,2}} = 950 l/mol.s$; $[M_{o_1}] = 4 mol/l$; $[M_{o_2}] = 0.13 mol/l$; $C^* = 0.01 mol/l$; $R_o = 0.001 cm$; $D_1 = D_2$
F1 - mol fraction of propylene in copolymer.

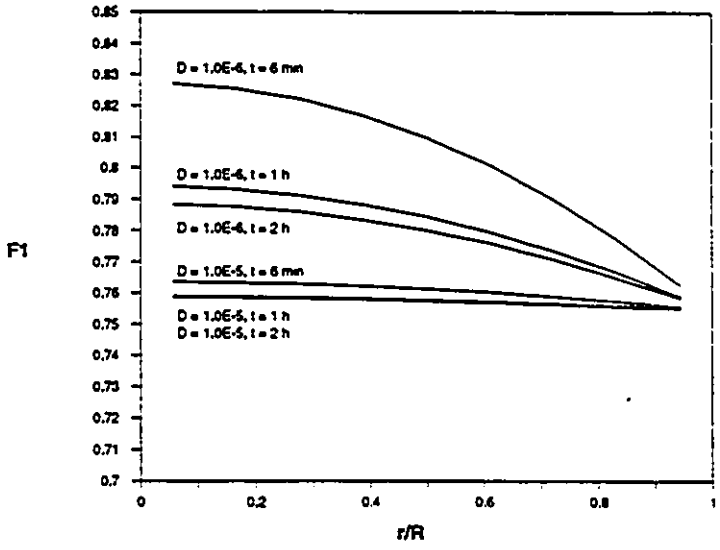

Figure 19 - Effect of monomer diffusivity for a low activity catalyst during copolymerization.
$k_{P_{1,1}} = k_{P_{2,1}} = 95 l/mol.s$; $k_{P_{2,2}} = k_{P_{1,2}} = 950 l/mol.s$; $[M_{o_1}] = 4 mol/l$; $[M_{o_2}] = 0.13 mol/l$; $C^* = 0.01 mol/l$; $R_o = 0.001 cm$; $D_1 = D_2$
F1 - mol fraction of propylene in copolymer; r/R - dimensionless radial position; R - polymeric particle radius (time function).

This behaviour gets even more important when highly active catalysts are used. Figure 20 shows the number average molecular weight for a highly active catalyst. Transfer to hydrogen constants were adjusted to keep the same molecular weight obtained for the low activity catalyst. Although the average chain lengths were not very much affected by the increase in reactivity of the catalyst, copolymer composition shows a significant change when monomer diffusivity is low, as illustrated in figure 21. Figure 22 shows the radial concentration profiles of both ethylene and propylene. Propylene, being less reactive, has an almost flat radial profile while the concentration of ethylene decreases significantly towards the center of the particle. Since the ratio of monomers varies in radial position and in time, the copolymer produced under these circumstances will be heterogeneous in composition. The significance of this heterogeneity in copolymer composition depends on the relative polymerization rates in the spherical shells.

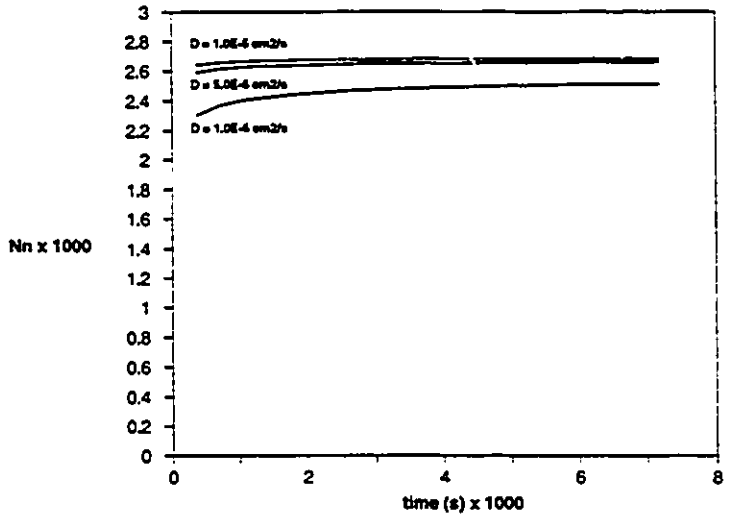

Figure 20 - Effect of monomer diffusivity for a high activity catalyst during copolymerization.

$k_{P_{1,1}} = k_{P_{2,1}} = 500 l/mol.s$; $k_{P_{2,2}} = k_{P_{1,2}} = 5000 l/mol.s$; $[M_{o_1}] = 4 mol/l$; $[M_{o_2}] = 0.13 mol/l$; $C^* = 0.01 mol/l$; $R_0 = 0.001 cm$; $D_1 = D_2$

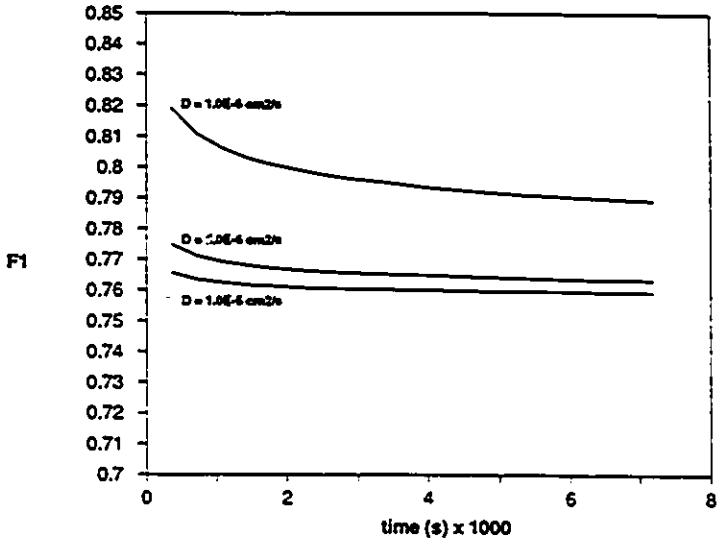

Figure 21 - Effect of monomer diffusivity for a high activity catalyst during copolymerization.
$k_{P_{1,1}} = k_{P_{2,1}} = 500 l/mol.s$; $k_{P_{2,2}} = k_{P_{1,2}} = 5000 l/mol.s$; $[M_{0_1}] = 4 mol/l$; $[M_{0_2}] = 0.13 mol/l$; $C^* = 0.01 mol/l$; $R_0 = 0.001 cm$; $D_1 = D_2$
F1 - mol fraction of propylene in copolymer.

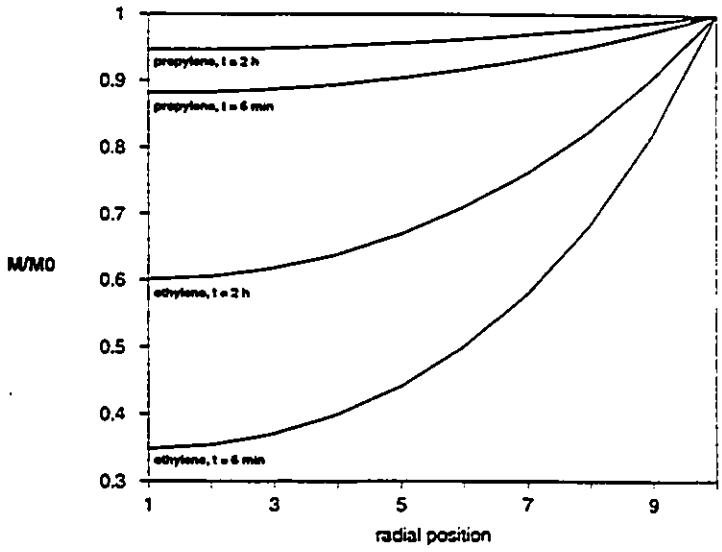

Figure 22 - Effect of monomer diffusivity for a high activity catalyst during copolymerization.
$k_{P_{1,1}} = k_{P_{2,1}} = 500 l/mol.s$; $k_{P_{2,2}} = k_{P_{1,2}} = 5000 l/mol.s$; $[M_{0_1}] = 4 mol/l$; $[M_{0_2}] = 0.13 mol/l$; $C^* = 0.01 mol/l$; $R_0 = 0.001 cm$; $D_1 = D_2$
M/M0 - dimensionless monomer concentration, M0 - monomer concentration in diluent; Radial position: 1 = particle centre, 11 = particle/diluent interface.

Copolymer CCDs for various layers of the model are shown in figure 23 for the high activity catalyst after two hours of polymerization. They indicate clearly that a significant composition distribution broadening is to be expected in this case. Polymer made in layers that are closer to the center of the particle is richer in the less reactive monomer than polymer made in the more exterior layers. The CCD for the whole particle is shown in figure 24.

Therefore, it seems that for the case of copolymerization, if the monomers have reactivities that differ considerably and the polymerization is carried out under conditions of significant mass transfer resistances, copolymer composition will be a function of both radial position and polymerization time. Notice that this effect can occur even in the total absence of monomer composition drift due to differences in reactivity ratios.

Intraparticle temperature gradients were not found to be significant in the range of parameters studied, confirming previous simulations using the multigrain model (Floyd, 1986d). It is well known, however, that fresh active catalyst fed into the gas-phase process (e.g. UNIPOL) can overheat leading to polymer melting and agglomeration. This is due to high heat generation during the early stages of polymerization and has been attributed to poor heat transfer in the external layer (Floyd,1986d). This phenomenon might be overcome by prepolymerization at low rates to build up polymer particle mass before it is fed to the reactor.

When more than one active site type is present on the catalyst the final properties of the whole polymer will be the average of the properties of the polymer made by each distinct catalytic species. In this case large polydispersities and heterogeneous composition can be easily obtained even in the absence of significant transfer resistances.

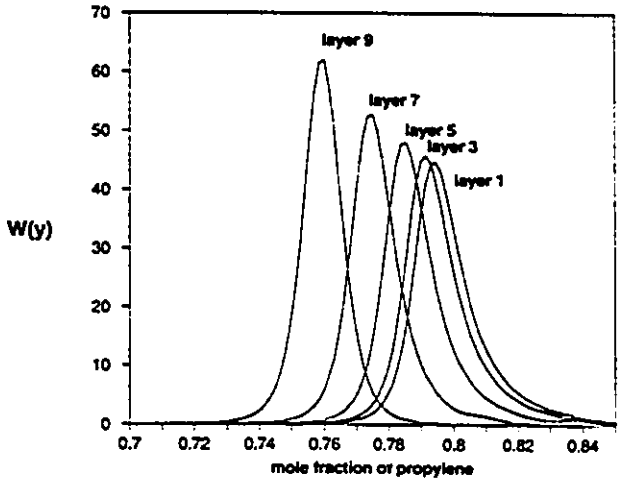

Figure 23 - CCD of different polymer layers for propylene-ethylene copolymerization.
$k_{p_{1,1}} = k_{p_{2,1}} = 500 l/mol.s$; $k_{p_{2,2}} = k_{p_{1,2}} = 5000 l/mol.s$; $[M_{0_1}] = 4 mol/l$; $[M_{0_2}] = 0.13 mol/l$;

$C^* = 0.01 mol/l$; $R_0 = 0.001 cm$; $D_1 = D_2 = 1.0 x 10^{-5} cm^2/s$; $t = 2h$

Layer 1 - innermost layer; layer 9 - external layer.

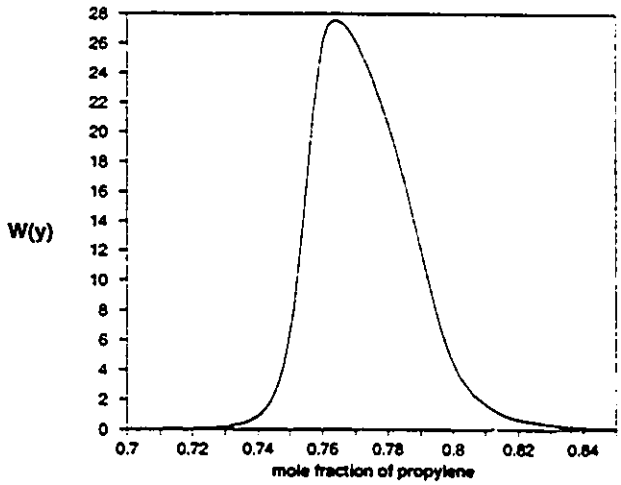

Figure 24 - average CCD for propylene-ethylene copolymerization.
$k_{p_{1,1}} = k_{p_{2,1}} = 500 l/mol.s$; $k_{p_{2,2}} = k_{p_{1,2}} = 5000 l/mol.s$; $[M_{0_1}] = 4 mol/l$; $[M_{0_2}] = 0.13 mol/l$;

$C^* = 0.01 mol/l$; $R_0 = 0.001 cm$; $D_1 = D_2 = 1.0 x 10^{-5} cm^2/s$; $t = 2h$

Figures 25 to 27 show some results for a catalyst with 3 site types. Even for a low activity catalyst and high monomer diffusivities the copolymer produced shows broad MWDs and CCDs. It is apparent that if the catalyst contains active site types which have greatly different ratios of propagation to transfer rates it will produce polymer with a very broad MWD. In the same way, if the reactivity ratios vary among the active site types, the final polymer will consist of a mixture of copolymer chains with different average compositions.

Figures 28 and 29 show the CCDs for this 3 site type catalyst. CCDs per site type over all layers are compared to the average CCDs of the whole particle in figure 28. Figure 29 shows the CCDs of some layers for all site types. Observe that additionally to the composition distribution broadening resulting from different site types, mass transfer resistances also cause spatial variation of composition in the particle.

Finally, figure 30 compares the chain length distributions of each site over all layers to the average chain length distribution of the polymer particle. As seen, the chain length distribution of the polymer particle is significantly broadened by the presence of site types with distinct rates of propagation to transfer reactions.

It is also illustrative to point out that this model can also be applied for the case of homogeneous Ziegler-Natta catalysis if one neglects mass and heat transfer resistances. A similar model was used to fit the experimental results of ethylene polymerization using bis(cyclopentadienyl) zirconium dichloride/methylaluminoxane as catalyst with considerable success (Soares et al., 1992; Vela-Estrada and Hamielec, 1994).

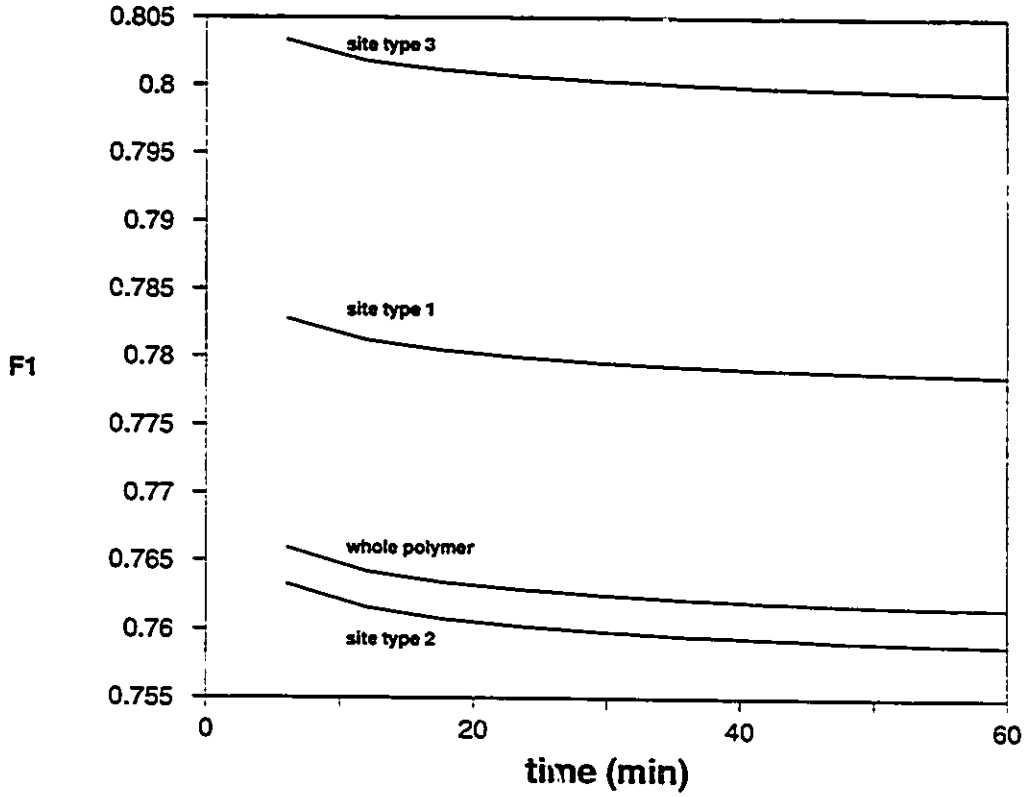

Figure 25 - Copolymerization over a 3 site type catalyst.

$k_{p_{1,1}}(1) = k_{p_{2,1}}(1) = 95 l/mol.s$; $k_{p_{2,2}}(1) = k_{p_{1,2}}(1) = 850 l/mol.s$;

$k_{p_{1,1}}(2) = k_{p_{2,1}}(2) = 950 l/mol.s$; $k_{p_{2,2}}(2) = k_{p_{1,2}}(2) = 9500 l/mol.s$;

$k_{p_{1,1}}(3) = k_{p_{2,1}}(3) = 9.5 l/mol.s$; $k_{p_{2,2}}(3) = k_{p_{1,2}}(3) = 75 l/mol.s$;

$C^*(1) = C^*(2) = C^*(3) = 0.0033 mol/l$; $[M_{0_1}] = 4 mol/l$; $[M_{0_2}] = 0.13 mol/l$;

$R_0 = 0.001 cm$; $D_1 = D_2 = 1x10^{-5} cm^2/s$

F1 - mol fraction of propylene in copolymer

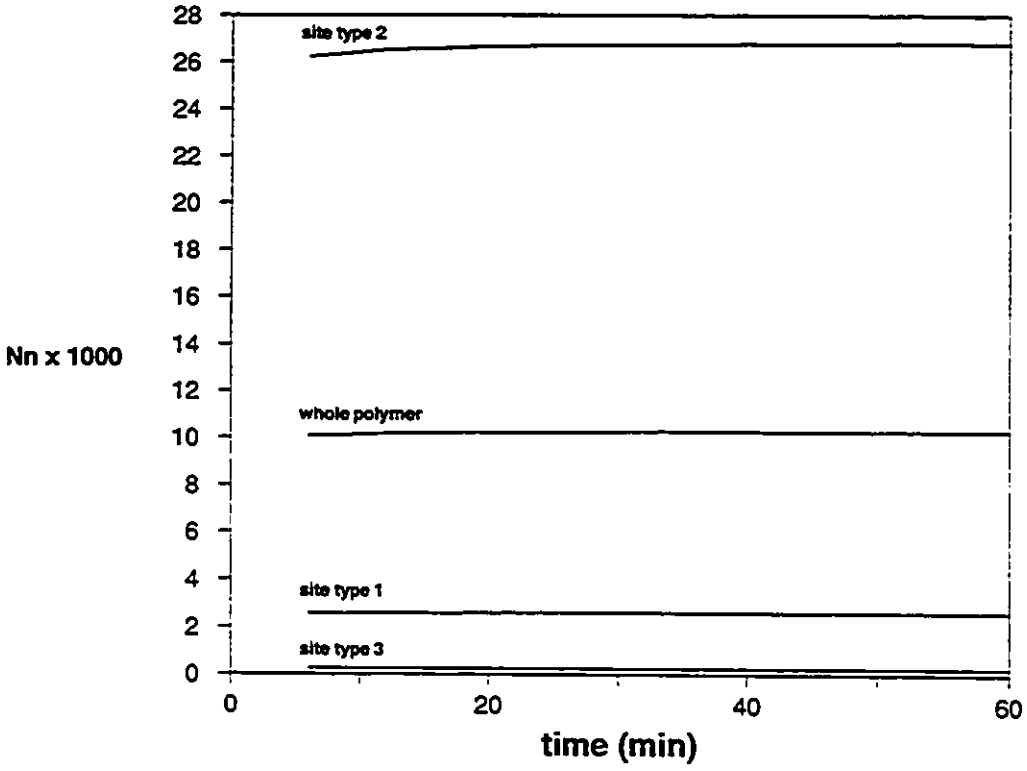

Figure 26 - Copolymerization over a 3 site type catalyst.

$K_{P_{1,1}}(1) = k_{P_{2,1}}(1) = 95 l/mol.s$; $k_{P_{2,2}}(1) = k_{P_{1,2}}(1) = 850 l/mol.s$;

$k_{P_{1,1}}(2) = k_{P_{2,1}}(2) = 950 l/mol.s$; $k_{P_{2,2}}(2) = k_{P_{1,2}}(2) = 9500 l/mol.s$;

$k_{P_{1,1}}(3) = k_{P_{2,1}}(3) = 9.5 l/mol.s$; $k_{P_{2,2}}(3) = k_{P_{1,2}}(3) = 75 l/mol.s$;

$C^*(1) = C^*(2) = C^*(3) = 0.0033 mol/l$; $[M_{0_1}] = 4 mol/l$; $[M_{0_2}] = 0.13 mol/l$;

$R_0 = 0.001 cm$; $D_1 = D_2 = 1x10^{-5} cm^2/s$

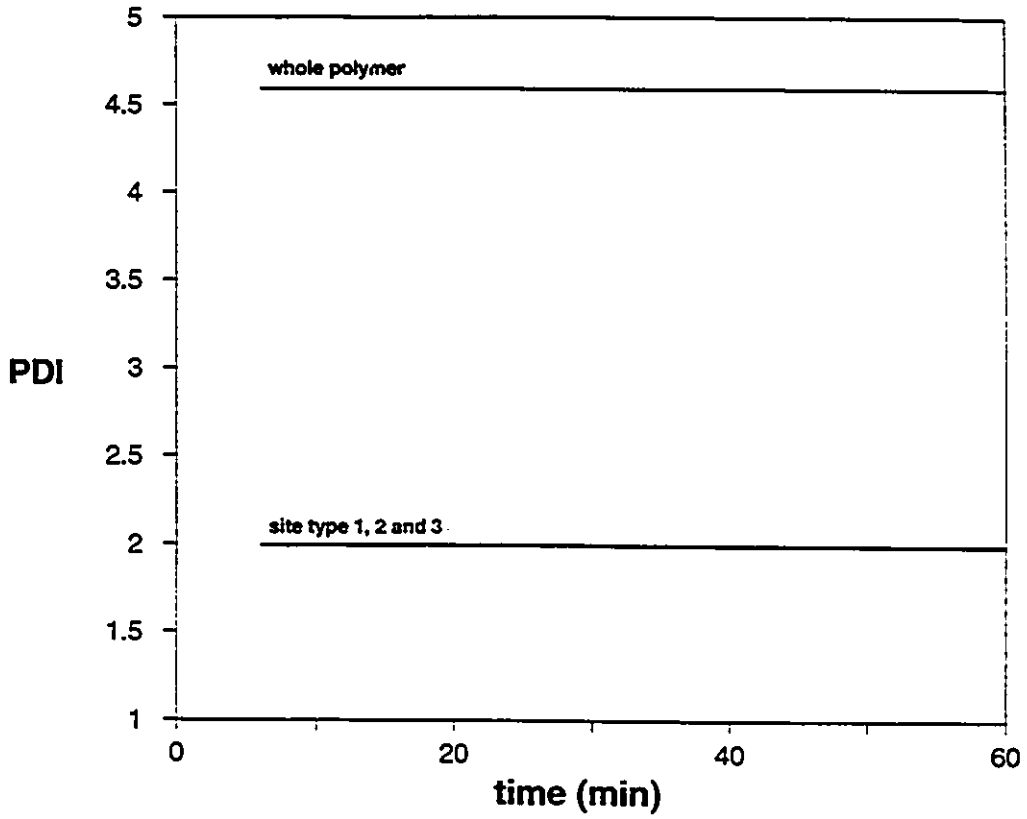

Figure 27 - Copolymerization over a 3 site type catalyst.

$k_{p_{1,1}}(1) = k_{p_{2,1}}(1) = 95 l/mol.s$; $k_{p_{2,2}}(1) = k_{p_{1,2}}(1) = 850 l/mol.s$;

$k_{p_{1,1}}(2) = k_{p_{2,1}}(2) = 950 l/mol.s$; $k_{p_{2,2}}(2) = k_{p_{1,2}}(2) = 9500 l/mol.s$;

$k_{p_{1,1}}(3) = k_{p_{2,1}}(3) = 9.5 l/mol.s$; $k_{p_{2,2}}(3) = k_{p_{1,2}}(3) = 75 l/mol.s$;

$C^*(1) = C^*(2) = C^*(3) = 0.0033 mol/l$; $[M_{0_1}] = 4 mol/l$; $[M_{0_2}] = 0.13 mol/l$;

$R_0 = 0.001 cm$; $D_1 = D_2 = 1x10^{-5} cm^2/s$

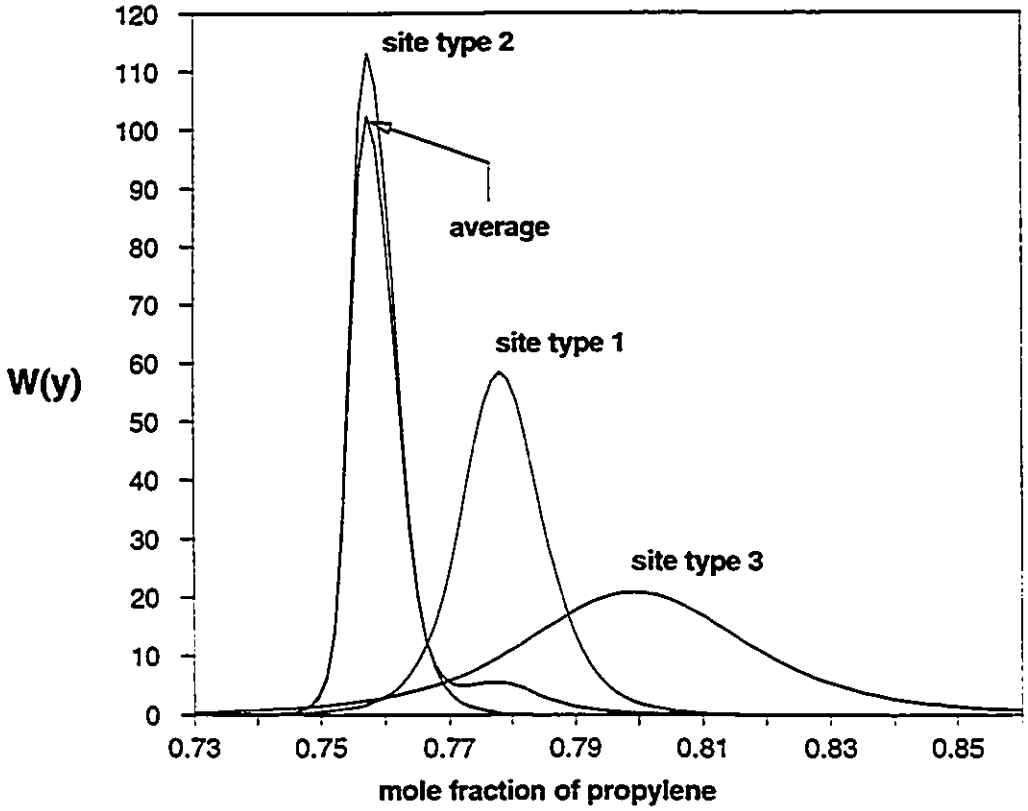

Figure 28 - CCD's for each site type over all layers for propylene-ethylene copolymerization.

$k_{P_{1,1}}(1) = k_{P_{2,1}}(1) = 95 l/mol.s$; $k_{P_{2,2}}(1) = k_{P_{1,2}}(1) = 850 l/mol.s$;

$k_{P_{1,1}}(2) = k_{P_{2,1}}(2) = 950 l/mol.s$; $k_{P_{2,2}}(2) = k_{P_{1,2}}(2) = 9500 l/mol.s$;

$k_{P_{1,1}}(3) = k_{P_{2,1}}(3) = 9.5 l/mol.s$; $k_{P_{2,2}}(3) = k_{P_{1,2}}(3) = 75 l/mol.s$;

$C^*(1) = C^*(2) = C^*(3) = 0.0033 mol/l$; $[M_{0_1}] = 4 mol/l$; $[M_{0_2}] = 0.13 mol/l$;

$R_0 = 0.001 cm$; $D_1 = D_2 = 1x10^{-5} cm^2/s$; $t = 1h$

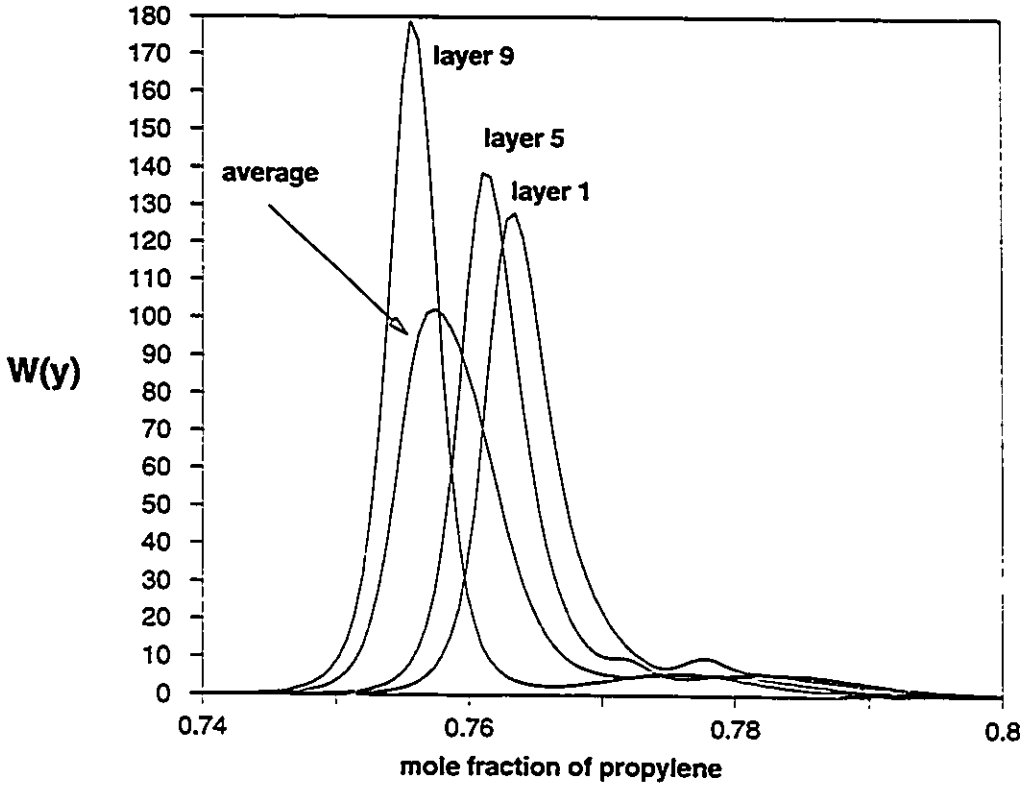

Figure 29 - CCD's considering all site types in different polymer layers for propylene-ethylene copolymerization.

$k_{p_{1,1}}(1) = k_{p_{2,1}}(1) = 95 l/mol.s$; $k_{p_{2,2}}(1) = k_{p_{1,2}}(1) = 850 l/mol.s$;

$k_{p_{1,1}}(2) = k_{p_{2,1}}(2) = 950 l/mol.s$; $k_{p_{2,2}}(2) = k_{p_{1,2}}(2) = 9500 l/mol.s$;

$k_{p_{1,1}}(3) = k_{p_{2,1}}(3) = 9.5 l/mol.s$; $k_{p_{2,2}}(3) = k_{p_{1,2}}(3) = 75 l/mol.s$;

$C^*(1) = C^*(2) = C^*(3) = 0.0033 mol/l$; $[M_{0_1}] = 4 mol/l$; $[M_{0_2}] = 0.13 mol/l$;

$R_0 = 0.001 cm$; $D_1 = D_2 = 1x10^{-5} cm^2/s$; $t = 1h$

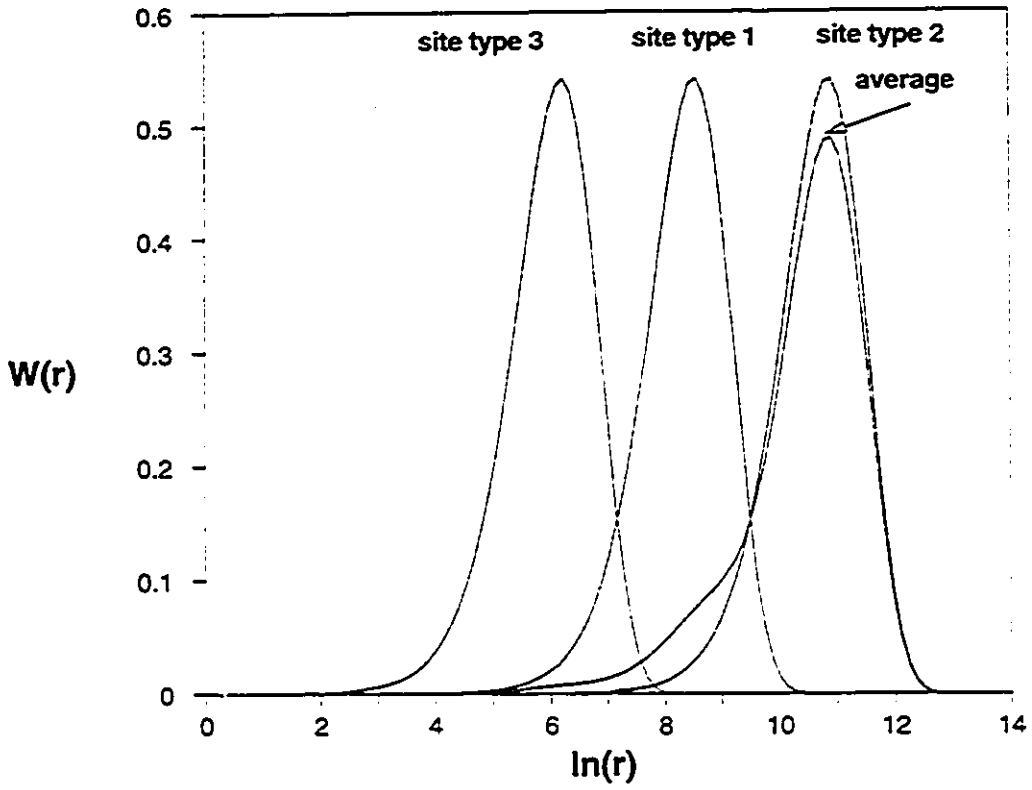

Figure 30 - Chain length distribution for each site type over all layers for propylene-ethylene copolymerization.

$k_{P_{1,1}}(1) = k_{P_{2,1}}(1) = 95 l/mol.s$; $k_{P_{2,2}}(1) = k_{P_{1,2}}(1) = 850 l/mol.s$;

$k_{P_{1,1}}(2) = k_{P_{2,1}}(2) = 950 l/mol.s$; $k_{P_{2,2}}(2) = k_{P_{1,2}}(2) = 9500 l/mol.s$;

$k_{P_{1,1}}(3) = k_{P_{2,1}}(3) = 9.5 l/mol.s$; $k_{P_{2,2}}(3) = k_{P_{1,2}}(3) = 75 l/mol.s$;

$C^*(1) = C^*(2) = C^*(3) = 0.0033 mol/l$; $[M_{0,1}] = 4 mol/l$; $[M_{0,2}] = 0.13 mol/l$;

$R_0 = 0.001 cm$; $D_1 = D_2 = 1x10^{-5} cm^2/s$; $t = 1h$

Conclusion

The polymeric multilayer model is a versatile model that can simulate both heterogeneous and homogeneous Ziegler-Natta polymerizations. Its formulation permits one to eliminate the mesoscale phenomena steps without changing the equations for the population balances, molecular weight averages and copolymer composition. For the special case of binary copolymerization of linear copolymers, chain length and chemical composition distributions can be estimated using Stockmayer's distribution.

Our simulation results confirm the predictions of other expansion models regarding the effects of mass and heat transfer resistances in the performance of heterogeneous Ziegler-Natta catalysts.

Mass transfer resistances alone can not account for the broad MWDs and CCDs for polymer made by heterogeneous Ziegler-Natta catalysts. This behaviour can be better explained by assuming that more than one active site type exists on the catalyst.

However, especially for large, high activity catalysts, mass transfer resistances can reduce the polymerization rate, decrease molecular weight averages and affect copolymer composition, thus contributing to the total broadening of MWD and CCD.

Particularly important for supported catalyst, high active site concentrations can increase mass transfer resistances and have undesirable results in catalyst performance and product quality. From the point of view of product quality control, production of polymer with well defined MWDs and CCDs is highly desirable.

Mass transfer resistance may also be a source of further composition heterogeneity for highly active and large catalyst particles, if the monomers have reactivities that differ significantly. In this case copolymer composition will be a function of both radial position and reaction time even in the total absence of

composition drift due to differing reactivity ratios. This is an especially important consideration for the technology of supported metallocene catalysts, where single site , highly active species may be subjected to mass and heat transfer resistances.

Temperature gradients in the polymeric particle are not expected to be a significant factor for reactions carried out in slurry reactors.

CHAPTER 4 - MATHEMATICAL MODELLING OF POLYMERIZATION IN A SERIES OF CONTINUOUS STIRRED TANK REACTORS USING ZIEGLER-NATTA CATALYSTS IN A SLURRY PROCESS

Model Development

This chapter defines the macroscale mathematical model for the dynamic simulation of copolymerization of olefins with Ziegler-Natta catalysts in a series of continuous stirred tank reactors (CSTRs).

The same kinetics of polymerization adopted for multiple site type catalysts in the previous chapter is used in the macroscale model, but intraparticle mass and heat transfer resistances are neglected.

Considering that mass and heat transfer resistances are generally of little significance when compared to the effect of multiple site types in heterogeneous Ziegler-Natta catalysts, the population balance equations derived for the multilayer model can be directly used in the macroscopic model to calculate molecular weight averages, composition averages, and conversion using bulk monomer concentrations in the diluent and the average polymerization temperature in the reactor.

Additional equations have to be developed only for the simulation of the macroscopic behaviour of the reactor such as gas-liquid equilibria, mass balance of chemical species in the reactor, energy balance around the reactor, and process control and residence time distribution (appendix B).

A schematic of the modelled reactor system is presented in figure 1 for a series of two reactors. A suspension of catalyst and cocatalyst in diluent is fed at a constant rate to the first reactor in the series (*stream 1*). A gas phase mixture of monomers, hydrogen, nitrogen or other inert compounds, and impurities is continuously fed to all of the reactors in the series (*stream 2*). The reactional diluent

phase containing dead and living polymer chains, catalyst, cocatalyst, and dissolved gases is transferred to the subsequent reactors at the same rate as stream 1 (*stream 3*). A vent line can be used to purge the reactor head space (*stream 4*).

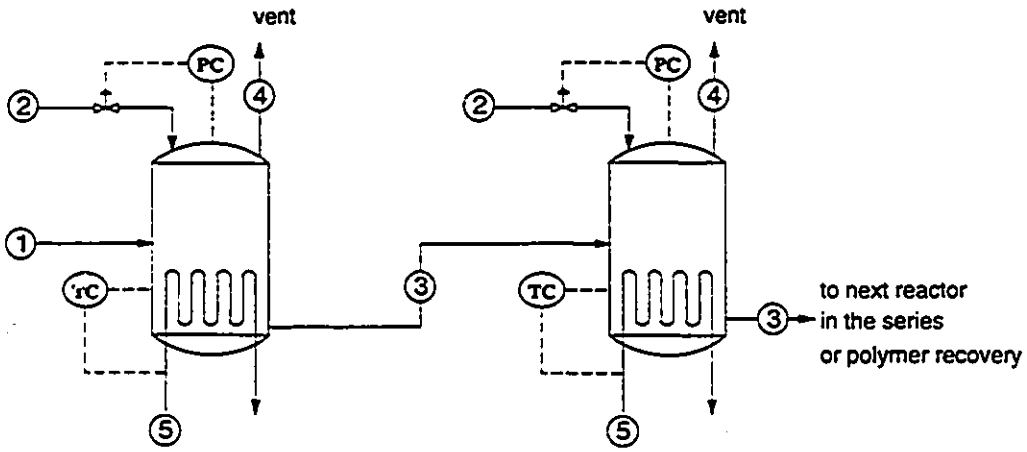

Figure 1 - Series of two CSTRs for the polymerization of olefins using Ziegler-Natta catalysts (Stream 1: diluent suspension of catalyst and cocatalyst. Stream 2: gaseous supply of monomers, hydrogen, inerts, and impurities. Stream 3: diluent suspension of polymer, catalyst, cocatalyst and dissolved gases. Stream 4: vent line. Stream 5: cooling water).

The reactor pressure is controlled by varying the flow of stream 2 using a PID controller. The reactor temperature is regulated using a PID controller by varying the temperature of cooling water (*stream 5*) to the polymerization reactor.

Polymerization of olefins in slurry CSTRs in series is commonly used for the commercial production of homopolymers, random copolymers and impact copolymers of olefins with Ziegler-Natta catalysts. Homopolymerization can be performed in one or more reactors in series. The same or different polymerization conditions can be used in each one of the reactors in the series for the production of distinct grades. Random copolymers are produced by feeding a mixture of comonomers to the reactors under polymerization conditions similar to those used for homopolymerization. Polymerization temperatures may be slightly lower than the ones used for homopolymerization to minimize reactor fouling by the stickier copolymer. The manufacture of impact copolymers requires at least two reactors in

series. Only one monomer type is fed to the first reactor or set of reactors, producing regular homopolymer. A mixture of comonomers is fed to the subsequent reactors in the series and therefore random copolymer is produced among the already formed homopolymer. The random copolymer fraction is responsible for increasing the impact strength of the homopolymer matrix formed in the first set of reactors. Impact copolymers are sometimes improperly called *block copolymers*, implying that their chains contain a block of homopolymer, formed in the first set of reactors, and a block of random copolymer, produced in the last set of reactors. However, since the lifetime of a polymer chain is much smaller then the reactor residence time, the amount of actual block copolymer produced is certainly negligible (Ver Strate, 1986; Whiteley et al., 1992).

Kinetics

The reaction kinetics include the steps of site formation, initiation, propagation, transfer to monomer, transfer to co-catalyst, transfer to hydrogen, spontaneous transfer (such as β-hydride elimination), deactivation and reaction with impurities, described in the previous chapter. Long chain branching reactions (addition of a polymeric macromonomer with terminal vinyl unsaturation to form trifunctional long chain branches) are not considered although they could be readily incorporated into the model.

Monomer and Temperature Radial Profiles in the Polymer-Catalyst Particle

Since heat and mass transfer resistances play a minor role in slurry polymerization of olefins using heterogeneous Ziegler-Natta catalysts as shown in the previous chapter and also demonstrated by several other theoretical and

experimental works (Chien et al., 1985; Zucchini and Cecchin, 1983; Usami et al., 1986; Ray, 1988), no mesoscale phenomena will be accounted for in the macroscale model proposed herein.

Population Balances

The same population balances for the active species defined for each concentric layer in the multilayer model, equations (25) to (42) of the previous chapter, will be used in the macroscale model with the bulk concentration of monomer in the diluent and with the average polymerization temperature in the reactor. The use of pseudo-kinetic rate constants as defined by equations (12) to (19) in the previous chapter will be again adopted to simplify the mathematical treatment of copolymerization.

Chain Length Averages and Copolymer Composition

Chain length averages and copolymer composition are estimated using the equations derived for the multilayer model, expressions (43) to (51) of the previous chapter.

Macroscopic Balance Around the Polymerization Reactor

Equations describing the total moles of each component in the reactor system are easily derived from a macroscopic mole balance around each reactor:

$$\frac{dN_i^T}{dt} = \dot{n}_{in,i}^s + \dot{n}_{in,i}^l - r_i V_r^l - \frac{N_i^l}{V_r^l}\dot{v}_{out}^l - \frac{N_i^s}{V_r^s}\dot{v}_{out}^s \tag{1}$$

$$\frac{dN_{H_2}^T}{dt} = \dot{n}_{in,H_2}^s + \dot{n}_{in,H_2}^l - r_{H_2} V_r^l - \frac{N_{H_2}^l}{V_r^l}\dot{v}_{out}^l - \frac{N_{H_2}^s}{V_r^s}\dot{v}_{out}^s \tag{2}$$

$$\frac{dN_{N_2}^T}{dt} = \dot{n}_{in,N_2}^g + \dot{n}_{in,N_2}^l - \frac{N_{N_2}^l}{V_r^l}\dot{v}_{out}^l - \frac{N_{N_2}^g}{V_r^g}\dot{v}_{out}^g \tag{3}$$

$$\frac{dN_D^T}{dt} = \dot{n}_{in,D}^l - \frac{N_D^l}{V_r^l}\dot{v}_{out}^l - \frac{N_D^g}{V_r^g}\dot{v}_{out}^g \tag{4}$$

$$\frac{dN_A^T}{dt} = \dot{n}_{in,A}^l - r_A V_r^l - \frac{N_A^l}{V_r^l}\dot{v}_{out}^l \tag{5}$$

$$\frac{dN_{imp}^T}{dt} = \dot{n}_{in,imp}^g + \dot{n}_{in,imp}^l - r_{imp} V_r^l - \frac{N_{imp}^l}{V_r^l}\dot{v}_{out}^l - \frac{N_{imp}^g}{V_r^g}\dot{v}_{out}^g \tag{6}$$

where,

N	moles of a given chemical component in the reactor.
t	time.
$\dot{n}_{in}$	mol flow rate of a given chemical component to the reactor, mol/time.
r	reaction rate of a given chemical component, mol/time.volume.
V_r	reactor volume.
$\dot{v}_{out}$	volumetric flow rate from reactor, volume/time.

The subscripts symbolize: i - monomer type, H_2 - hydrogen, N_2 - nitrogen or any other inert gas, D - diluent, A - cocatalyst, and *imp* - impurities or reversible catalyst poisons. The superscripts denote: T - liquid and gas phases, g - gas phase, and l - liquid phase.

The concentrations needed to calculate the polymerization rate are those of reagents dissolved in the diluent. These concentrations can be estimated using the gas-liquid treatment suggested by Kissin (1985) and De Carvalho et al. (1989). Ideal

behaviour is assumed for both gas and liquid phases while the ideal gas law is used to describe the gas phase. Henry's law is used to calculate the dissolution of monomers, hydrogen, inerts and impurities in the diluent. Raoult's law is applied to the diluent (Smith and Van Ness, 1987).

Therefore the gas-liquid equilibrium of monomer type i in the reactor is expressed as:

$$x_i k_i = y_i P \tag{7}$$

where,

x mol fraction of a given chemical species dissolved in the diluent, N_i^l / N_T^l.

y mol fraction of a given chemical species in gas phase, N_i^g / N_T^g.

k Henry's law constant.

P total reactor pressure.

Equivalent equations are easily derived for hydrogen, inerts, impurities and diluent:

$$x_{H_2} k_{H_2} = y_{H_2} P \tag{8}$$

$$x_{N_2} k_{N_2} = y_{N_2} P \tag{9}$$

$$x_{imp} k_{imp} = y_{imp} P \tag{10}$$

$$x_D P_D^{sat} = y_D P \tag{11}$$

where Raoult's law is used for the diluent in place of Henry's law. The cocatalyst is considered non-volatile.

A final system of (10+2m) algebraic equations and (10+2m) unknowns results, where m is the number of monomer types in the reactor:

$$\frac{N_i^l}{N_T^l}k_i = \frac{N_i^g}{N_T^g}P \tag{12}$$

$$\frac{N_{H_2}^l}{N_T^l}k_{H_2} = \frac{N_{H_2}^g}{N_T^g}P \tag{13}$$

$$\frac{N_{N_2}^l}{N_T^l}k_{N_2} = \frac{N_{N_2}^g}{N_T^g}P \tag{14}$$

$$\frac{N_{imp}^l}{N_T^l}k_{imp} = \frac{N_{imp}^g}{N_T^g}P \tag{15}$$

$$\frac{N_D^l}{N_T^l}P_D^{sat} = \frac{N_D^g}{N_T^g}P \tag{16}$$

$$N_T^l = \sum_{i=1}^{m} N_i^l + N_{H_2}^l + N_{N_2}^l + N_{imp}^l + N_D^l \tag{17}$$

$$N_T^g = \sum_{i=1}^{m} N_i^g + N_{H_2}^g + N_{N_2}^g + N_{imp}^g + N_D^g = \frac{PV_r^g}{RT} \tag{18}$$

$$N_i^T = N_i^l + N_i^g \tag{19}$$

$$N_{H_2}^T = N_{H_2}^l + N_{H_2}^g \tag{20}$$

$$N_{N_2}^T = N_{N_2}^l + N_{N_2}^g \tag{21}$$

$$N_{imp}^T = N_{imp}^l + N_{imp}^g \tag{22}$$

$$N_D^T = N_D^l + N_D^g \tag{23}$$

where,

P^{sat} saturated vapour pressure.

R molar gas constant.

T absolute temperature.

The above system of non-linear algebraic equations can be simplified by noticing that, for equation (12):

$$\frac{N_i^l}{N_T^l} k_i = \frac{N_i^T - N_i^l}{N_T^g} P \tag{24}$$

Using the ideal gas law to eliminate N_T^g:

$$N_i^l \left(\frac{k_i}{N_T^l} \frac{V_r^g}{RT} + 1 \right) - N_i^T = 0 \tag{25}$$

Similarly, for the remaining equations:

$$N_{H_2}^l \left(\frac{k_{H_2}}{N_T^l} \frac{V_r^g}{RT} + 1 \right) - N_{H_2}^T = 0 \tag{26}$$

$$N_{N_2}^l \left(\frac{k_{N_2}}{N_T^l} \frac{V_r^g}{RT} + 1 \right) - N_{N_2}^T = 0 \tag{27}$$

$$N_{imp}^l \left(\frac{k_{imp}}{N_T^l} \frac{V_r^g}{RT} + 1 \right) - N_{imp}^T = 0 \tag{28}$$

$$N_D^l\left(\frac{P_D^{sat}}{N_T^l}\frac{V_r^g}{RT}+1\right)-N_D^T=0 \tag{29}$$

The system of algebraic equations defined by (25) to (29) and (17) can be solved to estimate the number of moles of all reagents and inerts in the diluent phase: $N_i^l, N_{H2}^l, N_{N2}^l, N_{im}^l, N_D^l$. The total number of moles of chemical species in the reactor, $N_i^T, N_{H2}^T, N_{N2}^T, N_{im}^T, N_D^T$, are obtained at each time step by solving the system of ordinary differential equations defined by expressions (1) to (6).

An alternative way of solving the system of algebraic equations defined by expressions (25) to (29) and (17) is derived in appendix A. This method uses the fact that the fraction of diluent in the liquid phase is very close to unity to accelerate the convergence rate. This alternative algorithm proved to be faster then the Newton-Raphson method for the same convergence tolerance.

Energy Balance

Non-isothermal operation can be easily described by an energy balance around each reactor:

$$\sum_i C_{p_i} N_i^T \frac{dT}{dt} = UA(T_{cw}-T)-\sum_i \Delta H_i r_i V_r^l-\sum_i \dot{n}_{in,i}^g C_{p_i}\left(T-T_{i_0}\right) \tag{30}$$

$$-\sum_i \dot{n}_{in,i}^l C_{p_i}\left(T-T_{i_0}\right)$$

where i indicates monomer type, hydrogen, nitrogen, diluent, or impurities.

Process Control Equations

Equations for proportional-integral-derivative (PID) controllers are generally expressed as a continuous function of time for analog controllers:

$$c(t)=K_c\left[e(t)+\frac{1}{\tau_I}\int_0^t e(t)dt+\tau_D\frac{de(t)}{dt}\right] \tag{31}$$

or as a discrete function of time for digital controllers (Stephanopoulos, 1984):

$$C_n = K_c\left[\varepsilon_n + \frac{\Delta t}{\tau_I}\sum_{i=0}^{n}\varepsilon_i + \tau_D\frac{\varepsilon_n - \varepsilon_{n-1}}{\Delta t}\right] \tag{32}$$

where,

$c(t)$	analog controller action.
C_n	digital controller action at time n.
t	time.
$e(t)$	deviation from set point as a continuous function of time.
ε_n	deviation from set point at acquisition time n.
Δt	acquisition time interval.
K_c	proportional gain.
τ_I	integral time constant.
τ_D	derivative time constant.

As shown in figure 1, PID controllers are used to regulate the pressure and temperature of the polymerization reactors. The digital controller formulation was adopted in the simulation program for the macroscopic model since its implementation requires only minor modifications of the program code. The numerical method for the solution of the ODEs is in itself discrete in time and therefore the digital controller routine can be called outside the ODE solver at a determined acquisition time interval.

At a user determined time acquisition interval, that can be as small as the integration time interval automatically selected by LSODAR routine, the control variables, gas flow of reagents (stream 2) and temperature of cooling water (stream 5), are corrected using the equations:

$$(\dot{n}_{in}^{g})_{n+1} = (\dot{n}_{in}^{g})_n + C^{*}{}_n \quad , \qquad \dot{n}_{in}^{g} \geq 0 \tag{33}$$

$$(T_{cw})_{n+1} = (T_{cw})_n + C''_n \quad , \qquad T_{cw}^{min} < T_{cw} < T_{cw}^{max} \tag{34}$$

where,

n_{in}^g mole flow rate of gas mixture (stream 2) to reactor, mol/time.

T_{cw} temperature of cooling water.

C' pressure controller action, calculated by defining $\varepsilon_n = P^{sp} - P_n$ in equation (32).

C'' temperature controller action, calculated by defining $\varepsilon_n = T_n - T^{sp}$ in equation (32).

T_{cw}^{min} minimum temperature for cooling water.

T_{cw}^{max} maximum temperature for cooling water.

and the subscripts n, $n+1$ indicate iteration time, and sp indicates the control variable setpoint.

Numerical Solution

The final system of ordinary differential equations that comprises the macroscopic model is defined, for each reactor in the series, by equations (1) to (6) for the macroscopic mole balance around the reactor, by equation (30) for the energy balance around the reactor, and by several equations from the previous chapter: equations (25) to (42) for the population balance of active species in the reactor; equation (43) for the copolymer composition; and equations (49) to (51) for the moments of dead and living polymer. This system can be solved using several numerical methods for ordinary differential equations (Press et al., 1992).

We adopted the well established numerical package LSODAR (Hindmarsh). This numerical package automatically tests whether the system of ordinary differential equations is stiff or not and selects the integration step size according to a tolerance specified by the user.

The following general algorithm was used for solving the system of algebraic-differential equations:

1. Input data
2. Set initial conditions
3. Solve system of ODEs using LSODAR from $t + \Delta t$
4. Calculate pressure and temperature controller actions
5. Calculate copolymer composition
6. Calculate average molecular weights
7. Calculate polymer production
8. Increment time
9. If time less then end time then return to step 3
10. End

Results and Discussion

The macroscopic model was used to study the dynamics of a series of four CSTRs of equal volumes producing impact copolymer. The first two reactors in the series produce only homopolymer while the two last reactors produce random copolymer. Tables 1, 2, and 3 show the parameters used in the simulation. Those parameters were obtained for an industrial process for the production of propylene-ethylene impact copolymer in a series of CSTRs of equal volumes

Reactors volume (liquid phase)	1000 l
Reactors volume (gas phase)	150 l
Reactors pressure (set-point)	6 atm
Reactors temperature (set-point)	60 °C
PID controller parameters	
•Pressure - K_c, τ_I, τ_D	100, 1000, 0
•Temperature - K_c, τ_I, τ_D	1, 10, 0.1
Number of active site types	2
Concentration of active sites of type 1 in feed	2.7×10^{-6} mol/l
Concentration of active sites of type 2 in feed	2.7×10^{-6} mol/l
Mean residence time in reactors	2.1 h
Mole % of monomer 1 in feed (reactors 1 and 2)	99.99 %
Mole % of monomer 1 in feed (reactors 3 and 4)	50 %
Mole % of monomer 2 in feed (reactors 1 and 2)	0 %
Mole % of monomer 2 in feed (reactors 3 and 4)	50 %
Mole % of hydrogen in feed (reactors 1 and 2)	0.01 %
Mole % of hydrogen in feed (reactors 3 and 4)	0 %
Global heat transfer coefficient	2.0×10^4 cal/K.m^2.h
Total transfer area	200 m^2

Table 1 - Reactor operation conditions at beginning of simulation. If not explicitly indicated, conditions are equal for all reactors in the series.

	A	B	C
Diluent - P_D^{sat}	4.211	0.1686×10^4	0.5202×10^2
Monomer 1 - k_1	0.2756×10^3	0.1396×10^6	0.1793×10^8
Monomer 2 - k_2	0.422	0.7046×10^3	
Hydrogen - k_{H_2}	1×10^3		
Nitrogen - k_{N_2}	1×10^3		
Impurity - k_{imp}	1×10^3		

Table 2 - Physical properties of reagents.

Partial pressure of diluent: $$\log_{10} P_d^{sat} = A - \frac{B}{T(K) - C}$$

Henry's law constant:

monomer 1 $$k_1 = A - \frac{B}{T(K)} + \frac{C}{T(K)^2}$$

monomer 2 $$k_2 = A k_1 e^{B/T(k)}$$

others $$k_i = A \qquad i = H_2, N_2, imp$$

	i	k	site type 1	site type 2
k_f (1/s)			2000	4000
k_{d_s}(1/s)			0	0
k_{dM} (1/s)			2000	1000
k_{H_A} (1/s)			2000	4000
k_a (1/s)			0	0
k_{i_i} (l/mol.s)	1		600	2500
	2		2000	4000
k_{H_i} (l/mol.s)	1		600	2500
	2		2000	4000
k_{tH_i} (l/mol.s)	1		0.55	0.055
	2		0.55	0.055
k_{tD_i} (l/mol.s)	1		0	0
	2		0	0
k_{tA_i} (l/mol.s)	1		0	0
	2		0	0
$k_{P_{ik}}$ (l/mol.s)	1	1	200	400
	1	2	2000	4000
	2	1	200	400
	2	2	2000	4000
$k_{tm_{ik}}$ (l/mol.s)	1	1	0.03	0.003
	1	2	0.03	0.003
	2	1	0.03	0.003
	2	2	0.03	0.003

Table 3 - Polymerization kinetics parameters.

time (h)	Condition before change	Condition after change
50	M1/M2 = 1	M1/M2 = 2.33
100	$H2_{feed}$ = 0.01%	$H2_{feed}$ = 0.1%
150	P = 6 atm	P = 7 atm
200	$H2_{feed}$ = 0.1%	$H2_{feed}$ = 0.01%
250	M1/M2 = 2.33	M1/M2 = 1
300	P = 7 atm	P = 6 atm

Table 4 - Operation condition changes of impact copolymer manufacture in CSTR in series (figures 2 to 10). M1/M2 - molar ratio of monomer 1 and 2; $H2_{feed}$ - hydrogen molar concentration in gas feed; P - reactor pressure.

(De Carvalho et al., 1989b), except for the reactor volumes and heat transfer areas that were arbitrarily chosen. The physical properties of monomer 1 and monomer 2 are those of propylene and ethylene, respectively.

Table 4 shows how some of the reactor operation conditions vary during a 360 hour polymerization for the simulations illustrated in figures 2 to 10. Hydrogen is fed only to the two first reactors in the series.

Figure 2 shows the time profiles of number average molecular weight (M_n) of polymer produced in each one of the four reactors in the series. The increase in ratio of monomer 1 to monomer 2 at t = 50 h decreases M_n of polymer made in reactors 3 and 4, since monomer 1 is less reactive then monomer 2. M_n of polymer made in reactors 1 and 2 remains unaffected since those reactors only homopolymerize monomer 1. The increase in hydrogen concentration at t = 100 h immediately causes M_n to decrease in all four reactors, due to an intensification of chain transfer to hydrogen. The increase in polymerization pressure at t = 150 h has almost no effect on M_n; the observed perturbation is related to the pressure controller action.

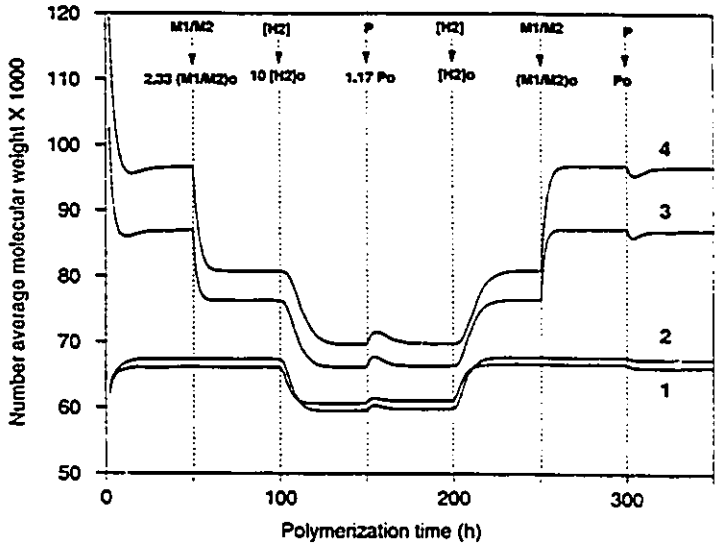

Figure 2 - Number average molecular weight profiles of a binary copolymerization of olefins with a two site type Ziegler-Natta catalyst in four CSTRs in series (M1/M2 - molar ratio of monomer 1 and 2; [H2] - hydrogen concentration in gas feed; P - reactor pressure, Po - initial reactor pressure).

Resetting the pressure of hydrogen, ratio of monomer 1 to monomer 2, and polymerization pressure at t = 200 h, 250 h, and 300 h, respectively, returns the values of M_n to those obtained in the beginning of the simulation.

The effect of changing the same polymerization conditions on the polydispersity index (PID) is shown in figure 3. The decrease of PID of reactors 3 and 4 with the increase of monomer 1/monomer 2 ratio at t = 50 h is a reflection of the process of making impact copolymer. Since reactors 1 and 2 make only homopolymer of monomer 1, increasing the relative amount of monomer 1 in reactors 3 and 4 approximates the operation conditions of those reactors to those obtained in reactors 1 and 2, thus decreasing the polydispersity. Notice how in figure 2, after the increase in monomer 1 concentration, M_n of polymer made in reactors 3 and 4 approximates that of polymer produced in the first two reactors. Increasing hydrogen concentration at t = 100 h immediately increases the polydispersity index, because of the accumulation of hydrogen in the reactor head space. Increase in polymerization

pressure has no effect on polydispersity; the observed perturbations are again caused by the pressure controller action. PIDs of polymer made in all reactors return to their initial values after all polymerization conditions are restored to their original values.

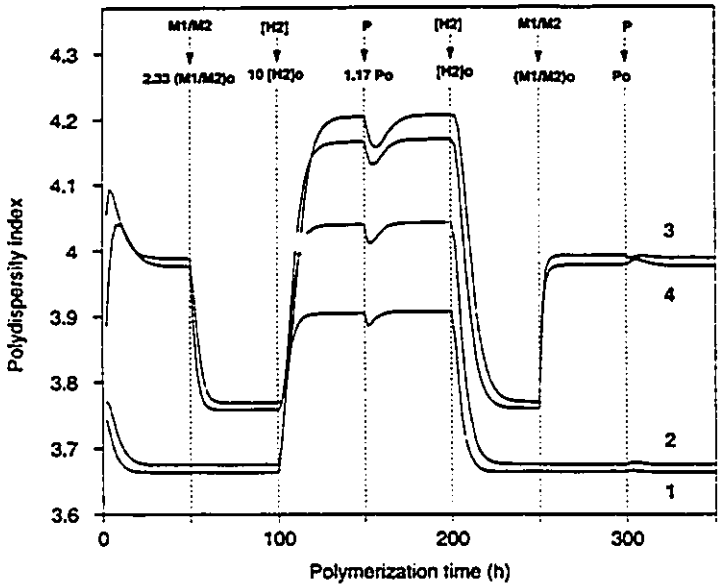

Figure 3 - Polydispersity index profiles of a binary copolymerization of olefins with a two site type Ziegler-Natta catalyst in four CSTRs in series (M1/M2 - molar ratio of monomer 1 and 2; [H2] - hydrogen concentration in gas feed; P - reactor pressure, Po - initial reactor pressure).

Figure 4 studies the effect of the polymerization conditions on copolymer composition. As expected, only the ratio of monomer 1 to monomer 2 has a permanent influence on copolymer composition in this system.

The actions of the pressure controller are illustrated in figure 5. As can be seen, the controller is able to regulate the total pressure of each reactor very well for the chosen tuning parameters. Variations of hydrogen concentration in the gas inlet stream are likely to have the most lasting impact on reactor pressure due to the lower reactivity of hydrogen.

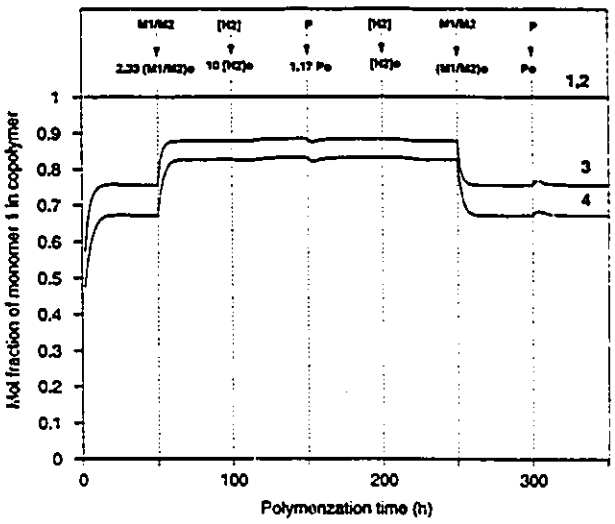

Figure 4 - Copolymer composition profiles of a binary copolymerization of olefins with a two site type Ziegler-Natta catalyst in four CSTRs in series (M1/M2 - molar ratio of monomer 1 and 2; [H2] - hydrogen concentration in gas feed; P - reactor pressure, Po - initial reactor pressure).

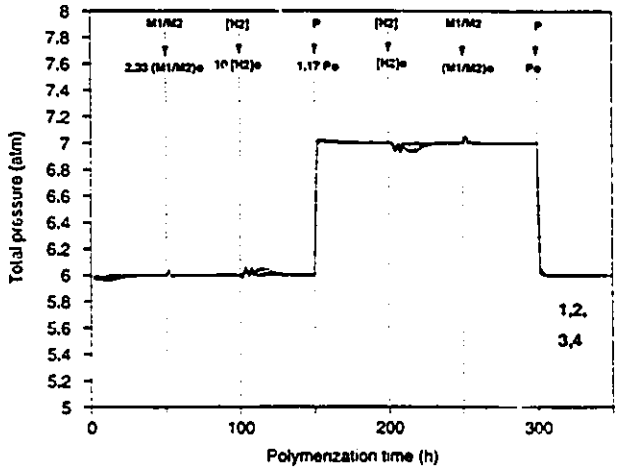

Figure 5 - Reactor pressure profiles of a binary copolymerization of olefins with a two site type Ziegler-Natta catalyst in four CSTRs in series (M1/M2 - molar ratio of monomer 1 and 2; [H2] - hydrogen concentration in gas feed; P - reactor pressure, Po - initial reactor pressure).

The total production of polymer in each reactor is shown in figure 6. The increase of the ratio of monomer 1 to monomer 2 decreases the polymer production of reactors 3 and 4 since monomer 1 is less reactive than monomer 2. Increase of hydrogen concentration also decreases the polymer production of all reactors. As a consequence of being less reactive than each monomer and of the reactor pressure control, hydrogen accumulates in the reactor, occupying space that would otherwise be used by monomer. In other to compensate for this effect, the total pressure of the reactor should be increased to keep constant the partial pressure of monomers. The increase of polymerization pressure at time $t = 100$ h increases polymer production since polymerization rate has a first order dependency on monomer concentration.

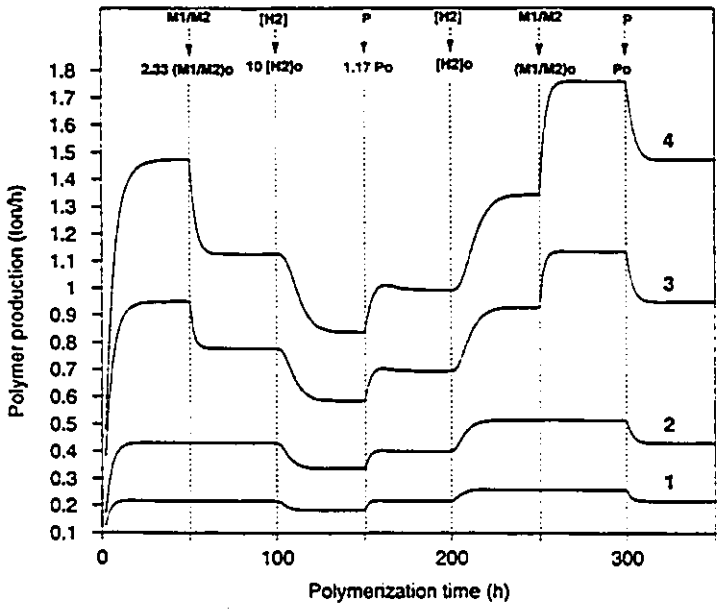

Figure 6 - Polymer yield profiles of a binary copolymerization of olefins with a two site type Ziegler-Natta catalyst in four CSTRs in series (M1/M2 - molar ratio of monomer 1 and 2; [H2] - hydrogen concentration in gas feed; P - reactor pressure, Po - initial reactor pressure).

Figure 7 shows the concentration profiles of monomer 1 in the gas phase of the reactors. The most interesting effect is the sharp drop in monomer concentration when the amount of hydrogen fed to the reactor is increased at $t = 100$. This effect is even more pronounced in reactor 2 since in addition to the fresh gas feed of

hydrogen, the diluent slurry transferred from reactor 1 already contains dissolved hydrogen. Being significantly less reactive than the monomers, hydrogen slowly accumulates in the head space of the reactor, causing the monomer concentration and polymer production to drop. Concentration of hydrogen in the gas phase of the reactor is shown in figure 8. In a similar way, the liquid phase concentration of monomer 1 in the reactor is presented in figure 9. The relationship between concentrations of monomers and hydrogen is shown in figure 10 in dimensionless form for the last reactor in the series.

During all operation conditions, the temperature controller was able to keep the reactor temperature regulated within 2 ^{0}C of the set-point.

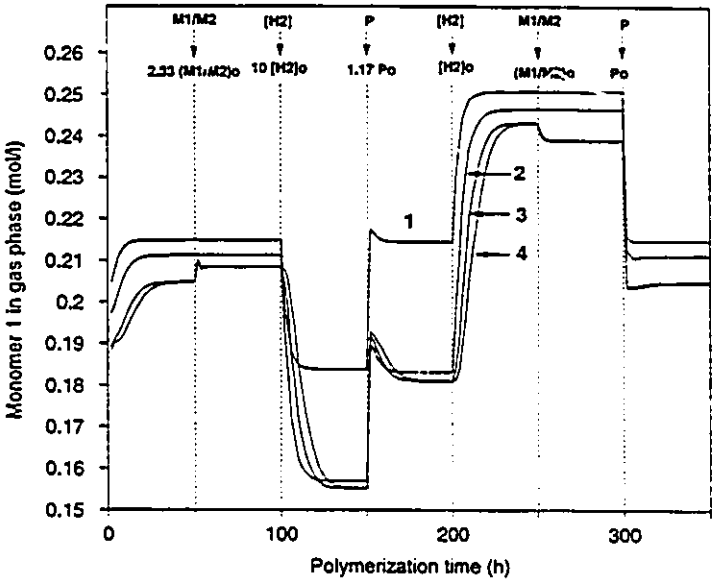

Figure 7 - Concentration profiles of monomer 1 in gas phase of a binary copolymerization of olefins with a two site type Ziegler-Natta catalyst in four CSTRs in series (M1/M2 - molar ratio of monomer 1 and 2; [H2] - hydrogen concentration in gas feed; P - reactor pressure, Po - initial reactor pressure).

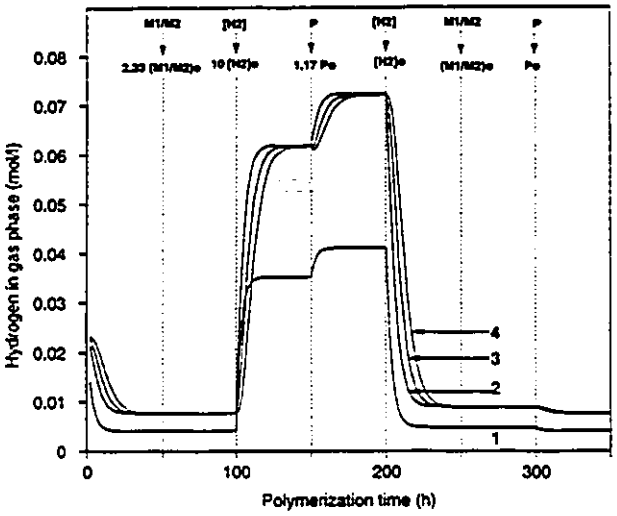

Figure 8 - Concentration profiles of hydrogen in gas phase of a binary copolymerization of olefins with a two site type Ziegler-Natta catalyst in four CSTRs in series (M1/M2 - molar ratio of monomer 1 and 2; [H2] - hydrogen concentration in gas feed; P - reactor pressure, Po - initial reactor pressure).

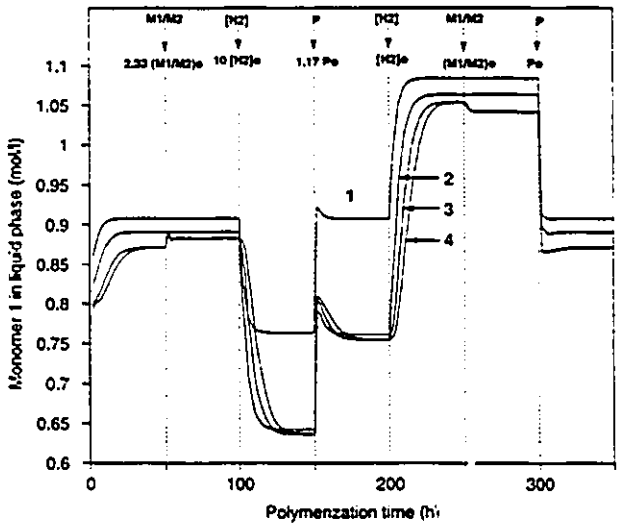

Figure 9 - Concentration profiles of monomer 1 in liquid phase of a binary copolymerization of olefins with a two site type Ziegler-Natta catalyst in four CSTRs in series (M1/M2 - molar ratio of monomer 1 and 2; [H2] - hydrogen concentration in gas feed; P - reactor pressure, Po - initial reactor pressure).

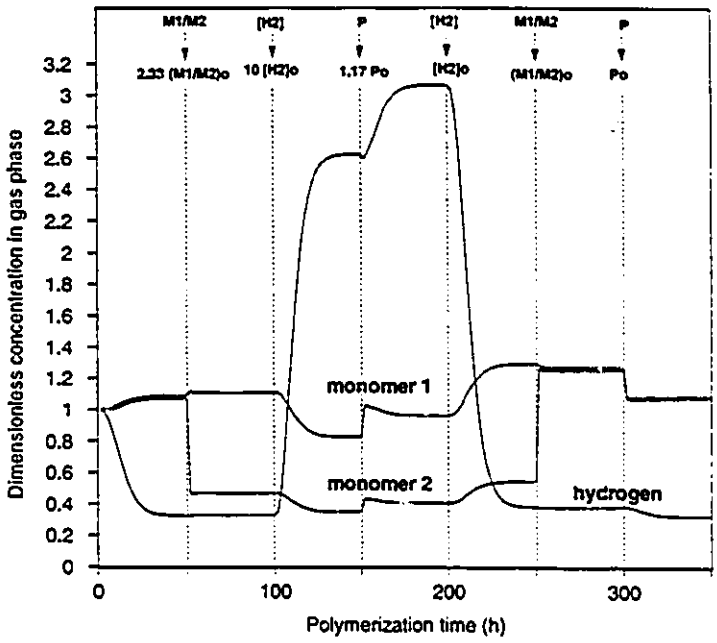

Figure 10 - Dimensionless concentration profiles of monomer 1, monomer 2, and hydrogen in gas phase of a binary copolymerization of olefins with a two site type Ziegler-Natta catalyst in four CSTRs in series (M1/M2 - molar ratio of monomer 1 and 2; [H2] - hydrogen concentration in gas feed; P - reactor pressure, Po - initial reactor pressure).

The study of the effect of catalyst poisons on polymerization rate and polymer properties is studied in the next set of figures.

A reversible catalyst poison is introduced in the first reactor through the gas inlet stream as a pulse of short duration (1 hour, 1% mole fraction). Profiles of poison concentration in all reactors are shown in figure 11.

The effect on introducing a catalyst poison on M_n is depicted in figure 12. The presence of poison causes a temporary increase in M_n since it preferentially deactivates the site types that make shorter polymer chains. Also as a consequence of this selective active site poisoning, one observes a significant decrease of PDI (figure 13).

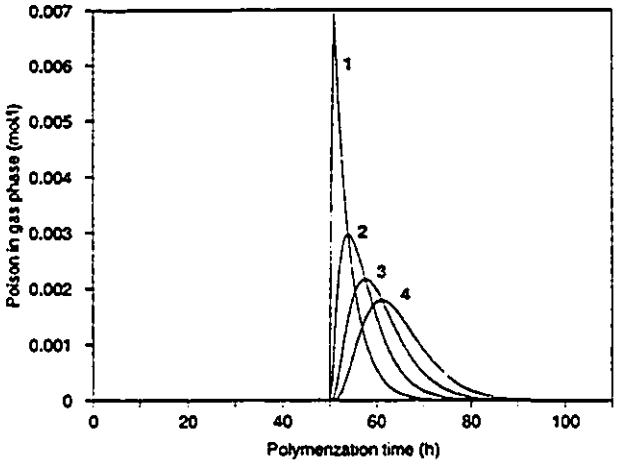

Figure 11 - Concentration profiles of poison in gas phase of a binary copolymerization of olefins with a two site type Ziegler-Natta catalyst in four CSTRs in series.

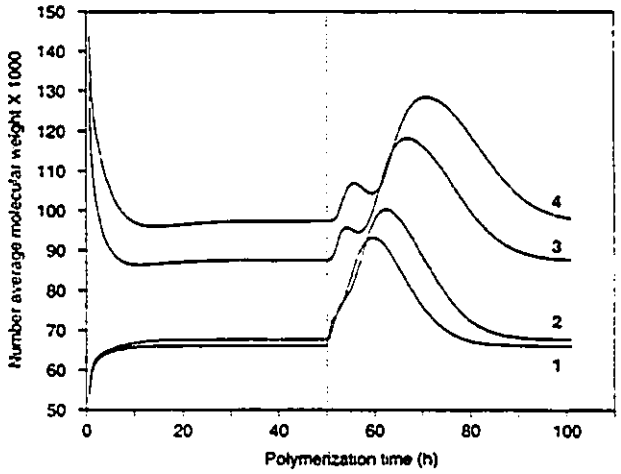

Figure 12 - Number average molecular weight profiles of a binary copolymerization of olefins with a two site type Ziegler-Natta catalyst in four CSTRs in series.

As expected, polymer production decreases as a consequence of catalyst deactivation, as shown in figure 14, but returns to original values after all poison is eliminated.

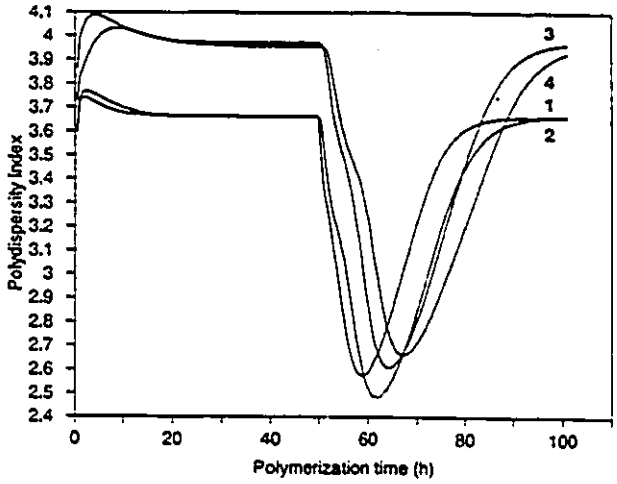

Figure 13 - Polydispersity index profiles of a binary copolymerization of olefins with a two site type Ziegler-Natta catalyst in four CSTRs in series.

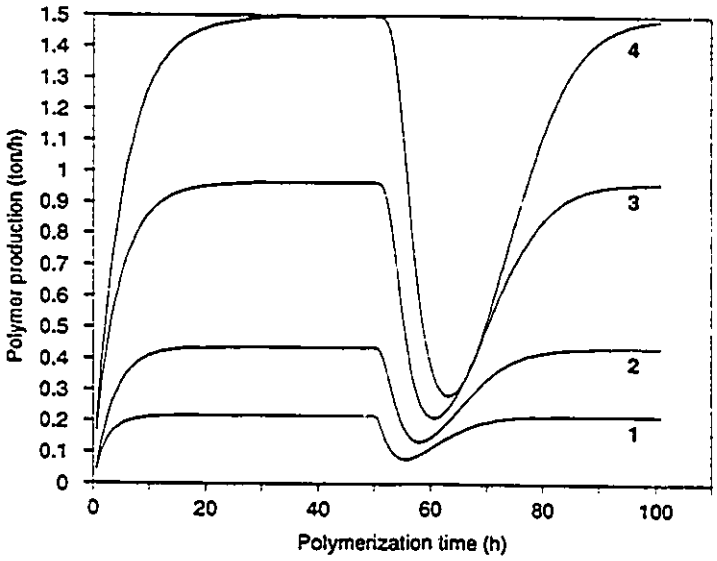

Figure 14 - Polymer production profiles of a binary copolymerization of olefins with a two site type Ziegler-Natta catalyst in four CSTRs in series.

The effect of reactor fouling by copolymer on temperature control is studied in the next set of figures.

It will be assumed that two CSTRs in series produce impact copolymer. The first reactor only polymerizes monomer 1 and is not affected by fouling. The second reactor in the series produces random copolymer. The manufacture of copolymers in slurry reactors can be asscciated with heat transfer problems. Copolymer chains are sticky (low glass transition temperature) and thus have a tendency to adhere to reactor walls and heat transfer surfaces, decreasing the global heat transfer coefficient. An arbitrary exponential decay law for the decrease of the global heat transfer coefficient is shown in figure 15.

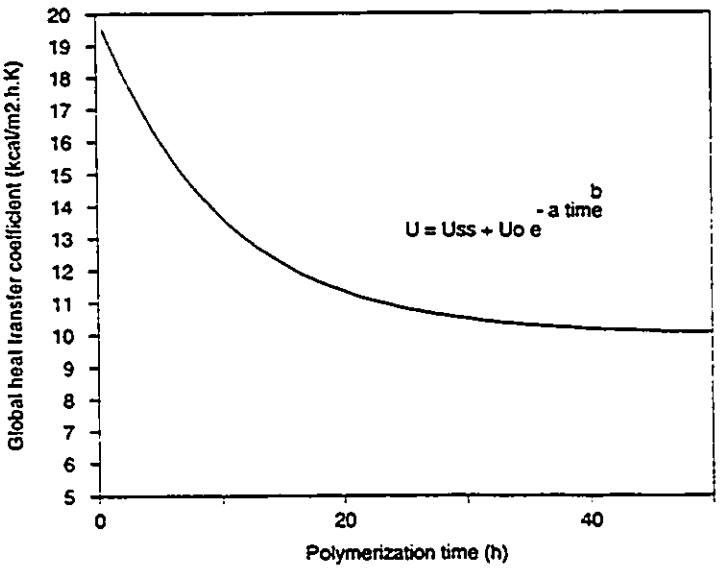

Figure 15 - Decrease of the global heat transfer coefficient in the second reactor due to fouling by copolymer.

The performance of the temperature controllers of the two reactors is shown in figure 16. While the temperature set-point is easily maintained in reactor 1 (no fouling), even a constant decrease of the cooling water temperature to its minimum value (35 ^{0}C) is not enough to avoid overheating of the second reactor under those circumstances.

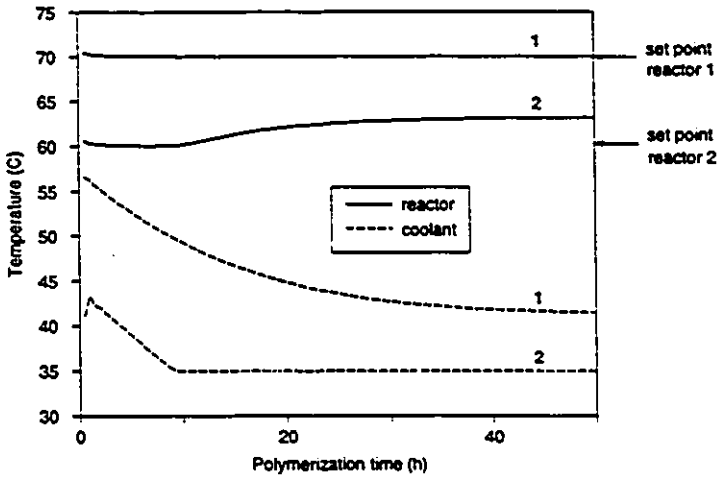

Figure 16 - Temperature profiles of polymerization reactor and cooling water during a binary copolymerization of olefins with a two site type Ziegler-Natta catalyst in two CSTRs in series.

As a consequence of overheating reactor 2, one can observe a decrease in M_n of polymer made in that reactor, caused by an increase of chain transfer reactions (figure 17). The effect on PDI is shown in figure 18. While the reactor temperature varies because of the decrease in the global heat transfer coefficient one can observe an increase in PDI due to the time variation of M_n.

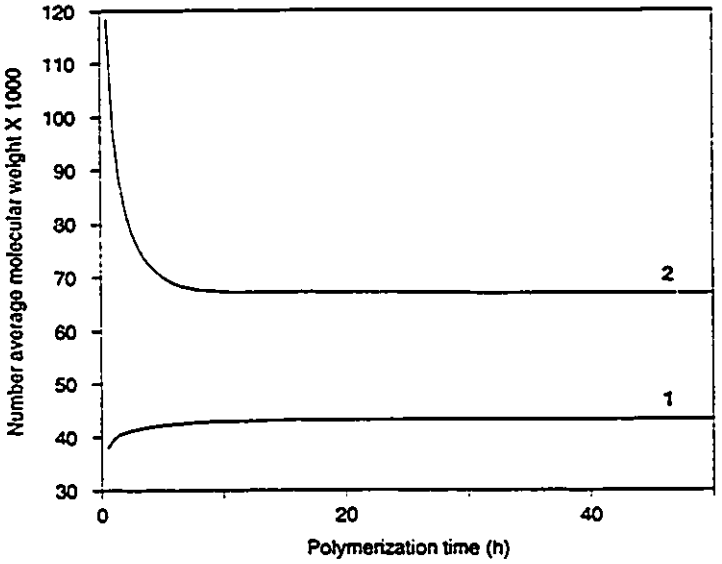

Figure 17 - Number average molecular weight profiles during a binary copolymerization of olefins with a two site type Ziegler-Natta catalyst in two CSTRs in series.

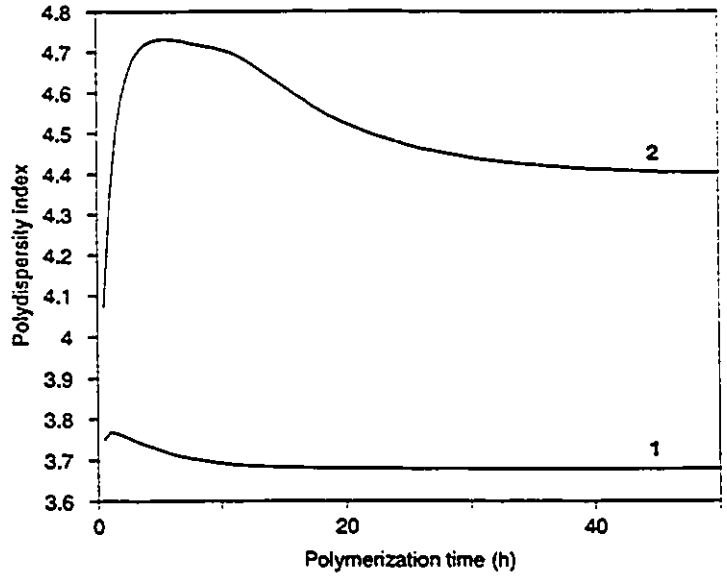

Figure 18 - Polydispersity index profiles during a binary copolymerization of olefins with a two site type Ziegler-Natta catalyst in two CSTRs in series.

CHAPTER 5 - POLYMERIZATION EXPERIMENTS

Introduction

All polymerizations were carried out in a one liter stainless steel autoclave reactor operated in semi-batch mode. Purified diluent was transferred to the reactor under nitrogen pressure through a transfer needle. Cocatalyst solution and catalyst slurry were injected in the reactor using gas-tight syringes. In all experimental runs, the order of injection was cocatalyst solution first, followed by the catalyst slurry. The interval between injections never exceeded 10 minutes. If necessary, the reactor was initially pressurized with hydrogen to act as chain transfer agent. Unless otherwise stated, hydrogen was not fed to the reactor at any other time during the polymerization. The polymerization was started by feeding gaseous monomer on demand to maintain a constant pressure in the reactor. The polymerization was interrupted by rapid depressurization of the head space of the reactor followed by quenching of the catalyst with methanol.

The catalyst used was LYNX 900, a second generation, ester modified titanium trichloride based catalyst, kindly donated by CRI, Catalyst Resources, Inc. The catalyst samples were obtained in 100 g glass containers as a purple powder in hexane slurry, at a weight fraction of approximately 0.20. In order to facilitate sampling and improve reproducibility, the catalyst slurry was further diluted using purified Shell isoparaffin 2025 to a weight fraction of approximately 0.04 and transferred to a Schlenk type storage bottle described below. No external bases were used to modify the catalyst performance.

The cocatalyst used was diethyl aluminum chloride (DEAC), purchased from Aldrich as a 1.0 M solution in hexanes. DEAC is provided in Sure/Pac™ metal containers, specially designed for handling air-sensitive materials outside a glove box. No further alteration of the cocatalyst solution was necessary.

The diluent used was isoparaffin 2025, kindly donated by Shell Canada. The purification of the diluent will be discussed below. Isoparaffin 2025 is used by Shell as diluent in Ziegler-Natta slurry reactors for the manufacture of polyolefins.

Polymerization grade propylene (99.5%) and research grade ethylene (99.99%) cylinders were purchased from Matheson. Ultra high purity nitrogen (99.999%) and ultra high purity hydrogen (99.999%) cylinders were purchased from Canadian Liquid Air/Alphagaz. Further purification of gaseous streams was provided by in-line oxygen traps and dessicator columns. All gas cylinders were provided with two-stage regulators to ensure precise pressure control during polymerization.

Catalyst and Cocatalyst Sampling

The manipulation of air-sensitive compounds such as catalysts and cocatalysts used in Ziegler-Natta polymerization requires specialized techniques to minimize contamination and avoid hazardous conditions. An excellent review of techniques for handling air-sensitive materials is available in Shriver (1969). Most of the techniques used in this work were adapted from his book.

The catalyst slurry was stored in a specially designed Schlenk-type glass bottle provided with a T sleeve septum adaptor inlet and a Teflon stopcock, as shown in figure 1. This bottle design is very useful for sampling air-sensitive compounds outside a glove box (Kramer et al., 1975). A constant positive pressure of dry nitrogen can be kept inside the bottle by connecting the side arm of the T inlet to a nitrogen line while the sample is withdrawn with a syringe needle through the vertical septum inlet. This procedure limits the chance of contamination by inflow of air to the bottle during sampling. The Teflon stopcock provides an effective way of isolating the bottle contents from external atmosphere and minimizes the chemical attack of both septa by the catalyst diluent. The cocatalyst solution was purchased in metal cylinders provided with a ball valve and a T septum adaptor inlet with the same features as the catalyst storage bottle.

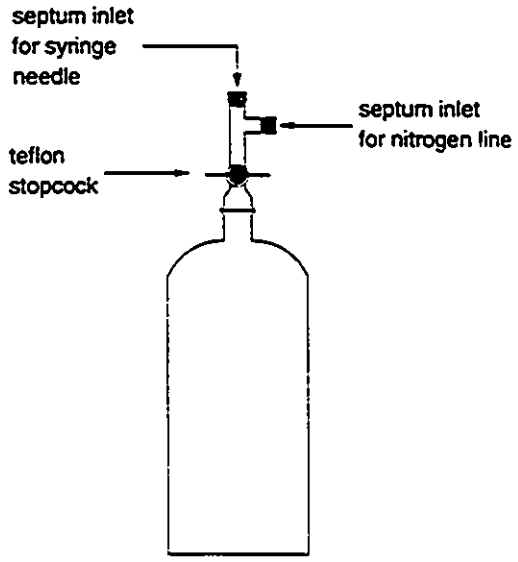

Figure 1 - Schlenk type catalyst slurry bottle.

All care was taken to avoid catalyst contamination by air during sampling. Dried gas-tight syringes (5.0 ml) provided with long stainless steel needles (16" long, gauge 16 and 18) were purified by purging at least five times with dry nitrogen and finally plugged with a rubber stopper. The side arm of the T septum adaptor was connected to a dry nitrogen line to guarantee a positive nitrogen pressure inside the catalyst and cocatalyst storage bottles during sampling. The desired amount of catalyst suspension or cocatalyst solution was sampled using the purified syringe. A small amount of nitrogen from the gas space of the bottle was also withdrawn to empty the needle and create a nitrogen blanket inside the syringe. The syringe needle was removed from the septum inlet and quickly inserted in a rubber stopper.

A more elaborate sampling procedure was also tested to eliminate the risk of contamination of the needle tip with air during syringe purification and sample withdrawing. A short glass tubing of about 4.0 cm in length provided with sleeve septa on both ends and purged with dry nitrogen was used in place of the rubber stopper. After syringe purification the syringe needle was inserted through one septum and kept inside the glass tubing in inert atmosphere. For sampling the catalyst or cocatalyst, the septum at the opposite end of the tubing was contacted with the septum at the T adaptor of the catalyst or cocatalyst storage bottle, and the syringe

needle inserted into the bottle by simultaneously perforating both septa. At the end of the sampling, the needle was withdrawn from the storage bottle but kept inside the closed glass tubing, therefore effectively eliminating exposure to the external atmosphere. This sampling procedure is illustrated in figure 2. No significant differences in catalyst activity were observed between polypropylene polymerizations carried out by using the first or the second sampling procedure. Due to its simplicity, the first sampling procedure was adopted for most polymerization runs.

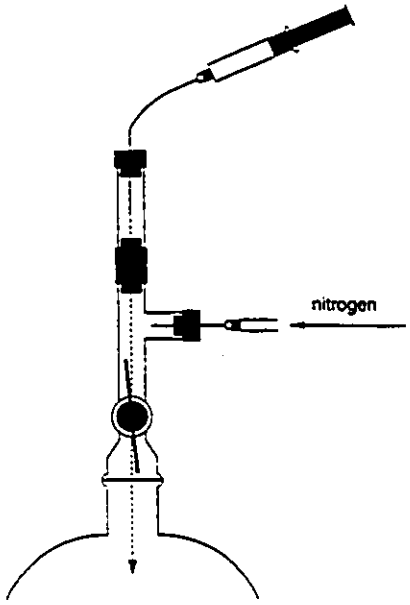

Figure 2 - Sampling procedure for catalyst slurry and cocatalyst solution.

Diluent Purification

Both catalyst and cocatalyst are very sensitive to water, carbon monoxide, carbon dioxide and oxygen. The diluent must be purified to reduce these contaminants to acceptable levels. Two methods of diluent purification were compared. No apparent difference in the rate of polymerization of propylene was noticed when diluent purified by either method was used.

With the first method, the diluent was refluxed with metallic sodium under nitrogen pressure using a conventional glass distillation apparatus. The whole apparatus was thoroughly evacuated and purged with dry nitrogen several times before adding the diluent. A small amount of benzophenone was also added to the distillation kettle as a moisture indicator. The solution turns dark blue when no moisture is present. The desired amount of diluent was distilled and collected immediately before the start of the polymerization and transferred to the polymerization reactor under nitrogen pressure through a transfer needle.

With the second method the diluent was directly transferred from its original container to a four liter storage bottle, provided with a two-hole rubber stopper, as shown in figure 3. About 500 g of Davidson molecular sieves 3A or 4A (Alumina-silicate with potassium or sodium cations, respectively) was added to the bottle to remove moisture from the diluent. The dip tube was connected to a dry nitrogen line and the septum adaptor was connected to a mineral oil bubbler through a plastic hose provided with a needle adaptor and a needle. Nitrogen was continuously bubbled into the diluent to remove any traces of absorbed gases, while the bubbler avoided backflow of air into the diluent storage bottle. The diluent was left under these conditions for at least three days before being used for polymerization. The desired amount of diluent was transferred to the reactor under nitrogen pressure through a transfer needle.

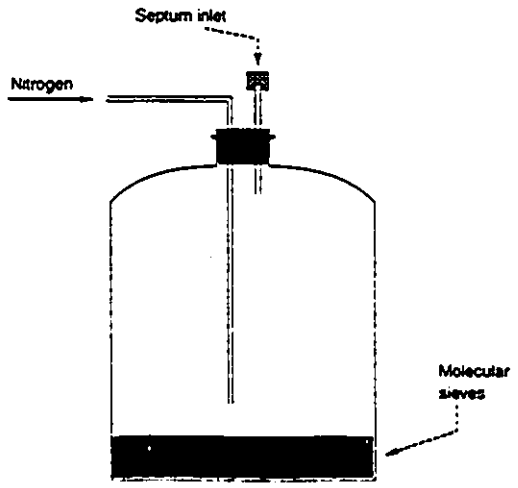

Figure 3 - Solvent storage and purification bottle.

Since no apparent advantage was obtained by using the more time consuming and hazardous diluent reflux method, the second method was almost exclusively used for purifying the diluent.

Polymerization Reactor System

The polymerization reactor is a one liter stainless steel autoclave, (height = 9 inches, inside diameter = 3 inches), from Autoclave Engineers (figure 4). The reactor is provided with a mechanical stirrer, an internal cooling coil and a heating mantle. A Thermo Electric temperature controller, model Tempstar III, regulates the heat output of the mantle to maintain the reactor at the desired polymerization temperature. The cooling coil is connected to a Lauda RM 20 thermostated circulator bath. A constant flow of cooling water is used to remove the heat of polymerization. The temperature control system was able to control the polymerization temperature within ± 1 °C of the set-point for all propylene and ethylene polymerizations.

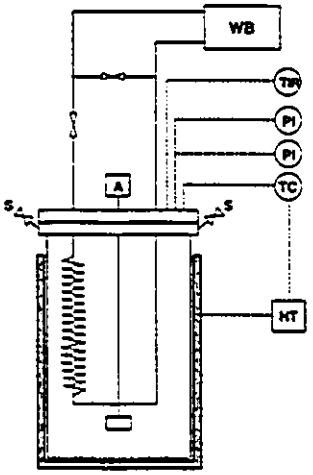

Figure 4 - Polymerization reactor (A = stirrer; S = septum inlet; WB = thermostated water bath; HT = heater; TC = temperature controller; PI = pressure indicator; TIR = temperature indicator & recorder.)

The reactor is also provided with two manometers with different pressure ranges (0 - 15 psi and 0 - 100 psi), an Omega RI-5000 digital temperature

indicator-recorder interface connected to a stripchart recorder, and two septum adaptors for admitting the diluent, the cocatalyst solution and the catalyst slurry to the reactor.

Propylene, ethylene, hydrogen and nitrogen cylinders are connected to the reactor via the gas feeding system shown in figure 5. All gaseous components are purified by means of on-line LABCLEAR oxygen trap columns and anhydrous $CaSO_4$ dehumidifier columns. An Alphagaz side-track mark II mass flow meter connected to a stripchart is used for measuring and recording the flow of ethylene and propylene to the reactor.

Purge and vacuum lines are used during reactor purification steps. The vacuum lines are connected to an Edwards high vacuum pump model E2M2. The purge lines are connect to a mineral oil bubbler to avoid backflow of air to the reactor.

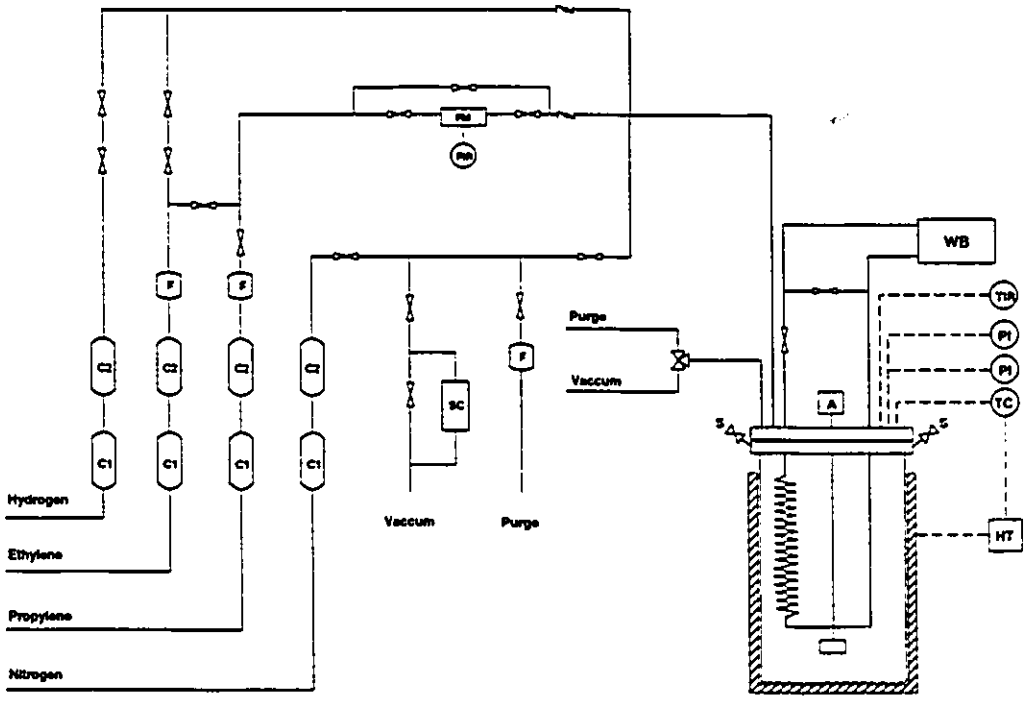

Figure 5 - Polymerization reactor system (A = stirrer; S = septum inlet; WB = thermostated water bath; HT = heater; TC = temperature controller; PI = pressure indicator; TIR = temperature indicator & recorder; C1 = oxygen trap column; C2 = dehumidifier column; F = in-line filter; FM = mass flow meter; FIR = flow indicator & recorder; SC = solvent condenser.)

Polymerization Procedure

The same reactor operation procedure was used for both ethylene and propylene polymerization.

The reactor body is dried in an oven for at least four hours at 120 °C to eliminate moisture and diluent residues from previous polymerizations. While still hot, the reactor body is transferred to its stand and connected to the top flange. The reactor is then thoroughly evacuated and pressurized with dry nitrogen at least five times to obtain an adequate inert atmosphere inside the reactor.

Diluent is transferred only after the reactor has been properly purified. The diluent is transferred under nitrogen pressure through a transfer needle. While keeping the diluent storage vessel under constant nitrogen pressure, one end of the transfer needle is inserted into the septum adaptor of the storage bottle. The transfer needle is flushed with nitrogen for some seconds to ensure proper evacuation of air and moisture. The reactor outlet valve is switched to the purge position, thus directing the gas flow to the mineral oil bubbler, and the free end of the transfer needle is inserted in the septum adaptor of the polymerization reactor. To start the diluent transfer, the end of the transfer needle that is inserted into the diluent bottle is lowered until it reaches the liquid level. A graduated scale attached to the diluent bottle measures the amount of diluent transferred to the reactor. When the transfer is complete, the transfer needle is raised to the gas space in the diluent bottle while the other end is removed from the septum inlet of the reactor.

To eliminate any residual contamination, the reactor is again submitted to at least three nitrogen pressurization and evacuation cycles. The stirrer is then turned on and the stirring speed is set to 1200 rpm, as measured by a stroboscope. The reactor is then warmed up to the desired polymerization temperature by turning on the temperature controller, while keeping a constant flow of nitrogen in the reactor headspace. At least one hour is allowed for this final nitrogen purge and temperature equilibration stage before the beginning of the polymerization.

The cocatalyst solution and the catalyst slurry, sampled by the syringe techniques described before, are only injected into the reactor after the reactor temperature is stable. The cocatalyst solution is injected firstly, immediately followed by the catalyst slurry injection.

When necessary, hydrogen is admitted to the reactor immediately after the injection of the catalyst until the desired pressure is obtained. Unless otherwise stated, hydrogen is not fed to the reactor at any other time during the polymerization.

The polymerization is started by pressurizing the reactor with monomer. The two-stage pressure regulator of the monomer cylinder keeps the pressure constant inside the reactor by suppling the amount of monomer consumed by the polymerization, as recorded by the on-line mass flow meter. In all polymerizations, the time interval between the injection of the cocatalyst and monomer pressurization was never greater than 15 minutes.

The polymerization is terminated by fast depressurization of the reactor through the purge line. About 100 ml of methanol is injected into the reactor through the septum adaptor to deactivate the catalyst. The reactor is allowed to cool down to room temperature. The produced polymer is filtered and washed with methanol and water to remove catalyst residues and dried in a vacuum oven at 50 °C overnight.

Estimate of Propylene and Ethylene Concentration in Diluent

The concentration of propylene and ethylene in the diluent as a function of reactor temperature and monomer pressure was estimated by a mass balance around the reactor system.

A carefully measured amount of diluent was transferred to the reactor and warmed-up to the desired temperature. Gas monomer was fed to the reactor until the desired pressure was established, while recording the flow by using the in-line mass flow meter. The total mass of monomer in the reactor can be obtained by integrating in time the mass flow of monomer to the reactor:

$$M_t = \int_0^{\bullet\bullet} \dot{m}\,dt \tag{1}$$

The mass of monomer in the head space of the reactor can be estimated by using the ideal gas law:

$$M_g = \frac{P(V_t - V_l)}{RT} mw \tag{2}$$

Therefore, the mass of monomer dissolved in the solvent can be estimated by:

$$M_l = M_t - M_g = \int_0^{\bullet\bullet} \dot{m}\,dt - \frac{P(V_t - V_l)}{RT} mw \tag{3}$$

Propylene concentrations at four pressure levels and three temperature values were estimated. As shown in figure 6, an almost linear relationship exists between propylene concentration in diluent and propylene pressure at a given temperature for the studied ranges of pressures and temperatures. The same is observed for the relationship between concentration of propylene in diluent and temperature for a given propylene pressure, as shown in figure 7.

Ethylene concentration in diluent was also measured for three temperatures and an ethylene pressure of 70 psi. As for propylene, a linear relation represents the dependency reasonably well, as depicted in figure 8.

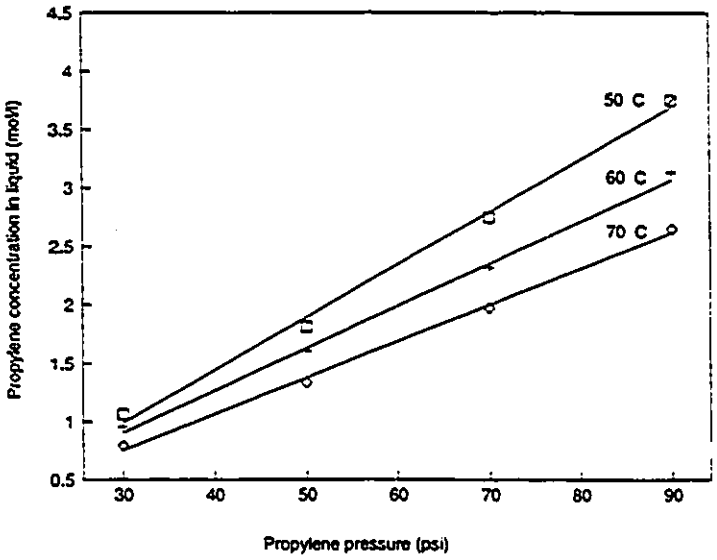

Figure 6 - Concentration of propylene in isoparaffin 2025 as a function of propylene pressure at different temperatures.

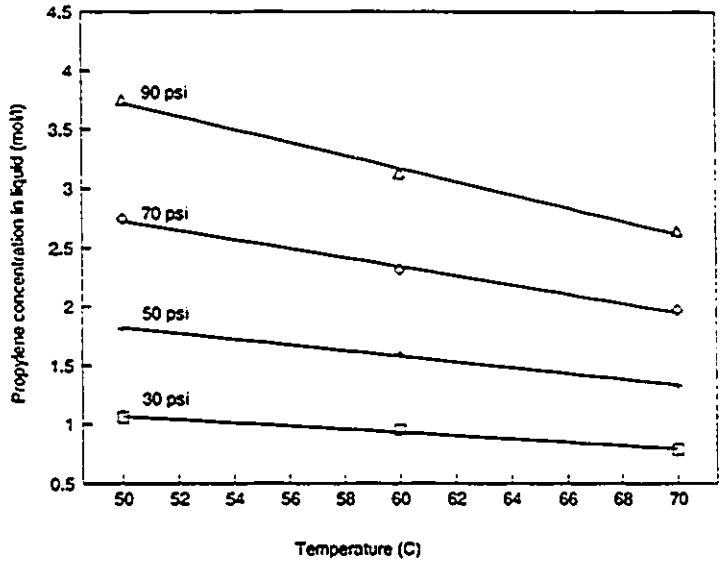

Figure 7 - Concentration of propylene in isoparaffin 2025 as a function of temperature at different partial pressures of propylene.

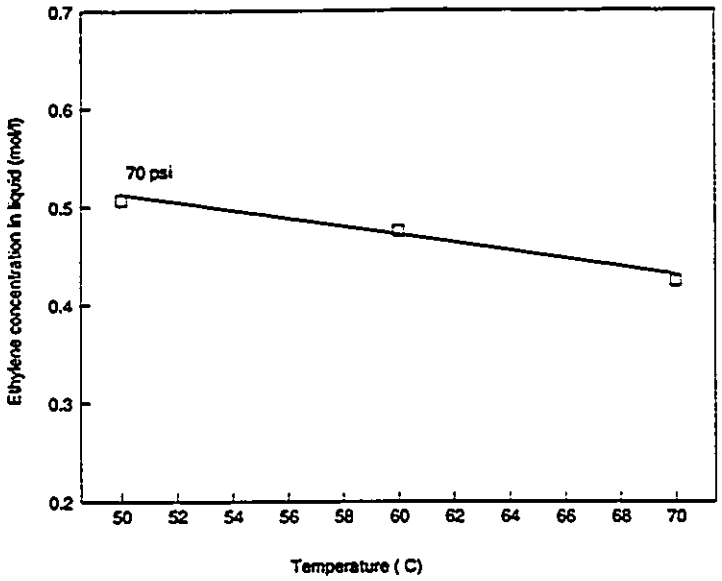

Figure 8 - Concentration of ethylene in isoparaffin 2025 as a function of temperature (partial pressure of ethylene = 70 psi).

Propylene Polymerization

Propylene was polymerized at three different temperatures and four different hydrogen pressures. Monomer partial pressure, catalyst and cocatalyst concentrations were kept constant for all runs. Table 1 summarizes the experimental design adopted for the propylene polymerizations and table 2 shows reactor operation conditions and polymer yields of each run.

The presence of hydrogen in the reactor significantly increases the catalyst activity for all three temperature levels studied. Figure 9 shows the polymerization kinetic curves of propylene at 70 °C in absence of hydrogen and at hydrogen partial pressures of 2, 5, and 10 psi. The initial decrease in propylene flow actually corresponds to the pressurization of the polymerization reactor and should not be considered as a catalytic decay period. The catalyst activity is significantly increased by initially pressurizing the reactor with even small pressures of hydrogen. Increasing hydrogen pressure from 2 to 10 psi does not seem to improve catalyst activity any

further. The same behaviour is noticed at polymerization temperatures of 60 °C and 50 °C as shown in figures 10 and 11. Table 3 shows the average rates of polymerization and standard deviations at each polymerization temperature in presence and absence of hydrogen.

T	P_{H2}	Replicates	
50	0	HP057	HP058
50	10	HP056	HP059
60	0	HP054	HP052
60	5	HP053	
60	10	HP051	HP055
70	0	HP045	HP046
70	2	HP050	
70	5	HP041	HP042
70	10	HP043	HP044

Table 1: Experimental design of propylene polymerization runs (T = polymerization temperature, °C; P_{H2} = hydrogen pressure, psi).

In order to test the reversibility of the hydrogen effect on polymerization rate, two additional experiments were designed for the polymerization temperature of 70 °C. In the first one, the polymerization of propylene was initiated with a hydrogen partial pressure of 10 psi. After 30 minutes the polymerization was shortly interrupted by stopping the monomer flow and depressurizing the reactor. The reactor was then connected to the vacuum line for five minutes to eliminate residual amounts of hydrogen dissolved in the diluent. The polymerization was restarted by pressurizing the reactor with propylene, this time in absence of hydrogen. This second stage of polymerization was interrupted after 30 minutes by quenching with methanol. In the second experiment, the reverse order was adopted. The polymerization was

Run #	T	$P_{propene}$	P_{H2}	$[TiCl_3]$	[DEAC]	[DEAC]/ $[TICl_3]$	Catalyst activity
HP057	50	70	0	1.76	7.98	4.53	164.7
HP058	50	70	0	1.76	8.02	4.56	148.5
HP056	50	70	10	1.74	8.02	4.61	245.6
HP059	50	70	10	1.76	8.00	4.55	259.8
HP054	60	70	0	1.56	8.02	5.14	230.0
HP052	60	70	0	1.74	8.00	4.60	262.9
HP053	60	70	5	1.72	7.92	4.60	418.4
HP051	60	70	10	1.74	8.00	4.60	432.0
HP055	60	70	10	1.76	8.02	4.56	493.7
HP045	70	70	0	1.76	8.10	4.60	382.7
HP046	70	70	0	1.76	7.14	4.06	408.8
HP050	70	70	2	1.76	8.02	4.56	716.1
HP041	70	70	5	1.78	8.12	4.56	748.7
HP042	70	70	5	1.76	8.00	4.55	768.8
HP043	70	70	10	1.80	8.08	4.49	765.9
HP044	70	70	10	1.76	8.06	4.58	733.5

Table 2: Experimental conditions and yield of propylene polymerization runs. (T = polymerization temperature, °C; $P_{propene}$ = partial pressure of propene, psi; P_{H2} = partial pressure of hydrogen, psi; $[TiCl_3]$ = catalyst concentration, mmol/l; [DEAC] = cocatalyst concentration, mmol/l; Catalyst activity = g polymer/g catalyst.mol.h)

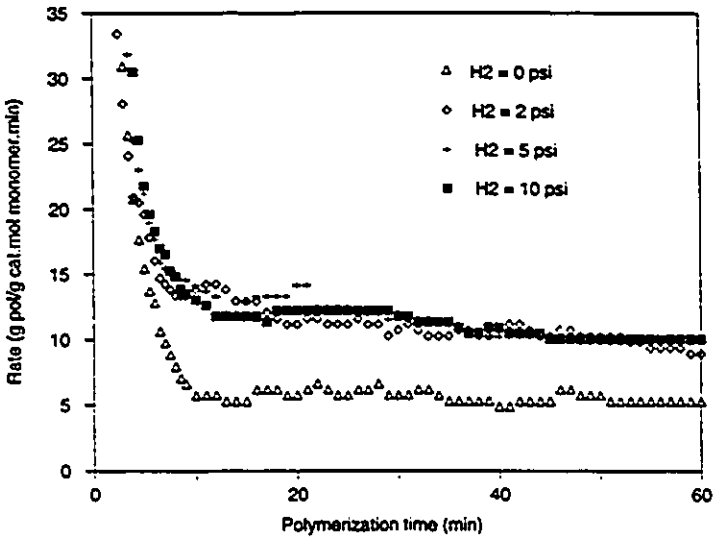

Figure 9 - Effect of hydrogen pressure on polymerization rate of propylene at 70 °C.

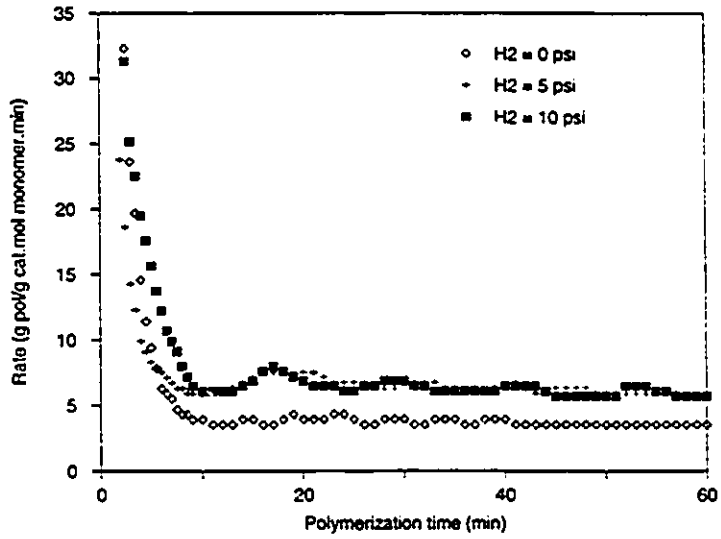

Figure 10 - Effect of hydrogen pressure on polymerization rate of propylene at 60 °C.

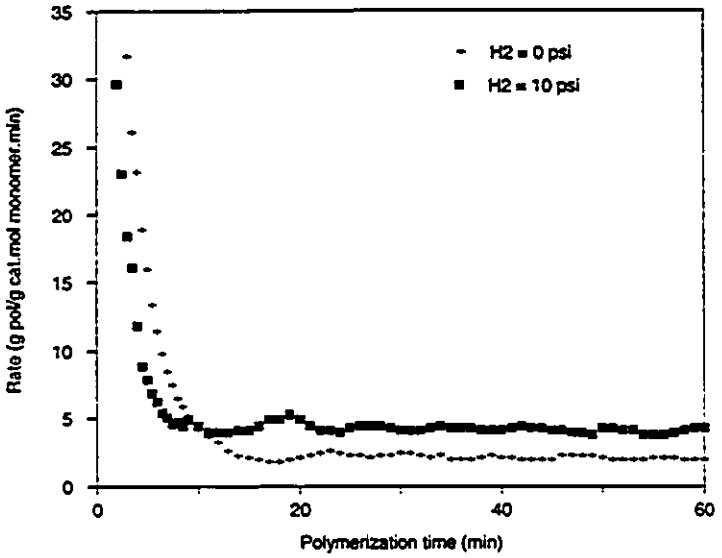

Figure 11 - Effect of hydrogen pressure on polymerization rate of propylene at 50 °C.

	$P_{H_2} = 0$		$P_{H_2} \neq 0$	
T	Catalyst activity	Standard deviation	Catalyst activity	Standard deviation
50	156.6	1i.5	252.7	10.0
60	246.5	23.3	448.0	40.1
70	395.8	18.5	746.6	22.2

Table 3: Effect of hydrogen on catalyst activity of propylene polymerization (P_{H2} = partial pressure of hydrogen; T = temperature, °C; Catalyst activity = g polymer/g catalyst.mol.h).

started in absence of hydrogen and after 30 minutes of polymerization the reactor was pressurized with 10 psi of hydrogen, after which the polymerization continued for an additional 30 minutes.

Figure 12 compares the two experiments described in the last paragraph with a polymerization in absence of hydrogen and another in which an initial partial pressure of hydrogen was used. The agreement between the curves is quite remarkable, leading to the conclusion that the effect of hydrogen on the catalytic activity of LYNX 900 for propylene polymerization is reversible. Admission of hydrogen to a polymerization started in absence of hydrogen immediately causes the rate of polymerization to increase to the level observed when the polymerization was started in the presence of hydrogen. In the same way, when hydrogen is evacuated from the reactor, the polymerization rate drops to the value obtained when no hydrogen is used throughout the polymerization.

As depicted in figures 6 to 12, after the steady-state is reached, there is very little catalyst activity decay during one hour of polymerization, either in absence or presence of hydrogen.

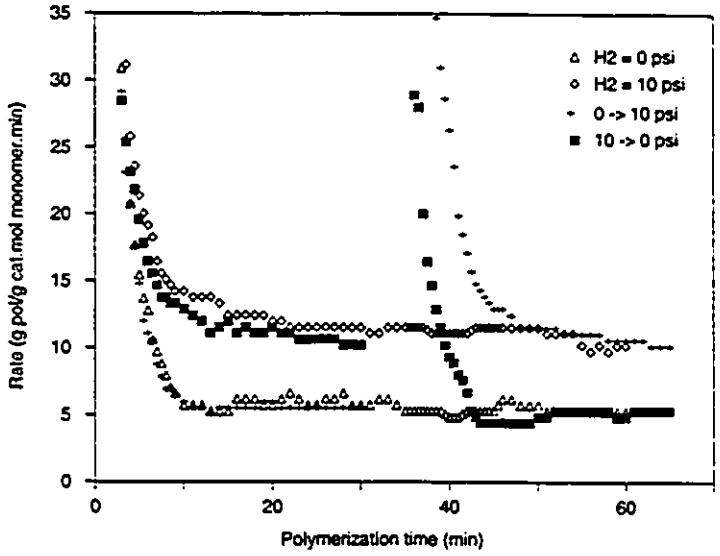

Figure 12 - Reversibility of hydrogen effect on polymerization rate of propylene at 70 °C.

The activation energy of polymerization defined by the Arrhenius law is expressed as:

$$Y = k_p[C^*][M] \tag{4}$$

$$Y = k_{p_0}\exp(-E/RT)[C^*][M] \tag{5}$$

$$\ln\frac{Y}{[M]} = -\frac{E}{R}\frac{1}{T} + \ln k_{p_0}[C^*] \tag{6}$$

The activation energy E can be thus estimated from the slope of the curve *ln Y/[M]* versus *1/T*.

Figures 13 and 14 show the plots of *ln Y/[M]* versus *1/T* with and without hydrogen. From the slopes of the curves it is possible to estimate an activation energy of 15,600 cal/mol for propylene polymerization in presence of hydrogen and of 13,800 cal/mol for propylene polymerization in absence of hydrogen. Those values are in the range commonly reported in the literature for the activation energy of propylene polymerization (Yuan et al., 1982).

Ethylene Polymerization

Ethylene was polymerized at three different temperatures and three different hydrogen pressures. The effect of prepolymerizing the catalyst with propylene prior to ethylene polymerization was also investigated. Monomer partial pressure, catalyst, and cocatalyst concentrations were kept constant for all runs. Table 4 summarizes the experimental design adopted for the ethylene polymerizations and table 5 shows reactor operation conditions and polymer yields of each run.

Prepolymerization of the catalyst with propylene prior to ethylene polymerization has a remarkable effect of the activity of the catalyst towards ethylene polymerization. As shown in figure 15, when the prepolymerized catalyst is used the polymerization rate of ethylene increases significantly when compared to the polymerization rates obtained with the regular catalyst. This acceleration rate effect

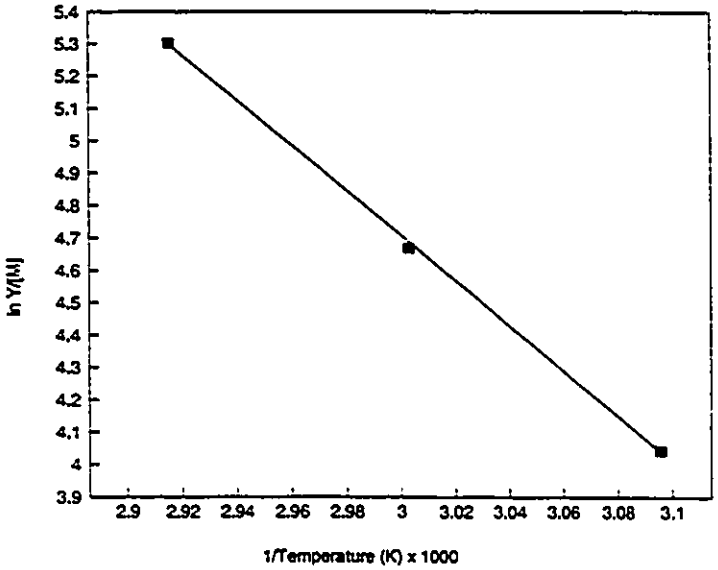

Figure 13 - Arrhenius law plot for polymerization of propylene in presence of hydrogen.

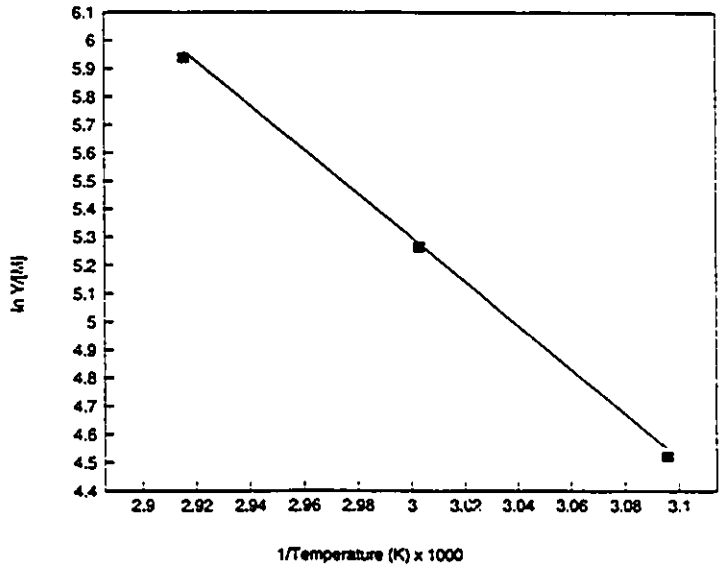

Figure 14 - Arrhenius law plot for polymerization of propylene in absence of hydrogen.

is observed either in the presence or in the absence of hydrogen. Table 6 shows the average polymerization rates of the regular and prepolymerized catalyst at the three temperature levels studied.

Prep	P_{H2}	T	Replicates	
Y	0	50	HE013	HE021
Y	0	60	HE009	HE016
Y	0	70	HE011	HE019
Y	5	60	HE014	
Y	10	50	HE012	HE022
Y	10	60	HE008	HE015
Y	10	70	HE010	HE020
N	0	60	HE004	HE006
N	10	60	HE005	HE007

Table 4: Experimental design of ethylene polymerization runs. (Prep: Y = catalyst prepolymerized with propylene, N = regular catalyst; P_{H2} = hydrogen pressure, psi; T = polymerization temperature, °C)

All effort was taken to minimize copolymerization effects that could occur if significant amounts of propylene stayed in the reactor after the prepolymerization. The catalyst was prepolymerized with propylene by pressurizing the reactor containing diluent, catalyst slurry and cocatalyst solution with a propylene partial pressure of 12 psi for 5 minutes. The prepolymerization was terminated by evacuating and venting the reactor with nitrogen exhaustively to assure the proper removal of the propylene absorbed in the diluent. The polymerization of ethylene was started immediately after propylene removal following the same experimental procedure adopted for propylene polymerization.

Run #	Prep	T	$P_{ethylene}$	P_{H2}	$[TiCl_3]$	[DEAC]	[DEAC]/ $[TiCl_3]$	Catalyst activity
HE004	N	60	70	0	1.83	8.29	4.53	657.0
HE006	N	60	70	0	1.78	8.00	4.50	522.5
HE005	N	60	70	10	1.79	8.14	4.54	549.2
HE007	N	60	70	10	1.78	8.01	4.50	602.4
HE013	Y	50	70	0	1.77	7.91	4.47	2117.4
HE021	Y	50	70	0	1.75	8.16	4.65	1779.5
HE012	Y	50	70	10	1.79	7.92	4.41	1583.6
HE022	Y	50	70	10	1.77	7.93	4.47	1534.7
HE009	Y	60	70	0	1.73	8.09	4.69	2713.1
HE016	Y	60	70	0	1.76	8.11	4.61	3055.7
HE014	Y	60	70	5	1.74	7.94	4.55	2978.8
HE008	Y	60	70	10	1.73	8.02	4.64	2703.6
HE015	Y	60	70	10	1.77	8.13	4.60	2956.7
HE011	Y	70	70	0	1.79	7.92	4.41	4833.2
HE019	Y	70	70	0	1.75	8.13	4.64	4084.6
HE010	Y	70	70	10	1.78	8.17	4.60	3918.2
HE020	Y	70	70	10	1.81	8.01	4.43	3274.7

Table 5: Experimental conditions and yield of ethylene polymerization runs. (Prep: Y = catalyst prepolymerized with propylene, N = regular catalyst; T = polymerization temperature, °C; $P_{ethylene}$ = partial pressure of ethylene, psi; P_{H2} = partial pressure of hydrogen, psi; $[TiCl_3]$ = catalyst concentration, mmol/l; [DEAC] = cocatalyst concentration, mmol/l; Catalyst activity = g polymer/g catalyst.mol.h)

	Regular catalyst		Prepolymerized catalyst	
T	Catalyst activity	Standard deviation	Catalyst activity	Standard deviation
50			1753.8	264.5
60	582.8	59.6	2881.6	162.4
70			4027.7	640.6

Table 6: Effect of prepolymerization with propylene in catalyst activity of ethylene polymerization (T = polymerization temperature, °C; Catalyst activity = g polymer/g catalyst.mol.h).

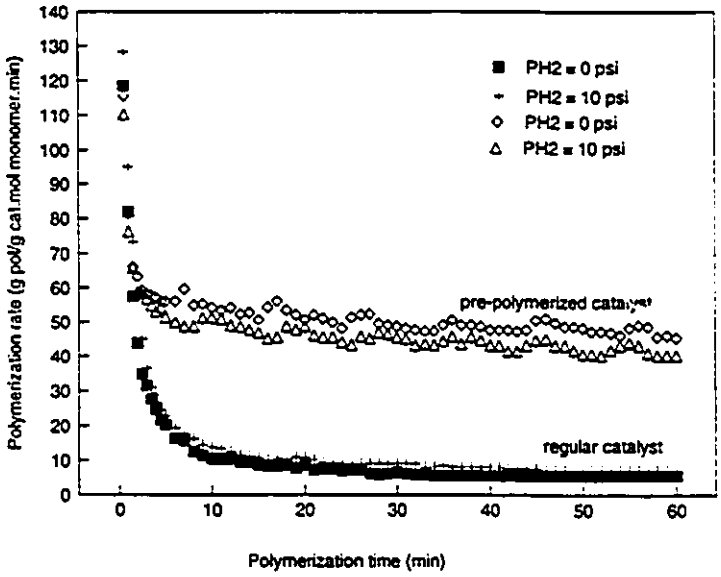

Figure 15 - Effect of catalyst prepolymerization with propylene on the polymerization rate of ethylene at 60° C.

The effect of hydrogen on the polymerization rate of ethylene is not so clear as for the polymerization rate of propylene. By inspection of table 5 for the case of the regular catalyst, there seems to be no significant influence of hydrogen on the polymerization rate of ethylene. On the other hand, for the prepolymerized catalyst, the presence of hydrogen apparently decreases slightly the catalyst activity, especially at 50 and 70 °C. However, these observed differences are not statistically significant. Table 7 shows the levels of probability of the null hypothesis for the influence of hydrogen in the polymerization rate of ethylene in relation to the Student's distribution (Box, G. E. P.; Hunter, W. G.; Hunter, J. S., 1978). The null hypothesis states that the average polymerization rate of ethylene in absence of hydrogen is equal to the average polymerization rate of ethylene in presence of hydrogen. The null hypothesis is clearly valid for both the regular and the prepolymerized catalyst at 60 °C. At 70 °C, the difference in average rate of polymerization is statistically significant at the 0.12 level of probability, which is still sufficiently high to support the null hypothesis. However, at 50 °C the difference in rates of polymerization is statistically significant at the smaller level of probability of 0.8. At this level of probability it is somewhat difficult to make a decisive distinction between accepting or rejecting the null hypothesis. However, since the polymerization rate of ethylene is clearly not considerably affected by the presence of hydrogen at 60 and likely not at 70 °C, it will be assumed that the same behaviour occurs at 50 °C.

Prep	T	t_0	ν	Pr
N	60	0.19	2	> 0.4
Y	50	2.28	2	0.8
Y	60	0.027	3	> 0.4
Y	70	1.75	2	0.12

Table 7: Statistical significance of the influence of hydrogen on the polymerization rate of ethylene (Prep: Y = catalyst prepolymerized with propylene, N = regular catalyst; T = polymerization temperature, °C; t_0 = normalized deviate, Pr = level of probability, ν = degrees of freedom)

Figure 16 shows the polymerization kinetic curves of ethylene at 60 °C in absence of hydrogen and at hydrogen partial pressures of 5 and 10 psi for the prepolymerized catalyst. As for the case of propylene, the initial decrease in ethylene flow actually corresponds to the pressurization of the polymerization reactor and should not be interpreted as decay in catalytic activity. Figure 17 shows the polymerization kinetic curves of ethylene at 60 ° C in absence of hydrogen and at hydrogen partial pressure of 10 psi for the regular catalyst. No significant hydrogen effects on the rate of polymerization were observed in both cases.

Table 8 shows the average rates of polymerization and standard deviations at each polymerization temperature in presence and absence of hydrogen.

As depicted in figures 15 to 17, after the steady-state is reached, there is very little catalyst deactivation in one hour polymerization, either in absence or presence of hydrogen.

The activation energy E for ethylene polymerization can also be estimated by the inclination of the curve $ln\ Y/[M]$ versus $1/T$.

		$P_{H_2}=0$		$P_{H_2}\neq 0$	
T	Prep	Catalyst activity	Standard deviation	Catalyst activity	Standard deviation
60	N	589.8	95.1	575.8	37.6
50	Y	1948.5	238.9	1559.2	34.6
60	Y	2884.4	242.3	2879.7	152.9
70	Y	4458.9	529.3	3596.5	455.0

Table 8: Effect of hydrogen on catalyst activity of ethylene polymerization (T = temperature, °C; Prep: Y = catalyst prepolymerized with propylene, N = regular catalyst; P_{H_2} = partial pressure of hydrogen, psi; Catalyst activity = g polymer/g catalyst.mol.h).

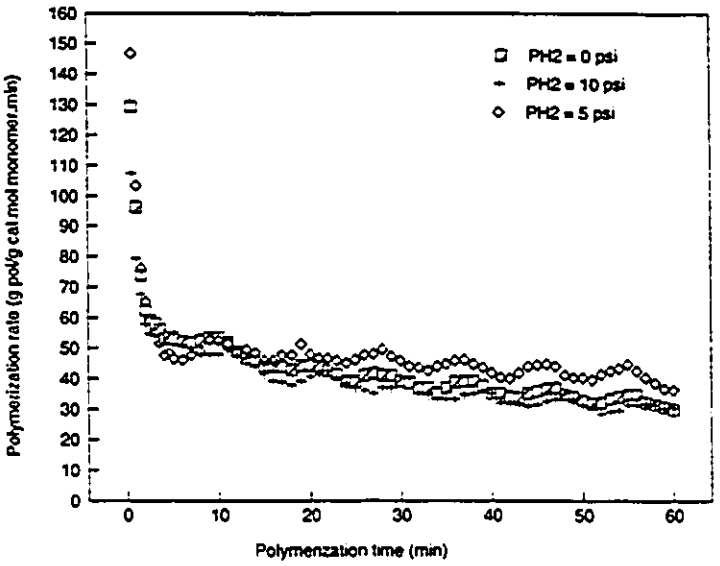

Figure 16 - Effect of hydrogen pressure on polymerization rate of ethylene at 60 °C with prepolymerized catalyst.

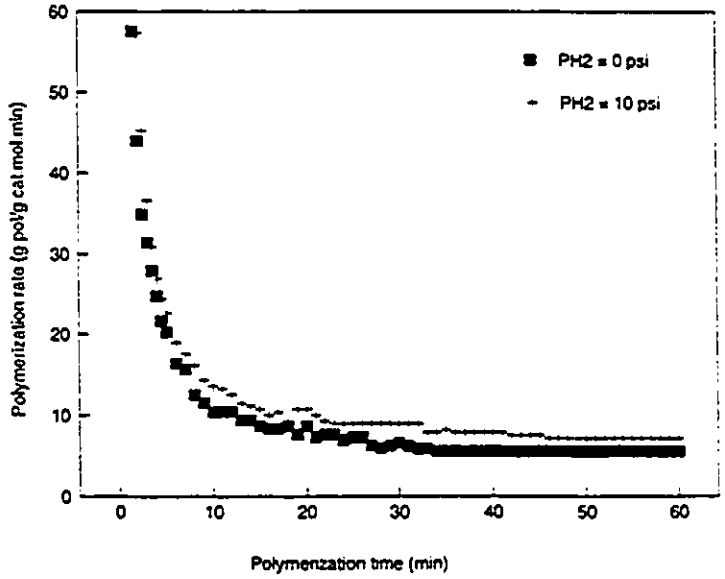

Figure 17 - Effect of hydrogen pressure on polymerization rate of ethylene at 60 °C with regular catalyst.

Figures 18 shows the plot of *ln Y/[M]* versus *1/T* for ethylene polymerization with the prepolymerized catalyst. From the slope of the curve it is possible to estimate an activation energy of 11,300 cal/mol for ethylene polymerization. This value is in the range commonly reported in the literature for activation energy of ethylene polymerization (Jejelowo et al., 1991).

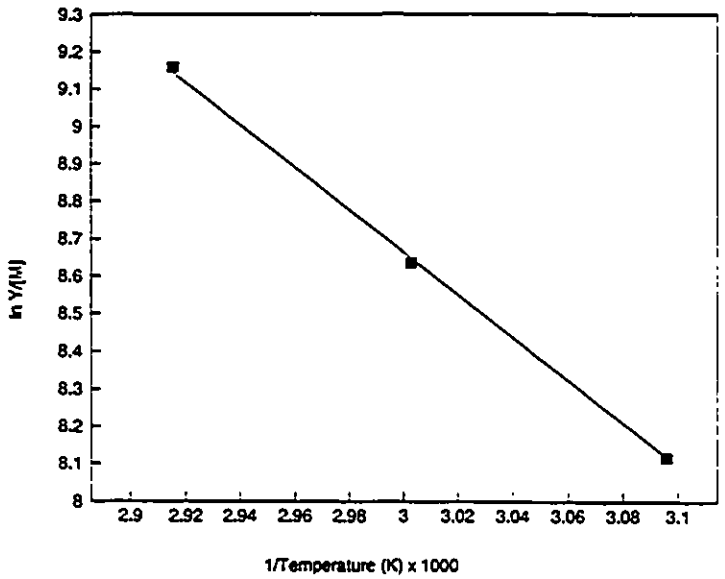

Figure 18 - Arrhenius law plot for polymerization of ethylene with catalyst prepolymerized with propylene, considering runs with and without hydrogen.

Discussion

The effect of hydrogen on the rate of olefin polymerization with Ziegler-Natta catalysts is rather complex and governed by insufficiently known mechanisms (Boor, 1979; Keii, 1988). Depending on the type of catalyst, cocatalyst, monomer, and polymerization conditions, the polymerization rate can either decrease (Natta, 1959; Berger and Grieveson, 1965; Keii, 1972; Böhm, 1981; Soga and Sino, 1982; Guastalla and Giannini, 1983), increase (Rayner, 1964; Okura et al., 1970; Mason and Schaffhausen, 1971; Pijpers and Roest, 1972; Bulls and Higgins, 1973; Guastalla and Giannini, 1983; Ross 1984), or remain unaffected (Yuan et al., 1982; Guastalla

and Giannini, 1983; Marques et al., 1993) in the presence of hydrogen. The reversibility of the hydrogen effect on polymerization rate has also been described by Natta (1959).

More interesting to our experimental results, Guastalla and Giannini (1983) studied the effects of hydrogen on the polymerization rate of propylene and ethylene using a $MgCl_2$ supported catalyst. It was found that the presence of hydrogen generally increased the rate of polymerization of propylene but decreased the rate of ethylene polymerization. At low polymerization temperatures (17°C), however, the rate of propylene polymerization was unaffected by the presence of hydrogen. No explanation was proposed to account for this behaviour.

According to Natta (1959) and also Soga and Sino (1982), the decrease in polymerization rate caused by hydrogen is due to a slow addition of the monomer to the catalyst-hydrogen bond formed in the chain transfer to hydrogen step.

Several hypotheses have been proposed to account for the polymerization rate enhancement of hydrogen. Okura et al. (1970) suggested that hydrogen and cocatalyst interact to further reduce the catalytic surface forming new active sites, not available when the cocatalyst is the single oxidizing agent. The formation of additional active sites has also been proposed by Bulls and Higgins (1973) and by Mortimer et al. (1978).

Pijpers and Roest (1972) explained the increase in polymerization rate in terms of a complexation mechanism between the active center and the dead polymer chain. The rate of polymerization in absence of hydrogen is lower because polymer chains terminated by β-hydride elimination possess a terminal double-bond that can interact with the transition metal at the active center and compete with or prevent monomer insertion. On the other hand, chain ends of polymers terminated by transfer to hydrogen are saturated and can not complex with the active site. Alternatively, the decrease in molecular weight caused by hydrogen could also facilitate chain migration from the active sites, thus favoring monomer diffusion through the polymer layer (Boucheron, 1975). Both hypotheses have been contested by Barbe et al. (1987).

Ross (1984) proposed a dual mechanism to explain the rate enhancement-lowering effect of hydrogen: atomic hydrogen would be responsible for polymerization inhibition, while molecular hydrogen, particularly at high monomer and hydrogen concentrations, would account for the formation of new active sites, thus increasing the polymerization rate. This model would explain the discrepancy between the rate-enhancement effect observed by Guastalla and Giannini (polymerization pressure of 3 - 4 kg/cm^2) and Soga (polymerization carried out at atmospheric pressure). However, some recent polymerization data of ethylene using a supported $MgCl_2$ catalyst contradict this hypothesis. Marques et al. (1993) reported that the rate of ethylene polymerization is enhanced by hydrogen at pressures below 2 bars, but that higher hydrogen pressures first lower and then do not alter the rate of polymerization.

The enhancement in the rate of propylene polymerization observed using the catalyst LYNX 900 and DEAC can therefore be related to similar observations in the literature. Although there is not significant experimental support for this hypothesis, apparently hydrogen interacts with the catalyst surface, probably with help of the monomer, creating more active site types, thus increasing the rate of propylene polymerization. The reversibility of the hydrogen effect can also be explained by this hypothesis. When hydrogen is removed from the reactor, the hydrogen-activated active sites lose their activity and, consequently, the polymerization rate decreases. If hydrogen is admitted again to the reactor, the hydrogen-activated sites become once more available, increasing the rate of polymerization. Additional support for this hypothesis comes from the molecular weight distributions of polymer made in the presence and absence of hydrogen and will be discussed in the next chapter.

Hydrogen has a minimal effect on polymerization rate of ethylene with the regular or prepolymerized catalyst. If the activation mechanism by hydrogen is based on an interaction of hydrogen-monomer-catalyst as proposed by Ross (1984), then hydrogen would not interact with ethylene to form new active sites on LYNX 900. This mechanism is only tentative and only with more extensive experimental data could one establish its validity. Alternatively, the hydrogen-activated sites might not be active for ethylene polymerization.

The enhancement of the rate of ethylene polymerization caused by the presence of an α-olefin has been studied in industrial and academic laboratories (Chien, 1993). Two principal experimental conditions may lead to this phenomenon: 1) prepolymerization of the catalyst with an α-olefin prior to the addition of ethylene to the reactor; 2) copolymerization of ethylene and an α-olefin. The rate of propylene homopolymerization can also be increased by prepolymerization of the catalyst at milder conditions with propylene (Yano et al., 1986).

Several explanations have been proposed to account for rate enhancement by prepolymerization: 1) controlled fracturing of the catalyst during prepolymerization, exposing more active sites (Fink and Kinkelin, 1988, Xu et al., 1990); 2) activation of dormant sites or formation of additional sites by the α-olefin (Spitz et al., 1988; Tait, 1988; Ystenes, 1991); 3) displacement of complexed molecules, such as donor molecules formed during catalyst synthesis or added on purpose as external Lewis bases, by the α-olefin (Tait, 1988); 4) change of the distribution of the titanium oxidation states (Calabro and Lo, 1988); and 5) alteration of the association state of the titanium (Chien, 1993). Reduction of diffusional mass transfer resistances of the cocatalyst and monomer through the polymeric layer surrounding the active sites has also been suggested for the case of rate enhancement of copolymerization of ethylene and α-olefins (Soga et al., 1988).

It is difficult to determine which one of the described mechanisms is responsible for the increase in the polymerization rate of ethylene using prepolymerized LYNX 900 catalyst. Due to the complex nature of heterogeneous Ziegler-Natta catalysts, it is probable that several of those mechanisms are present simultaneously in different degrees as a function of the polymerization conditions and type of catalytic system and of monomer.

CHAPTER 6 - POLYMER CHARACTERIZATION

Introduction

An integrated methodology for polymer characterization using size exclusion chromatography (SEC), temperature rising elution fractionation (TREF) and carbon-13 nuclear magnetic resonance spectroscopy (^{13}C NMR) has been developed and used for characterizing polypropylene, polyethylene, and ethylene-propylene impact copolymers produced with the LYNX 900 catalyst system. This combined methodology permits the determination of the distributions of chemical composition, stereoregularity, and molecular weight which then permit one to estimate number of active site types and to better understand the catalysis mechanisms.

Molecular weight and stereoregularity distributions of polypropylene made with LYNX 900 are also compared with those of a polypropylene produced with a metallocene/aluminoxane soluble catalyst, ethylenebis(indenyl) zirconium dichloride and methylaluminoxane ($Et(Ind)_2ZrCl_2$/MAO, see Huang and Rempel, 1992).

Determination of Molecular Weight Distributions of Ethylene and Propylene Homopolymers with High Temperature SEC

Experimental Details

Molecular weight distributions (MWD) of the polyolefin samples were measured with a Waters-Millipore SEC instrument model 150-C. The Waters-Millipore SEC model 150-C is today the standard equipment for measuring the MWD of polyolefins (Haddam and Hay, 1988).

Data were acquired on-line using a data acquisition/processing computer software installed in a NEC powermate SX plus microcomputer (Intel 386SX microprocessor, 16 MHz). This software was also used for fitting molecular weight calibration curves and molecular weight distributions and averages (Maxima/Baseline - Gel Permeation Chromatography Option: Operator's Manual, Dynamic Solutions Division of Millipore, Ventura, California, 2nd edition, 1989).

Three SEC columns from American Polymer Standards Corporation were used and these had the following specifications: 1) pore size X molecular weight range: linear X 1,000-5,000,000; 500 Å X 0-10,000; and 10^6 Å X 500,000-10,000,000; 2) particle size diameter - 15 µm; 3) column size - 7.8 mm ID x 30 cm; 4) packing - crosslinked styrene-divinyl benzene copolymer.

The mobile phase and sample solvent used was HPLC grade trichlorobenzene from Fischer Chemicals.

The following operation conditions were adopted: 1) column and sample compartment temperature - 145 °C, 2) flow rate of mobile phase - 1.0 ml/min, 3) sample injection volume - 200 µl, 4) equilibrium delay - 10 min, 5) initial delay - 2 hours, 6) sample run time - 50 min, 7) no sample spinning, 8) no sample filtering.

Polymer samples were prepared in 4 ml SEC glass vials at a concentration no higher then 0.1 wt % in trichlorobenzene. Antioxidant (Irganox 1010 from Ciba-Geigy) was also added to the sample vials at a concentration of 0.1 wt % to prevent oxidative thermal degradation of the polymer samples in the SEC oven and columns. No antioxidant was added to the mobile phase.

To eliminate aggregates of polymer chains in the mobile phase (Grinshpun et al., 1984; Grinshpun and Rudin, 1985), polyethylene and polypropylene samples were allowed to dissolve for at least 24 hours prior to injection. However, to avoid oxidative thermal degradation of the samples, the maximum dissolution time used was 40 hours (Ekamnis and Skinner, 1991; Lew et al., 1988a).

Molecular weight distributions and averages were determined using the universal calibration curve obtained with narrow MWD polystyrene standards from Tosoh Corporation (table 1). Polystyrene samples for calibration were prepared by the procedure used for polypropylene and polyethylene, but at dissolution times of only two hours. Polystyrene standards were injected every week to detect changes

in the calibration curve; a new calibration curve was determined whenever necessary. Calibration curves were usually adequately fit with a 3rd degree polynomial (figure 1).

Standard	M_w (LS)	M_w (GPC)	M_w/M_n	M_n
A-500		500	1.14	440
A-1000		870	1.10	790
A-2500	2,980	2,740	1.11	2,470
A-5000	5,570	5,240	1.03	5,090
F-1	9,100	9,830	1.02	9,640
F-2	19,600	19,100	1.01	18,900
F-4	37,900	37,200	1.01	36,800
F-10	96,400	98,900	1.01	97,900
F-20	190,000	189,000	1.04	182,000
F-40	355,000	354,000	1.02	347,000
F-80	706,000	707,000	1.05	673,000
F-128	1,090,000	1,110,000	1.08	1,030,000

Table 1 - Polystyrene standards of narrow MWD used for SEC calibration (Tosoh Corporation).

Polymer type	K	a	Reference
Polystyrene	1.21×10^{-4}	0.707	Lew et al., 1988
Polypropylene	1.37×10^{-4}	0.750	Lew et al., 1988
Polyethylene	3.92×10^{-4}	0.725	Wagner, 1985

Table 2 - Mark-Houwink constants for universal calibration curve of SEC (Mark - Houwink equation: $[\eta] = KMW^{a}$).

The Mark-Houwink constants used with the universal calibration curve are shown in table 2.

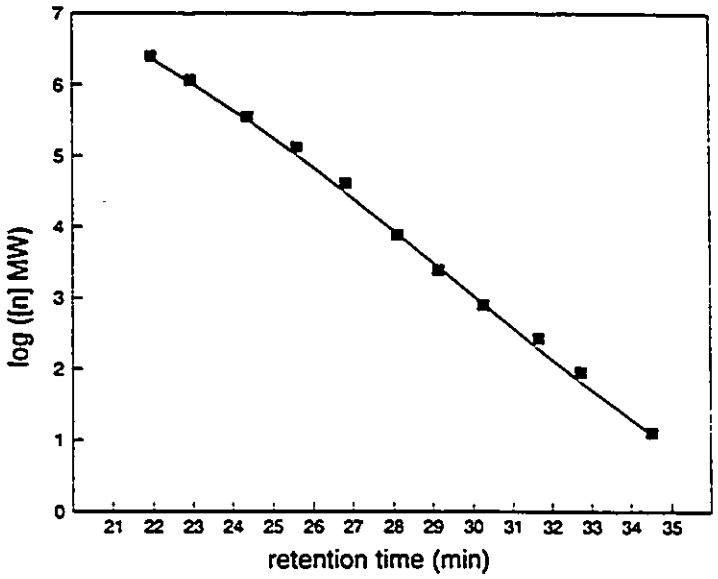

Figure 1 - Universal calibration curve for SEC using narrow MWD polystyrene standards.

Evaluation of SEC - Sample Degradation, Reproducibility, and Peak Broadening

SEC analysis of highly crystalline polyolefins can be complicated by imperfect dissolution and/or sample degradation (Grinshpun et al., 1984; Grinshpun and Rudin, 1984). Polymer aggregates can be present in the sample vial if the dissolution time is insufficient to ensure complete dissolution of the polyolefin sample. These aggregates must be eliminated since they interfere with SEC measurements. Longer dissolution times or dissolution at higher temperatures can be employed to eliminate these polymer aggregates. However, thermal degradation of the samples may take place under these circumstances (Lew et al., 1988a).

During SEC analysis an operation window of 24 to 40 hours for dissolution time at 145 °C was adopted. Figure 2 shows the number, mass and z average chain lengths of two different polypropylene samples as a function of dissolution time. These averages vary within 5% of the first measured value even after 100 hours of

dissolution time for the lower molecular weight sample. This suggests that during this period, no noticeable polymer degradation took place. It is likely that stable aggregates are not present after 24 hours of dissolution since no molecular weight changes are noticed in the figure. Shorter dissolution times were not used to avoid plugging the injection lines of SEC with undissolved polymer.

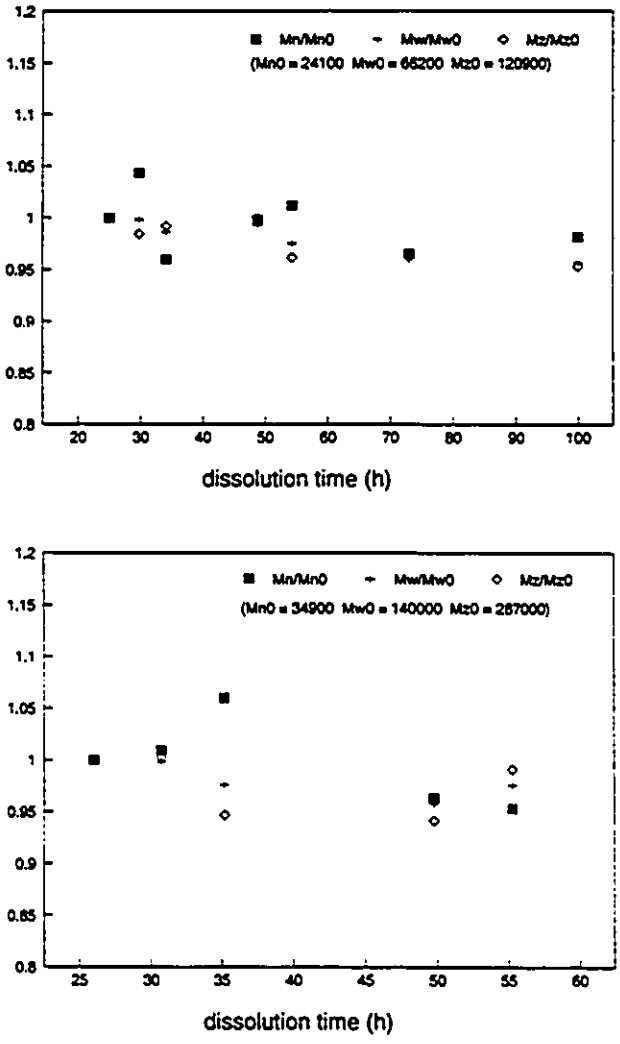

Figure 2 - Degradation of polypropylene as a function of dissolution time at 145 ^{0}C.

The molecular weight averages shown in figure 2 indicate good reproducibility of SEC results, even when long time intervals exist between two consecutive sample injections. SEC reproducibility was further assessed with successive injections (spaced over only 1 hour) of polypropylene samples made with LYNX 900 (table 3). As can be seen, all molecular weight averages are within 10% of the average estimated value.

	Sample 1		Sample 2	
#	M_n	M_w	M_n	M_w
1	42468	170081	52395	199968
2	40347	145174	51736	196341
3	40922	150047	52989	189634
avg	41246	155101	52373	195314
std	896	10778	512	4281
	Sample 3		Sample 4	
#	M_n	M_w	M_n	M_w
1	43699	171021	56992	205820
2	48763	186372	60855	210217
3	47377	189859	54873	201057
4	46470	173778	50211	197249
5	45678	172594	53170	195417
avg	46397	178725	55220	201952
std	1695	7796	3586	5457

Table 3 - Reproducibility of SEC using polypropylene (avg - average, std - standard deviation).

Peak broadening and skewing of SEC was evaluated using the method proposed by Hamielec (1980). In this method, skewing and symmetrical broadening are estimated by comparing previously known number and mass average molecular weights of polymer standards with those averages estimated for the same polymer with SEC, using the equations:

$$M_n(c) = M_n(uc)\left(1+\frac{sk}{2}\right)\exp\left[\frac{(D_2\sigma)^2}{2}\right] \quad (1)$$

$$M_w(c) = M_w(uc)\left(1+\frac{sk}{2}\right)\exp\left[-\frac{(D_2\sigma)^2}{2}\right] \quad (2)$$

where,

M_n number average molecular weight.

M_w mass average molecular weight.

(c) previously known standard averages (absolute values usually determined by osmometry and light scattering).

(uc) averages determined with SEC.

The parameter *sk* is related to the detector response skewing, and should be less then 0.1 for satisfactory SEC operation. Symmetrical broadening is described by the expression $\exp[(D_2\sigma)^2/2]$ and should not exceed 1.05.

The polystyrene samples used for obtaining the calibration curve were analyzed by SEC in order to evaluate peak broadening. These results are presented in table 4 and indicate that no significant peak broadening takes place during SEC analysis.

Standard	M_n (c)	M_w (c)	M_n(uc)	M_w(uc)	skewing broadening	symmetrical broadening
A-1000	790	870	885	958	-0.10	0.99
A-2500	2,470	2,740	2,681	3,025	-0.09	1.01
A-5000	5,090	5,240	5,164	5,569	-0.04	1.02
F-1	9,640	9,830	10,239	11,017	-0.08	1.03
F-2	18,900	19,100	19,210	20,807	-0.05	1.04
F-4	36,800	37,200	37,618	40,788	-0.06	1.04
F-10	97,900	98,900	88,748	96,260	0.06	1.04
F-20	182,000	189,000	175,237	189,400	0.02	1.02
F-40	347,000	354,000	337,400	368,065	-0.01	1.03
F-80	673,000	707,000	677,659	714,352	-0.01	1.00
F-128	1,030,000	1,110,000	964,076	1,004,548	0.09	0.98

Table 4 - Evaluation of symmetrical and skewing peak broadening in SEC with polystyrene standards.

Experimental SEC Results for Polypropylene and Polyethylene

The molecular weight distributions of polypropylene and polyethylene samples produced with LYNX 900 were determined by SEC following the procedures described above.

Table 5 shows the results for the number and mass average molecular weights and polydispersity of the polypropylene samples. All SEC measurements were replicated two times, except for the last sample at $P_{H_2} = 0$ psi and $T = 70$ °C, which was analyzed only once.

P_{H_2}(psi)	T (°C)	M_n	M_w	PDI
10	50	49,300±760	226,700±15,000	4.60±0.24
10	60	38,100±4,100	166,500±20,800	4.36±0.07
10	70	33,200±120	145,600±2200	4.39±0.05
5	60	57,400±4,400	248,600±9,500	4.34±0.16
5	70	55,700±3,700	225,200±9,200	4.04±0.11
0	50	301,300±11,600	581,000±17,200	1.93±0.14
0	60	243,900±12,500	536,900±24,100	2.2±0.15
0	70	165,500	434,800	2.59

Table 5 - Molecular weight averages and polydispersities of polypropylene made with LYNX 900 (measured by high temperature SEC).

As expected, the molecular weight averages of propylene produced at any hydrogen pressure decrease with increasing temperature, because of the normally higher activation energies for chain transfer than for propagation reactions. Polydispersities, however, do not change appreciably with polymerization temperature when hydrogen is present in the reactor.

Surprisingly, polypropylene made in the absence of hydrogen shows a very narrow polydispersity for a polyolefin made with heterogeneous Ziegler-Natta catalyst. The polydispersity of those samples also increases slightly with increasing temperature. Two explanations might be given for this behaviour.

First, because of the high molecular weight of the samples, part of the polypropylene chains might have reached the *exclusion limit* of the SEC columns. If the polymer chain volumes in solution are larger then the largest pore volumes in the columns, they will be excluded from all pores and be eluted all at the same time. If this phenomenon happens to a large fraction of the polymer chains the SEC peak will be severely skewed to low retention times. Although it is not possible to

completely rule out this hypothesis from our data, there is evidence that indicates that most if not all polypropylene chains are within the exclusion limit volume. First, the SEC peaks are not skewed to low retention times, as shown in figure 3. As shown by the shaded area in this figure, only about 20 wt% of the polymer chains elute at retention times smaller then the retention time for the highest molecular weight polystyrene standard. This indicates that most of the distribution falls inside the range of retention times described by the calibration curve and that only a small part of this distribution is calculated by extrapolation.

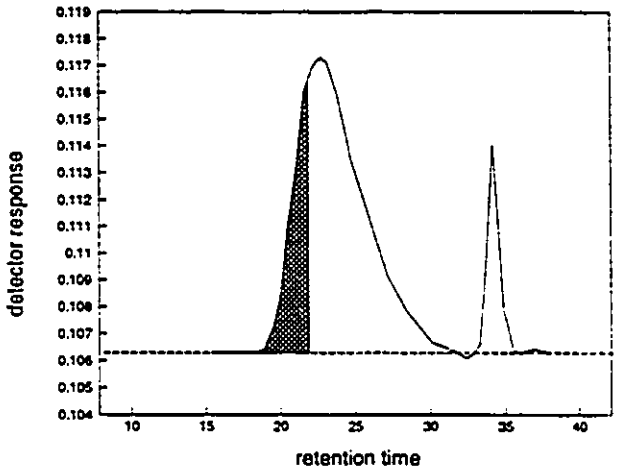

Figure 3 - SEC curve of a high molecular weight polypropylene sample made with LYNX 900 ($T = 60$ °C, $P_{H_2} = 0$). Shaded area indicates retention times lower than the one for the highest molecular weight polystyrene standard used to establish the molecular weight calibration curve.

Further evidence can be obtained using the calibration curve, figure 1. As can be seen, the exclusion limit has not been reached for the highest molecular weight standard of polystyrene (MW = 1,100,000). To evaluate the equivalent MW for polypropylene, one can use the Mark-Houwink equation and the fact that SEC fractionation of polymers is according to the hydrodynamic volume of the polymer chains, $[\eta]MW$. Therefore:

$$MW_{ps}[\eta]_{ps} = MW_{pp}[\eta]_{pp} \tag{3}$$

$$K_{ps}MW_{ps}^{a_{ps}+1} = K_{pp}MW_{pp}^{a_{pp}+1} \tag{4}$$

$$MW_{pp} = \left(\frac{K_{ps} MW_{ps}^{a_{ps}+1}}{K_{pp}} \right)^{1/(a_{pp}+1)} \quad (5)$$

where *ps* and *pp* indicate polystyrene and polypropylene, respectively.

Substituting the values of the Mark-Houwink constants for ethylene and propylene (table 2) in equation 5, one obtains MW_{pp} = 728,000 when MW_{ps} = 1,100,000. This means that polystyrene chains of MW = 1,100,000 and polypropylene chains of MW = 728,000 will elute from the SEC columns at the same time. If one uses the nominal exclusion limit of the largest pore size column (10,000,000 for the 10^6 Å column) then MW_{pp} = 6,268,734, which means that the 10^6 Å column is rated to fractionate polypropylene with MW up to about 6,300,000.

Even if one chose to disregard the nominal rating of the column, the number and mass average molecular weights measured for the polypropylene samples are still significantly smaller then the limit encountered by comparison with the polystyrene standard of highest molecular weight.

Considering that the molecular weight distributions measured by SEC are adequate or at least not severely biased, a possible explanation for the narrowing of the molecular weight distribution of polypropylene produced without hydrogen is that some site types are active only in the presence of hydrogen. This hypothesis is clearly supported by the decrease in catalytic activity observed when hydrogen is removed from the polymerization reactor as discussed in the previous chapter.

Therefore, for propylene polymerization, hydrogen seems to activate site types that are dormant in its absence, increasing the catalyst activity and broadening the molecular weight distribution of the formed polymer.

For the case of ethylene polymerization, hydrogen does not seem to have a marked influence on catalyst activity, as presented in the previous chapter. However, prepolymerization with propylene before introduction of ethylene causes a marked increase in the polymerization rate of ethylene. The molecular weight averages of polyethylene samples polymerized at 60 °C with or without prepolymerization and in presence or absence of hydrogen are shown in table 6. Prepolymerization of the catalyst with propylene increases the average molecular weights but does not alter polydispersity. The presence of hydrogen again increases polydispersity but not as significantly as for the case of propylene polymerization.

Pre-polym.	P_{H_2}(psi)	T (^{0}C)	M_n	M_w	PDI
Yes	10	60	112,400	330,000	2.94
No	10	60	97,700	311,200	3.18
Yes	0	60	188,300	440,900	2.34
No	0	60	178,500	416,800	2.34

Table 6 - Molecular weight averages and polydispersities of polyethylene made with LYNX 900 (measured by high temperature SEC).

Based on these results, we can tentatively propose that prepolymerization with propylene generates sites with higher propagation constants and smaller ratios of chain transfer to propagation rates than those created when the catalyst is directly contacted with ethylene, but not necessarily produces different types of active sites. This hypothesis is supported by the higher catalytic activities and polymer with higher molecular weight averages obtained with the prepolymerized catalyst with no or little change in polydispersities.

One can envision a polymerization process in which ethylene when put in contact directly with the catalyst, due to its very high reactivity, polymerizes very fast with incomplete break-up of the original particle or even restricting access of monomer to the active sites by encapsulating them.

On the other hand, prepolymerizing the catalyst with the less reactive propylene might lead to a more controlled break-up of the particles and the formation of a catalyst-polymer particle of high porosity where ethylene can be polymerized with higher activities.

Determination of Stereoregularity and Chemical Composition Distributions Using TREF and ^{13}C NMR

Experimental Details

All TREF runs were performed in the fractionation apparatus shown in figures 4 and 5. It can be run in preparative and in analytical modes.

The precipitation step is done independently of the elution step in the 2 liter glass kettle illustrated in figure 4. The glass kettle is inserted in a thermostated oil bath and circulator (Haake model F3-C digital) equipped with a programmable temperature controller (Haake model PG20), and provided with a nitrogen inlet, a glass condenser in the vent outlet, a digital thermometer, and a mechanical stirrer (Caframo model RZR50).

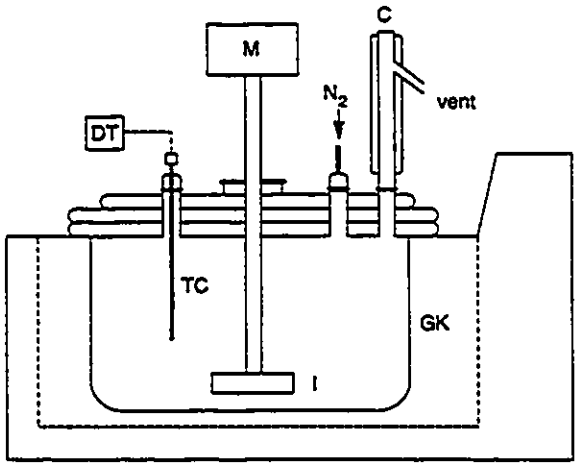

DT = DIGITAL THERMOMETER
M = MOTOR
I = IMPELLER
C = CONDENSER
TC = THERMOCOUPLE
GK = GLASS KETTLE
OB = OIL BATH

Figure 4 - Cooling Section of TREF.

The solvent, polymer sample, support and stabilizer (0.2 wt% Irganox 1010 from Ciba-Geigy) are added to the glass kettle in the desired proportions. Nitrogen is fed continuously to the glass kettle to minimize sample oxidation. The stirrer is turned on. The temperature is then increased rapidly to a value in which all polymer chains are soluble in trichlorobenzene (usually 145 °C) and maintained at that temperature for at least two hours. The mixture is then slowly cooled to room temperature at a constant degree of cooling of no more than 2 °C/h. The polymer coated support is then transferred to the TREF column.

The elution apparatus is shown in figure 5. The TREF column (MODcol column, model MB-2030, pressure rate 2000 psi) is positioned inside a mechanical convection oven (Precision, model µP control 625) with a microprocessor band ramping control (WATLOW, series 920). Fresh trichlorobenzene (HPLC grade from Fischer Chemicals) mixed with stabilizer (Irganox 1010 from Ciba-Geigy) at a concentration of 0.1 wt% is fed to the column by a LC pump (Millipore-Waters, programmable solvent deliver module model 590) through a 4-port switching valve. The column effluent can be directly collected outside the oven in the case of preparative fractionation or is sent to an on-line IR detector (Foxboro, model MIRAN-1A) in the case of analytical TREF.

In the case of preparative TREF, the temperature is increased at predetermined intervals. Temperature is only increased when the collected polymer solution does not show any further precipitation of polymer when methanol is added. In the case of analytical TREF the temperature is raised continuously and the concentration of eluted polymer is monitored by the IR detector.

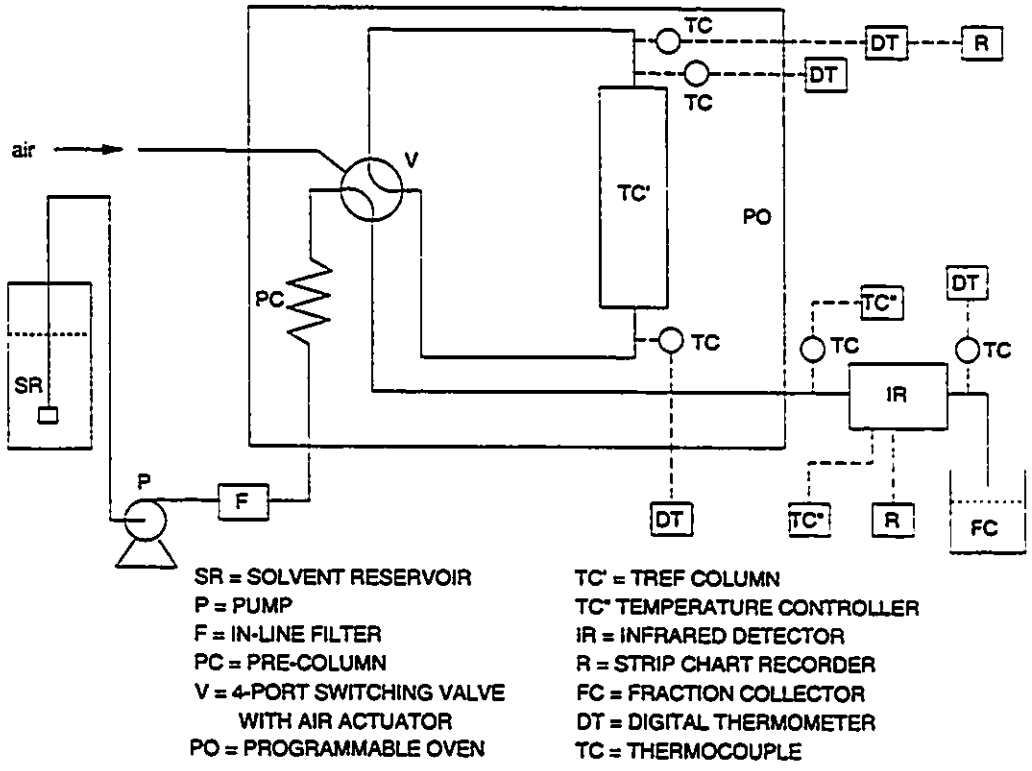

Figure 5 - Heating Section of TREF.

The samples that will be discussed in the next section were all fractionated by using TREF in preparative mode. The operational conditions used and characteristics of the TREF apparatus are shown in table 7.

PRECIPITATION STAGE	
Type of support	Chromosorb P (250 - 177μm)
Polymer concentration	0.004 g/ml
Solvent type	Trichlorobenzene
Antioxidant type	Irganox 1010
Antioxidant concentration	0.002 g/ml
Temperature range	145 °C - room temperature
Cooling rate	1.8 °C/h
Stirring speed	800 rpm
Nitrogen pressure	2 psi
ELUTION STAGE	
Column size	30 cm x 5 cm I.D.
Solvent type	Trichlorobenzene
Temperature range	Room temperature - 145 °C
Solvent flow rate	4.0 ml/min
Size of fractions	Fractions are collected until polymer stops precipitating from solution when methanol is added

Table 7 - Characteristics and operational conditions TREF apparatus.

Experimental Results for TREF Fractionation

Ethylene-1-Octene Copolymer (LLDPE)

LLDPE is certainly the polyolefin that has been most thoroughly studied by TREF. The TREF profile of a commercial LLDPE (ethylene/1-octene) determined by Vela-Estrada and Hamielec (1993) using the TREF apparatus described before is shown in figure 6.

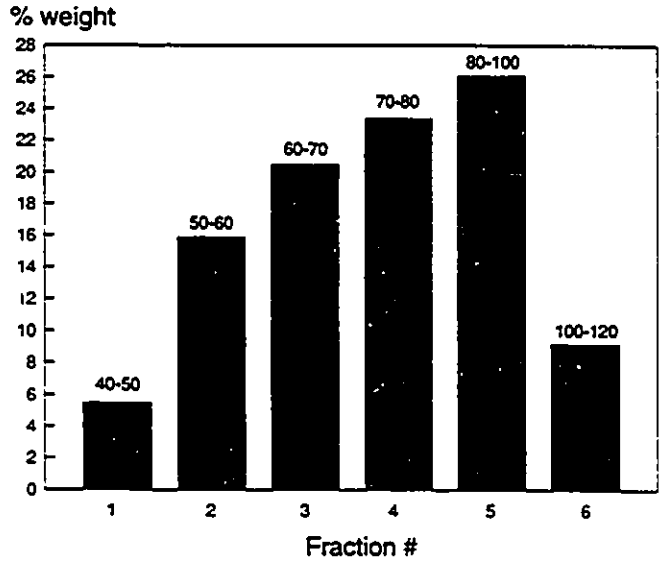

Figure 6 - Preparative TREF profile for a ethylene-1-octene copolymer (LLDPE) made with a heterogeneous Ziegler-Natta catalyst (Vela-Estrada and Hamielec, 1993) (legends on top of bars indicate the temperature interval, in °C, in which the fraction was obtained).

The degree of short chain branching of the TREF fractions was determined by ^{13}C NMR and is shown as a function of elution temperature in figure 7. There is an inverse relationship between degree of short chain branching and elution temperature, since the crystallinity of the polyethylene chains decrease with increasing degree of short chain branching.

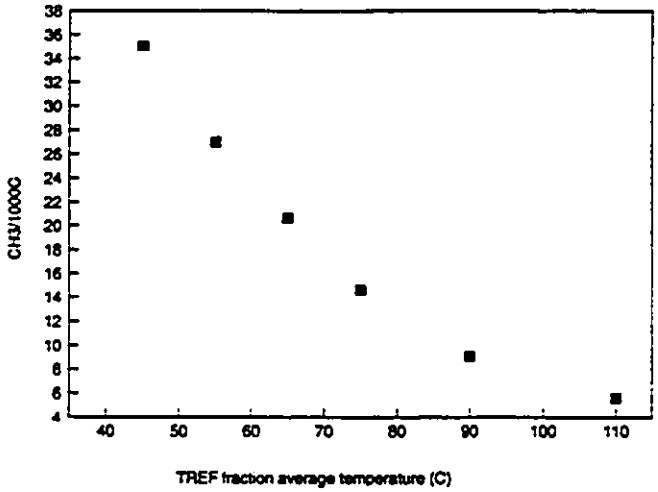

Figure 7 - Relation between short chain branching and TREF fraction average elution temperature for an ethylene-1-octene copolymer (LLDPE) made with a heterogeneous Ziegler-Natta catalyst (Vela-Estrada and Hamielec, 1993)

Propylene-Ethylene Impact Copolymer

A commercial propylene-ethylene impact copolymer produced with a Ti-based heterogeneous Ziegler-Natta catalyst (LYNX 900) in an industrial process operating with five slurry CSTRs in series was fractionated by preparative TREF.

The distribution of TREF fractions as a function of elution temperature is shown in table 8 and in figure 8. Two distinct regions are clearly observed in this distribution. Approximately 25 wt% of the polymer is eluted below 90 °C while the rest of the polymer is distributed in several fractions from 90 to 140 °C. Since this copolymer is a mixture of polypropylene and ethylene-propylene copolymer, one intuitively associates the fraction obtained at low temperature to the less crystalline copolymer and the fraction obtained at higher temperature to isotactic polypropylene. Analyses of these TREF fractions by ^{13}C NMR, FTIR and DSC confirm these assumptions.

fraction #	ΔT (°C)	sample weight (g)	% weight
1	RT-60	0.3728	11.9
2	60-90	0.3633	11.6
3	90-95	0.0304	1.0
4	95-100	0.0730	2.3
5	100-105	0.2215	7.1
6	105-110	0.2801	9.0
7	110-120	1.2535	40.2
8	120-140	0.526	16.9
total polymer recovered		3.1206	
total polymer injected		3.36	
efficiency		92.9%	

Table 8 - TREF fractionation results for ethylene-propylene impact copolymer made with LYNX 900 (RT - room temperature, efficiency = total polymer recovered / total polymer injected x 100).

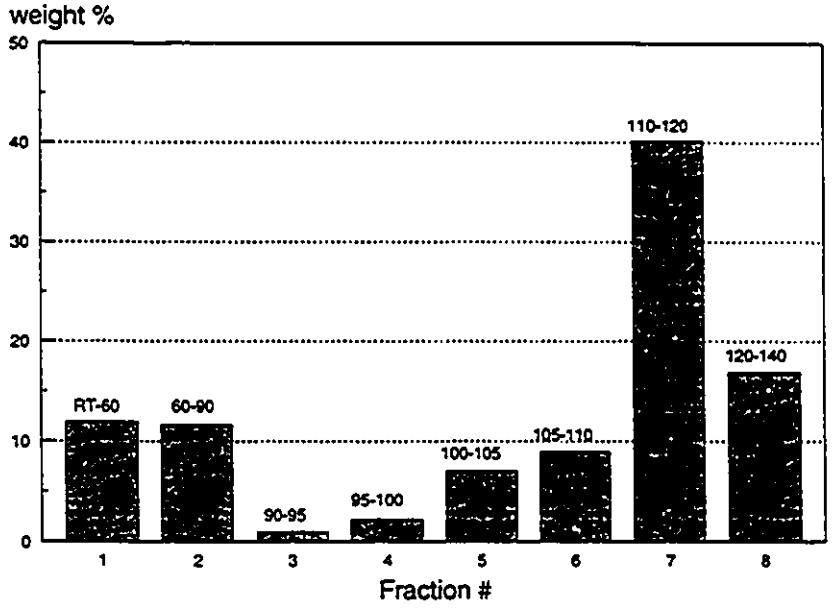

Figure 8 - Preparative TREF profile of propylene-ethylene impact copolymer made with LYNX 900 (legends on top of bars indicate the temperature interval, in °C, in which the fraction was obtained).

Polymer obtained below 90 °C can be further fractionated in smaller fractions as shown in figure 9. Unfortunately the amount of polymer in each sample is not enough for proper analysis with ^{13}C NMR to obtain the copolymer composition of each fraction separately. A higher amount of copolymer was used to try to obtain larger TREF fractions at the lower elution temperatures. However, this more concentrated solution caused excessively high pressure increase in the TREF column and the fractionation had to be interrupted.

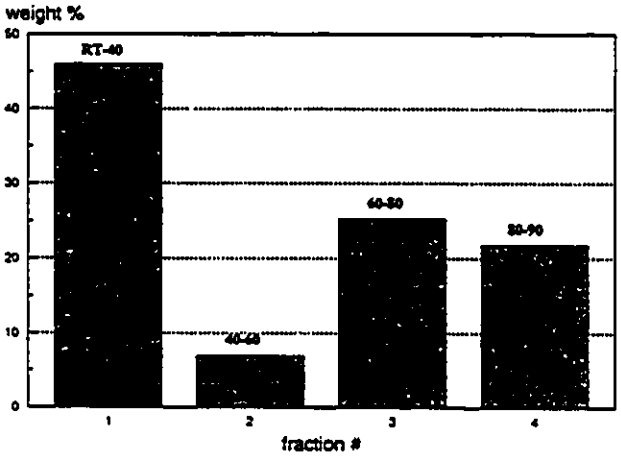

Figure 9 - Preparative TREF fractionation of propylene-ethylene impact copolymer made with LYNX 900 below 90 °C (legends on top of bars indicate the temperature interval, in °C, in which the fraction was obtained).

The melting points and heats of fusion of the TREF fractions measured by differential scanning calorimetry (DSC - DuPont model 910) are shown in table 9. The polymer samples were transferred to the DSC hermetic pans, melted at 160 °C and cooled to room temperature at a rate of 5°C/min before the DSC measurements. Melting curves for fractions 1 and 3 could not be determined. Fraction 1 was almost completely amorphous and does not have well defined melting peaks. Fraction 3 was too small for adequate analysis. Fractions 2, 4, and 5 have multimodal DSC curves which indicates that they are still heterogeneous, while the other fractions have unimodal melting curves, with well defined, sharp peaks and melting temperatures. The DCS curves of these TREF fractions are shown in figure 10. There is a consistent change towards sharper melting curves and higher melting temperatures as one goes from fractions obtained at lower temperatures to the ones obtained at higher temperatures.

fraction #	ΔT (°C)	T_m (°C)	ΔH_f(J/g)
2*	60-90	134.4	34.06
4*	95-100	151.2	36.80
5*	100-105	157.9	97.3
6	105-110	163.0	116.9
7	110-120	163.8	126.2
8	120-140	165.7	130.2

Table 9 - Differential scanning calorimetry measurements of melting point temperature (maximum peak temperature, T_m) and heats of fusion, ΔH_f, of TREF fractions of ethylene-propylene impact copolymer made with LYNX 900. Fractions marked with * have multimodal melting curves; only highest temperature peak is indicated.

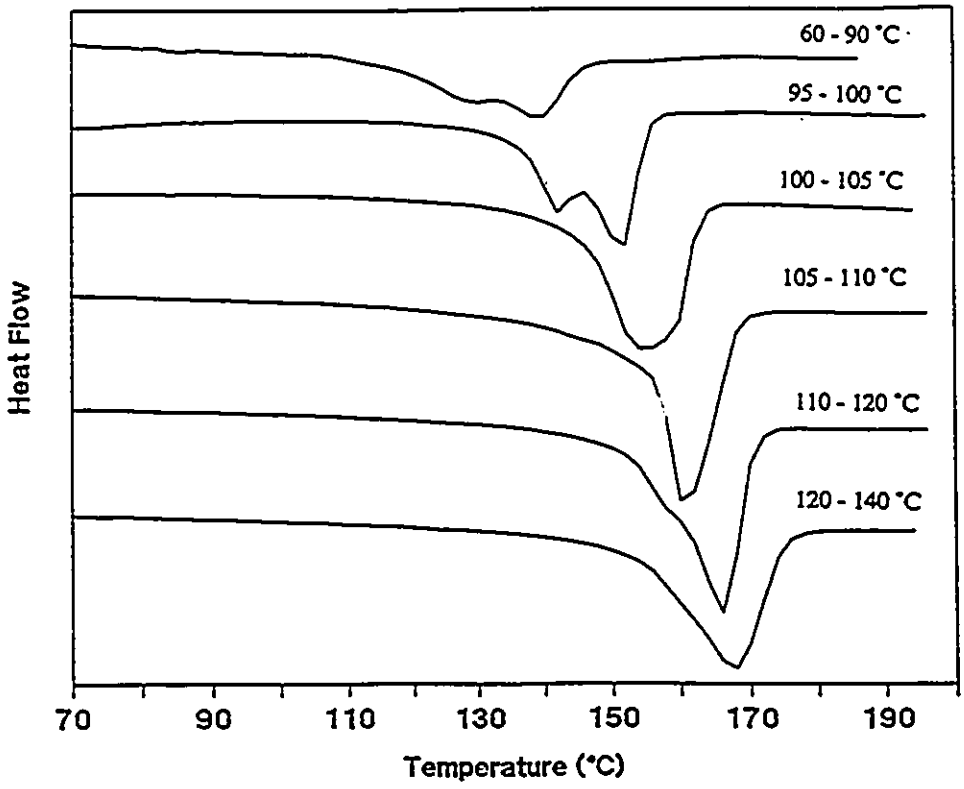

Figure 10 - DSC curves of TREF fractions of propylene-ethylene impact copolymer made with LYNX 900.

Fourier transform infrared spectroscopy (FT-IR) can be used to qualitatively assess the amount of ethylene in the copolymer. Figure 11 shows the FT-IR spectra of some of the TREF fractions using a pressed film technique for preparing the samples. An adequate film of fractions 1 and 2 could not be prepared because of the rubbery nature of the polymer. The peaks in the absorbance region 720 cm^{-1} are related to CH_2 rocking vibrations and are commonly used for determining the amount of ethylene units in propylene-ethylene copolymers (Wei, 1961; Drushel and Iddings, 1963; Gardner et al., 1971). Regioregular polypropylene, containing only isolated CH_2 groups, has no absorption in this region. From figure 11, it is easily seen that TREF fractions 6 to 8 do not contain any appreciable amount of ethylene, while fractions 4 and 5 absorb infrared radiation in the 720 cm^{-1} range and therefore contain some ethylene-propylene copolymer.

It is difficult to obtain quantitative measurements of copolymer composition using FT-IR since this analytical technique requires a calibration curve and copolymer standards are difficult to obtain. Those quantitative results can be obtained more easily using an absolute method such as ^{13}C NMR (see appendix C for experimental conditions).

Detailed structural information about the polymer chains can be obtained by analyzing the ^{13}C NMR spectra of the fractions. Figure 12 shows the ^{13}C NMR spectrum with peak assignments (Cheng, 1984) of the fraction collected between 60 - 90 °C using standard NMR techniques for polyolefins (Randall, 1977). P,S,T indicate primary (methyl), secondary (methylene) and tertiary (methine) carbon atoms respectively. The Greek letters refer to the location of the nearest primary carbons in each side of the chain as suggested by Carman and Wilkes (1971). Therefore, an $S_{\alpha\alpha}$ carbon is a secondary carbon that is adjacent to two primary carbon atoms, an $S_{\alpha\beta}$ carbon is a secondary carbon that is adjacent to a primary carbon atom and is one carbon atom away from a primary carbon and so on up to a $S_{\delta\delta}$ carbon that is three carbon atoms away from a primary carbon atom from both sides of the chain. ^{13}C NMR resolution can only distinguish up to δδ carbon atoms, longer separations being also treated as δδ carbon atoms.

The chain microstructures detected in the ^{13}C NMR spectrum for the methylene carbons of ethylene-propylene copolymer are:

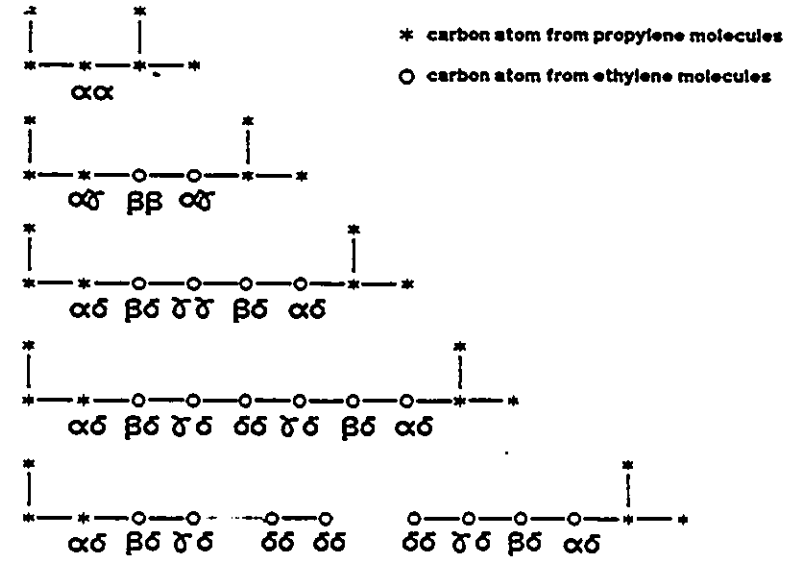

and for the methyl and methine carbons:

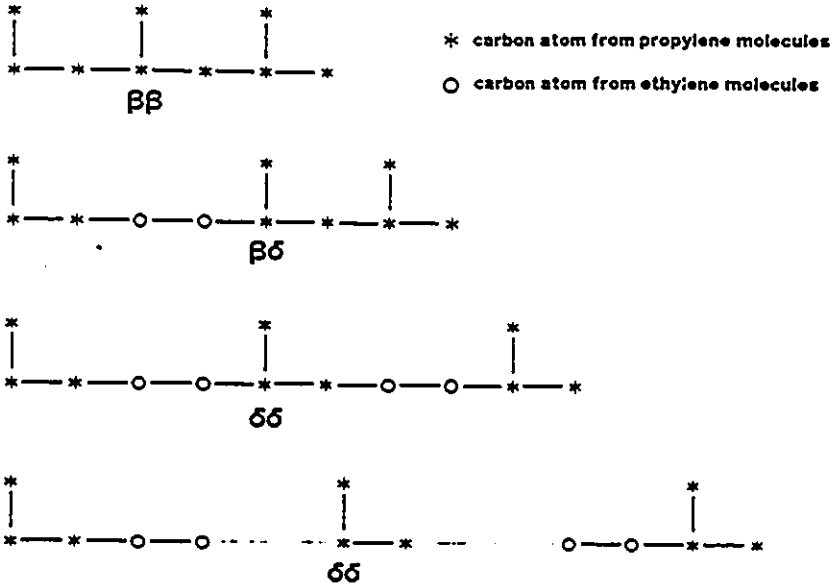

As can be seen, the spectra describes an ethylene-propylene copolymer without monomer inversions.

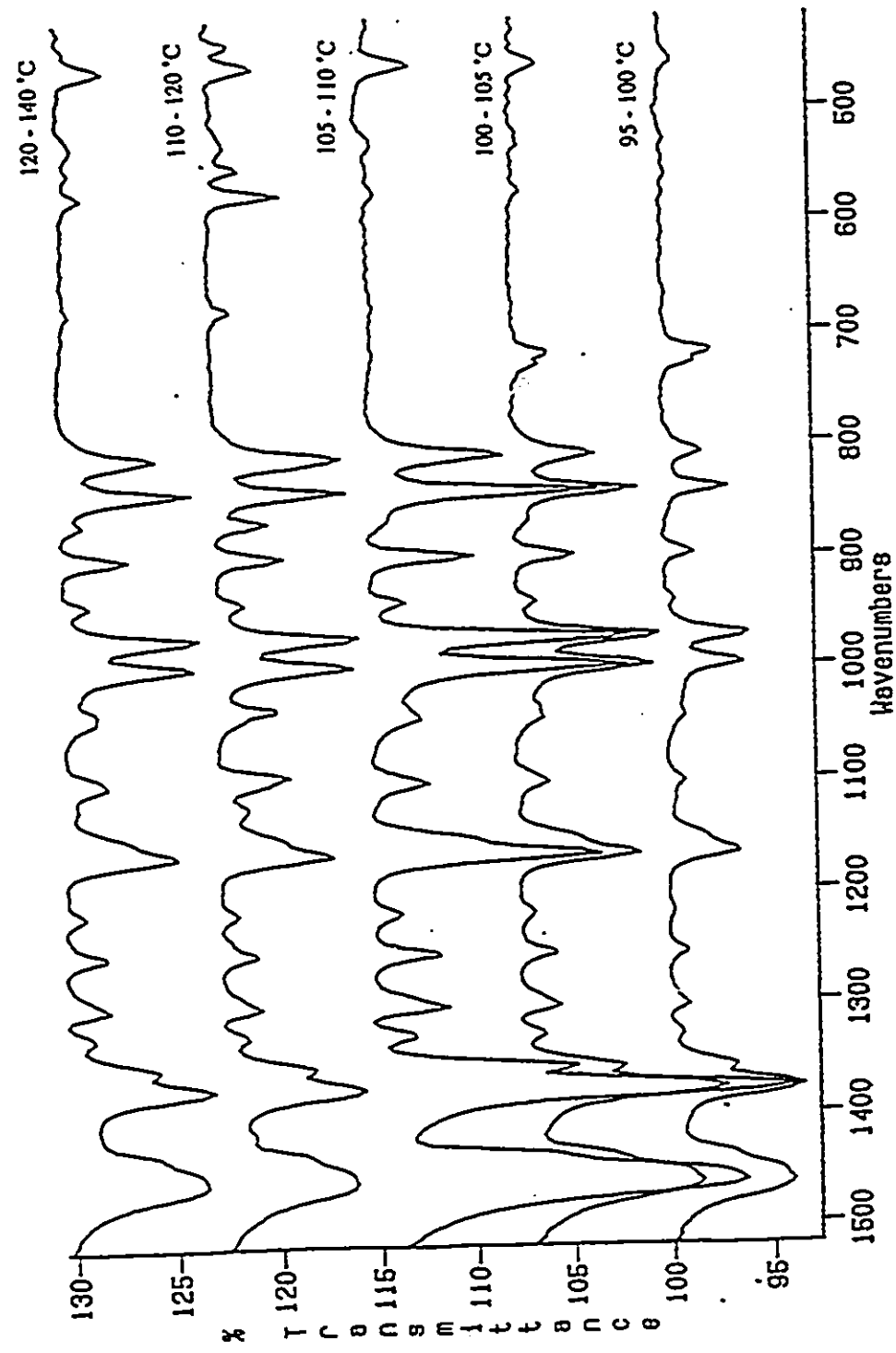

Figure 11 - FTIR spectra of TREF fractions of propylene-ethylene impact copolymer made with LYNX 900.

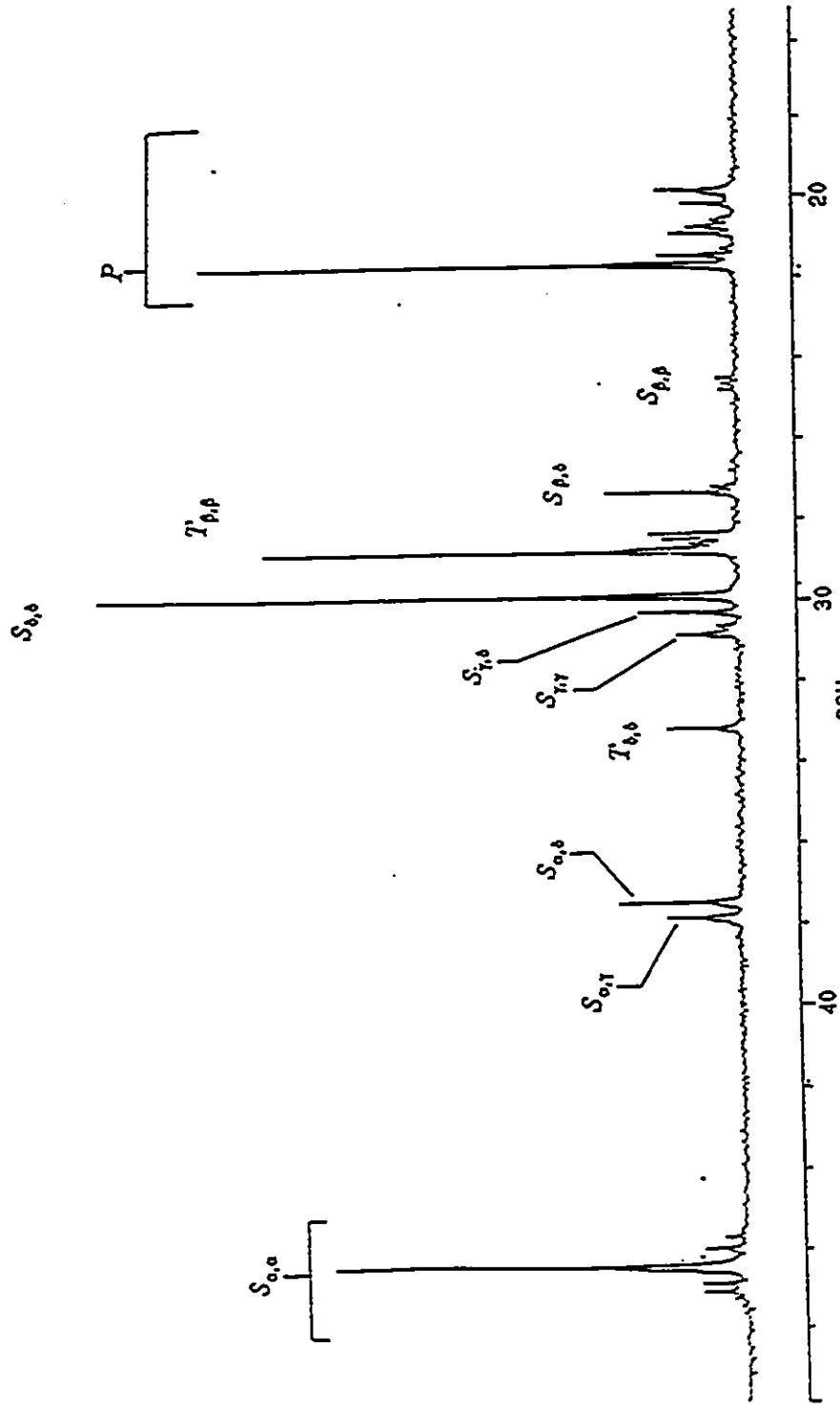

Figure 12 - ^{13}C NMR peak assignments of the TREF fraction of propylene-ethylene impact copolymer made with LYNX 900 collected between 60 - 90 °C.

In figure 13 the ^{13}C NMR spectra of six TREF fractions are compared. The peaks associated with ethylene units decrease rapidly from the fraction obtained between 60 - 90 °C to the one obtained between 100 - 105 °C.

The amounts of ethylene units in the TREF fractions can be estimated from ^{13}C NMR peak intensities using the relationships suggested by Cheng (1984). If we call E and P the total amounts of ethylene and of propylene in the copolymer, then:

$$s = \sum_{i,j} S_{i,j} = k(2E + P) \tag{6}$$

where i,j can be $\alpha, \beta, \gamma, \delta$ and k is the NMR signal proportionality constant. E is multiplied by 2 because there are two secondary carbons in one ethylene monomeric unit.

In the same way, for primary and tertiary carbons:

$$p = \sum_{i,j} P_{i,j} = t = \sum_{i,j} T_{i,j} = kP \tag{7}$$

Combining equations (6) and (7) one easily obtains the following relations for the mole fractions of ethylene and propylene:

$$\frac{E}{E+P} = \frac{s-t}{s+t} = \frac{s-p}{s+p} \tag{8}$$

$$\frac{P}{E+P} = \frac{2t}{s+t} = \frac{2p}{s+p} \tag{9}$$

Alternative computational schemes have been published in the literature (Randall, 1978a; Cheng, 1984). For quantitative spectra, these different computational schemes must give consistent results.

The amounts of ethylene units in the first three fractions as calculated by equations (8) and (9) are 42.0%, 23.9% and 3.3%, respectively (temperature range 60 - 105 °C).

No peaks related to ethylene units can be detected for the other three fractions, in good agreement with the qualitative results of FT-IR. The main factor regulating the fractionation at higher temperatures is the stereoregularity of the polypropylene chains. By analysis of the methyl area of the spectra the following triad distribution was found:

	mm	mr	rr
105-110	97.86	1.54	0.61
110-120	99.04	0.96	
120-140	100		

where m refers to a meso (isotactic) placement and r to a racemic (syndiotactic) placement, as illustrated below:

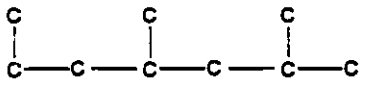

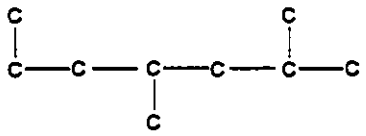

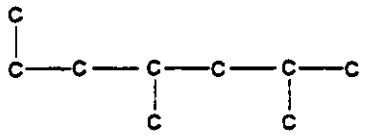

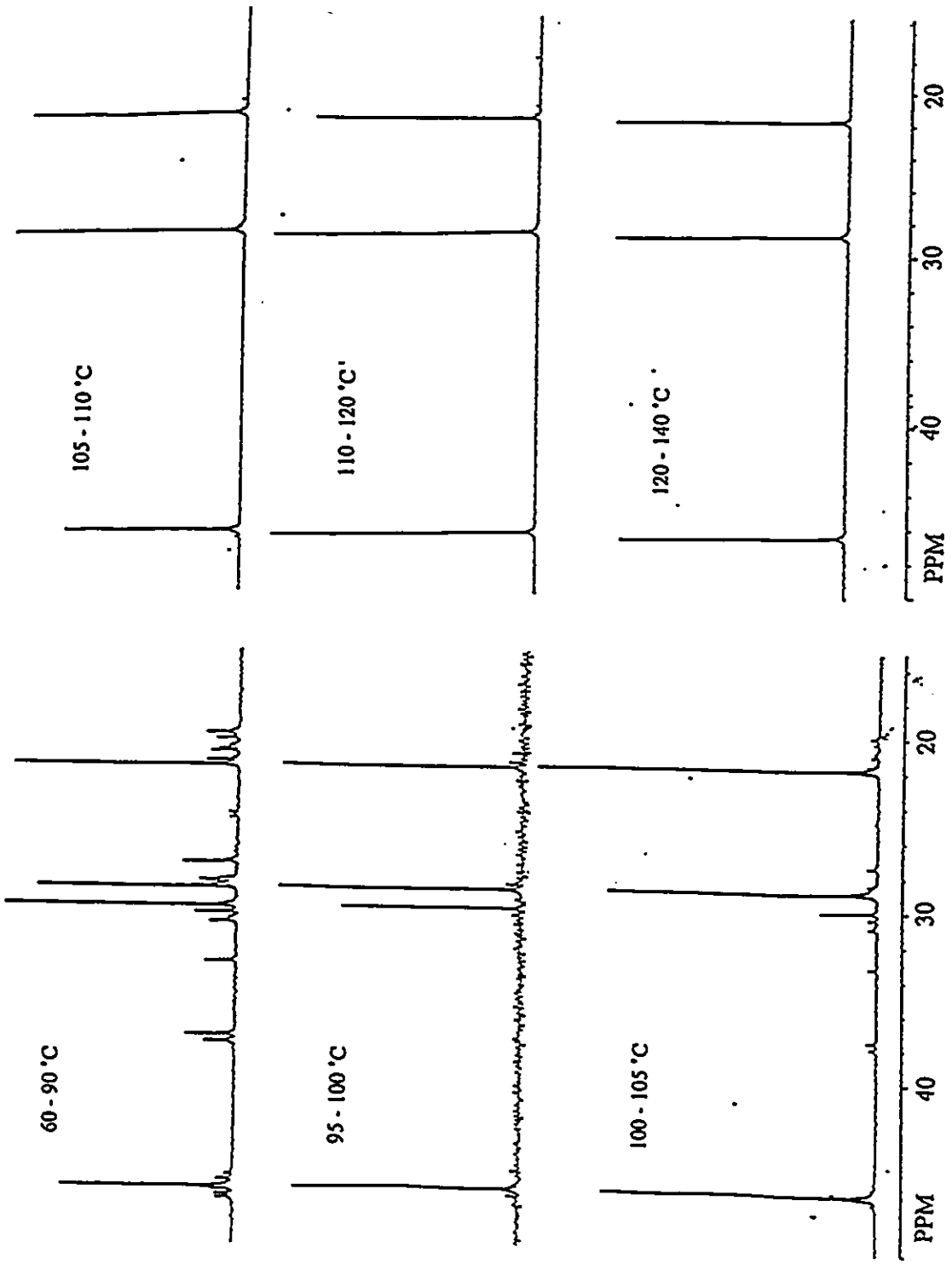

Figure 13 - ^{13}C NMR of TREF fractions of propylene-ethylene impact copolymer made with LYNX 900.

Polypropylene Made by Heterogeneous Ziegler-Natta Catalyst

Table 10 and figure 14 show the TREF profile of a polypropylene made using LYNX 900 at polymerization temperature of 70 °C and partial pressure of hydrogen of 5 psi. As can be seen, although most of the polymer is recovered between 100 to 125 °C, some fractions can be collected either above or below this temperature range. Since there is only one monomer unit, and ruling out the effect of molecular weight (Wild, 1990), the fractionation should be solely controlled by the stereo and regioregularity of the chains.

fraction #	ΔT (°C)	sample weight (g)	% weight
0	RT	0.213	0.6
1	RT-40	0.0179	0.5
2	40-90	0.0566	1.7
3	90-100	0.2416	7.1
4	100-105	0.1149	3.4
5	105-110	0.4499	13.3
6	110-115	0.7780	23.0
7	115-120	0.7157	21.2
8	120-125	0.9315	27.6
9	125-130	0.0128	0.4
10	130-140	0.0414	1.2
total polymer recovered		3.3816	
total polymer injected		3.45	
efficiency		98%	

Table 10 - TREF fractionation results for polypropylene made with LYNX 900 at 70 °C and partial pressure of hydrogen of 5 psi. (RT - room temperature, efficiency = total polymer recovered / total polymer injected x 100).

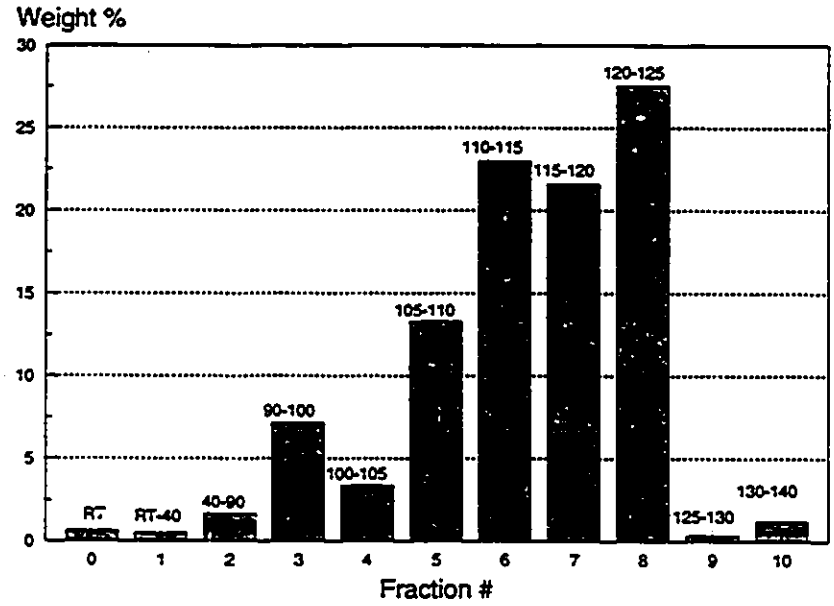

Figure 14 - Preparative TREF profile of polypropylene made with LYNX 900 at 70 °C and hydrogen partial pressure of 5 psi (legends on top of bars indicate the temperature interval, in °C, in which the fraction was obtained).

This broad elution profile agrees with the hypothesis of multiple site types on the catalysts, since sites of different types would likely have different stereochemical control.

This TREF profile also has implications for the interpretation of the fractionation of ethylene-propylene impact copolymer. From inspection of figure 14, it is evident that polypropylene also elutes at low temperatures, which means that in the case of impact copolymer, polypropylene and ethylene-propylene copolymer will be eluted together. Consequently, the average fraction of ethylene units in the copolymer in the three first fractions in figure 13 will be actually higher than the values measured by ^{13}C NMR.

Figure 15 shows the ^{13}C NMR spectra of some TREF fractions. ^{13}C NMR spectra of pure isotactic polypropylene should have only three single peaks, one for each nonequivalent carbon type in the chain (methylene, methine, and methyl). The TREF fraction obtained in the temperature interval 40-90 °C shows several secondary peaks associated with stereoirregularities in the methyl region. Those peaks gradually disappear from the spectrogram for TREF fractions obtained at higher temperatures,

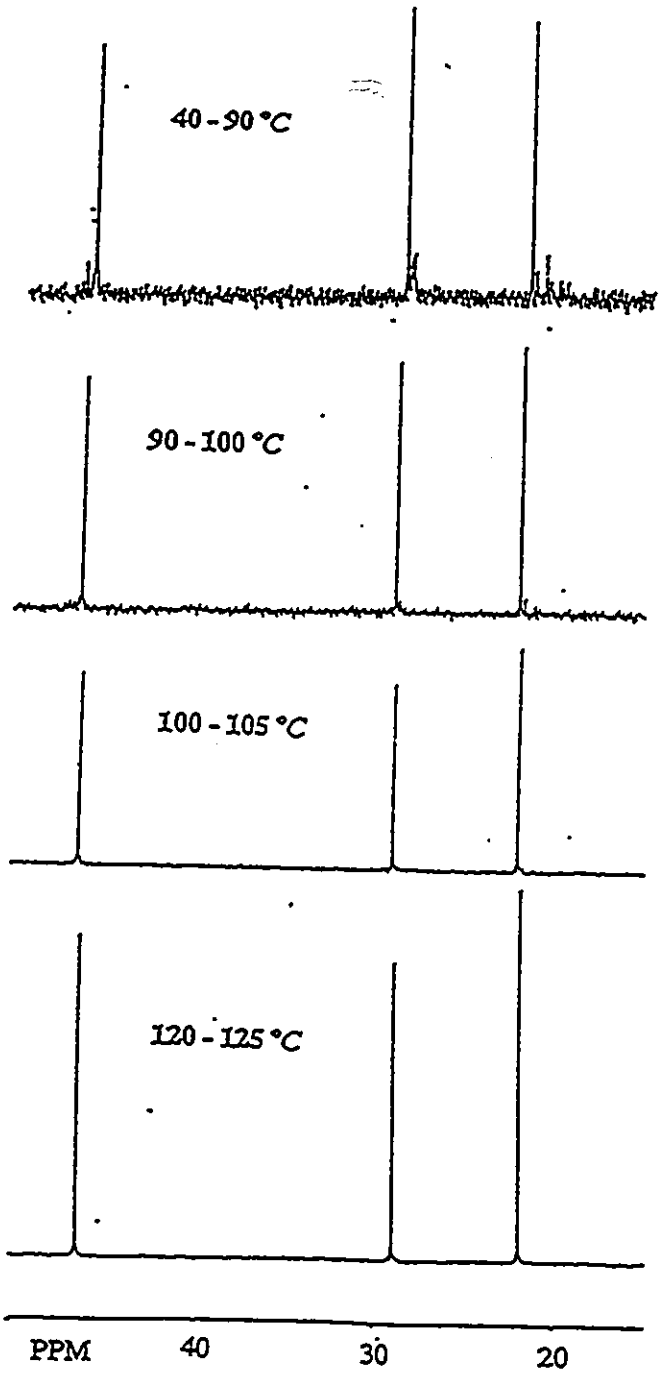

Figure 15 - ^{13}C NMR of TREF fractions of polypropylene with LYNX 900.

which indicates that the fractionation mechanism is mainly regulated by the stereoregularity of the polypropylene chains, in good agreement with the results obtained for the fractionation of the ethylene-propylene impact copolymer.

Figure 16 and table 11 present the preparative TREF profile for polypropylene produced in absence of hydrogen. This profile is remarkably different from the one shown in figure 14 when $P_{H_2} = 5$ psi. Almost no polymer is recovered below 110 °C and practically all polymer elutes from the column between 110-135 °C. This result agrees well with SEC analysis of polypropylene produced in the absence of hydrogen. The narrow molecular weight distributions observed for this polymer indicate that there are only a few active site types. Few site types imply smaller variances in stereoregularity and molecular weight distributions.

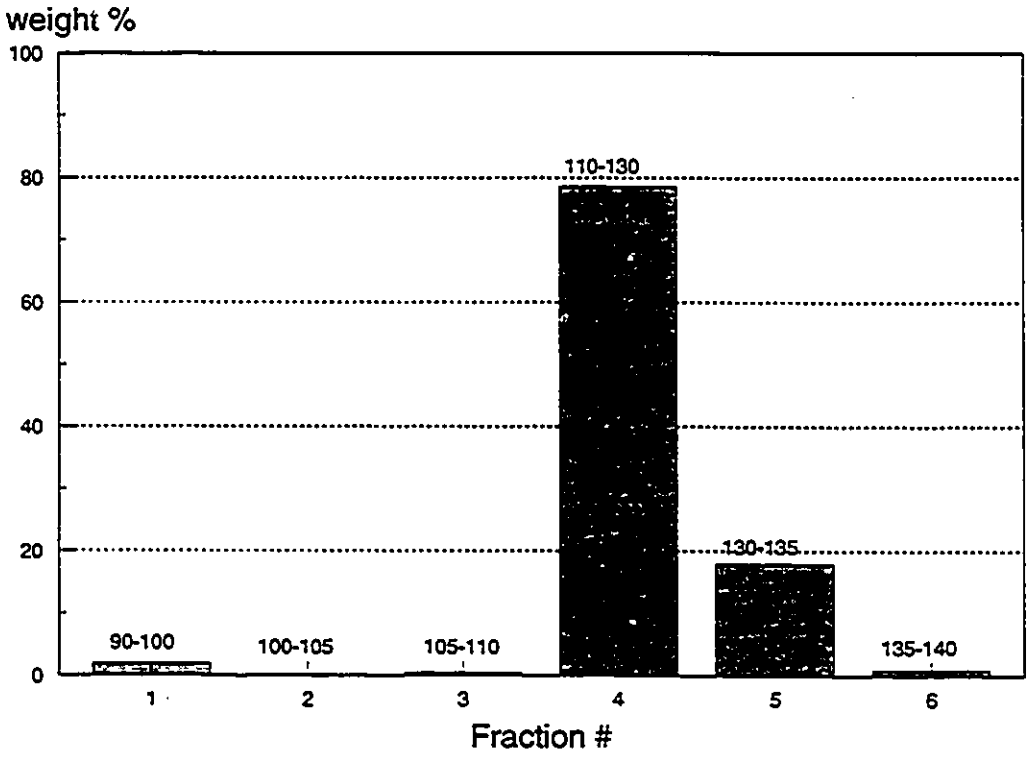

Figure 16 - Preparative TREF profile of polypropylene made with LYNX 900 at 70 °C in absence of hydrogen (legends on top of bars indicate the temperature interval, in °C, in which the fraction was obtained).

fraction #	ΔT (°C)	sample weight (g)	% weight
1	90-100	0.0695	1.9
2	100-105	0.0031	0.1
3	105-110	0.0201	0.5
4	110-130	2.9400	78.6
5	130-135	0.6744	18.0
6	135-140	0.0320	0.9
total polymer recovered		3.7391	
total polymer injected		4.00	
efficiency		93.5%	

Table 11 - TREF fractionation results for polypropylene made with LYNX 900 at 70 °C in absence of hydrogen. (RT - room temperature, efficiency = total polymer recovered / total polymer injected x 100).

Polypropylene Made by a Metallocene Catalyst

The potential for industrial production of polyolefins by metallocene catalysts is great. Polyolefins made by these catalysts have narrower molecular weight and composition distributions than ones produced by conventional heterogeneous Ziegler-Natta catalysts, permitting greater control over the blend of polymer properties required for many commercial applications. TREF is a suitable technique to help understand the novel properties of these new polymers.

The TREF profile of a polypropylene made by a metallocene catalyst is presented in figure 17 and table 12. This sample was synthesized using $Et(Ind)_2ZrCl_2$/MAO (Huang and Rempel, 1992). Its TREF profile differs significantly from the TREF profile for the polypropylene synthesized using classical heterogeneous Ziegler-Natta catalysts shown in figure 14.

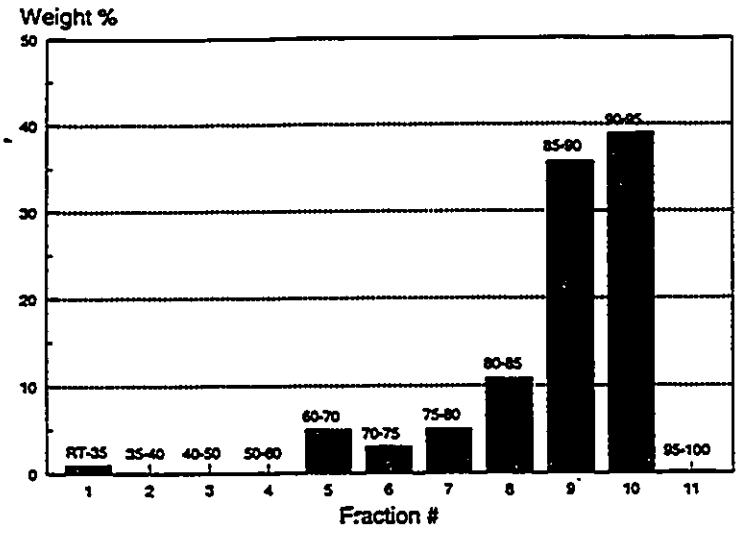

Figure 17 - Preparative TREF profile of propylene made with $Et(Ind)_2ZrCl_2$/MAO.

The lower elution temperatures of the polypropylene made with the metallocene catalyst are probably due to reduced chain crystallinity because of chain defects such as atactic placements, regioregular defects (head-to-head and tail-to-tail placements), or 1-3 monomer insertions. Those types of chain defects have been reported in the literature for polypropylene made with this metallocene catalyst and are reflected in the complex ^{13}C NMR spectra of the whole polymer shown in figure 18. Some of those secondary carbon peaks are shown in detail in figure 19 with peak assignments that correspond to the following structures:

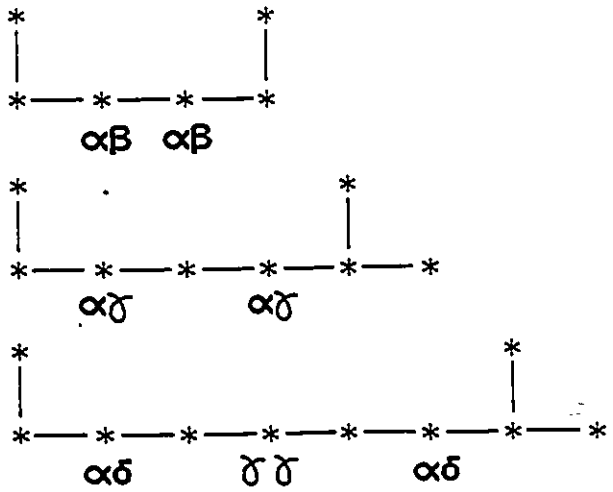

Notice that those structures are only possible if propylene insertions of type tail-to-tail and 1-3 occur.

The preparative TREF elution profile of this polypropylene is significantly narrower then the one obtained for the propylene produced with LYNX 900 in the absence of hydrogen. This result is expected, since metallocene catalysts have one or at most two site types and produce polymer that is more homogeneous than the ones produced with conventional heterogeneous Ziegler-Natta catalysts.

fraction #	ΔT (°C)	sample weight (g)	% weight
0	RT	0	0
1	RT-35	0.0281	1.0
2	35-40	0	0
3	40-50	0	0
4	50-60	0.0022	0.1
5	60-70	0.1433	5.0
6	70-75	0.0902	3.1
7	75-80	0.1475	5.1
8	80-85	0.3121	10.8
9	85-90	1.0306	35.7
10	90-95	1.1293	39.0
11	95-100	0.0054	0.2
total polymer recovered		2.8887	
total polymer injected		3.36	
efficiency		86%	

Table 12 - TREF fractionation results for polypropylene made with $Et(Ind)_2ZrCl_2$/MAO (RT - room temperature, efficiency = total polymer recovered / total polymer injected x 100).

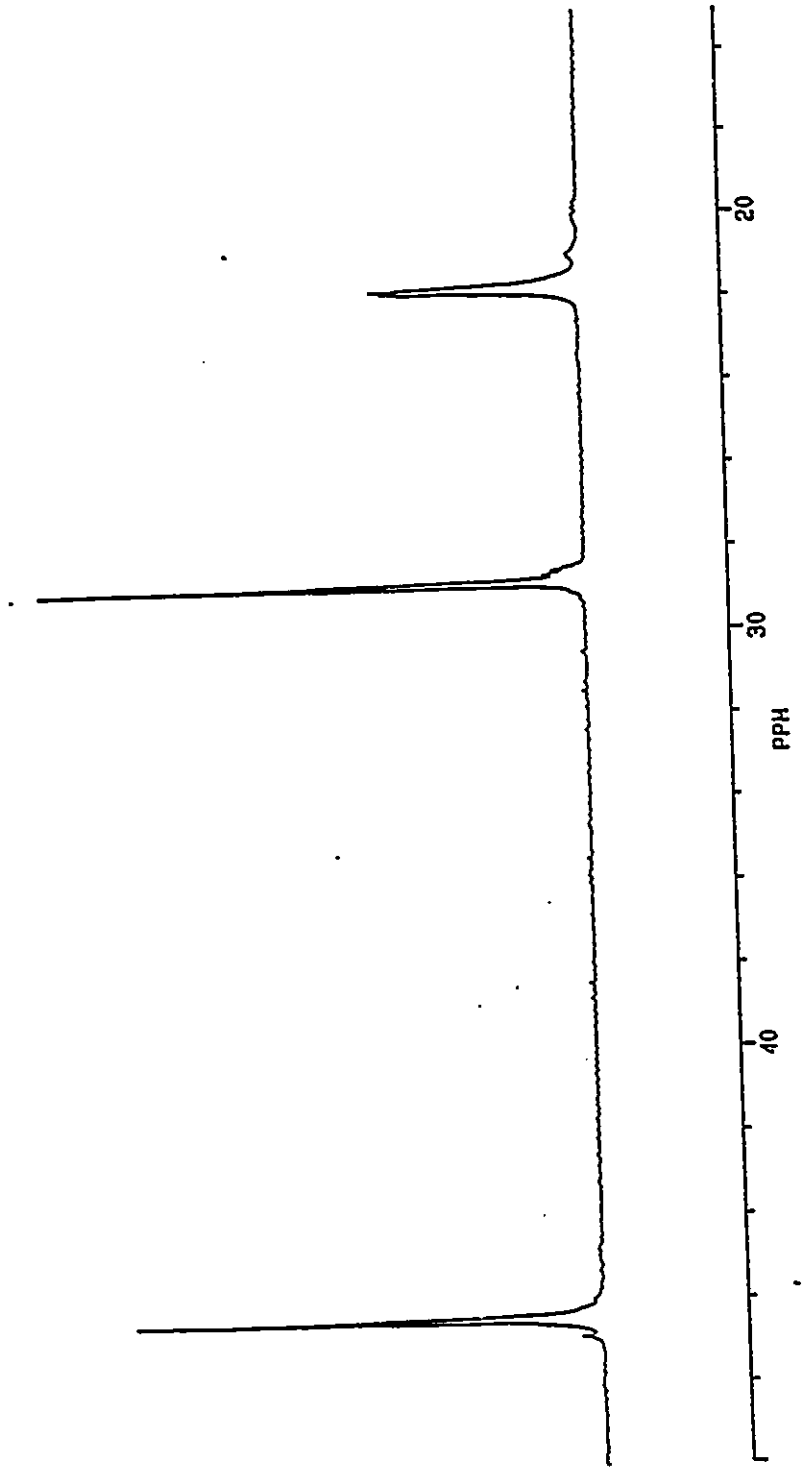

Figure 18 - ^{13}C NMR of TREF polypropylene made with $Et(Ind)_2ZrCl_2/MAO$.

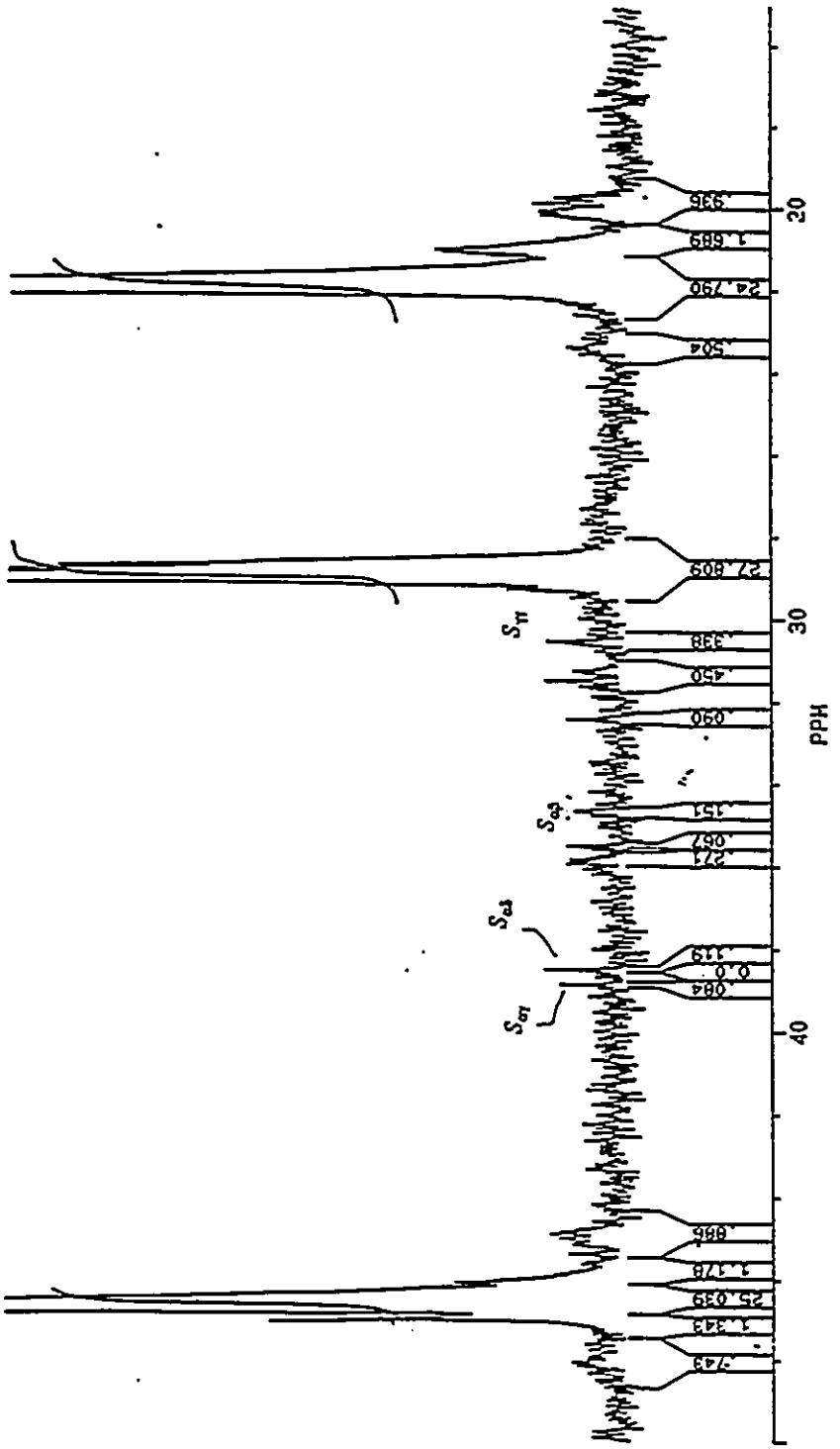

Figure 19 - ^{13}C NMR of TREF of polypropylene made with $Et(Ind)_2ZrCl_2$/MAO.

CHAPTER 7 - MATHEMATICAL MODELLING OF SEC AND TREF

Introduction

In this chapter, size exclusion chromatography (SEC) and temperature rising elution fractionation (TREF) responses are analyzed using mathematical models based on the most probable weight chain length distribution and the Stockmayer bivariate distribution to aid in the interpretation of SEC and TREF measurements and provide information on the types of active sites on the catalyst used for producing these polyolefins. In other words, imbedded in SEC and TREF responses is information which can reveal the mechanism by which catalyst site types operate. These mathematical modelling techniques are designed to clearly reveal this information.

Deconvolution of SEC Chromatograms

Under most industrial polymerization conditions where conventional Ziegler-Natta catalysts are used, the effect of multiple site types is far more important than mass and heat transfer resistances. During polymerization, each site type instantaneously produces dead polymer chains that have the most probable weight chain length distribution (WCLD). Therefore, the instantaneous WCLD of the total polymer produced instantaneously can be considered an average of that produced by the individual site types, weighted by the weight fraction of polymer produced by each site type.

Assuming that the polymerization conditions are such that the WCLD of the accumulated polymer is equal to the instantaneous WCLD, it is possible to obtain information about the number and the nature of catalytic species by decomposing the WCLD of the whole polymer into individual most probable WCLD for each site type. The nature of the site type, in this context, is related to a dimensionless group

of rate constants which appears in the most probable chain length distribution. This approach using SEC was suggested by Vickroy et al. (1993), but very few details were given about their numerical method and polymerization conditions required for its validity. In this section we will compare two numerical methods for performing the necessary deconvolution and propose an efficient methodology for its use with experimental WCLD measured by SEC.

Representation of WCLD as a weighted sum of most probable WCLDs

The most probable WCLD of linear homo and multicomponent copolymers may be expressed by the equation:

$$w(r,j) = \tau^2(j) r e^{-\tau(j) r} \tag{1}$$

where,

$w(r,j)$	most probable WCLD (weight fraction of polymer of chain length r produced on site type j instantaneously)
$\tau(j)$	ratio of rate of production of dead polymer chain to rate of propagation
r	polymer chain length
j	active site type

Dead polymer chain can be produced by β-hydride elimination and chain transfer to a small molecule, as well as by other reaction types. It is assumed that for batch and semi-batch polymerizations $\tau(j)$ is time or monomer conversion independent and for continuous processes also spatially independent.

The instantaneous WCLD of the whole polymer is obtained by averaging the distributions of each individual site type:

$$\hat{W}(r) = \sum_{j=1}^{n} m(j) w(r,j) \tag{2}$$

where,

$\hat{W}(r)$ instantaneous WCLD of the whole polymer produced by n site types

$m(j)$ weight or mass fraction of polymer made by site type j

n number of active site types

Equation (2) is modified to include the constraint:

$$\sum_{j=1}^{n} m(j) = 1 \tag{3}$$

and is finally expressed as,

$$\hat{W}(r) = w(r,n) + \sum_{j=1}^{n-1} m(j)\,[w(r,j) - w(r,n)] \tag{4}$$

We want to minimize the difference between $\hat{W}(r)$ computed by equation (4) and the measured distribution $W(r)$ in order to determine the adjustable parameters $\tau(1), \tau(2), \ldots, \tau(n)$ and $m(1), m(2), \ldots, m(n)$.

Equation (4) is valid for describing an instantaneous WCLD formed by the superposition of several individual most probable WCLDs. However, in practice one has information only about WCLDs for polymer accumulated over a finite polymerization time. Therefore, to apply the proposed model to experimental WCLDs we must assume that the WCLD for the accumulated polymer is essentially the same as the instantaneous WCLD. This assumption is valid when:

- The polymerization reactor is operated at steady-state conditions and the WCLD is spatially independent.
- The ratio of transfer to propagation rates of all active sites does not change during the polymerization.
- The relative amounts of polymer made by each site type do not change during the polymerization.
- Mass and heat transfer effects are negligible, since these effects could give instantaneous WCLD which are spatially dependent.

Numerical solution

Two numerical methods were compared by fitting the model equation (4) to a theoretical and to an experimental WCLD: The Levenberg-Marquardt method (Bates and Watts, 1988) and the method proposed by Golub and Pereyra (1973).

The Levenberg-Marquardt method has become a standard method of nonlinear least-squares routines. We used Press's FORTRAN routine for this algorithm (Press et al., 1992). It defines a chi-square merit function and determines best-fit parameters by its minimization:

$$\chi^2 = \sum_{i=1}^{m} \left[\frac{W(r)_i - \hat{W}(r)_i}{\sigma(r)_i} \right]^2 \tag{5}$$

where m is the number of experimental points and $\sigma(r)$ is the standard deviation of the experimental points

If the Levenberg-Marquardt method is used to estimate $\tau(j)$ and $m(j)$ directly, it often converges to values that have no physical meaning, such as negative values for $\tau(j)$ and values greater than one for $m(j)$, especially when many site types are used. To overcome this problem, we defined new fitting variables according to the transformations:

$$\tau(j) = \frac{1}{1 + \exp[-T(j)]} \tag{6}$$

$$m(j) = \frac{1}{1 + \exp[-M(j)]} \tag{7}$$

The adjustable parameters are now $T(j)$ and $M(j)$, thus restraining the values of $\tau(j)$ and $m(j)$ to the interval [0,1].

In the model defined by equation (4), the parameters $m(j)$ are called conditionally linear parameters (Bates and Watts, 1988). The optimal values of these parameters, for fixed values of the nonlinear parameters $\tau(j)$, can be estimated by linear least squares. The model of equation (4) can be partitioned into expressions containing only linear or nonlinear parameters:

$$W(\tau, m) = A(\tau)m \tag{8}$$

where the matrix A_{mxn} depends only on the nonlinear parameters. For any given set of τ values, the estimated value of m is given by:

$$\hat{m}(\tau) = A^{+}(\tau)W \tag{9}$$

where A^{+} is the pseudoinverse of A, defined by:

$$A^{+} = (A^{T}A)^{-1}A^{T} \tag{10}$$

Golub and Pereyra (1973) proposed a method to minimize:

$$r_2(\tau) = \| W - A(\tau)\hat{m}(\tau) \|^2 \tag{11}$$

which depends only on the nonlinear parameters. The objective function is first optimized in relation to the nonlinear parameters $\tau(j)$ and then the linear parameters $m(j)$ are calculated. By using this method, we need to estimate only the first estimates of the n nonlinear parameters $\tau(j)$.

We used the Golub-Pereyra method as implemented in the FORTRAN subroutine VARPRO. This subroutine is easily obtained from NETLIB through INTERNET (Dongarra and Grosse, 1987).

Obtaining first estimates and increasing the number of site types

It is possible to estimate $\tau(1), \tau(2)$, and $m(1)$ from the knowledge of the number, mass and z average chain lengths ($\overline{n}_n, \overline{n}_w, \overline{n}_z$), which are easily available from the experimental WCLD. Although only two most probable WCLD may not be sufficient to adequately represent the global WCLD, at least they provide an educated guess to start the decomposition algorithm.

For a two site type model, the chain length averages are defined by the equations:

$$\overline{n}_n = \frac{1}{m(1)\tau(1) + m(2)\tau(2)} \tag{12}$$

$$\overline{n}_w = 2\left[\frac{m(1)}{\tau(1)} + \frac{m(2)}{\tau(2)}\right] \tag{13}$$

$$\overline{n}_z = 3\left[\frac{m(1)}{\tau^2(1)} + \frac{m(2)}{\tau^2(2)}\right]\left[\frac{m(1)}{\tau(1)} + \frac{m(2)}{\tau(2)}\right]^{-1} \tag{14}$$

Equations (12) to (14) are easily solved by any algorithm for finding the roots of systems of non-linear algebraic equations, such as Newton's method (Press et al., 1992).

The following "rules of thumb" proved to be useful in helping achieve the convergence and to decide when to stop increasing the number of site types. For the Golub-Pereyra method, it is not necessary to obtain first estimates for *m(j)*:

- Obtain first guesses for $\tau(1), \tau(2)$, and *m(1)* by solving equations (12) to (14).
- Start running the estimation program using those estimates.
- Gradually increase the number of site types by estimating $\tau(n+1)$ and *m(n+1)*:
  - $\tau(n+1) = \sum_{j=1}^{n} \tau(j)m(j)$
  - *m(n+1)* as the average between the *m(j)* corresponding to the $\tau(j)$ adjacent to $\tau(n+1)$ and normalizing the new values so that $\sum_{j=1}^{n+1} m(j) = 1$.
- χ^2 generally decreases significantly when site types that are needed to improve the fit are added.
- The number of site types should be considered adequate when the sum of the squares of the residuals does not improve significantly by adding another site type and when the residuals are not correlated.

Simulation results

We will first analyze the performance of the two numerical methods and the proposed methodology for estimating the site types using a WCLD produced by a model catalyst containing six site types. In this way we can verify if the methods work well for a case in which all of our assumptions about the catalyst are valid, since the global WCLD is the actual result of the superposition of six individual instantaneous most probable WCLDs. Next we will use the above methods to decompose an experimental WCLD of a polypropylene sample measured by high temperature SEC.

Table 1 presents the parameters $\tau(j)$ and $m(j)$ used to obtain the model WCLD of figure 1.

By solving equations (12) to (14) we obtain the following estimates for the parameters:

$$\tau(1) = 0.00108, \quad \tau(2) = 0.00017, \quad m(1) = 0.503$$

Those estimates are used as first guesses in both numerical methods. The following discussion is valid for both methods, since they converge to the same parameters, provided that their initial guesses are the same.

Figure 2 illustrates the fitted curve when only two and three site types are used. It is readily seen that two or three sites can not describe properly the whole distribution. Figure 3 compares a four site types predicted curve with the model curve. The agreement is very good and one might been tempted to stop the regression at this point. However, the residuals are still significantly correlated as presented in the bottom part of this figure. Correlated residuals are a good indication of model inadequacy (Bates and Watts, 1988). The same is observed for a five site type curve, as shown in figure 4. Finally, for the six site types model one gets a very good agreement between prediction and model curve (as expected for this case) and residuals that are almost randomly distributed, as seen in figure 5. The small discrepancies observed in the residuals were caused by round-off errors when generating and fitting the model distribution.

Site type (j)	$\tau(j)$	m(j)
1	0.00010	0.10
2	0.00015	0.15
3	0.00025	0.25
4	0.00050	0.25
5	0.00100	0.15
6	0.00250	0.10

Table 1 - Model chain length distribution parameters.

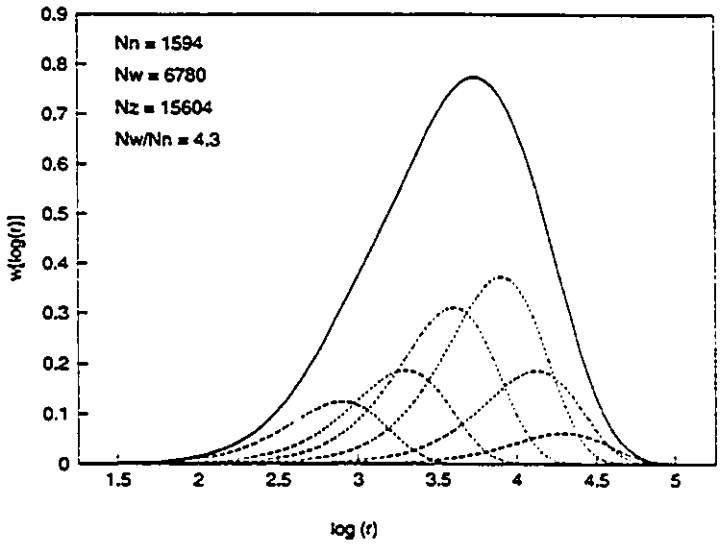

Figure 1 - Model chain length distribution generated for a six site type catalyst.

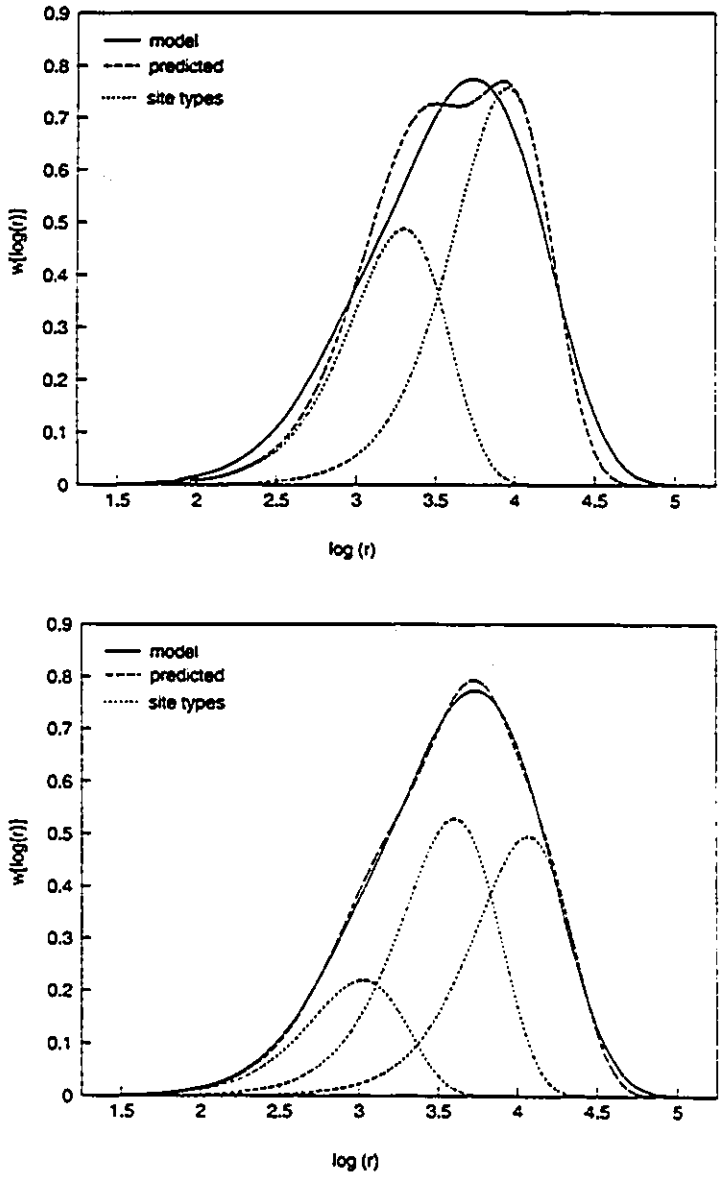

Figure 2 - Deconvolution of a model chain length distribution generated for a six site type catalyst into two and three most probable chain length distributions.

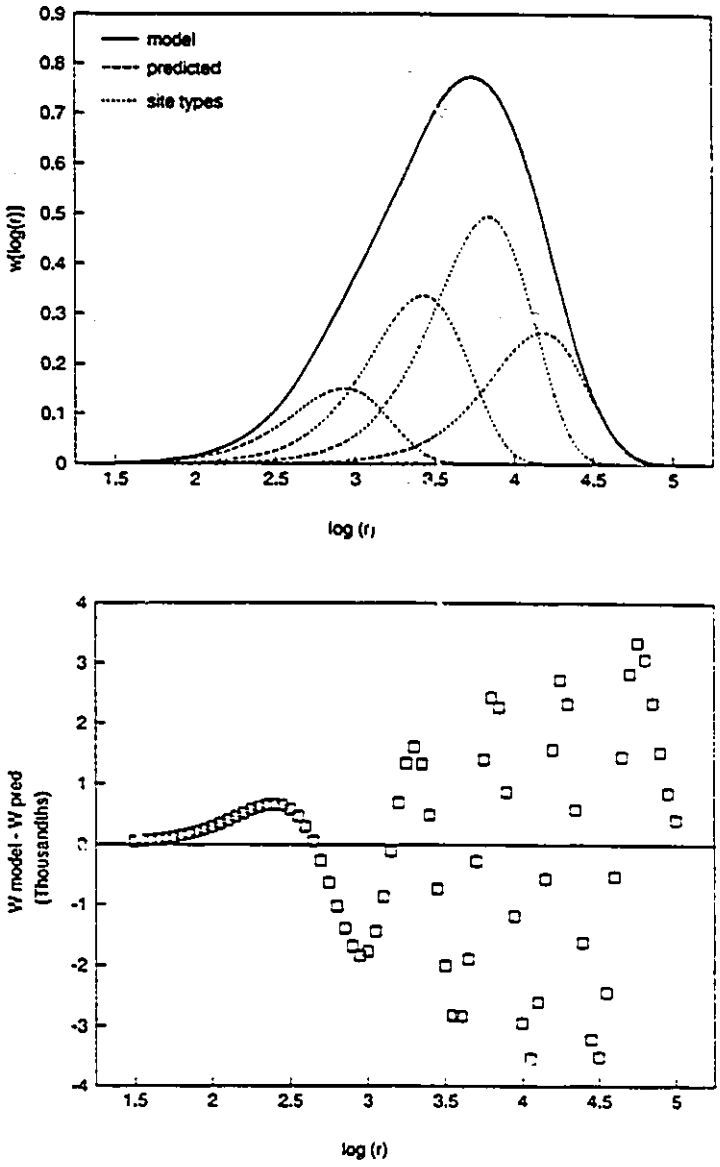

Figure 3 - Deconvolution of a model chain length distribution generated for a six site type catalyst into four most probable chain length distributions and residuals of the predicted four site type chain length distribution and the model six site type chain length distribution.

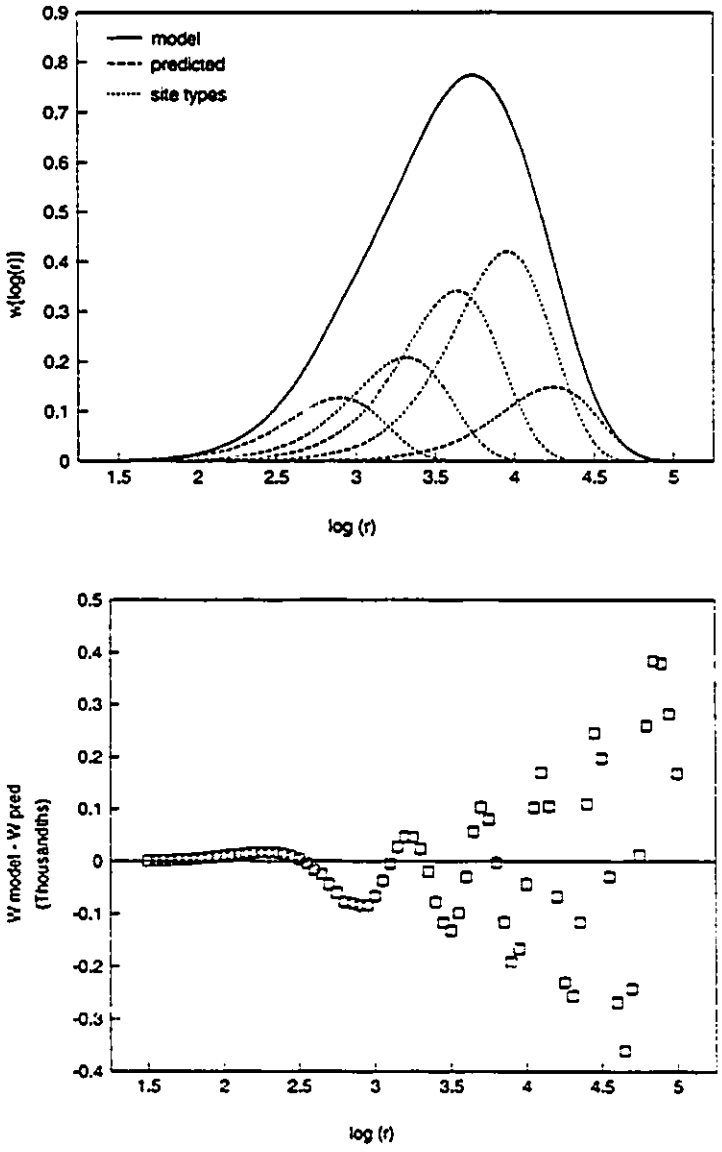

Figure 4 - Deconvolution of a model chain length distribution generated for a six site type catalyst into five most probable chain length distributions and residuals of the predicted five site type chain length distribution and the model six site type chain length distribution.

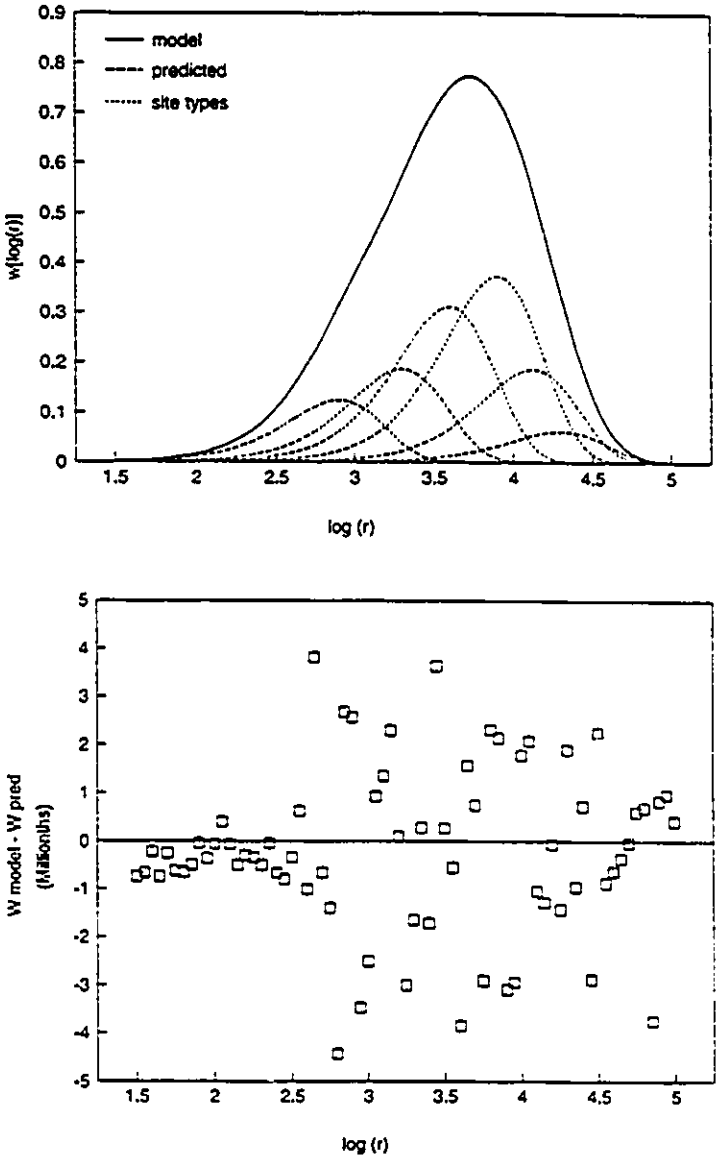

Figure 5 - Deconvolution of a model chain length distribution generated for a six site type catalyst into six most probable chain length distributions and residuals of the predicted six site type chain length distribution and the model six site type chain length distribution.

It is also illustrative to observe how the sum of the squares of the residuals changes with the use of additional site types. Table 2 shows how this value decreases significantly when site types that are needed to improve the fitting are added to the model. Observe how the sum of the squares of the residuals is significantly smaller for the six site types model than for the five site types model but almost does not decrease for the seven site types model.

Number of site types	$\Sigma(residuals)^2$
2	1.40×10^{-1}
3	6.76×10^{-3}
4	1.80×10^{-4}
5	1.22×10^{-6}
6	2.14×10^{-10}
7	2.09×10^{-10}

Table 2 - Sum of the squares of residuals as a function of number of site types for prediction of the model chain length distribution.

Table 3 compares the number of iterations and computational time required by both methods. Although they both converge for the same values, the Golub-Pereyra method requires fewer iterations and is much faster then the Levenberg-Marquardt method, especially when the number of site types considered approaches that used in generating the model WCLD. For six site types, the Levenberg-Marquardt method converges very slowly while the convergence rate of the Golub-Pereyra method is not significantly reduced.

	Marquardt		Golub	
Number of site types	Time (s)	Iter.	Time(s)	Iter.
2	2	6	5	23
3	16	27	6	16
4	15	14	9	20
5	19	12	10	17
6	870	465	22	30
total	922	524	52	106

Table 3 - Computational times and number of iterations required for convergence as a function of number of site types for the model chain length distribution.

The two methods were also used to fit an experimental WCLD distribution of an isotactic polypropylene sample made by a heterogeneous Ziegler-Natta catalyst (LYNX 900) under steady-state polymerization conditions and no significant deactivation at 70 °C and P_{H_2}= 10 psi. The experimental SEC curve and chain length averages are shown in figure 6.

The same systematic approach was used for decomposing the polypropylene WCLD. First guesses were obtained by solving equations (12) to (14) using average chain lengths and the number of site types was increased one at a time. Again, both methods converge to the same values, but the Golub-Pereyra method is significantly faster.

Figure 7 shows the experimental and the predicted WCLD for a four site type model. From visual inspection the fit seems adequate, but the residuals are still strongly correlated. The fit can be improved by using a five site types model, as shown in figure 8. The residuals do not seem to be very correlated, except for the low molecular weight tail. Adding one more site type does not significantly improve the fit or the residual correlations, as can be seen in figure 9.

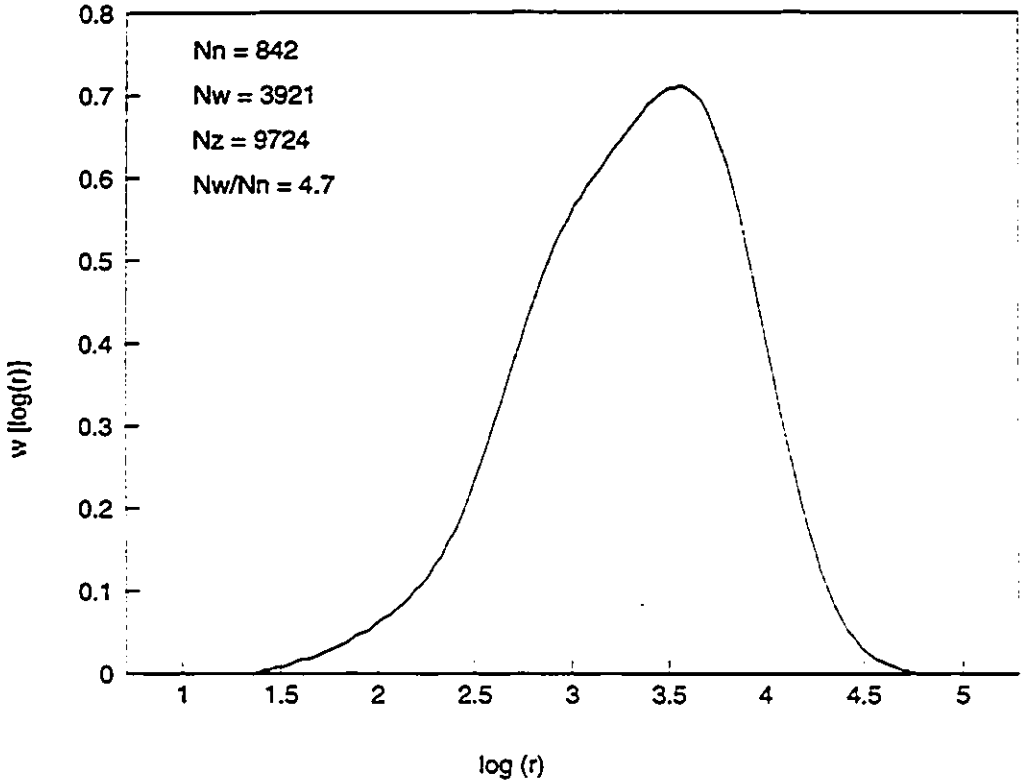

Figure 6 - Experimental polypropylene chain length distribution.

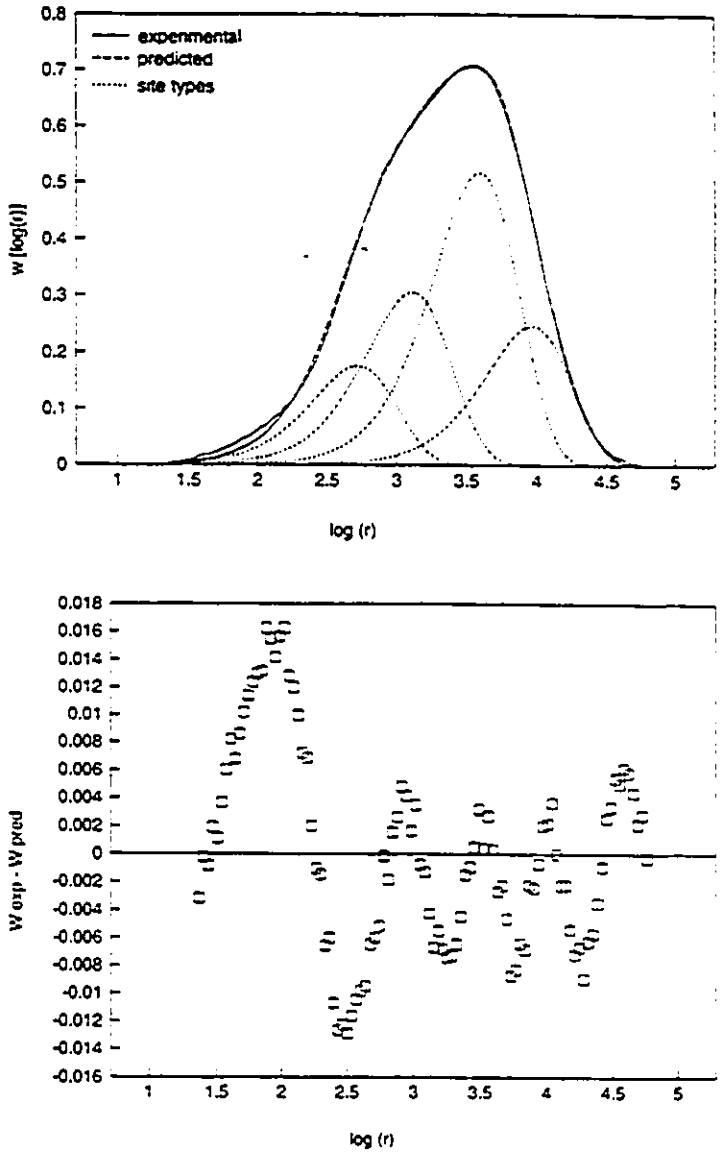

Figure 7 - Deconvolution of an experimental polypropylene chain length distribution into four most probable chain length distributions and residuals of the predicted four site type chain length distribution and the experimental polypropylene chain length distribution.

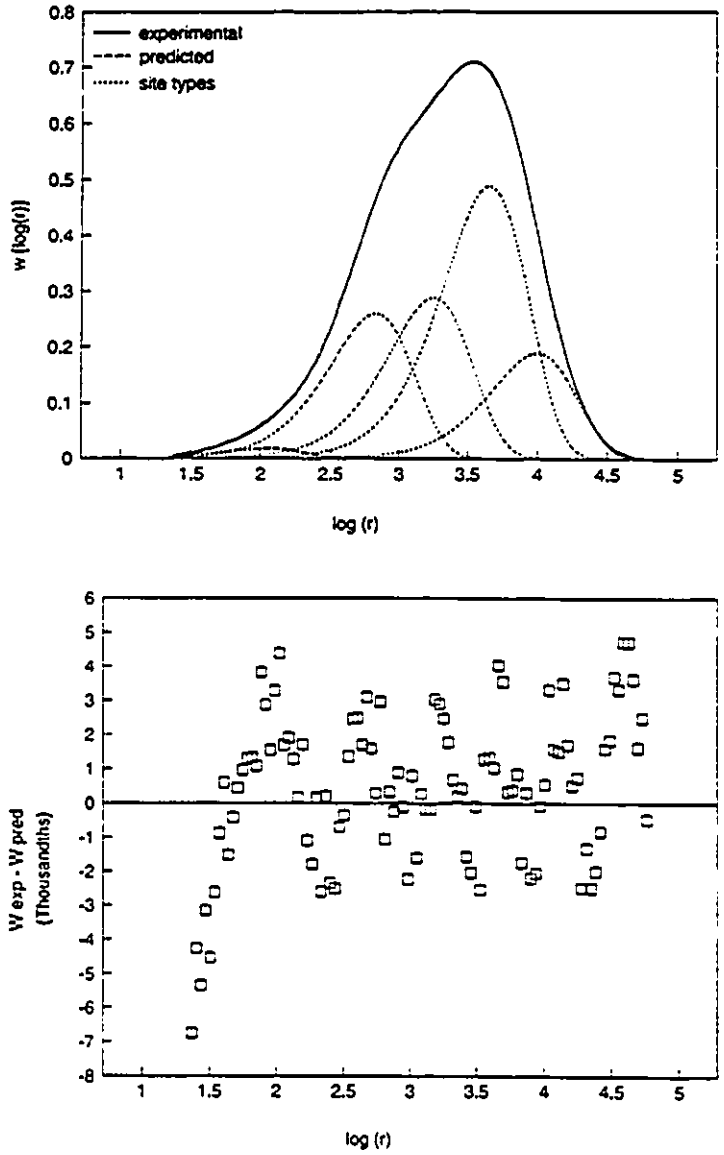

Figure 8 - Deconvolution of an experimental polypropylene chain length distribution into five most probable chain length distributions and residuals of the predicted five site type chain length distribution and the experimental polypropylene chain length distribution.

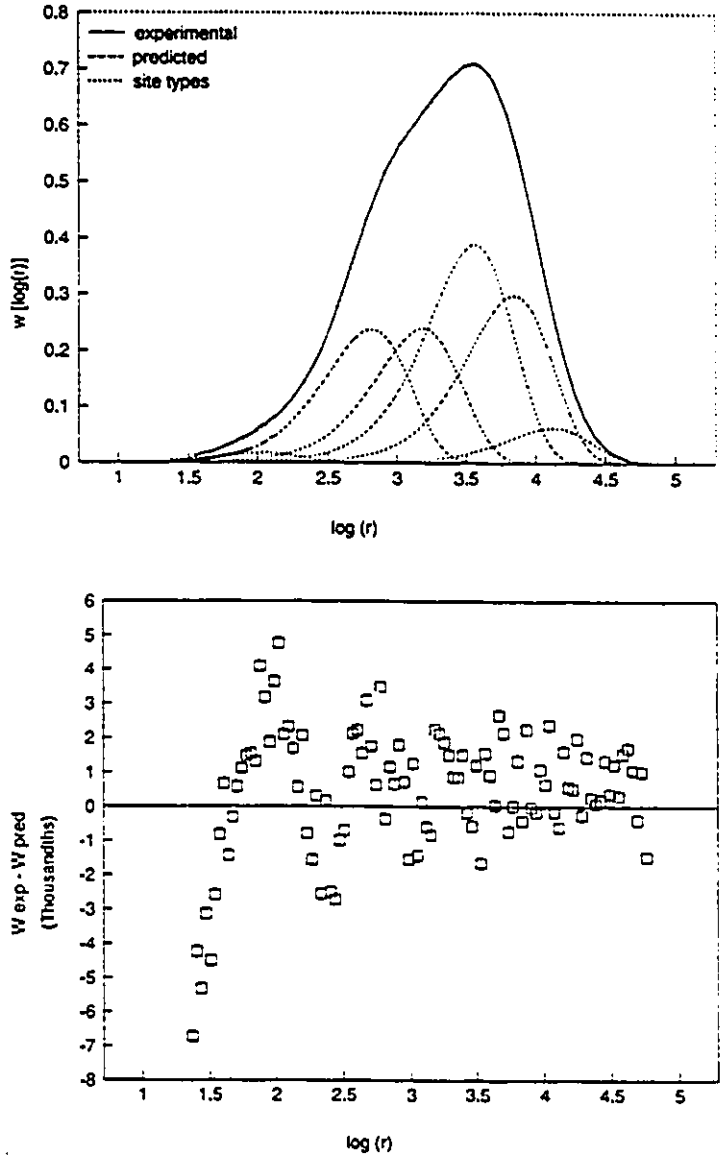

Figure 9 - Deconvolution of an experimental polypropylene chain length distribution into six most probable chain length distributions and residuals of the predicted six site type chain length distribution and the experimental polypropylene chain length distribution.

Table 4 shows the sum of the squares of the residuals for models containing two to seven site types. As mentioned before, the five and six site types model are almost equivalent and no improvement is noticed by using a seven site type model. Therefore, it is reasonable to assume that the analyzed polypropylene sample was produced by a catalyst containing five or, less likely, six different site types. The correlated residuals observed for the low molecular weight tail are probably related to higher chromatogram noise levels and increased variance of the observations or to peak broadening. For this polypropylene sample, TREF/^{13}C NMR measurements have shown chains at significant concentration levels having quite different stereoregularity. The SEC relationship of molecular weight versus retention time may differ for chains with different microstructure and of course this may make SEC analysis of whole polypropylene samples suspect.

Number of site types	$\Sigma(residuals)^2$
2	1.98×10^{-1}
3	1.62×10^{-2}
4	5.08×10^{-3}
5	5.12×10^{-4}
6	3.75×10^{-4}
7	3.76×10^{-4}

Table 4 - Sum of the squares of residuals as a function of number of site types for prediction of the GPC chain length distribution of polypropylene.

The close similarity of results obtained for the model WCLD and the experimental WCLD, plus the good fitting of the five or six site types model, indicates that our initial assumptions about the nature of active sites of the catalyst are reasonable. The converged parameters for the polypropylene sample are shown in table 5.

	5 site types model		6 site types model	
Site types	τ	m	τ	m
1	0.000199	0.152	0.000151	0.051
2	0.000439	0.393	0.000287	0.240
3	0.00111	0.232	0.000549	0.311
4	0.00295	0.208	0.00130	0.193
5	0.0182	0.015	0.00306	0.191
6			0.00186	0.014

Table 5 - Converged parameters of the five and six site types model for the GPC chain length distribution of polypropylene.

Computational times and number of iterations required by each method are compared in table 6 for the polypropylene sample. As for the case of the model catalyst, the Golub-Pereyra method is also faster and requires less iterations for decomposing the experimental WCLD.

	Marquardt		Golub	
Number of site types	Time (s)	Iter.	Time (s)	Iter.
2	2	7	4	21
3	6	11	5	15
4	9	10	19	38
5	24	19	15	23
6	197	120	20	22
total	238	167	63	119

Table 6 - Computational times and number of iterations required for convergence as a function of number of site types for the GPC chain length distribution of polypropylene.

Mathematical Modelling of TREF Using Stockmayer's Bivariate Distribution

For the first time, the Stockmayer bivariate distribution is used to model ideal TREF behaviour for the linear copolymers of olefins. It can also be used to simulate molecular weight distributions of the different fractions and therefore help to interpret the SEC analysis of these fractions.

We use the term ideal TREF behaviour to indicate that the fractionation is controlled only by copolymer composition or stereoregularity, free of cocrystallization effects, molecular weight influences and peak broadening due to axial dispersion and crystallization kinetics. These ideal conditions can be met when TREF is done properly.

In our analysis, we assume that each catalytic site type produces instantaneous copolymer chains that have an individual Stockmayer bivariate distribution.

Having determined the bivariate distribution for each site type it is possible to derive expressions for the whole polymer and TREF fractions as will be described below.

To date, no publication has shown the use of Stockmayer's bivariate distribution as a mathematical model to describe TREF fractionation. A model for predicting the molecular weight distribution of fractions of polyethylene and polypropylene using the solvent gradient method was proposed by Ogawa and Inaba (1978). Good agreement was obtained between experimental and simulated results. However, contrarily to TREF fractionation, the mechanism of fractionation by the solvent gradient method is regulated by the molecular weight of the polymer chains (Soares and Hamielec, 1994d).

Cheng et al. (1992) simulated the chemical composition distribution of linear binary copolymers using Monte Carlo methods. Four causes of compositional heterogeneity were examined: 1) statistical or instantaneous broadening; 2) conversion heterogeneity (also known as compositional drift); 3) multistage heterogeneity; and 4) polymerization process heterogeneity. A simulated chemical composition distribution curve was proposed for an ethylene/butene-1 copolymer

using three components and an arbitrary Gaussian broadening of σ = 0.06. The resulting distribution approximates TREF curves of LLDPE. A similar approach was proposed for describing the tacticity distribution of polypropylene (Cheng and Kasehagen, 1993) using a four component Monte Carlo model. The tacticity distribution curve was shown to be similar to an experimental TREF curve.

However, even though several experimental fractionations of polyolefins have been reported in the literature using TREF, to our knowledge no mathematical model has been proposed to quantitatively interpret TREF spectra and the molecular weight distribution of TREF fractions.

Equations for each site type

The instantaneous chain length and composition distribution proposed by Stockmayer and corrected for differing monomer molecular weights is given by:

$$w(r,y,j)drdy = [1 + y(j)\delta(j)]\tau^2(j) r \exp(-\tau(j)r)dr \times \frac{1}{\sqrt{2\pi\beta(j)/r}} \exp(-y^2(j)r/2\beta(j))dy \tag{15}$$

where,

$$\beta(j) = \overline{F}_1(j)(1-\overline{F}_1(j))K \tag{16}$$

$$K = \{1 + 4\overline{F}_1(j)(1-\overline{F}_1(j))(r_1(j)r_2(j)-1)\}^{0.5} \tag{17}$$

$$\delta(j) = \frac{(1-M_2/M_1)}{M_2/M_1 + \overline{F}_1(j)(1-M_2/M_1)} \tag{18}$$

$$\tau(j) = \frac{k_{tm}(j)}{k_p(j)} + \frac{k_\beta(j)}{k_p(j)[M]} + \frac{k_{tH_2}(j)[H_2]}{k_p(j)[M]} \tag{19}$$

and,

r	chain length
y	deviation from average copolymer composition
$\overline{F}_1(j)$	average mole fraction of monomer type 1 of copolymer made on site type j
r_1, r_2	reactivity ratios
j	active site type
$k_p(j)$	propagation rate constant of site type j
$k_{tm}(j)$	transfer to monomer rate constant of site type j
$k_\beta(j)$	β-hydride elimination rate constant of site type j
$k_{tH_2}(j)$	transfer to hydrogen rate constant of site type j
$[M]$	monomer concentration
$[H_2]$	hydrogen concentration
M_1, M_2	molecular weights of monomers type 1 and 2

To obtain the instantaneous weight chain length distribution, we integrate equation (15) with respect to y, from $-\infty$ to ∞:

$$w(r,j) = \tau^2(j) r e^{-\tau(j)r} \tag{20}$$

which is a form of Flory's most probable distribution.

The instantaneous number average and mass average chain lengths are calculated as follows:

$$\overline{n_N}(j) = \left\{ \int_0^{\infty} \frac{w(r,j)}{r} dr \right\}^{-1} = \frac{1}{\tau(j)} \tag{21}$$

$$\overline{n_W}(j) = \int_0^{\infty} r w(r,j) dr = \frac{2}{\tau(j)} \tag{22}$$

Notice that each site *instantaneously* produces dead polymer with polydispersity equal to 2.

Analogously, for composition distribution over all chain lengths:

$$w(y,j) = \int_0^{\infty} w(r,y,j) dr \tag{23}$$

$$= \frac{3[1+\delta(j)y(j)]}{4\sqrt{2\beta(j)\tau(j)}(1+y^2(j)/2\beta(j)\tau(j))^{5/2}}$$

Equations for the total polymer produced on all of the active site types, instantaneously

The previous equations apply for the individual active site types. The properties of the total polymer produced instantaneously can be obtained by averaging the expressions for the individual site types over all site types. Then, if *m(j)* is the mass fraction of polymer produced on sites of type j, chain length and composition distributions of the accumulated polymer made by *n* different site types can be expressed as:

$$w(r) = \sum_{j=1}^{n} m(j) w(r,j) \tag{24}$$

$$w(y) = \sum_{j=1}^{n} m(j) w(y,j) \tag{25}$$

Molecular weight and composition averages of the accumulated polymer can be calculated from these new distributions:

$$\overline{n_N} = \left\{ \int_0^{\infty} \frac{w(r)}{r} dr \right\}^{-1} = \left\{ \sum_{j=1}^{n} \frac{m(j)}{\overline{n_N}(j)} \right\}^{-1} \tag{26}$$

$$\overline{n_W} = \int_0^{\infty} r w(r) dr = \sum_{j=1}^{n} m(j) \overline{n_W}(j) \tag{27}$$

$$\overline{F}_1 = \int_{-\infty}^{+\infty} w(y) (F_1 - \overline{F}_1) dF_1 \tag{28}$$

Equations for TREF fractions

The chain length distribution of TREF fraction k can be obtained for each site type by integrating equation (15) over the composition range of the considered fraction:

$$w_k(r,j) = \frac{\int_{y(j)}^{y(j)+\Delta y_k} w(r,y,j) dy}{\int_{y(j)}^{y(j)+\Delta y_k} \int_0^{\infty} w(r,y,j) dr dy} \tag{29}$$

The denominator of equation (29) is the weight fraction of polymer produced on site type j within the considered composition range in relation to the total amount of polymer made on site type j. Equation (29) has the following analytical solution:

$$\psi_k(j) = \frac{y(j)\{2\beta(j)\tau(j) + 2[y^2(j) + 2\beta(j)\tau(j)]\}}{4[y^2(j) + 2\beta(j)\tau(j)]^{1.5}} \Bigg|_{y(j)}^{y(j)+\Delta y_k} \tag{30}$$

$$-\delta(j)\frac{[2\beta(j)\tau(j)]^2}{4\{y^2(j) + [2\beta(j)\tau(j)]^2\}^{1.5}} \Bigg|_{y(j)}^{y(j)+\Delta y_k}$$

The chain length distribution of TREF fraction k for the total polymer can be expressed as:

$$w_k(r) = \frac{\sum_{j=1}^{n} m(j) w_k(r,j) \psi_k(j)}{\sum_{j=1}^{n} m(j)\psi_k(j)} = \sum_{j=1}^{n} \eta(j) w_k(r,j) \tag{31}$$

where $\eta(j)$ is the mass fraction of polymer made in site type j within the considered composition range in relation to the total polymer made by the catalyst.

With equation (31) one can easily obtain the molecular weight averages of the TREF fractions:

$$\overline{n_{N_k}} = \left\{ \int_0^\infty \frac{w_k(r)}{r} dr \right\}^{-1} = \left\{ \frac{\sum_{j=1}^{n} m(j) I_0(j)}{\sum_{j=1}^{n} m(j)\psi_k(j)} \right\}^{-1} \tag{32}$$

$$\overline{n_{W_k}} = \int_0^\infty r w_k(r) dr = \frac{\sum_{j=1}^{n} m(j) I_1(j)}{\sum_{j=1}^{n} m(j)\psi_k(j)} \tag{33}$$

where,

$$I_0(j)=\frac{y(j)\tau(j)}{2\sqrt{y^2(j)+2\beta(j)\tau(j)}}\Bigg|_{y(j)}^{y(j)+\Delta y_k} \tag{34}$$

$$-\delta(j)\frac{\tau^2(j)\beta(j)}{\sqrt{2\beta(j)\tau(j)+y^2(j)}}\Bigg|_{y(j)}^{y(j)+\Delta y_k}$$

$$I_1(j)=\frac{2y^5(j)+10\beta(j)\tau(j)y^3(j)+15\beta^2(j)\tau^2(j)y(j)}{2\tau(j)\left[y^2(j)+2\beta(j)\tau(j)\right]^{5/2}}\Bigg|_{y(j)}^{y(j)+\Delta y_k} \tag{35}$$

$$-\delta(j)\frac{3\tau^2(j)\beta^3(j)}{\left[2\beta(j)\tau(j)+y^2(j)\right]^{5/2}}\Bigg|_{y(j)}^{y(j)+\Delta y_k}$$

Simulation results and discussion

The model equations were coded in FORTRAN77 using Microsoft FORTRAN compiler version 2.1. The program was installed in an IBM compatible microcomputer with an 8386 processor and an 80386 math coprocessor with a clock of 33 MHz. The integrals that do not have analytical solutions were solved by Simpson's rule or Romberg method (Gerald and Wheatley, 1989).

The Stockmayer's distribution was used to determine chain length and composition distribution of a polymer made by a model catalyst containing six different types of active sites. The distribution parameters are shown in table 7. The results were compared to the ones obtained from the original Stockmayer distribution to assess the importance of the correction term for differing monomer molecular weights. For the case studied we considered $M_1=28$ and $M_2=42$, which corresponds to the molecular weights of ethylene and propylene.

Random copolymerization is assumed to occur at all site types and the affinity for monomer type 1 and propagation to transfer rate ratios increase continually from site type 1 to site type 6.

j	$m(j)$	$\tau(j)$	r_1	$r_1.r_2$	$\overline{F}_1$
1	0.20	0.00250	8	1	0.889
2	0.15	0.00100	10	1	0.909
3	0.10	0.00050	15	1	0.938
4	0.10	0.00025	20	1	0.952
5	0.20	0.00015	22	1	0.958
6	0.25	0.00010	25	1	0.962
average	1.00				0.934

Table 7 - Simulation parameters.

Table 8 shows the number and mass average chain lengths for all site types and for the whole polymer. Each site type makes polymer with polydispersity equal to 2 but the total polymer has polydispersity of 7.3. This is not an unusual value for polyolefins produced by heterogeneous Ziegler-Natta catalysts. The active site types make polymer from the very low number average chain length of 400 to a high average of 10,000.

SITE	$n_N(j)$	$n_W(j)$	$n_W(j)/n_N(j)$
1	400	800	2.0
2	1000	2000	2.0
3	2000	4000	2.0
4	4000	8000	2.0
5	6667	13333	2.0
6	10000	20000	2.0
whole	1282	9327	7.3

Table 8 - Averages per site type and whole polymer.

Figure 10 shows the simulated TREF curve of this copolymer. The vertical dotted lines indicate the composition ranges of the TREF fractions. As can be seen, the mole fraction of monomer 1 in the copolymer varies from 0.84 to 0.98, according to the different reactivity ratios of the active site types. In the bottom part of this figure this average curve is decomposed into its normalized individual components. Notice that the higher the average chain length the narrower the composition distribution. This means that copolymer chains made by site types that have large transfer to propagation ratios will have broader composition distribution than the ones made by sites that have lower transfer to propagation ratios and therefore are expected to interfere more strongly with other site types. Observe how the composition distribution of chains made by site type 1 considerably overlaps the composition distribution of polymer chains made by site type 2, even though the average composition of polymer chains made by those two site types is significantly different.

For our particular case, the separation of polymer made by different site types would not be significantly improved by increasing the number of fractions, especially for site type 1 and 2 and site types 4, 5 and 6. A better strategy would be to change the fraction boundaries so that some of them would contain polymer from only one or two site types. Unfortunately, in practice one does not know a priori the individual distributions and this decision has to be made by trial-and-error until an optimal fractionation scheme is devised. An optimal fractionation scheme would provide TREF fractions with narrower composition distributions and thus ones that are more suitable for SEC analysis.

Figure 11 shows the simulated chain length distribution of the whole polymer and its averages, as well as the normalized chain length distributions of each site type.

Table 9 shows the TREF fractionation summary. Seven fractions were separated in the composition range F_0 - F_1. For the first two fractions the polydispersity is less than 2 and for the last five fractions it is higher than 2.

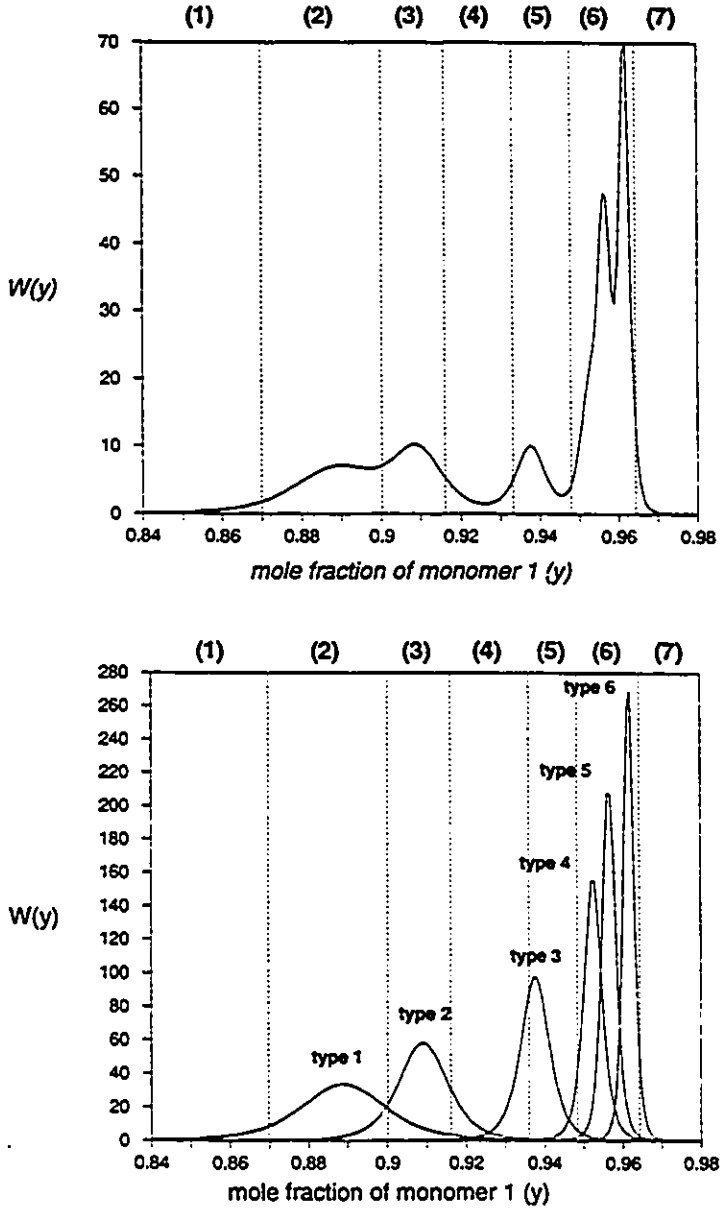

Figure 10 - TREF curve of whole polymer and of active site types.

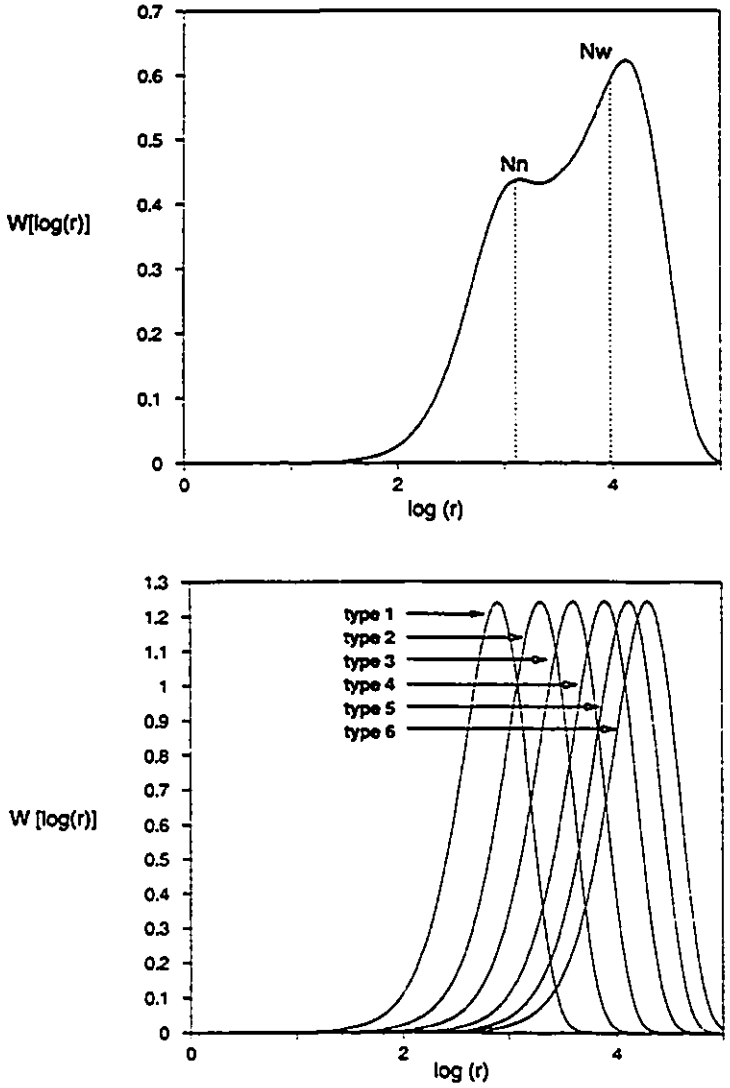

Figure 11 - Chain length distribution of whole polymer and of active site types.

Fraction	F_0	F_1	n_N	n_W	n_W/n_N
1	0.840	0.870	236	403	1.7
2	0.870	0.900	552	913	1.6
3	0.900	0.916	836	1963	2.3
4	0.916	0.932	576	1594	2.8
5	0.932	0.948	1695	4140	2.4
6	0.948	0.964	6634	15739	2.4
7	0.964	0.980	1925	8751	4.5

Table 9 - TREF fraction averages.

Polydispersities that are less than 2 are due to the fractionation of only part of the complete molecular weight distribution of one site type. In fraction 1, only part of the distribution of site type 1 is separated thus decreasing the polydispersity. This behaviour gets more important when there are site types that produce low molecular weight chains, since in this case broad composition distributions are expected for statistical reasons. Notice in figure 10 how the polymer made by site type 1 will be present in fractions 1 to 4.

Polydispersities higher than 2 are caused by the overlapping of distributions from different site types. Fraction 6 is a good example of this behaviour. In its composition range, 0.948 to 0.964, the distributions from site types 4, 5 and 6 overlap significantly and broaden the chain length distribution.

Figure 12 shows the amount of polymer coming from different site types in each TREF fraction. Again it is possible to observe how the polymer from different site types, even under ideal fractionation conditions, will not be totally isolated by TREF.

Finally, figure 13 depicts the chain length distribution of each TREF fraction. The superimposing of different composition distributions broadens the chain length distributions of the fractions.

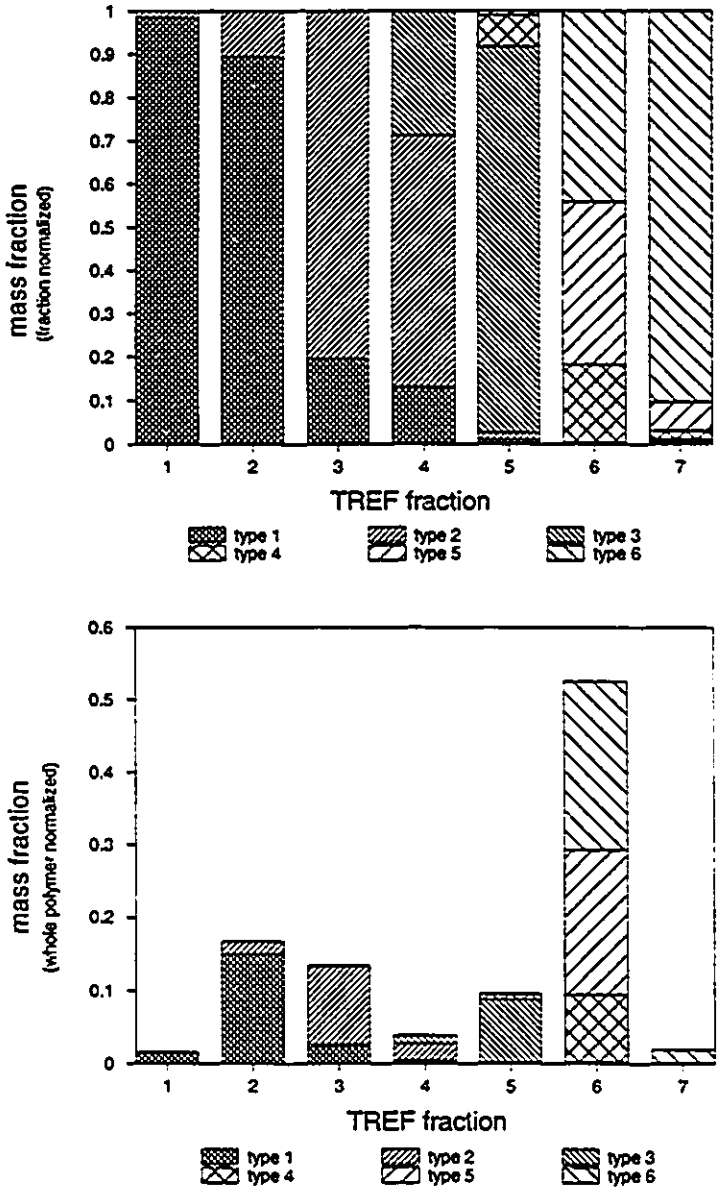

Figure 12 - Composition of TREF fractions.

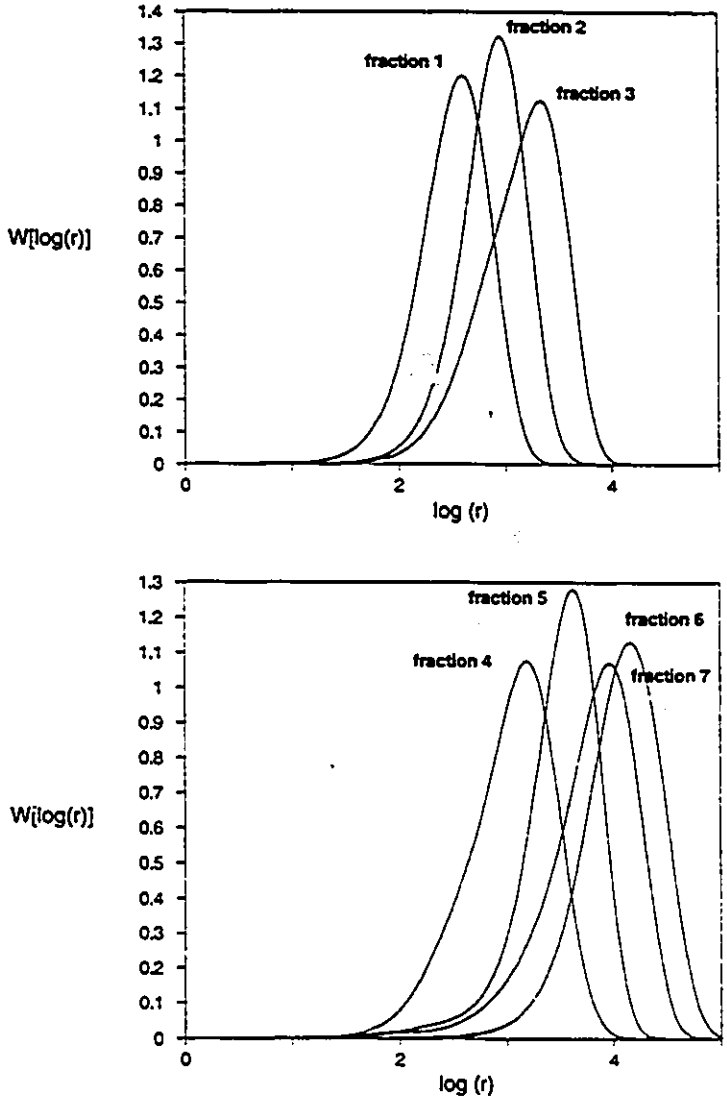

Figure 13 - Chain length distribution of TREF fractions 1 to 7.

The correction for differing monomer molecular weights will be less significant for polymer made on sites with small transfer to propagation ratio. In this case the deviations from the average composition are very small, which decreases the correction term of the distribution.

The differences between the corrected and uncorrected composition distributions (wt%) are shown in figure 14. The correction term is a linear function of $y(j)$ and is equal to zero when the composition is the same as the average copolymer composition. Notice that, as we move away from the average copolymer composition, the amount of polymer decreases. Therefore, the larger corrections apply only to a small fraction of the total polymer.

The effect of the correction for differing monomer molecular weights on the chain length averages of the polymer obtained in each TREF fraction is presented in table 10. The fractions that contain shorter chains and composition ranges far from the mean compositions of the sites that produced the polymer show the bigger deviation from the Stockmayer distribution uncorrected for differing molecular weights.

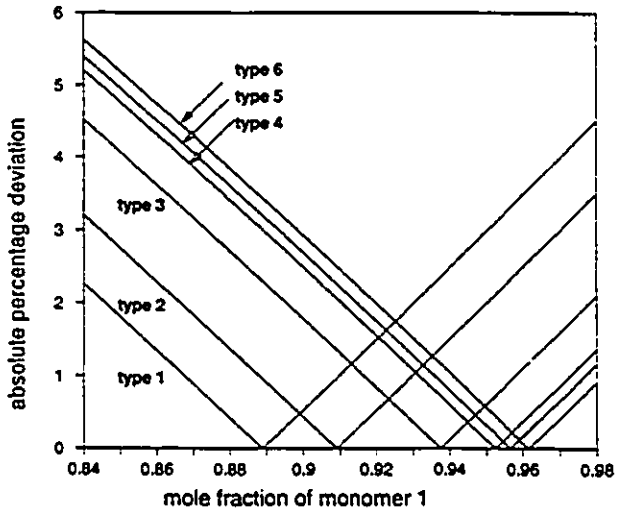

Figure 14 - Absolute percentage deviations (wt%) between corrected and uncorrected composition distributions for differing monomer molecular weights.

Fraction	F_0	F_1	Absolute % deviation	
			n_N	n_W
1	0.840	0.870	3.62	3.99
2	0.870	0.900	2.19	2.29
3	0.900	0.916	1.88	2.20
4	0.916	0.932	2.73	3.35
5	0.932	0.948	0.40	0.21
6	0.948	0.964	0.31	0.00
7	0.964	0.980	1.03	0.50

Table 10 - Deviation between chain length averages of TREF fractions calculated by uncorrected and corrected Stockmayer's distributions.

As mentioned in the literature review, the analytical TREF profile of LLDPE made with conventional heterogeneous Ziegler-Natta catalysts is generally bimodal, showing a sharp higher elution temperature peak and a broader lower elution temperature peak. This type of curve is simulated using a five site type model catalyst and is shown in figure 15 for the simulation parameters in table 11, neglecting the correction for differing molecular weights. The curve resembles closely the experimental TREF profiles published in the literature. Average molecular weights are presented in table 12 for each site type and in table 13 for the TREF fractions. It can be again observed that the polydispersity of TREF fractions can vary significantly as a function of overlapping or incomplete recovery of individual distributions.

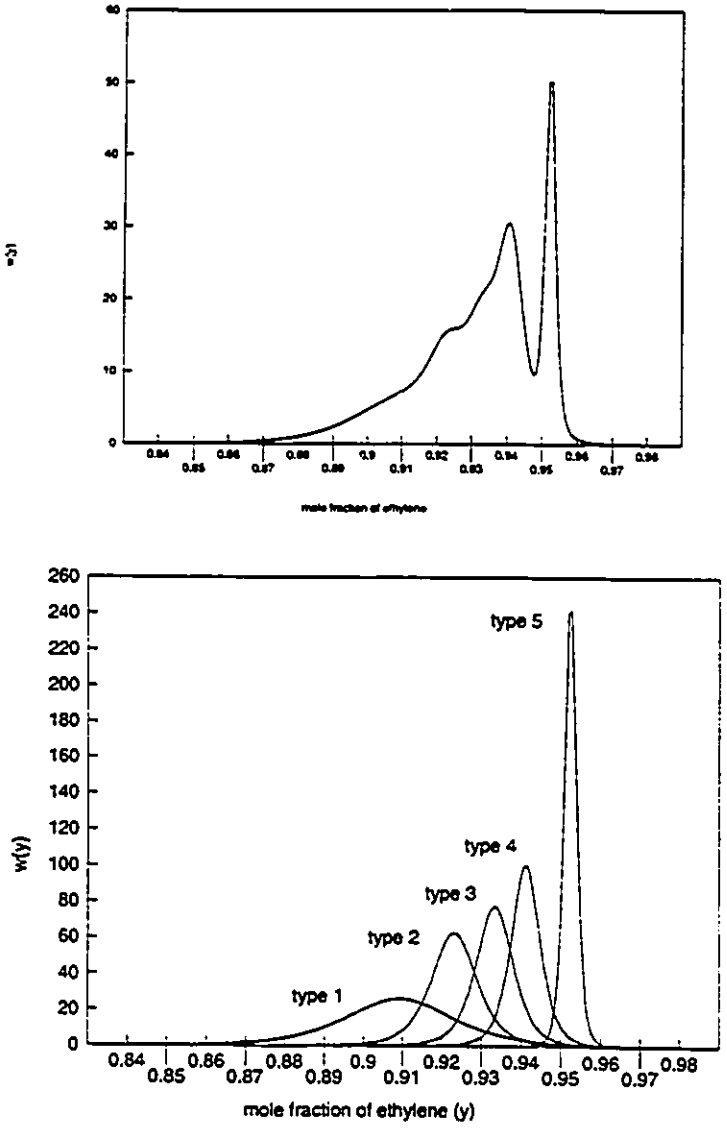

Figure 15 - Theoretical TREF curve of a LLDPE made with a five site type catalyst.

j	$m(j)$	$\tau(j)$	r_1	$r_1 \cdot r_2$	$\overline{F}_1$
1	0.22	0.00500	10	1	0.909
2	0.16	0.00100	12	1	0.923
3	0.17	0.00075	14	1	0.933
4	0.25	0.00050	16	1	0.941
5	0.20	0.00010	20	1	0.952
average	1.00				0.932

Table 11 - Simulation parameters (LLDPE).

SITE	$n_N(j)$	$n_W(j)$	$n_W(j)/n_N(j)$
1	200	400	2.0
2	1000	2000	2.0
3	1333	2666	2.0
4	2000	4000	2.0
5	10000	20000	2.0
whole	653	5861	9.0

Table 12 - Averages per site type and whole polymer (LLDPE).

F_0	F_1	n_N	n_W	n_W/n_N	*mass fraction*
0.84	0.88	97	178	1.8	0.012
0.88	0.90	218	374	1.7	0.051
0.90	0.92	373	894	2.4	0.158
0.92	0.94	905	2615	2.9	0.391
0.94	0.96	1943	12183	6.3	0.384
0.96	0.98	100	597	6.0	0.004

Table 13 - TREF fraction averages (LLDPE).

A similar approach can be used for modelling TREF curves of stereoregular homopolymers. In this case, the governing mechanism of the fractionation is chain stereoregularity. If we consider atactic placements as a comonomer unit, we can use the Stockmayer bivariate distribution to describe the distribution of monomer inversions in the polymer chain. Figure 16 shows the simulated TREF curve of an isotactic polypropylene made by the five site type model catalyst described in tables 14 and 15, and the TREF profiles of polymer chains made by each site type.

j	$m(j)$	$\tau(j)$	r_1	$r_1.r_2$	$\overline{F}_1$
1	0.10	0.00100	14	1	0.933
2	0.15	0.00075	16	1	0.941
3	0.15	0.00050	18	1	0.947
4	0.30	0.00020	20	1	0.952
5	0.30	0.00010	22	1	0.956
average	1.00				0.949

Table 14 - Simulation parameters (isotactic polypropylene).

SITE	$n_N(j)$	$n_W(j)$	$n_W(j)/n_N(j)$
1	1000	2000	2.0
2	1333	2666	2.0
3	2000	4000	2.0
4	5000	10000	2.0
5	10000	20000	2.0
whole	653	10200	3.9

Table 15 - Averages per site type and whole polymer (isotactic polypropylene).

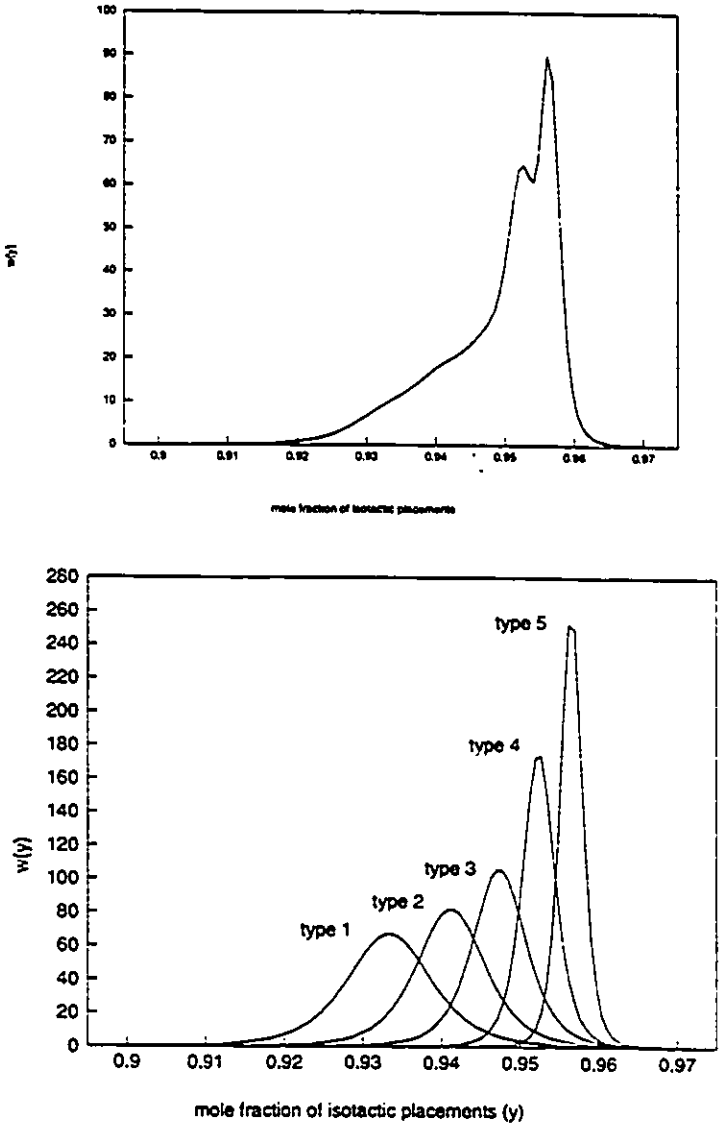

Figure 16 - Theoretical TREF curve of isotactic polypropylene made with a five site type catalyst.

Conclusion

The instantaneous chain length distribution of polymers made by multiple site type catalysts and synthesized under appropriate polymerization conditions can be described reasonably well as a weighted sum of most probable chain length distributions. If polymerization conditions are such that the cumulative WCLD is close to the instantaneous WCLD, then this model can be extended to describe polymer samples obtained under realistic experimental conditions.

The deconvolution of the global WCLD can be performed by several non-linear optimization techniques. The algorithm proposed by Golub and Pereyra takes advantage of the conditional linear parameters of the model and is generally faster then the Levenberg-Marquardt method, although both algorithms converge to the same values when the same initial conditions are used. One additional advantage of the Golub-Pereyra method is that it is not necessary to provide a first estimate of the linear parameters of the model.

The proposed methodology of obtaining first estimates for a two site type model and of systematically increasing the number of site types of the model is capable of obtaining an optimum solution for the deconvolution problem, as attested by the correct deconvolution of a model six site type WCLD. It can also be successfully employed for deconvoluting experimental WCLDs.

Finally, the good agreement between the multiple site type model and the experimental WCLD of a polypropylene sample supports the hypothesis that heterogeneous Ziegler-Natta catalysts possess multiple active site types, each one instantaneously producing polymer chains with a most probable chain length distribution.

TREF is a powerful technique for fractionating and characterizing semicrystalline polymers. When TREF is properly executed, it is regulated by the crystallinity of a homopolymer and is effectively independent of molecular weight and cocrystallization influences.

Preparative TREF is a time consuming procedure but when combined with complementary analytical techniques, such as ^{13}C NMR, can provide very detailed information about polymer microstructure.

The information obtained by analytical TREF is more limited than that available with preparative TREF and its use depends on the determination of a reliable calibration curve. However its much faster operation makes it more attractive for industrial applications such as quality control than preparative TREF.

The Stockmayer bivariate distribution is a useful technique for the interpretation of individual TREF curves or for the cross-fractionation of polymer samples by TREF-SEC techniques.

The Stockmayer bivariate distribution can be successfully used to interpret the TREF fractionation of binary copolymers with broad molecular weight and composition distributions.

The general conclusions that can be drawn about TREF fractionation of copolymers made by multisite type catalysts are the following:

- For most practical fraction sizes, TREF fractions will contain mixtures of polymers made by different catalytic site types.
- Chain length distributions of TREF fractions will be narrower than that of the whole polymer but the polydispersity will not necessarily be equal to 2.
- Superposition of individual distributions tends to increase the polydispersity of the TREF fraction while the incomplete recovery of polymer chains made by one site type decreases the polydispersity.
- Active sites that make low molecular weight chains with broad composition distribution will interfere more in the ability of TREF to separate polymer chains made on different site types.

It is important to stress that several restrictions apply to the use of the proposed methodology. Other effects besides copolymer composition may play an important role in TREF fractionation and therefore the ideal composition cuts used in this analysis would not be obtained. Axial diffusion effects together with crystallization kinetics may also have a significant effect in peak broadening. Additionally,

Stockmayer distribution can only be applied to instantaneous composition and chain length. Compositional drift and unstable polymerization conditions may affect significantly the chemical composition and tacticity distributions. Consequently the proposed methodology can only be applied to polymer obtained under steady-state conditions with no spatial variations of temperature and concentration in the reactor.

However, even in the face of all these restrictions, the present treatment is able to give a good qualitative description of TREF profiles and can be usefully applied as a limiting case and as a conceptual tool for the understanding of TREF results.

SIGNIFICANT RESEARCH CONTRIBUTIONS TO POLYMER SCIENCE AND ENGINEERING

I believe that significant contributions to polymer science and engineering have been made in this research and these follow in order of importance:

1) The development and application of an integrated methodology based on Stockmayer's bivariate distribution for the dynamic mathematical modelling of the kinetics of olefin polymerization. This includes kinetic parameter estimation methodology using information obtained from the characterization of polyolefins by size exclusion chromatography (SEC), temperature rising elution fractionation (TREF), and carbon-13 nuclear magnetic resonance (^{13}C NMR) for polyolefins synthesized using homogeneous and heterogeneous Ziegler-Natta catalysts.

The interpretation of the molecular weight distribution (MWD) and chemical composition distribution (CCD) of linear homopolymers and binary copolymers of olefins made with Ziegler-Natta catalysts as a weighted average of individual Stockmayer's bivariate distributions associated to different site types. This conceptual approach is theoretically sound and proved to be very useful not only in explaining and modelling the broad MWDs and CCDs generally associated with polyolefins produced with heterogeneous Ziegler-Natta catalysts but also in obtaining information about catalytic site types from MWD and CCD measurements with SEC and TREF.

The development of a novel and versatile mathematical model for the dynamic simulation of binary copolymerization of olefins using Ziegler-Natta catalysts, the polymeric multilayer model. The most important innovation introduced with the polymeric multilayer model is the dynamic modelling of MWDs and CCDs of linear homopolymers and binary copolymers of olefins made with catalysts containing multiple site types and subject to intraparticle mass and heat transfer resistances. Similar mathematical models in the literature are only able to model

chemical composition and molecular weight averages. However, the present model calculates the complete distributions of compositions and molecular weight, a significant step forward in polymerization modelling fundamentals.

Additionally, the polymeric multilayer model has a very attractive mathematical formulation that permits easy adaptation to situations in which intraparticle mass and heat transfer resistances are negligible. It can also be conveniently combined with mathematical models for the dynamic macroscopic simulation of polymerization reactors and used in process simulation, optimization and control studies.

2) The presence of hydrogen during the polymerization of propylene with a conventional heterogeneous Ziegler-Natta catalyst was found to increase the rate of propylene polymerization by creating new active site types. This was clearly shown using SEC and TREF analyses of the polypropylenes. It appears that this phenomenon of rate enhancement caused by hydrogen via the generation of new active site types has never been confirmed with TREF/SEC analysis of the product polymer.

3) The development of a systematic methodology for the deconvolution of MWD measured by SEC into individual Flory's chain length distributions using the Golub-Pereyra method. Although a similar study has been publish in the literature, this is the first time that all the limiting hypotheses of this approach were clearly identified, that a systematic approach for the deconvolution steps is clearly explained, and that a numerical method that takes advantage of the conditional linearity of the optimization problem is proposed as an alternative to the conventional Levenberg-Marquardt method.

The development of a mathematical model to simulate ideal TREF fractionation of binary copolymers made with multiple site type catalysts using Stockmayer's bivariate distribution. This is the first time a mathematical model is proposed to describe the MWD of TREF fractions using a phenomenological approach considering the influence of the bivariate distribution of molecular weights

and copolymer composition in the fractionation. The modelling of TREF with this model provides an ideal limiting case for the fractionation of binary linear copolymers with broad molecular weight and composition distributions and is useful in interpreting TREF fractionation results.

APPENDIX A: Alternative Numerical Method for Solving the Gas-Liquid Equilibrium Equations of the Macroscopic Model

The gas-liquid equilibrium equations for the slurry reactors can be described using Henry's and Raoult's law:

$$x_i k_i = y_i P \tag{A.1}$$

$$x_{H_2} k_{H_2} = y_{H_2} P \tag{A.2}$$

$$x_{N_2} k_{N_2} = y_{N_2} P \tag{A.3}$$

$$x_{imp} k_{imp} = y_{imp} P \tag{A.4}$$

$$x_D P_D^{sat} = y_D P \tag{A.5}$$

Remembering that,

$$x_i = \frac{N_i^l}{N_T^l} \quad , \qquad y_i = \frac{N_i^g}{N_T^g} \quad , \qquad N_T^g = \frac{P V_r^g}{RT} \tag{A.6}$$

equation (A.1) can be transformed to:

$$\frac{N_i^l}{N_T^l} k_i = \frac{N_i^g}{N_T^g} P = N_i^g \frac{RT}{V_r^g} \tag{A.7}$$

Rearranging equation (A.7):

$$N_i^g = k_i \frac{V_r^g}{RT} \frac{N_i^l}{N_T^l} = k_i C x_i \tag{A.8}$$

Similar expressions can be derived for equations (A.2) to (A.5):

$$N_{H_2}^{g} = k_{H_2} C x_{H_2} \tag{A.9}$$

$$N_{N_2}^{g} = k_{N_2} C x_{N_2} \tag{A.10}$$

$$N_{imp}^{g} = k_{imp} C x_{imp} \tag{A.11}$$

$$N_{D}^{g} = P_{D}^{sat} C x_{D} \tag{A.12}$$

where,

$$N_{T}^{g} = \sum_{i=1}^{m} N_{i}^{g} + N_{H_2}^{g} + N_{N_2}^{g} + N_{imp}^{g} + N_{D}^{g} \tag{A.13}$$

$$N_{T}^{l} = \sum_{i=1}^{m} N_{i}^{l} + N_{H_2}^{l} + N_{N_2}^{l} + N_{imp}^{l} + N_{D}^{l} \tag{A.14}$$

Substituting the expressions:

$$N_{i}^{T} = N_{i}^{l} + N_{i}^{g} \tag{A.15}$$

$$N_{H_2}^{T} = N_{H_2}^{l} + N_{H_2}^{g} \tag{A.16}$$

$$N_{N_2}^{T} = N_{N_2}^{l} + N_{N_2}^{g} \tag{A.17}$$

$$N_{imp}^{T} = N_{imp}^{l} + N_{imp}^{g} \tag{A.18}$$

$$N_{D}^{T} = N_{D}^{l} + N_{D}^{g} \tag{A.19}$$

into equations (A.8) to (A.12), one finally obtains:

$$N_{i}^{l} = N_{i}^{T} (1 + C k_{i} / N_{T}^{l})^{-1} \tag{A.20}$$

$$N_{H_2}^l = N_{H_2}^T\left(1 + Ck_{H_2}/N_T^l\right)^{-1} \tag{A.21}$$

$$N_{N_2}^l = N_{N_2}^T\left(1 + Ck_{N_2}/N_T^l\right)^{-1} \tag{A.22}$$

$$N_{imp}^l = N_{imp}^T(1 + Ck_{imp}/N_T^l)^{-1} \tag{A.23}$$

$$N_D^l = N_D^T(1 + CP_D^{sat}/N_T^l)^{-1} \tag{A.24}$$

The system of algebraic equations defined by expressions (A.20) to (A.24) can not be explicitly solved since N^T_l is a function of N_i^l, $N_{H2}{}^l$, $N_{N2}{}^l$, $N_{im}{}^l$, and $N_D{}^l$. However, since under normal Ziegler-Natta polymerization conditions in slurry reactors, the fraction of diluent in the liquid phase approximates unity, the following algorithm can be devised to solve the above system of equations:

1. Assume that $N_T^l \approx N_D^l$. Call this first estimate $N_T^{l,1}$, where *1* denotes the first iteration.

2. Estimate $N_T^{l,1}$ from equation (A.24) as $N_T^{l,1} \equiv N_D^l = N_D^T - CP_D^{sat}$.

3. Solve equations (A.20) to (A.24) substituting N_T^l by $N_T^{l,k}$ obtained in step 2 (k indicates the iteration number) to obtain estimates of N_i^l, $N_{H2}{}^l$, $N_{N2}{}^l$, $N_{im}{}^l$, and $N_D{}^l$.

4. Estimate $N_T^{l,k+1}$ using equation (A.14).

5. If $| N_T^{l,k} - N_T^{l,k+1} | > \varepsilon$, repeat steps 3 and 4 with the new estimate $N_T^{l,k+1}$.

The proposed algorithm converges to the same results obtained when the system of algebraic equations defined by expression (25) to (29) and (17) in chapter 4 is solved using the Newton-Raphson method. The computation time of the proposed algorithm is, however, significantly lower since it does not compute function derivatives.

APPENDIX B: Particle Size Distribution in a Series of Continuous Stirred Tank Reactors Using Heterogeneous Ziegler-Natta Catalysis in a Slurry Polymerization Process

It is well known that the PSD of polymer particles of olefins produced with heterogeneous Ziegler-Natta catalysts approximately replicates the PSD of the original catalyst particles (*replication factor*). This is an important phenomenon because it permits one to readily predict the PSD of the produced polymer particles. The PSD of the polymer particles is an important variable in designing and operating polymer recovery, treatment, and processing units.

However, the necessary condition to obtain a perfect replication of the catalyst PSD is that the residence time of all catalyst particles in the reactor be the same. This requirement is only possible in plug flow reactors.

In this appendix, a simplified polymerization model is derived and used to study the effects of residence time distribution (RTD) in series of CSTRs on the final particle size distribution (PSD) of polymer particles produced with heterogeneous Ziegler-Natta catalysts.

- Equations for particle growth when there is no catalyst deactivation

The initial moles of active sites in the catalyst particle can be expressed as:

$$C^* = V_p^0[C^*] = \frac{\pi D_p^{0^3}}{6}[C^*] \tag{B.1}$$

where,

V_p^0 initial volume of catalyst particle.

D_p^0 initial diameter of catalyst particle.

C^* moles of active sites in the catalyst.

$[C^*]$ concentration of active sites in the catalyst particle.

The catalyst particle volume exiting the reactor is calculated as:

$$V_p = V_p^0 + \Delta V_p \tag{B.2}$$

$$\frac{\pi D_p^3}{6} = \frac{\pi D_p^{0^3}}{6} + \frac{\pi D_p^{0^3}}{6} \frac{k_p[M][C^*]t_p\overline{mw}}{\rho_{pol}} \tag{B.3}$$

where,

V_p volume of polymer-catalyst particle exiting the reactor.

ΔV_p volume increase of polymer-catalyst particle due to polymerization.

D_p diameter of polymer-catalyst particle exiting the reactor.

k_p average (over all site types) propagation constant, volume/mol.time.

t_p polymerization time.

$\overline{mw}$ average molecular weight of comonomers.

ρ_{pol} polymer density, weight/volume

$[M]$ monomer concentration near active sites.

Equation (B.3) can be rearranged into the more convenient form shown as follows:

$$D_p = D_p^0(1 + \alpha t_p)^{1/3} \tag{B.4}$$

$$\alpha = \frac{k_p[M][C^*]\overline{mw}}{\rho_{pol}} \tag{B.5}$$

and therefore,

$$\frac{dD_p}{dt} = \frac{D_p^0}{3}(1+\alpha t_p)^{-2/3}\alpha \tag{B.6}$$

The particle size distribution, $F(D_p)$, can be related to the residence size distribution in the reactor, $E(t)$, by:

$$F(D_p)dD_p = E(t)dt \tag{B.7}$$

$$F(D_p)\frac{dD_p}{dt} = E(t) \tag{B.8}$$

Substituting (B.6) in (B.8) one obtains an expression relating $F(D_p)$ to $E(t)$:

$$F(D_p) = \frac{3(1+\alpha t_p)^{2/3}}{\alpha D_p^0}E(t) \tag{B.9}$$

For n CSTRs of equal volumes in series, equation (B.9) can be used substituting the well known expression for $E(t)$ (Fogler, 1986):

$$F(D_p) = \frac{3(1+\alpha t_p)^{2/3}}{\alpha D_p^0}\frac{t_p^{n-1}}{(n-1)!\tau^n}e^{-t_p/\tau} \tag{B.10}$$

where τ is the mean residence time in the reactors and t can be expressed as a function of D_p rearranging equation (B.4):

$$t_p = \left[\left(\frac{D_p}{D_p^0}\right)^3 - 1\right]\frac{1}{\alpha} \tag{B.11}$$

If the CSTRs do not have the same volumes, equations (B.10) and (B.11) can still be used for the first reactor in the series. For the subsequent reactors one must express the increase in particle volume per reactor as:

$$\frac{\pi D_p^{i^3}}{6} = \frac{\pi D_p^{i-1^3}}{6} + \frac{\pi D_p^{0^3}}{6} \frac{k_p [M] [C^*] t_p^i \overline{mw}}{\rho_{pol}} \tag{B.12}$$

where,

D_p^i diameter of polymer-catalyst particle exiting reactor i.

D_p^{i-1} diameter of polymer-catalyst particle exiting reactor i-1 and entering reactor i.

t_p^i polymerization time in reactor i.

Rearranging equation (B.12):

$$D_p^i = D_p^0 \left[\left(\frac{D_p^{i-1}}{D_p^0} \right)^3 + \alpha t_p^i \right]^{1/3} \tag{B.13}$$

Substituting the time derivative of (B.13) in (B.8) one obtains a general relationship for the $F(D_p)$ and $E(t)$ in a series of CSTRs of any volumes:

$$F(D_p^i) = \frac{3\left[(D_p^{i-1}/D_p^0)^3 + \alpha t_p^i \right]^{2/3}}{\alpha D_p^0} E(t) \tag{B.14}$$

Equation (B.14) can be used with any residence time distribution for any one of the reactors in the series. For an ideal CSTR:

$$F(D_p^i) = \frac{3\left[(D_p^{i-1}/D_p^0)^3 + \alpha t_p^i \right]^{2/3}}{\alpha D_p^0} \frac{e^{-t_p^i/\tau}}{\tau} \tag{B.15}$$

where t_p can be easily obtained from (B.13):

$$t_p = \frac{1}{\alpha} \left[\left(\frac{D_p^i}{D_p^0} \right)^3 - \left(\frac{D_p^{i-1}}{D_p^0} \right)^3 \right] \tag{B.16}$$

- Equations for particle growth when there is catalyst deactivation

It is assumed that the active sites on the catalyst can be divided into stable and unstable sites. The unstable sites deactivate following an exponential decay rate with two adjustable parameters, *a* and *b*. The total number of sites at any time can be calculated by:

$$[C^*] = [C^*_{uns}]e^{-at^b} + [C^*_{ss}] \tag{B.17}$$

where,

$[C^*]$ concentration of all active sites in the catalyst as a function of time.

$[C_{uns}^*]$ initial concentration of unstable active sites in the catalyst.

$[C_{ss}^*]$ concentration of stable active sites in the catalyst.

Using the above relation, equation (B.4) for the first reactor in the series becomes:

$$D_p = D_p^0[1 + \alpha_{uns}\phi(t_p) + \alpha_{ss}t_p]^{1/3} \tag{B.18}$$

where,

$$\alpha_{uns} = \frac{k_p[M][C^*_{uns}]\overline{mw}}{\rho_{pol}} \tag{B.19}$$

$$\alpha_{ss} = \frac{k_p[M][C^*_{ss}]\overline{mw}}{\rho_{pol}} \tag{B.20}$$

$$\phi(t) = e^{-at_p^b}t_p \tag{B.21}$$

In an equivalent way, for the other reactors in the series, equation (B.13) becomes:

$$D_p^i = D_p^{i-1}\left[\left(\frac{D_p^{i-1}}{D_p^0}\right)^3 + \alpha_{uns}\phi(t_p^i) + \alpha_{ss}t_p^i\right]^{1/3} \tag{B.22}$$

The particle size distribution of any reactor in the series is easily obtained by substituting the time derivative of equations (B.18) or (B.22) in expression (B.8):

$$F(D_p^i) = \frac{3\left[(D_p^{i-1}/D_p^0)^3 + \alpha_{uns}\phi(t_p^i) + \alpha_{ss}t_p^i\right]^{2/3}}{D_p^0\left[\alpha_{uns}\exp\left(-at_p^{i^b}\right)\left(1-abt_p^{i^b}\right)+\alpha_{ss}\right]} \tag{B.23}$$

where D_p^{i-1}/D_p^0 is equal to 1 for the first reactor.

For the case of catalyst deactivation, t can not be obtained explicitly as a function of D_p. Both equations (B.18) and (B.22) have to be solved using a numerical method for finding the roots of non-linear algebraic equations such as Newton's method (Press et al., 1992).

- Algorithm for Solving the Equations

The particle size distribution of the original catalyst particles is input as a histogram of average particle size *versus* number fraction:

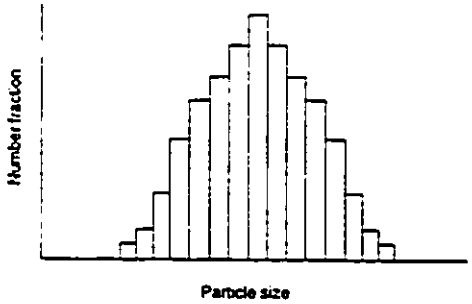

Each particle size class of the histogram is followed individually during the polymerization throughout all reactors, since each one is associated with an individual initial diameter and consequently with a distinct number of active sites.

During polymerization, each class of particle size generates a new distribution of particle sizes that have to be added in the end of the simulation to obtain the global particle size distribution exiting the reactor (figure B.1).

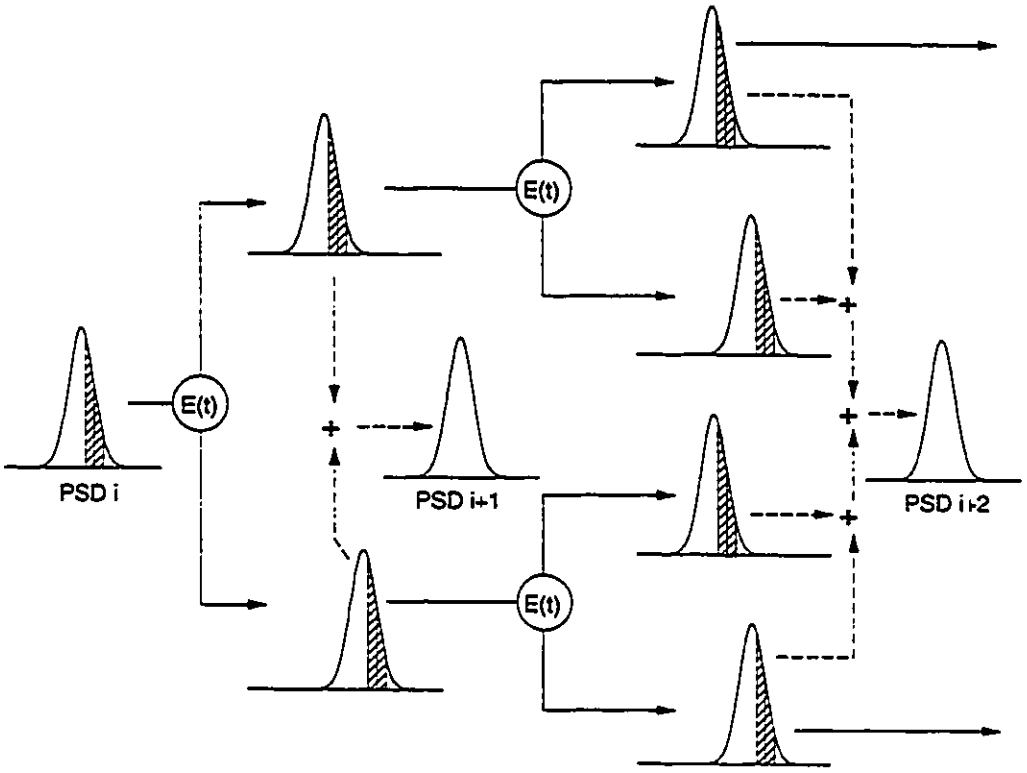

Figure B.1 - Each particle size class entering the reactor generates a particle size distribution (PSD). All PSDs are added up in the end of the simulation to obtain the PSD of all polymer-catalyst particles exiting the reactor.

For the case of catalyst deactivation, it is necessary to solve equations (B.18) and (B.22) numerically, using the Newton-Raphson method. Noticing that both equations can be expressed as:

$$f(t) = \alpha_{uns}\phi(t) + \alpha_{ss}t + c \tag{B.24}$$

where, $c = 1 - (D_p/D_p^0)^3$ for reactor 1, and $c = (D_p^{i-1}/D_p^0)^3 - (D_p^i/D_p^0)^3$ for reactors 2, 3,...,n., estimates for t can be obtained using the recursive formula:

$$t^{k+1} = t^k - \frac{f(t^k)}{f'(t^k)} \tag{B.25}$$

$$f'(t) = \alpha_{uns}\phi'(t) + \alpha_{ss} \tag{B.26}$$

$$\phi'(t) = e^{-at^b}(1 - abt^b) \tag{B.27}$$

- Simulation Results

Some simulation results will be presented to illustrate the use of the equations derived herein.

A model catalyst was assumed with a particle size distribution (PSD) commonly encountered in commercial catalysts (figure B.2).

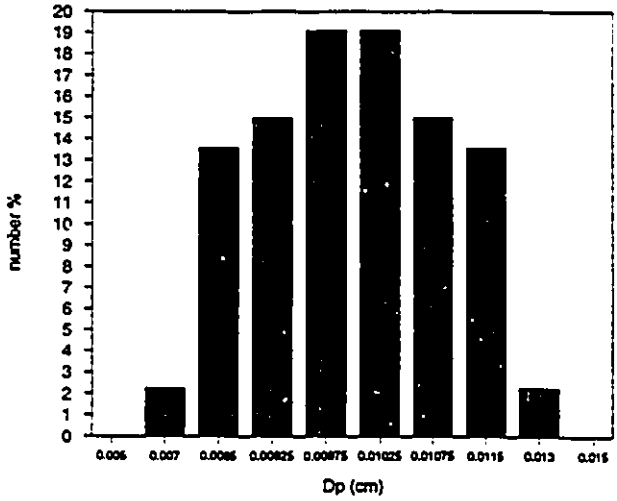

Figure B.2 - Particle size distribution of catalyst before polymerization.

Figure B.3 compares the PSD obtained when the polymerization takes place in five CSTRs of equal volumes in series with that obtained in only one CSTR with the same volume of the series of CSTRs. As expected, PSD is narrower for the series of reactors. Evidently, for an infinite number of CSTRs in series, the PSD would approach that obtained with a plug flow reactor.

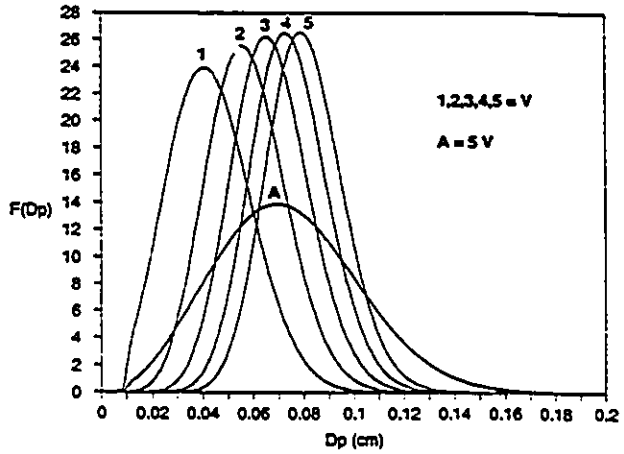

Figure B.3 - Comparison of particle size distribution of polymer made in five CSTRs of volume V in series and that obtained when only one CSTR with volume equal $5V$ is used.
(τ = 60 min; k_p = 1.0 x 10^5 l/mol.min; [M] = 4.0 mol/l; [C^*] = 1.0 x 10^{-4} mol/l; $\overline{mw}$ = 42; ρ_{pol} = 900 g/l.)

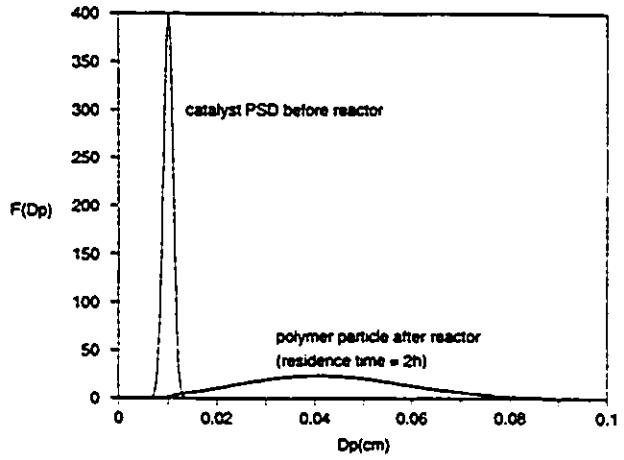

Figure B.4 - Particle size distribution of polymer-catalyst particles after and before polymerization.
(τ = 120 min; k_p = 1.0 x 10^5 l/mol.min; [M] = 4.0 mol/l; [C^*] = 1.0 x 10^{-4} mol/l; $\overline{mw}$ = 42; ρ_{pol} = 900 g/l.)

Figure B.4 compares the PSD before and after one single reactor with residence time of two hours. There is significant broadening of the PSD, which is an important result for polymer recovery and processing in later stages of polymer production.

Non-ideal residence time distributions can have an important effect on PSD. Figure B.5 shows a non-ideal RTD as a linear combination of two ideal RTDs for CSTRs. By combining the two ideal RTDs of average residence times of 2 hours and 6 hours, respectively, it is possible to model the non-ideal RTD of a CSTR containing stagnant sections. The effect of those stagnant sections is to increase the residence time in the reactor and consequently broaden the PSD. This result is shown in figure B.6 for the first and last reactor of a series of five CSTRs.

Catalyst deactivation has the opposite effect: it tends to narrow the PSD as compared to that obtained with stable catalyst. Figure B.7 shows the deactivation profile of a model catalyst according to equation (B.17). Figure B.8 compares the PSDs of polymer made by a stable catalyst with those obtained if the catalyst deactivates following the profile shown in figure B.7. Both catalysts have the same active site concentration in the beginning of the polymerization and the reactors in the series follow the nonideal RTD depicted in figure B.5. Not only are average particle sizes lower for the unstable catalyst but also the PSDs are narrower.

These simulation results, although simplified, are useful for predicting how reactor configurations, residence time distributions and catalyst deactivation can influence the particle size distribution of polymers made using heterogeneous Ziegler-Natta catalysts.

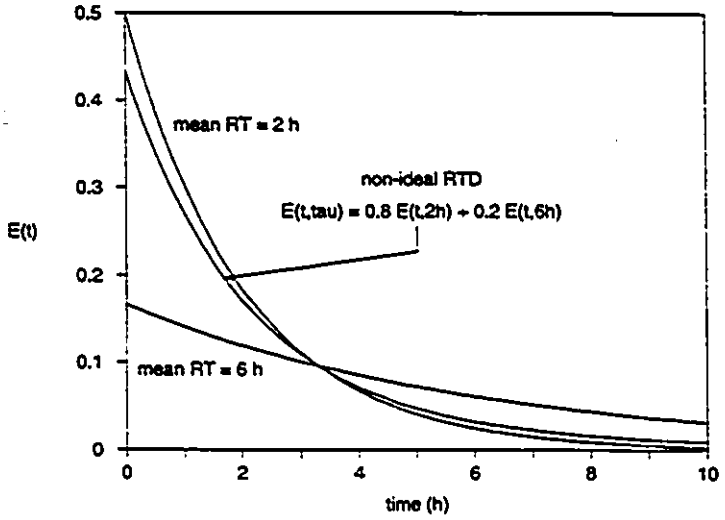

Figure B.5 - Non-ideal residence time distribution (RTD) obtained as a linear combination of two ideal RTDs.

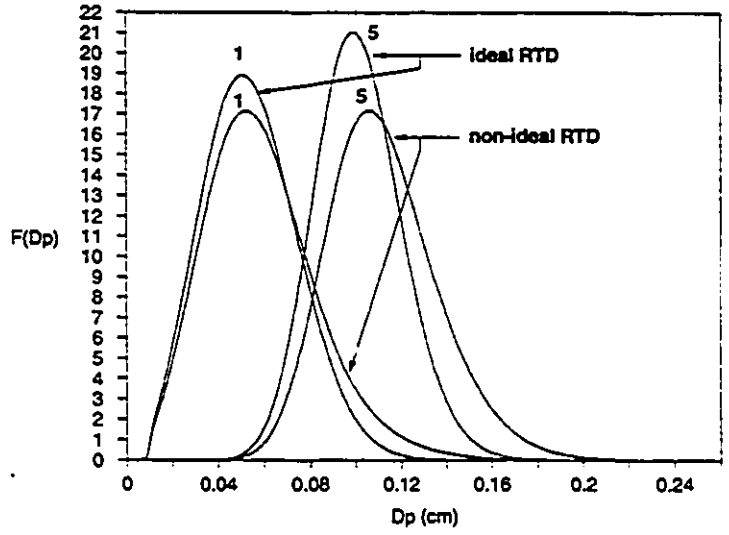

Figure B.6 - Effect of nonideal residence time distribution on the particle size distribution.
(k_p = 1.0 x 10^5 l/mol.min; [M] = 4.0 mol/l; [C^*] = 1.0 x 10^{-4} mol/l; $\overline{mw}$ = 42; ρ_{pol} = 900 g/l.)

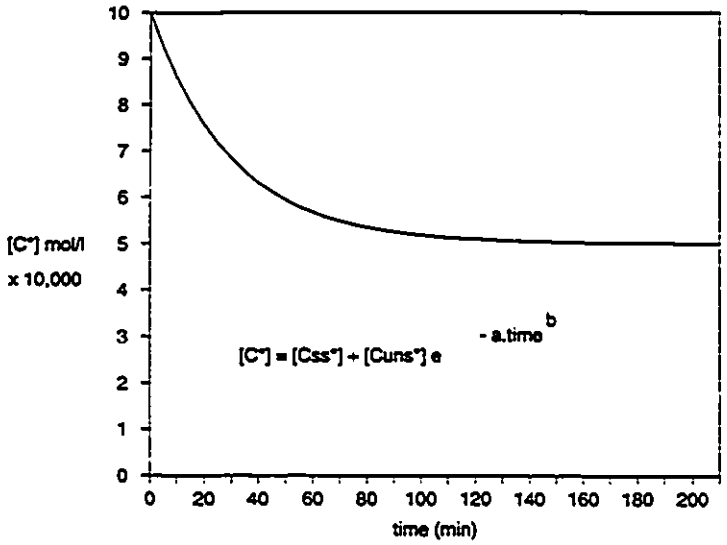

Figure B.7 - Deactivation profile of a model catalyst composed of stable (C^*_{ss}) and unstable (C^*_{uns}) active sites ($[C^*_{ss}] = [C^*_{uns}] = 5.0 \times 10^{-5}$ mol/l; $a = 0.033$; $b = 1.0$).

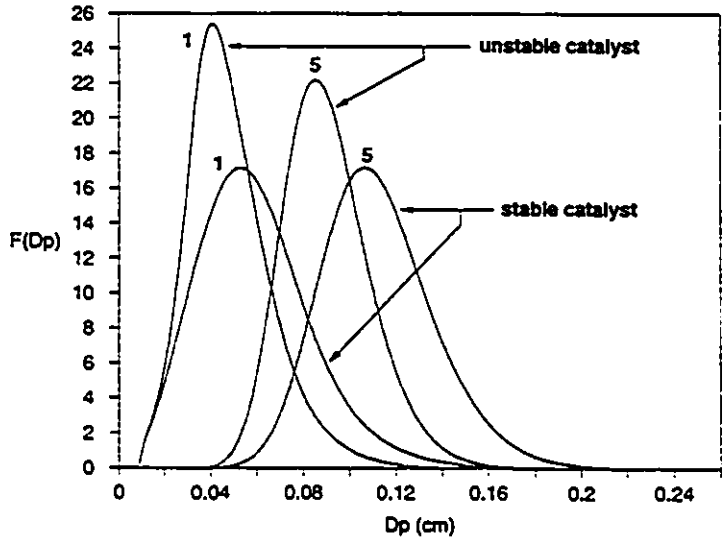

Figure B.8 - Effect of catalyst deactivation on particle size distribution.
(τ = for non-ideal RTD as described in figure B.5; $k_p = 1.0 \times 10^5$ l/mol.min; $[M]$ = 4.0 mol/l; $\overline{mw} = 42$; $\rho_{pol} = 900$ g/l.)

APPENDIX C: ^{13}C NMR - Experimental Conditions

All reported ^{13}C NMR spectra of polyolefins were measured using a BAUKER AC 300 spectrometer under the following experimental conditions:

- Spectral frequency 75.5 MHz
- Memory size 32 K bytes
- Spectral width 12,800 Hz
- Pulse width 4.3 μsec
- Pulse angle 90°
- Relaxation delay 15 sec
- Acquisition time 0.64 sec
- Number of scans 924
- Temperature 120 °C
- Sample concentration 15 wt% in ODCB

REFERENCES

Abis, L.; Bacchilega, G.; Milani, F. (1986) Makromol. Chem., **187**, 1877.

Andressen, A.; Cordes, H. G.; Herwig, J.; Kaminsky, W.; Merck, A.; Mottweiller, R; Pein, J.; Sinn, H.; Vollmer, H. J. (1976) Angew. Chem. Int. Ed. Engl., **15**, 630.

Antberg, M.; Bohm, L.; Rohrmann, J. (1991) Process for the preparation of a heterogeneous metallocene catalyst component. **U.S. Pat. 5,071,808.**

Antberg, M.; Spaleck, W.; Rohrmann, J.; Luker, H.; Winter, A. (1992a) Process for the preparation of an ethylene/propylene copolymer. **U.S. Pat. 5,086,134.**

Antberg, M.; Herrmann, H. F.; Rohrmann, J. (1992b) Metallocene (co)polymers, process for their preparation and their use as catalysts. **U.S. Pat. 5,169,818.**

Antberg, M; Liiker, H.; Bohm, L. (1993) Process for the preparation of a 1-olefin polymer. **U.S. Pat. 5,202,398.**

Arlman, J. (1964) Proc. Int. Congr. Catal., **2**, 957.

Bailly, J. C.; Bres, P.; Chabrand, C.; Daire, E. (1992) Catalyst and prepolymer used for the preparation of polyolefins. **U.S. Pat. 5,106,804.**

Balke, S. T.; Hamielec, A. E.; LeClair, B. P.; Pearce, S. L. (1969) Ind. Eng. Chem., Proc. Res. Dev., **8**, 54.

Barbe, P. C.; Cecchin, G.; Noristi, L. (1987) Adv. Polym. Sci., **81**, 1.

Bates, D. M.; Watts, D. G. (1988) Nonlinear Regression Analysis and its Applications, John Wiley & Sons, New York.

Berger, M. N.; Grieveson, B. M. (1965) Makromol. Chem., **83**, 80.

Bergstrom, C.; Avela, E. (1979) J. Appl. Polym. Sci., **23**, 163.

Biesenberg, J. A.; Sebastian, D. H. (1983) Principles of Polymerization Engineering, John Wiley & Sons, New York.

Billingham, N. C. (1989) In Comprehensive Polymer Science, 3, Sir G. Allen (ed.), Pergamon Press, New York, 43.

Bohm, L. L. (1978) Polymer, **19**, 545.

Bohm, L. L. (1981) Makromol. Chem., **182**, 3291.

Boor, J., Jr. (1979) Ziegler-Natta Catalysts and Polymerization., Academic Press, New York.

Box, G. E. P.; Hunter, W. G.; Hunter, J. S. (1978) Statistics for Experimenters., John Wiley & Sons, New York.

Brekner, M. J.; Rohrmann, J.; Spaleck, W.; Antberg, M. (1992) Process for the preparation of cycloolefin polymers. **U.S. Pat. 5,087,677.**

Brockmeier, N. F.; Rogan, J. B. (1976) AIChE Symp. Ser., 72, 29.

Brockmeier, N. F. (1983) In Transition Metal Catalyzed Polymerization, **4**, R. P. Quirk (ed.), Harwood, New York, 671.

Bueschges, U.; Chien, J. C. W. (1989) J. Polym. Sci.: Part A: Polym. Chem., **27**, 1525.

Buls, V. W.; Higgins, T. L. (1970) J. Polym. Sci.: Part A1, **8**, 1037.

Buls, V. W.; Higgins, T. L. (1973) J. Polym. Sci.: Polym. Chem. Ed., **11**, 925.

Burfield, D. R.; Tait, P. J. T.; McKenzie, I. D. (1972) Polymer, **13**, 321.

Burfield, D. R.; McKenzie, I. D.; Tait, P. J. T. (1976) Polymer, **17**, 130.

Calabro, D. C.; Lo, F. Y. (1988) In Transition Metal Catalyzed Polymerization, R. D. Quirk (ed.), Cambridge University Press, New York, 729.

Canich, J. A. M. (1991) Olefin polymerization catalysts. **U.S. Pat. 5,055,438.**

Carman, C. J.; Wilkes, C. E. (1971) Rub. Chem. Tech., **44**, 781.

Carman, C. J.; Tarpley, A. R., Jr.; Goldstein, J. H. (1973) Macromolecules, **6**, 719.

Carman, C. J.; Harrington, R. A.; Wilkes, C. E. (1977) Macromolecules, **10**, 536.

Caunt, A. D. (1977) In Catalysis, **1**, 234.

Chang, M. (1989a) Method for preparing a supported metallocene-alumoxane catalyst for gas-phase polymerization. **Eur. Pat. 323,716.**

Chang, M. (1989b) Method for preparing an active metallocene-alumoxane catalyst in situ during polymerization. **Eur. Pat. 308,177.**

Chang, M. (1990a) Method for preparing a silica gel supported metallocene-alumoxane catalyst for gas phase polymerization. **U.S. Pat. 4,912,075.**

Chang, M. (1990b) Method for preparing polyethylene wax by gas phase polymerization. **U.S. Pat. 4,914,253.**

Chang, M (1990c) Method for utilizing triethylaluminum to prepare an alumoxane support for an active metallocene catalyst. **U.S. Pat. 4,925,821.**

Chang, M (1990d) Supported metallocene-alumoxane catalyst for high pressure polymerization of olefins and a method of preparing and using the same. **U.S. Pat. 4,935,397.**

Chang, M. (1990e) Method for utilizing triethylaluminum to prepare an alumoxane support for an active metallocene catalyst. **U.S. Pat. 4,937,217.**

Chang, M. (1990f) Method for preparing a silica gel supported metallocene-alumoxane catalyst. **U.S. Pat. 4,937,301.**

Chang, M. (1990g) Method for utilizing triethylaluminum to prepare an alumoxane support for an active metallocene catalyst. **U.S. Pat. 4,937,217.**

Chang, M. (1991a) Olefin polymerization catalyst from trialkylaluminum mixture, silica gel and a metallocene. **U.S. Pat. 5,006,500.**

Chang, M. (1991b) Method for preparing a silica gel supported metallocene-alumoxane catalyst. **U.S. Pat. 5,008,228.**

Chang, M. (1991c) Supported catalysts for 1-olefin and 1,4-diolefin copolymerization. **U.S. Pat. 5,017,665.**

Chang, M. (1991d) Supported vanadium catalyst for polymerization of olefins and a process of preparing and using the same. **U.S. Pat. 5,032,652.**

Chang, M. (1992a) Method for preparing a silica gel supported metallocene-alumoxane catalyst. **U.S. Pat. 5,086,025.**

Chang, M. (1992b) Polymerization process using a silica gel supported metallocene-alumoxane catalyst. **U.S. Pat. 5,147,949.**

Cheng, H. N. (1982) Anal. Chem., **54**, 1828.

Cheng, H. N. (1984) Macromolecules, **17**, 1950.

Cheng, H. N. (1988) J. Appl. Polym. Sci., **35**, 1639.

Cheng, H. N.; Ewen, J. A. (1989) Makromol. Chem., **190**, 1931.

Cheng, H. N.; Kakugo, M. (1991) Macromolecules, **24**, 1724.

Cheng, H. N.; Tam, S. B.; Kasehagen, L. J. (1992) Macromolecules, **25**, 3779.

Cheng, H. N.; Kasehagen, L. J. (1993) Macromolecules, **26**, 4774.

Chien, J. C. W. J. (1979) J. Polym. Sci.: Polym. Chem. Ed., **17**, 2555.

Chien, J. C.; Kuo, C.; Ang, T. J. (1985) J. Polym. Sci.: Polym. Chem. Ed., **23**, 723.

Chien, J. C. W.; Razavi, A. (1988a) J. Polym. Sci.: Part A: Polym. Chem., **26**, 2369.

Chien, J. C. W.; Wang, B. P. (1988b) J. Polym. Sci.: Part A: Polym. Chem., **26**, 3089.

Chien, J. C. W.; Wang, B. P. (1988c) J. Polym. Sci.: Part A: Polym. Chem., **26**, 3009.

Chien, J. C. W.; Wang, B. P. (1989) J. Polym. Sci.: Part A: Polym. Chem., **27**, 1539.

Chien, J. C. W.; Wang, B. P. (1990) J. Polym. Sci.: Part A: Polym. Chem., **28**, 15.

Chien, J. C. W.; He, D. (1991a) J. Polym. Sci.: Part A: Polym. Chem., **29**, 1603.

Chien, J. C. W.; Sugimoto, R. (1991b) J. Polym. Sci.: Part A: Polym. Chem., **29**, 459.

Chien, J. C. W., Llinas, G. H.; Rausch, M. D.; Lin, G. Y.; Winter, H. H., Atwood, J. L.; Bott, S. G. (1991c) J. Am. Chem. Soc., **113**, 8569.

Chien, J. C. W.; Tsai, W. M.; Rausch, M. D. (1991d) J. Am. Chem. Soc., **113**, 8570.

Chien, J. C. W. (1992a) Makromol. Chem., Macromol. Symp., **63**, 209.

Chien, J. C. W.; Xu, B. (1993) Makromol. Chem., Rapid Commum., **14**, 109.

Chien, J. C. W.; Nozaki, T. (1993) J. Polym. Sci.: Part A: Polym. Chem., **31**, 227.

Chumaevskii, N. B.; Zakharov, V. A.; Bukatov, G. D.; Kuznetzova, G. I.; Yermakov, Y. I. (1976) Makromol. Chem., **117**, 747.

Collins, S.; Kelly, W. M.; Holden, D. A. (1992) Macromolecules, **25**, 1780.

Cooper, W. (1976) In Chemical Kinetics, **15**, C. H. Bamford and C. F. H. Tipper (eds.), Elsevier, New York, 133.

Corish, P. J. (1961) Anal. Chem., **33**, 1798.

Corish, P. J.; Tunnicliffe, M. E. (1964) J. Polym. Sci.: Part C, **7**, 187.

Corradini, P.; Busico, V.; Guerra, G. (1989) In Comprehensive Polymer Science. Sir G. Allen (ed.), Oxford, Pergamon Press, **4**, 24.

Cossee, P. (1960) Tetrahedron Lett., **17**, 12.

Cossee, P. (1964) J. Catal., **3**, 80.

Cozewith, C.; VerStrate, G. (1971) Macromolecules, **4**, 482.

Crank, J. (1990) The Mathematics of Diffusion., Oxford University Press, New York, 2nd edition.

Crapo, C. C.; Malpass, D. B. (1992) Catalyst for polymerization of olefins. **U.S. Pat. 5,086,024.**

De Carvalho, A. B.; Gloor, P. E.; Hamielec, A. E. (1989) Polymer, **30**, 280.

De Carvalho, A. B.; Gloor, P. E.; Hamielec, A. E. (1989b) Modelling the Ziegler-Natta Copolymerization in Slurry Type Reactor Trains. Internal Report, Polipropileno S.A., Pólo Petroquímico do Nordeste, Rua Hidrogênio s/n, Camaçari, Ba, Brazil.

Desreux, V.; Spiegels, M. C. (1950) Bull. Soc. Chim. Belges., **59**, 476.

Doi, Y.; Morinaga, A.; Keii, T. (1980) Makromol. Chem., Rapid Commun., **1**, 193.

Doi, Y.; Ohnishi, R.; Soga, K. (1983) Makromol. Chem., Rapid Commun., **4**, 169.

Dolle, V.; Antberg, M.; Rohrmann, J.; Winter, A. (1993) Process for the preparation of a polyolefin. **U.S. Pat. 5,216,095**.

Dongarra, J. J.; Grosse, E. (1987) Commun. ACM, **30**, 403.

Drogemuller, H.; Heiland, K.; Kaminsky, K. (1988) In Transition Metals and Organometallics as Catalysts for Olefin Polymerization, W. Kaminsky and H. Sinn (eds.), 303.

Drushel, H. V.; Iddings, F. A. (1963) Anal. Chem., **35**, 28.

Dusseault, J. J. A.; Hsu, C. C. (1993) J.M.S.- Rev. Macromol. Sci., **C33** (2), 103.

Ekmanis, J. L.; Skinner, R. A. (1991) J. Appl. Polym. Sci.; Appl. Polym. Symp., **48**, 57.

Elder, M. J.; Razavi, A.; Ewen, J. A. (1992) Process and catalyst for producing syndiotactic polyolefins. **U.S. Pat. 5,155,080**.

Elias, H. G. (1992) In Ullman's Encyclopedia of Industrial Chemistry, **A20**, B. Elvers, S. Hawkins, G. Schultz (eds.), VCH Publishers, New York, 543.

Ewen, J. A. (1984) J. Am. Chem. Soc., **106**, 6355.

Ewen, J. A. (1985) Isotactic-stereoblock polymers of alpha-olefins and process for producing the same. **U.S. Pat. 4,522,982**.

Ewen, J. A. (1986) In Catalytic Polymerization of Olefins, T. Keii and K. Soga (eds.), 271.

Ewen, J. A.; Haspeslagh, L.; Elder, M. J.; Atwood, J. L.; Zhang, H.; Cheng, H. N. (1988a) In Transition Metals and Organometallics as Catalysts for Olefin Polymerization, W. Kaminsky and H. Sinn (eds.), pg. 281.

Ewen, J. A.; Jones, R. L.; Razavi, A.; Ferrara, J. D. (1988b) J. Am. Chem. Soc., **110**, 6255.

Ewen, J. A. (1988c) Hafnium metallocene catalyst for the polymerization of olefins. **U.S. Pat. 4,794,096.**

Ewen, J. A.; Razzavi, A. (1990a) Process and catalyst for producing syndiotactic polyolefins. **U.S. Pat. 4,892,851.**

Ewen, J. A.; Welborn, H. C., Jr. (1990b) Process and catalyst for producing polyethylene having a broad molecular weight distribution. **U.S. Pat. 4,935,474.**

Ewen, J. A.; Welborn, H. C., Jr. (1990c) Process and catalyst for producing reactor blend polyolefins. **U.S Pat. 4,937,299.**

Ewen, J. A. (1990d) Catalyst systems for producing polyolefins having a broad molecular weight distribution. **U.S. Pat. 4,975,403.**

Ewen, J. A. (1991) Catalyst for producing hemiisotactic polypropylene. **U.S. Pat. 5,036,034.**

Fink, G.; Kinkelin, E. (1988) In Transition Metal Catalyzed Polymerization. R. D. Quirk (ed.), Cambridge University Press, New York, 161.

Flory, P. J. (1953) Principles of Polymer Chemistry, Ithaca, Cornell University Press, 568.

Floyd, S.; Choi, K. Y.; Taylor, T. W.; Ray, W. H. (1986a) J. Appl. Polym. Sci., **31**, 2231.

Floyd, S.; Choi, K. Y.; Taylor, T. W.; Ray, W. H. (1986b) J. Appl. Polym. Sci., **32**, 2935.

Floyd, S.; Hutchinson, R. A.; Ray, W. H. J. (1986c) J. Appl. Polym. Sci., **32**, 5451.

Floyd, S. (1986d) Ph.D. Thesis, Department of Chemical Engineering, University of Wisconsin-Madison.

Floyd, S.; Heiskanen, T.; Taylor, T. W.; Mann, G. E.; Ray, W. H. (1987) J. Appl. Polym. Sci., **33**, 1021.

Floyd, S.; Heiskanen, T.; Ray, W. H. (1988) Chem. Eng. Prog., **84**, 56.

Floyd, S.; Hoel, E. L. (1993) Process for the production of high molecular weight EPDM elastomers using a metallocene-alumoxane catalyst system. **U.S. Pat. 5,229,478.**

Fogler, H. S. (1986) Elements of Chemical Reaction Engineering, Prentice-Hall, Englewood Cliffs.

Froment, G. F.; Bischoff, B. (1979) Chemical Reactor Analysis and Design, John Wiley & Sons, New York.

Fujita, T. (1990) Polymerization of ethylene. **U.S. Pat. 4,931,517.**

Galli, P.; Luciani, L.; Cecchin, G. (1981) Ang. Makromol. Chem., **94**, 63.

Galli, P.; Haylock, J. C. (1991) Prog. Polym. Sci., **16**, 443.

Galli, P.; Haylock, J. C. (1992) Macromol. Chem., Macromol. Symp., **63**, 19.

Galvan, R.; Tirrell, M. (1986a) Comp. Chem. Eng., **10**, 77.

Galvan, R.; Tirrell, M. (1986b) Chem. Eng. Sci., **41**, 2385.

Gardner, I. J.; Cozewith, C.; VerStrate, G. (1971) Rubber Chem. Technol., 1015.

Gerald, C. F.; Wheatley, C. F. (1989) Applied Numerical Analysis, Addison-Wesley Pub. Co., Reading, Massachussetts, 4th ed.

Giannetti, E.; Nicoletti, G. M.; Mazzocchi, R. (1985) J. Polym. Sci.: Polym. Chem. Ed., **23**, 2117.

Glockner, G. (1990) J. Appl. Polym. Sci.: Appl. Polym. Symp., **45**, 1.

Golub, G. H.; Pereyra, V. (1973) SIAM J. Numer. Anal., **10**, 413.

Grassi, A.; Zambelli, A.; Resconi, L.; Albizzati, E.; Mazzocchi,R. (1988) Macromolecules, **21**, 617.

Guastalla, G.; Giannini, U. (1983) Makromol. Chem. Rapid Commun., **4**, 519.

Haddam, M. R.; Hay, J. N. (1988) In Size Exclusion Chromatography, B. J. Hunt and S. R. Holding (eds.), Blackie and Son, 57.

Hamielec, A. E. (1980) J. Liq. Chromat., **3**, 381.

Hamielec, A. (1982) Pure Appl. Chem., **54**, 293.

Hamielec, A. E.; MacGregor, J. F. (1983) In Polymer Reaction Engineering, K. H. Reichert and W. Geiseler (eds.), Munich, Hansa Publishers, 21.

Hamielec, A. E.; MacGregor, J. F.; Penlidis, A. (1987) Makromol. Chem., Macromol. Symp., **10/11**, 521.

Hamielec, A.; MacGregor, J.; Penlidis, A. (1989) In Comprehensive Polymer Science, 3, Sir Geoffrey Allen (ed.), Oxford, Pergamon Press, 17.

Hawkins, S. W.; Smith, H. (1958) J. Polym. Sci., **28**, 341.

Hayashi, T.; Inoue, Y.; Chujo, R. (1988) Macromolecules, **21**, 3139.

Hazlit, L. G.; Moldovan, D. G. (1989) **U.S. Patent 4,798,081.**

Hazlit, L. G. (1990) J. Appl. Polym. Sci.: Appl. Polym. Symp., **45**, 25.

Herfert, N.; Montag, P.; Fink, G. (1993) Makromol. Chem., **194**, 3167.

Hindmarsh, A. C. ODEPAC, A Systematic Collection of ODE Solvers. In Scientific Computing, S. Stepleman et al. (ed.), North Holland, Amsterdan, 55.

Hlatky, G. G.; Turner, H. W. (1992) Catalyst system of enhanced productivity. **U.S. Pat. 5,153,157.**

Hock, C. W. (1966) J. Polym. Sci.: Part A-1, **4**, 3055.

Hoel, E. L. (1989a) Process for production of a high molecular weight ethylene a-olefin elastomer with a metallocene alumoxane catalyst. **U.S. Pat. 4,871,705.**

Hoel, E. L. (1991) Process for production of a high molecular weight ethylene α-olefin elastomer with a metallocene alumoxane catalyst. **U.S. Pat. 5,001,205.**

Honig, J. A. J.; Gloor, P. E.; MacGregor, J. F.; Hamielec, A. E. (1987) J. Appl. Polym. Sci., **34**, 829.

Huang, J.; Rempel, G. L. (1992) Progress in Catalysis, 169.

Hutchinson, R. A.; Ray, W. H. (1988) AIChE Meeting., November 28 - December 2.

Hutchinson, R. A.; Chen, C. M.; Ray, W. H. (1992) J. Appl. Polym. Sci., **44**, 1414.

Inoue, Y.; Itabashi, Y.; Chujo, R.; Doi, Y. (1984) Polymer, **25**, 1640.

Janiak, C.; Rieger, B.; Voelkel, R.; Braun, H. G. (1993) J. Polym. Sci.: Part A: Polym. Chem., **31**, 2959.

Jejelowo, M. O.; Lynch, D. T.; Wanke, S. E. (1991) Macromolecules, **24**, 1755.

Jordan, R. F.; Bajgur, C. S.; Willett, R.; Scott, B. (1986) J. Am. Chem. Soc., **108**, 7410.

Jordan, R. F. (1988). Symposium on Catalysis and Organometallic Chemistry, **65**, 285.

Jordan, R. F.; Crowther, D. J. (1993) Cyclopentadienyl dicarbollide complexes of titanium, zirconium and hafnium. **U.S. Pat. 5,214,173.**

Kakugo, M.; Naito, Y.; Mizunuma, K.; Miyatake, T. (1982) Macromolecules, **15**, 1150.

Kakugo, M.; Miyatake, T.; Mizunuma, K.; Kawai, Y. (1988) Macromolecules., **21**, 2309.

Kakugo, M.; Naito, Y.; Mizunuma, K.; Miyatake, T. (1989) Makromol. Chem., **190**, 849.

Kakugo, M.; Sedatoshi, H.; Sakai, J.; Yokoyama, M. (1989) Macromolecules, **22**, 3172.

Kakugo, M.; Miyatake, T.; Mizunuma, K. (1991) Macromolecules, **24**, 1469.

Kamatah, P. M.; Wild, L. (1966) Polym. Eng. Sci., **6**, 213.

Kaminaka, M.; Soga, K. (1991) Makromol. Chem., Rapid Commun., **12**, 367.

Kaminaka, M.; Soga, K. (1992) Polymer, **33**, 1105.

Kaminsky, W.; Miri, M.; Sinn, H.; Woldt, R. (1983a). Makromol. Chem., Rapid Commun., **4**, 464.

Kaminsky, W.; Miri, M.; Sinn, H.; Woldt, R. (1983b). Makromol. Chem., Rapid Commun., **4**, 417.

Kaminsky, W.; Luker, H. (1984) Makromol. Chem. Rapid. Commun., 5, 225.

Kaminsky, W.; Kulper, K.; Brintzinger, H. H.; Wild, F. R. W. P. (1985a) Angew. Chem. Int. Ed. Engl., 24, 507.

Kaminsky, W.; Miri, M. (1985b) J. Polym. Sci.: Polym. Chem. Ed., 23, 2151.

Kaminsky, W.; Hahnsen, H. (1985c). **U.S. Pat. 4,544,762.**

Kaminsky, W. (1986a) In Catalytic Polymerization of Olefins, T. Keii and K. Soga (eds.), 225.

Kaminsky, W. (1986b) In Catalytic Polymerization of Olefins, T. Keii and K. Soga (eds.), 293.

Kaminsky, W.; Schlobohm, M. (1986c) Makromol. Chem., Macromol. Symp., 4, 103.

Kaminsky, W. (1986d) Angew. Makromol. Chem., **145/146**, 149.

Kaminsky, W.; Kulper, K.; Niedoba, S. (1986e) Makromol. Chem., Macromol Symp., 3, 377.

Kaminsky, W.; Bushermohle, M. (1987) In Recent Advances in Mechanistic and Synthetic Aspects of Polymerization, M. Fontanille and A. Guyot (eds.), 514.

Kaminsky, W.; Bark, A.; Spiehl, R.;Moller-Lindenhof,N.;Niedoba,S. (1988a) In Transition Metals and Organometallics as Catalysts for Olefin Polymerization, W. Kaminsky and H. Sinn (eds.), 291.

Kaminsky, W.; Steiger, R. (1988b) Polyhedron, 7 (22/23), 2375.

Kaminsky, W.; Buschermohle, M. (1989a) Process for the preparation of a 1-olefin stereoblock polymer. **U.S. Pat. 4,841,004.**

Kaminsky, W.; Buschermohle, M. (1989b) 1-Olefin stereoblock polymer, and a process for its preparation. **U.S. Pat. 4,849,487.**

Kaminsky, W.; Bark, A.; Arndt, M. (1991a) Makromol. Chem., Macromol. Symp., 47, 83.

Kaminsky, W. (1991b) Catalysis Society of Japan, 33 (8), 536.

Kaminsky, W.; Bark, A. (1992a) Polym. Inter., **28**, 251.

Kaminsky, W.; Bark, A.; Steiger, R. (1992b) J. Mol. Catal., **74**, 109.

Kaminsky, W.; Renner, F. (1993a) Makromol. Chem., Rapid Commun., **14**, 239.

Kaminsky, W.; Spiehl, R. (1993b) Process for the preparation of an olefin polymer, **U.S. Pat. 5,204,429**.

Karbashewski, E.; Rudin, A.; Kale, L.; Tchir, J. (1993) Polym. Eng. Sci., **33**, 1370.

Keii, T. (1972) Kinetics of Ziegler-Natta Polymerization, Kodansha, Tokyo.

Keii, T. (1982) Makromol. Chem., **183**, 2285.

Keii, T.; Doi, Y.; Suzuki, E.; Tamura, M.; Murata, M.; Soga, K. (1984) Makromol. Chem., **185**, 1537.

Keii, T. (1988) In Transition Metal Catalyzed Polymerization, R. P. Quirk (ed.), Harwood, New York, 84.

Kelusky, E. C.; Elston, C. T.; Murray, R. (1987) Polym. Eng. Sci., **27**, 1562.

Kioka, M.; Kashiwa, N.; Tsutsui, T.; Toyota, A. (1993) Catalyst for polymerizing an olefin and process for polymerizing an olefin, **U.S. Pat. 5,206,199**.

Kioka, M.; Makio, H.; Mizuno, A.; Kashiwa, N. (1994) Polymer, **35**, 580.

Kissin, Y. V. (1985) Isospecific Polymerization of Olefins, Springer-Verlag, New York.

Kissin, Y. V.; Brandolini, A. J. (1991) Macromolecules, **24**, 2632.

Kok, A. C.; Oomens, A. C. (1982) J. Liq. Chromat., **5**, 807.

Kramer, G. W.; Levy, A. B.; Midland, M. M. (1975) In Organic Synthesis via Boranes, H. C. Brown (ed.), John Wiley & Sons, New York, 191.

Kulin, L.I.; Meijerink, N.L.; Sturck, P.S. (1988) Pure and Appl. Chem., **60**, 1404.

Lai, S. Y.; Land, S.; Wilson, J. R.; Knight, G. W.; Steven, J. C.; Chum, P. W. S. (1993) Elastic Substantially Linear Olefin Polymers, **U.S. Pat. 5,272,236.**

Lee, I. M.; Gauthier, W. J.; Ball, J. M.; Iyengas, B.; Collins, S. (1992) Organometallics, **11**, 2115.

Lew, R.; Suwanda, D.; Balke, S. T. (1988a) J. Appl. Polym. Sci., 35, 1049.

Lew, R.; Suwanda, D.; Balke, S. T. (1988b) J. Appl. Polym. Sci., 35, 1065.

Lieberman, R. B.; Barbe, P. C. (1986) In Encyclopedia of Polymer Science and Engineering, J. I. Kroschwitz (ed.).

Locatelli, P.; Sacchi, M. C.; Tritto, I.; Zannoni, G. (1988) Makromol. Chem.: Rapid Commum., **9**, 575.

Lorenzini, Pascal; Bertrand, Pascale; Villermaux, Jacques. (1991) Can. J. Chem. Eng., **69**, 682.

Luker, H. (1991) Polyethylene wax, and a process for the preparation thereof. **U.S. Pat. 5,023,388.**

Malanga, M. T.; Newmann, T. H. (1990) Suspension polymerization of vinyl aromatic monomers to polymer having high syndiotacticity. **U.S. Pat. 4,950,724.**

Mallin, D. T.; Rausch, M. D.; Lin, Y. G.; Dong, S.; Chien, J. C. W. (1990) J. Am. Chem. Soc., **112**, 2030.

Marques, M. M. V.; Nunes, P. C.; Tait, P. J. T.; Dias, A. R. (1993) J. Polym. Sci.: Part A: Polym. Chem., **31**, 209.

Martuscelli, E.; Avella, M.; Segre, A. L.; Rossi, E.; Di Drusco, G.; Galli, P.; Simonazzi, T. (1985) Polymer, **26**, 259.

Mason, C. D.; Schaffhausen, R. J. (1971) J. Polym. Sci., **B9**, 661.

McAuley, K. B.; MacGregor, J. F.; Hamielec, A. E. (1990) AIChE J., **36**, 850.

McMurry, J. (1984) Organic Chemistry, Brooks/Cole Publishing Co., Monterey, California.

Mirabella Jr., F. M. (1987a) International GPC Symposium 87, May 11-13, Itasca, IL, 180.

Mirabella Jr., F. M.; Ford, E. A. (1987b) J. Polym. Sci.: Part B: Polym. Phys., **25**, 777.

Mirabella Jr., F. M. (1992) J. Appl. Polym. Sci.: Appl. Polym. Symp., **51**, 117.

Mirabella Jr., F. M. (1993) Polymer, **34**, 1729.

Mirabella Jr., F. M. (1994) J. Liq. Chrom., in press.

Mise, T.; Miya, S.; Yamazaki, H. (1989) Chem. Lett., 1853.

Mortimer, G. A.; Ort, M. R.; Mottus, E. H.(1978) J Polym. Sci.: Polym. Chem. Ed., **16**, 2337.

Munoz-Escalona, A.; Villalba, J. (1977) Polymer, **18**, 179.

Nagel, E. J.; Kirilov, V. A.; Ray, W. H. (1980) Ind. Eng. Chem., Prod. Res. Dev., 19, 372.

Nakano, S.; Goto, Y. (1981) J. Appl. Polym. Sci., **26**, 4217.

Natta, G. (1959a) Adv. Catal., **11**, 1.

Natta, G. (1959b) J. Polym. Sci., **34**, 21.

Natta, G.; Mazzanti, G. (1960) Tetrahedron, **8**, 86.

Ogawa, T.; Inaba, T. (1978) J. Appl. Polym. Sci., **22**, 262.

Okura, I.; Kojima, A.; Soga, K.; Keii, T. (1970) J. Polym. Sci.: Part A-1, **8**, 2717.

Piccolrovazzi, P.; Pino, P.; Consiglio, G.; Sironi, A.; Moret, M. (1990) Organometallics, **9**, 3098.

Pijpers, E. J.; Roest, B. C. (1972) Eur. Polym. J., **8**, 1151.

Press, W. H.; Teukolsky, S. A.; Vetterling, W. T.; Flannery, B. P. (1992) Numerical Recipes in FORTRAN, Cambridge University Press, Cambridge, 2nd ed.

Randall, J. C. (1977) Polymer Sequence Distribution, Carbon-13 NMR Method., Academic Press, New York.

Randall, J. C. (1978a) Macromolecules, **11**, 33.

Randall, J. C. (1978b) Macromolecules, **11**, 592.

Ray, G. J.; Johnson, P. E.; Knox, J. R. (1977) Macromolecules, **10**, 773.

Ray, W. H. (1988) In Transition Metal Catalyzed Polymerization, R. P. Quirk (ed.), Harwood, New York, 563.

Rayner, L. S. (1964) Comm. J. Polym. Sci. Part C, **4**, 125.

Razavi, A. (1992) Process for the preparation of metallocenes. **U.S. Pat. 5,117,020.**

Resconi, L.; Giannini, U.; Albizzati, E. (1992) Catalysts for the polymerization of olefins. **U.S. Pat. 5,126,303.**

Rieger, B.; Mu, X.; Mallin, D. T.; Rausch, M. D.; Chien, J. C. W. (1990) Macromolecules, **23**, 3559.

Rieger, B.; Brintzinger, H.; Roell, W.; Reinmuth, A.; Barsties, E. (1992) Soluble catalyst systems for the polymerization of C2- to C10 alk-1-enes. **U.S. Pat. 5,132,262.**

Rincon-Rubio, L. M.; Wilen, C. E.; Lindfors, L. E. (1990) Eur. Polym. J., **26**, 171.

Rohrmann, J.; Herrmann, W. A. (1992) Process for the preparation of a chiral stereorigid metallocene. **U.S. Pat. 5,103,030.**

Ross, J. F. (1984) J. Polym. Sci.: Polym Chem. Ed., **22**, 2255.

Sarkar, P.; Gupta, S. K. (1991) Polymer, 32, 2842.

Schmeal, W. R.; Street, J. R. (1971) AIChE J., **17**, 1189.

Schmeal, W. R.; Street, J. R. (1972) J. Polym. Sci.: Polym. Phys. Ed., **10**, 2173.

Scholte, T. H. G.; Meijerink, N. L. J.; Schoffeleers, H. M.; Brands, A. M. G. (1984) J. Appl. Polym. Sci., **29**, 3763

Schouterdan, P.; Groeninckx, G.; der Heijden, B. Van, Jansen, F. (1987) Polymer., **28**, 2099.

Shirayama, K.; Okada, T.; Kita, S. I. (1965) J. Polym. Sci.: Part A, **3**, 907.

Shriver, D. F. (1969) The Manipulation of Air-Sensitive Compounds., McGraw-Hill, New York.

Simha, R.; Branson, H. J. (1944) Chem. Phys., **12**, 253.

Simonazzi, T.; Cecchin, G.; Mazzaullo, S. (1991) Prog. Polym. Sci., **16**, 303.

Singh, D.; Merrill, R. P. (1971) Macromolecules, **4**, 599.

Sinn, H.; Kaminsky, W.; Volmer, H. J.; Woldt, R. (1980) Angew. Chem. Int. Ed. Engl., **19** (5), 390.

Sinn, H.; Kaminsky, W. (1980) Adv. Organomet. Chem., **18**, 99.

Sinn, H. et al. (1988) In Transition Metals and Organometallics as Catalyst for Olefin Polymerization. W. Kaminsky and H. Sinn (eds.), 257.

Slaugh, L. H.; Schoenthal, G. W. (1987) Stabilization of metallocene/aluminoxane catalysts. **U.S. Pat. 4,665,047**.

Smith, J. M.; Van Ness, H. C. (1987) Introduction to Chemical Engineering Thermodynamics, New York, McGraw-Hill, 4th ed.

Smith, W. H.; Stoffer, R. L.; Hannan, R. B. (1962) J. Polym. Sci., **61**, 39.

Soares, J. B. P.; Vela-Estrada, J. M.; Hamielec, A. E. (1992) 75th Canadian Chemical Conference and Exhibition, Edmonton, Alberta, 265-ID-G2

Soares, J. B. P.; Hamielec, A. E. (1994a) Analyzing TREF Results by Stockmayer's Bivariate Distribution. Macromol. Theory Simul., accepted for publication, 10/94.

Soares, J. B. P.; Hamielec, A. E. (1994b) General Dynamic Mathematical Modelling of Heterogeneous and Homogeneous Ziegler-Natta Copolymerization with Multiple Site Types and Mass and Heat Transfer Resistances. Polym. Reac. Eng., submitted for publication.

Soares, J. B. P.; Hamielec, A. E. (1994c) Deconvolution of Chain Length Distributions of Linear Polymers Made by Multiple Site Type Catalysts. Polymer, accepted for publication, 10/94.

Soares, J. B. P.; Hamielec, A. E. (1994d) Fractionation of Linear Polyolefins by TREF. Polymer, accepted for publication, 08/94.

Soares, J. B. P.; Hamielec, A. E. (1994e) Metallocene/Aluminoxane Catalysts for Olefin Polymerization. A Review. Polym. Reac. Eng., accepted for publication, 10/94.

Soga, K.; Sino, T. (1982) Polym. Bull., **8**, 261.

Soga, K.; Shiono, T.; Takemura, S.; Kaminsky, W. (1987) Makromol. Chem., Rapid. Commun., **8**, 305.

Soga, K.; Yanagihara, H.; Lee, D. H. (1988) In Transition Metal Catalyzed Polymerization, R. D. Quirk (ed.), Cambridge University Press, New York, 995.

Soga, K.; Kaminaka, M. (1992) Makromol. Chem., Rapid Commun., **13**, 221.

Soga, K.; Kaminaka, M. (1993) Makromol. Chem., **194**, 1745.

Spaleck, W.; Antberg, M.; Dolle, V.; Klein, R.; Rohrmann, J.; Winter, A. (1990) News J. Chem., **14**, 499.

Spitz, R. (1987) In Recent Advances in Mechanistic and Synthetic Aspects of Polymerization, M. Fontanille and A. Guyot (eds.), D. Reidel Publishing Co., New York, 485.

Spitz, R.; Duranel, L.; Masson, P.; Darricades-Lauro, M. F.; Guyot, A. (1988) In Transition Metal Catalyzed Polymerization. R. D. Quirk (ed.), Cambridge University Press, New York, 719.

Stephanopoulos, G. (1984) Chemical Process Control. Prentice-Hall, Englewood Cliffs.

Stevens, J. C.; Neithamer, D. R. (1992) Metal complex compounds. **U.S. Pat. 5,132,380.**

Stockmayer, W. H. (1945) J. Chem. Phys., **13**, 199.

Stricklen, P. M. (1991) Process for producing polyolefins and polyolefin catalysts. **U.S. Pat. 5,064,797.**

Styring, M. K.; Hamielec, A. E. (1989) In Chemical Analysis, **103**, A. R. Cooper (ed.), John Wiley & Sons, New York, 263.

Tacx, J. C. J. F.; Linssen, H. N.; German, A. L. (1988) J. Polym. Sci.:Part A: Polym. Chem., **26**, 61.

Tait, P. J. T. (1988) In Transition Metal Catalyzed Polymerization, R. D. Quirk (ed.), Cambridge University Press, New York, 834.

Tait, P. J. T.; Booth, B. L.; Jejelowo, M. O. (1988) Makromol. Chem., Rapid Commun., **9**, 393.

Tait, P. J. T.; Wang, S. (1988) Brit. Polym. J., **20**, 499.

Tait, P. J. T. (1989) In Comprehensive Polymer Science. Sir G. Allen (ed.), Oxford, Pergamon Press, **4**, 1.

Tait, P. J. T.; Watkins, N. D. (1989) In Comprehensive Polymer Science. Sir G. Allen (ed.), Oxford, Pergamon Press, **4**, 533.

Tait, P. J. T.; Berry, I. G. (1989) In Comprehensive Polymer Science. Sir G. Allen (ed.), Oxford, Pergamon Press, **4**, 575.

Taylor, T. W.; Choi, K. Y.; Yuan, H.; Ray, W. H. (1983). MMI Press Symp. Ser., **4**, 191.

Tsutsui, T.; Ishimaru, N.; Mizuno, A.; Toyota, A.; Kashiwa, N. (1989a) Polymer, **30**, 1350.

Tsutsui, T.; Mizuno, A.; Kashiwa, N. (1989b) Makromol. Chem., **190**, 1177.

Tsutsui, T.; Yoshitsugu, K.; Toyota, A.; Kashiwa, M. (1992) Solid catalyst for polymerizing an olefin. **U.S. Pat. 5,126,301.**

Turner, H. W. (1988a) New polymerization catalyst. **U.S. Pat. 4,752,597.**

Turner, H. W. (1988b) New polymerization catalyst. **U.S. Pat. 4,791,180.**

Turner, H. W.; Hlatky, G. G.; Eckman, R. R. (1993) Ionic metallocene catalyst compositions. **U.S. Pat. 5,198,401.**

Usami, T.; Gotoh, Y.; Takayama, S. (1986) Macromolecules, **19**, 2722.

Usami, T.; Gotoh, Y.; Umemoto, H.; Takayama, S. (1993) J. Appl. Polym. Sci.: Appl. Polym. Symp., **52**, 145.

Vela-Estrada, J. M.; Hamielec, A. E. (1993) Polym. Reac. Eng. J., **1**, 171.

Vela-Estrada, J.M.; Hamielec, A.E. (1994) Polymer, **19**, 808.

Ver Strate, G. (1986) In Encyclopedia of Polymer Science and Engineering, J. I. Kroschwitz (ed.).

Vickroy, V. V.; Schneider, H.; Abbott, R. F. (1993) J. Appl. Polym. Sci., **50**, 551.

Wagner, H. L. (1985) J. Phys. Chem. Ref. Data, **14**, 511.

Waymouth, R. M. (1993) Stereoregular cyclopolymers and method. **U.S. Pat. 5,208,304.**

Wei, P. A. (1961) Anal. Chem., **33**, 215.

Welborn, H. C., Jr. (1987) Supported polymerization catalyst. **U.S. Pat. 4,701,432.**

Welborn, H. C., Jr. (1989) Supported polymerization catalyst. **U.S. Pat. 4,808,561.**

Welborn, H. C., Jr. (1990) Polymerization process. **U.S. Pat. 4,897,455.**

Welborn, H. C., Jr. (1991a) New supported polymerization catalyst. **U.S. Pat. 5,077,255.**

Welborn, H. C., Jr. (1991b) Metallocene, hydrocarbylaluminum and hydrocarbylboroxine olefin polymerization catalyst. **U.S. Pat. 5,001,244.**

Welborn, H. C., Jr. (1991c) Silicon-bridged transition metal compounds. **U.S. Pat. 5,017,714.**

Welborn, H. C., Jr. (1992a) Supported polymerization catalyst. **U.S. Pat. 5,124,418.**

Welborn, H. C., Jr.; Speed, C. S. (1992b) High pressure, high temperature polymerization of ethylene. **U.S. Pat. 5,084,534.**

Welborn, H. C., Jr. (1992c) Silicon-bridged transition metal compounds. **U.S. Pat. 5,120,867.**

Welborn, H. C., Jr. (1993) Polymerization process using a new supported polymerization catalyst. **U.S. Pat. 5,183,867.**

Whiteley, K. S.; Heggs, T. G.; Koch, H.; Mawer, R. L.; Immel, W. (1992) In Ulmann's Encyclopedia of Industrial Chemistry, **A21**, B. Elvers, S. Hawkins, G. Schultz (eds.), Weinheim, VHC Publishers Inc., 487.

Wijga, P. W. O.; Van Schooten, J.; Boerma, J. (1960) Makromol. Chem., **36**, 115.

Wilchinsky, Z. W.; Looney, R. W.; Tornquist, G. M. (1973) J. Catal., **28**, 351.

Wild, F. R. W. P.; Zsolnai, L.; Huttner, G.; Brintzinger, H. H. (1982) J. Organomet. Chem., **232**, 233.

Wild, F. R. W. P.; Wasiucionek, M.; Huttner, G.; Brintzinger, H. H. (1985) J. Organomet. Chem., **288**, 63.

Wild, L.; Ryle, T. (1977) Polym. Prep., Am. Chem. Soc., Polym. Chem. Div., **18**, 182.

Wild, L.; Ryle, T. R.; Knolbeloch, D. C.; Peat, I. R. (1982) J. Polym. Sci.: Polym. Phys. Ed., **20**, 441.

Wild, L.; Ryle, T.; Knobeloch, D. (1986) Polymer Preprints., **23**, 133.

Wild, L. (1990) Adv. Polym. Sci., **98**, 1.

Wilfong, D. L.; Knight, G. W. (1990) J. Polym. Sci.: Part B: Polym. Phys., **28**, 861.

Winter, A.; Antberg, M.; Rohrmann, J. (1990a) 1-Olefin stereoblock polymer wax, and a process for the preparation thereof. **U.S. Pat. 4,962,248.**

Winter, A.; Antberg, M.; Rohrmann, J. (1990b) 1-Olefin polymer wax, and a process for the preparation thereof. **U.S. Pat. 4,962,262.**

Winter, A.; Volker, D.; Antberg, M.; Rohrmann, J. Bohm, L.; Spaleck, W. (1992a) Polypropylene wax and process for the production thereof. **U.S. Pat. 5,081,322.**

Winter, A.; Volker, D.; Antberg, M.; Rohrmann, J. Bohm, L.; Spaleck, W. (1992b) Process for the preparation of a syndiotactic polyolefin. **U.S. Pat. 5,132,381.**

Xu, Z.; Zhu, Q.; Feng, L.; Yang, S. (1990) Makromol. Chem. Rapid Commum., **11**, 79.

Yano, T.; Inoue, T.; Ikai, S.; Kai, Y.; Tamura, M.; Shimizu, M. (1986) Makromol. Chem. Rapid Commum., **7**, 491.

Yoon, J. S; Ray, W. H. (1987) Ind. Eng. Chem. Res., **26**, 415.

Ystenes, M. (1991) J. Catal., **129**, 383.

Yuan, H. G.; Taylor, T. W.; Choi, K. Y.; Ray, W. H. (1982) J. Appl. Polym. Sci., **27**, 1691.

Zakharov, V. A.; Bukatov, G. D.; Yermakov, Y. F. (1983) Adv. Polym. Sci., **51**, 61.

Zambelli, A.; Ammendola, P. (1988) In Transition Metals and Organometallics as Catalysts for Olefin Polymerization. W. Kaminsky and H. Sinn (eds.), 329.

Zambelli, A.; Longo, P.; Grassi, A. (1989) Macromolecules, **22**, 2186.

Zhu, S. N.; Yang, X. Z.; Chujo, R. (1983) Polym. J., **15**, 859.

Zucchini, U.; Cecchin, G. (1983) Adv. Polym. Sci., **51**, 101.